



UNIVERSIDAD NACIONAL AUTÓNOMA DE MÉXICO

Doctorado en Ciencias Biomédicas

**Estudio del poro inespecífico mitocondrial de la levadura
Saccharomyces cerevisiae.**

TESIS

QUE PARA OPTAR POR EL GRADO DE:

Doctor en Ciencias

PRESENTA:

Norma Lilia Morales García

DIRECTOR DE TESIS:

Dr. Salvador Uribe Carvajal
[Instituto de Fisiología Celular](#)

COMITÉ TUTOR:

Dra. Bertha González Pedrajo
[Instituto de Fisiología Celular](#)
Dr. Oscar Flores Herrera
[Facultad de Medicina](#)

Ciudad de México. Octubre, 2022



Universidad Nacional
Autónoma de México

Dirección General de Bibliotecas de la UNAM

Biblioteca Central



UNAM – Dirección General de Bibliotecas
Tesis Digitales
Restricciones de uso

DERECHOS RESERVADOS ©
PROHIBIDA SU REPRODUCCIÓN TOTAL O PARCIAL

Todo el material contenido en esta tesis esta protegido por la Ley Federal del Derecho de Autor (LFDA) de los Estados Unidos Mexicanos (México).

El uso de imágenes, fragmentos de videos, y demás material que sea objeto de protección de los derechos de autor, será exclusivamente para fines educativos e informativos y deberá citar la fuente donde la obtuvo mencionando el autor o autores. Cualquier uso distinto como el lucro, reproducción, edición o modificación, será perseguido y sancionado por el respectivo titular de los Derechos de Autor.

ÍNDICE GENERAL

1. RESUMEN	1
2. INTRODUCCIÓN	2
2.1. El metabolismo aerobio en eucariontes	2
2.2. La glucólisis	4
2.3. Estructura de la mitocondria	5
2.4. Fosforilación Oxidativa (OxPhos)	7
2.5. Cadena de Transporte de Electrones (CTE)	11
2.5.1.Complejo I	12
2.5.2.Complejo II	14
2.5.3.Complejo III	15
2.5.4.Complejo IV	17
2.6. Complejo V	18
2.7. Mecanismo de acoplamiento mitocondrial	20
2.8. Las especies reactivas de oxígeno (EROs). Producción y detoxificación	20
2.9. Prevención de la sobreproducción de EROs	26
3. ANTECEDENTES	29
3.1. El poro de transición de la permeabilidad; estructura y función.	29
4. PLANTEAMIENTO DEL PROBLEMA	32
5. HIPÓTESIS	32
6. OBJETIVOS	33
6.1. OBJETIVO GENERAL	33
6.2. OBJETIVO PARTICULAR	33
7. MÉTODOS	34
8. RESULTADOS	38
9. DISCUSIÓN	47
10. CONCLUSIONES	50
11. PERSPECTIVAS	51
12. BIBLIOGRAFÍA	52
13. ANEXOS	59
13.1 Publicaciones	59

ÍNDICE DE FIGURAS

Figura 1. Esquema de una cresta mitocondrial	8
Figura 2. Apoptosis mitocondrial.....	10
Figura 3. Complejo I ..	14
Figura 4. Complejo II	15
Figura 5. Complejo III.....	17
Figura 6. Complejo IV.	18
Figura 7. Generación de especies reactivas de oxígeno..	24
Figura 8. Producción de las ERO _s y sus destinos.....	27
Figura 9. Arquitectura de las crestas mitocondriales en presencia de 0.1 mM Pi y 2 mM Pi.	41
Figura 10. Hinchamiento mitocondrial 2 mM Pi titulando ATP.....	43
Figura 11. Hinchamiento mitocondrial en 0.1 mM Pi titulando con diferentes concentraciones de ADP.....	43
Figura 12. Efecto antagónico del ATP y ADP en el hinchamiento mitocondrial..	44
Figura 13. Efecto del Pi sobre el potencial transmembranal.	45
Figura 14. Consumo de oxígeno	48
Figura 15. Producción de especies reactivas de oxígeno en mitocondrias aisladas..	49
Figura 16. Reversibilidad parcial adicionando ADP a diferentes tiempo en <i>S. cerevisiae</i> ..	50

ÍNDICE DE ECUACIONES

Ecuación 1. Ecuación global de la glucólisis	5
Ecuación 2. Descarboxilación oxidativa del piruvato	5
Ecuación 3. Balance del ciclo de Krebs	6
Ecuación 4. Fuerza protónmotriz	11

ABREVIATURAS

ADP	Adenosin difosfato
ANT	Adenine nucleotide translocator (Translocador de adenil nucleótidos)
AOX	Alternative oxidase (Oxidasa alterna)
Apaf-1	Apoptotic protease-activating factor-1 (Factor activador de proteasa apoptótico)
ATP	Adenosín trifosfato
BAT	Brown adipose tissue (Tejido adipose marron)
CCCP	p-clorocarbonilcianurofenilhidrazona
CJ	Cristae junctions (Uniones cretales)
CR	Control respiratorio
EGTA	Etilen glicol bis (2-aminoetil eter)-N N N'N'-ácidotetraacético
EIM	Espacio intermembranal
ERCI	Especie reactiva de cloro
ERNs	Especies reactivas de nitrógeno
EROs	Especies reactivas de oxígeno
FAD	Flavin adenosina dinucleótido
FMN	Flavin mononucleótido
GSH	Glutación reducido
H4B	Tetrahidrobiopterina
IBM	Inner boundary membrane (Membrana limitante interna)
MEM	Membrana externa mitocondrial
MES	Ácido 4-Morfolineatanesulfonico monohidratado
MICOS	Mitochondrial contact site and cristae organizing system (Sistema organizador de crestas y sitios de contacto mitocondrial)
MIM	Membrana interna mitocondrial
MUC	Mitochondrial unspecific channel (Canal inespecífico mitocondrial)
<i>D_h</i> MUC	<i>D. hanseni</i> of mitochondrial unspecific channel
<i>Sc</i> MUC	<i>S. cerevisiae</i> of mitochondrial unspecific channel
ND2	NADH deshidrogenasa tipo 2
ONS	Óxido nítrico sintasa
OPA1	Proteína de fusión de atrofia óptica tipo 1
Pi	Fosfato
PiC	Acarreador de fosfato
PTP	Poro de la transición de la permeabilidad
SOD	Superóxido dismutasa
TMPD	Tetrametilfenilendiamina
UCPs	Uncoupling proteins (Proteínas desacoplantes)
VDAC	Voltage-dependent anion channel (Canal aniónico dependiente de voltaje)
$\Delta\Psi$	Potencial transmembranal

AGRADECIMIENTOS

A la Universidad Nacional Autónoma de México y al Programa de Doctorado de Ciencias Biomédicas.

Al Dr. Salvador Uribe Carvajal, por su apoyo, paciencia y amistad.

A la técnica académico Dra. Natalia Chiquete Félix, por su apoyo técnico y personal.

A los miembros de mi comité tutor, conformado por el Dra. Bertha González Pedrajo y al Dr. Oscar Flores Herrera, por sus consejos y comentarios que enriquecieron este proyecto.

A los miembros del jurado de examen: Dr. Antonio Peña Díaz (IFC, UNAM), Dra. María del Carmen Beltrán Núñez (IBT, UNAM), Dr. Ricardo Jasso Chávez (Instituto Nacional de Cancerología), Dra. Ana Cecilia Zazueta Mendizabal (Instituto Nacional de Cardiología) y Dr. Oscar Flores Herrera (FM, UNAM), por la revisión y comentarios para mejorar este trabajo.

Se agradece el apoyo al laboratorio 306 oriente del Instituto por permitirme el uso de equipos y reactivos de su laboratorio, sobre todo a la Dra. Norma Silvia Sánchez y la Dra. Martha Calahorra Fuertes por sus comentarios y aportaciones a este proyecto.

A la Unidad de Microscopía Electrónica del IFC, en específico a la Dra. Ruth Rincón Heredia y al M.C. Rodolfo Paredes Díaz por su apoyo técnico.

A la técnica académico Dra. Yolanda Margarita Camacho Villasana, por su apoyo técnico para la realización de este proyecto.

Agradezco a cada integrante del laboratorio 305 oriente y el IFC que me apoyaron en mi formación personal y académica: Caro, Emilio, Mona, Cris, Alf, Pau, Ulrik, Félix, Xóchitl, Itza, Nat y Aldo.

A mi familia de Facultad de Medicina que me dio apoyo académico y profesional en todo este proceso.

Al Instituto de Fisiología Celular y a la Unidad del bioterio, por la aprobación del protocolo por el Comité institucional para el cuidado y uso de animales de laboratorio del IFC (SUV124-19).

Este trabajo fue apoyado parcialmente con una beca del Consejo Nacional de Ciencia y Tecnología (CONACYT) con CVU 695222 a la sustentante, Norma Lilia Morales García.

El trabajo fue apoyado parcialmente por un donativo de la DGAPA-PAPIIT IN208821.

A ti, Acatonalli; que siempre has estado en la buenas, malas y peores durante 17 años de mi vida y me regalaste al amor de mi vida. Gracias por ser en mi vida algo más que un instante, algo más que una sombra y algo más que un afán.

A mi madre, mis hermanas y sobrino que han sido mi apoyo incondicional.

A los que ya no están a mi lado y siempre me dieron su cariño

A mi padre que siempre me dio su mano, apoyo y su amor incondicional Y estoy segura de que lo veré en la otra vida.

1. RESÚMEN

En diversos organismos se ha reportado un poro inespecífico mitocondrial que permite el transporte no selectivo de moléculas de hasta 1.5 kDa provocando el abatimiento del potencial transmembranal e hinchamiento mitocondrial. En los mamíferos se ha propuesto que este poro participa en la expulsión del calcio mitocondrial y la irreversibilidad de su apertura lleva a la muerte celular. En la levadura *Saccharomyces cerevisiae* se detectó un poro similar al que se denominó $scMUC$ por sus siglas en inglés (*S. cerevisiae* Mitochondrial Unespecific Channel). Originalmente, este poro se describió en mamíferos desde los años 70's y al principio se consideró un artefacto. Sin embargo, con el paso del tiempo su importancia se ha hecho evidente. En cuanto a su posible estructura, se han propuesto diversos componentes y no se ha llegado a un consenso. Los efectores de este canal son muchos. Pueden ser fisiológicos (calcio, magnesio, ATP, ADP, NADH) o moléculas ajenas a la célula (atractilósido, ácido bongkrékico o polietilenglicol). En el caso de la levadura, además de la estructura, no se ha llegado a identificar la función del $scMUC$, pues se mantiene abierto por largos periodos sin matar a la célula; al contrario del poro de los mamíferos, en las levaduras se observó que este canal se cierra al aumentar el calcio extramitocondrial y se abre al quelarlo con EGTA. El objetivo de este trabajo fue corroborar la reversibilidad de la apertura del canal adicionando en secuencia efectores antagónicos fisiológicos buscando las condiciones en que este canal funciona como un desacoplante fisiológico que participa en la regulación del metabolismo de la levadura.

2.INTRODUCCIÓN

El metabolismo aerobio en eucariontes

Los procariontes y los organismos eucariontes, son muy diferentes tanto en tamaño, como en su fecha de aparición en el árbol filogenético. Los primeros en aparecer fueron los procariontes y hace unos 2700 millones de años aparecieron los eucariontes (Soo *et al.*, 2017). Los eucariontes nacieron de la asociación de varios organismos donde el núcleo probablemente evolucionó a partir de un adenovirus, los cloroplastos de una cianobacteria y las mitocondrias nacieron de una proteobacteria (Soo, Hemp & Hugenholtz 2019). Todos se asociaron dentro del citoplasma de otro procarionte, probablemente de mayor tamaño. Las endosimbiosis resultantes se consolidaron a través de una coevolución con intercambio de información genética (Martin, Garg & Zimorski 2015). Así, al exportar parte de su genoma al nuevo núcleo de la recién formada célula eucarionte, los cloroplastos y las mitocondrias perdieron su capacidad para existir libremente y se convirtieron en organelos (Margulis & Bermudes 1985).

En los eucariontes ya existían las cadenas respiratorias, sólo que, en lugar de oxígeno, se usaban como aceptores finales de electrones el nitrato, el nitrito, el dimetil sulfóxido y otras moléculas oxidadas; un ejemplo es *Chlamydomonas reinhardtii* su supervivencia en anoxia depende de sus aceptores finales diferentes al O₂ (Mia *et al.*, 2019). Los primeros eucariontes tenían mitocondrias con cadenas respiratorias anaerobias (Dodson 1979).

El repentino aumento del oxígeno atmosférico sobrevino porque los minerales del suelo encargados de secuestrarlo se saturaron. Esto se debió a la gran producción del gas por las cianobacterias acuáticas que proliferaron masivamente gracias a la fotosíntesis (Hsia *et al.*, 2013). Así, la atmósfera fue cambiando para quedar compuesta por bióxido de carbono y oxígeno. El alza en la concentración de oxígeno de 0 a 20-30% (Andrulis 2011) llevó a la primera gran extinción masiva. Cerca del

60% de los organismos perecieron, mientras que los sobrevivientes tuvieron que lidiar con este elemento (Grenfell *et al.*, 2010; Nunn 1998).

El O_2 es un ávido aceptor de electrones ($O_2/H_2O = +0.82$ V comparado con $NAD^+/NADH + H^+ = -0.32$ V) lo que es la base de su toxicidad, pero también dotó de grandes ventajas a los organismos que aprendieron a utilizarlo. La reducción parcial no catalizada del O_2 resulta en la generación de radicales libres; aquellos que son derivados del oxígeno se conocen como especies reactivas de oxígeno (EROs) y son capaces de combinarse con otras moléculas desorganizándolas y eventualmente destruyéndolas. Lo que hace diferentes a las EROs de otros radicales libres es que difunden rápidamente extendiendo el daño a diversas moléculas alrededor de su sitio de formación. En contraste con el daño causado por las EROs, el oxígeno es muy eficiente como aceptor de electrones y por ello fue adoptado por diversos organismos tanto procariontes como eucariontes como el aceptor final de electrones en la cadena respiratoria. Los organismos que usan oxígeno en su cadena respiratoria se denominan aerobios (McCord, 2000).

El metabolismo aerobio optimiza la extracción de energía de los nutrientes. Por ejemplo, un mol de glucosa metabolizado anaeróbicamente produce dos moles de ATP. En contraste, un mol de glucosa metabolizado aeróbicamente puede producir hasta 38 moles de ATP.

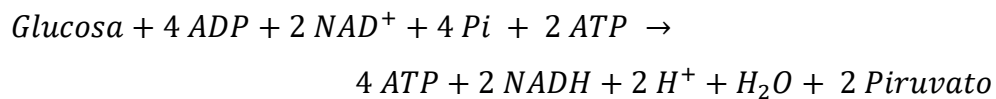
El metabolismo aerobio, muy probablemente, fue decisivo para que aparecieran los organismos pluricelulares. Otra vez, esto obedeció a dos factores. Por un lado, las células asociadas entre sí se protegen contra las elevadas concentraciones de O_2 . Por el otro, el alto rendimiento energético posibilitó la síntesis de moléculas y estructuras complicadas en los organismos con especialización tisular y sistemas de suministro de nutrientes y de O_2 . Con respecto a la evasión frente al oxígeno hay ejemplos en unicelulares de estrategias como la formación de biopelículas donde solamente las células de la superficie se tienen que enfrentar al O_2

mientras que la médula de la biopelícula permanece en anaerobiosis. (Uribe-Alvarez *et al.*, 2016; Wu *et al.*, 2015).

La glucólisis

La glucólisis es muy conservada y se considera que fue la primera vía de obtención de energía que apareció en los seres vivos; en este camino metabólico, una hexosa produce una ganancia neta de 2 moléculas de ATP y 2 de NADH + H⁺ y dos moléculas de piruvato (Ecuación 1).

ECUACIÓN 1. Ecuación global de la glucólisis.



Como se aprecia en la ecuación 1, la glucólisis invierte dos moléculas de ATP y produce cuatro, con ganancia neta de dos. En contraste, en las células aerobias se usan NAD/NADH y O₂ para oxidar al piruvato obteniendo CO₂ y agua, obteniendo mucho más ATP por cada molécula de glucosa.

El piruvato generado por la oxidación de la glucosa tiene dos destinos en la célula 1) en ausencia de O₂ se realiza el proceso llamado fermentación (en condiciones anaeróbicas) y 2) en presencia de O₂ ocurre el proceso llamado respiración (condiciones aeróbicas).

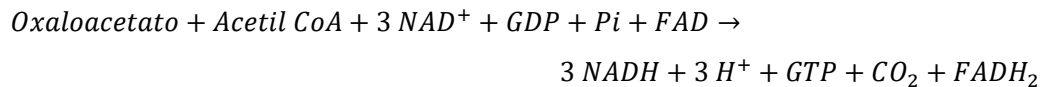
En el metabolismo aerobio de los eucariontes, el piruvato es captado por la mitocondria por una proteína transmembranal (transportador de piruvato); en la matriz mitocondrial el piruvato es descarboxilado por un complejo de tres enzimas llamado piruvato deshidrogenasa que genera 1 molécula de acetil CoA, CO₂ y NADH (Ecuación 2).

ECUACIÓN 2. Descarboxilación oxidativa del piruvato.



El acetil CoA es una molécula que no sólo es generada por la descarboxilación oxidativa del piruvato sino también de otras macromoléculas (como lípidos) y puede ingresar al ciclo de Krebs y generar NADH y FADH₂ (Ecuación 3).

ECUACIÓN 3. Balance del ciclo de Krebs



El NADH y FADH₂ que se generan son usados por un sistema complejo de enzimas incorporadas en la membrana interna mitocondrial que realizan la fosforilación oxidativa (OxPhos), que es un proceso metabólico que produce ATP, consumiendo O₂. Con este proceso se producen teóricamente 38 moléculas de ATP en vez de los 2 ATP que se generan anaeróticamente en la glucólisis, este proceso resalta la importancia de la mitocondria.

Estructura de la mitocondria

Como se ha descrito arriba, la hipótesis endosimbiótica propone que las células procariontes anaerobias engulleron a una bacteria primitiva lo que permitió que ambos organismos establecieran una interacción endosimbiótica para poder generar energía en forma de ATP a través de la cadena respiratoria (Margulis & Bermudes 1985).

La mitocondria se compone de dos membranas una interna (MIM) y otra externa (MEM), las cuales delimitan a la matriz mitocondrial y el espacio intermembranal (EIM) respectivamente. Las membranas tienen diferente composición; por ejemplo, la MEM tiene 20% de proteínas mientras que la MIM tiene 70%. También, en la MIM hay cardiolipina, un fosfolípido necesario para la función adecuada de diversas proteínas. La composición lipídica de la MEM es muy similar a la de la membrana

plasmática de la célula eucariota y presenta alta permeabilidad a diferentes solutos (Falabella *et al.*, 2021).

La MIM se pliega en una serie de invaginaciones hacia la matriz mitocondrial las cuales son llamadas crestas, en estas estructuras se encuentra principalmente la maquinaria de la fosforilación oxidativa. Hay secciones de la MIM que no forman crestas y que corren paralelamente con la MEM a éstas se le conoce como IBM (por sus siglas en inglés inner boundary membrane) y la unión entre las crestas y los IBM se conocen uniones de cresta (CJ, cristae junctions) (Gottschalk *et al.*, 2022).

El número de crestas, y en general la organización de éstas, depende de varios factores como los requerimientos celulares de energía o señales apoptóticas, las cuales las hacen más o menos compactas. Estas modificaciones en la arquitectura de las crestas se generan con ayuda de varias proteínas que regulan las CJ. Las CJ son parte del sistema de organización de crestas y de sitios de contacto mitocondrial (MICOS: Mitochondrial contact site and cristae organizing system) y la proteína de fusión de atrofia óptica tipo 1 (OPA1) (Khosravi & Harner 2020).

El cambio en la conformación de la arquitectura de las crestas de la mitocondria ha creado un modelo en el cual se propone la variación local del pH que pueden ser muy bajos cerca de los bordes de las crestas. En el extremo más profundo de las crestas tiende a acumularse mayor concentración de cargas lo cual hace más eficiente el acoplamiento de protones a nivel local teniendo un pH en la matriz aproximado de 7.9 mientras que en el espacio intracrestal es de 7.3; es decir, se establece ΔpH de 0.6 (Figura 1).

Se había descrito que para el funcionamiento de la ATPasa se requería de un ΔpH de 2, pero en este sistema se ha estimado un pH de 7.3. Otro sitio en donde el movimiento de protones entre la matriz y el espacio intracrestal genera un valor de pH muy localizado (7) es el sitio donde se encuentra el Complejo IV (Plecitá-Hlavatá & Ježek 2016).

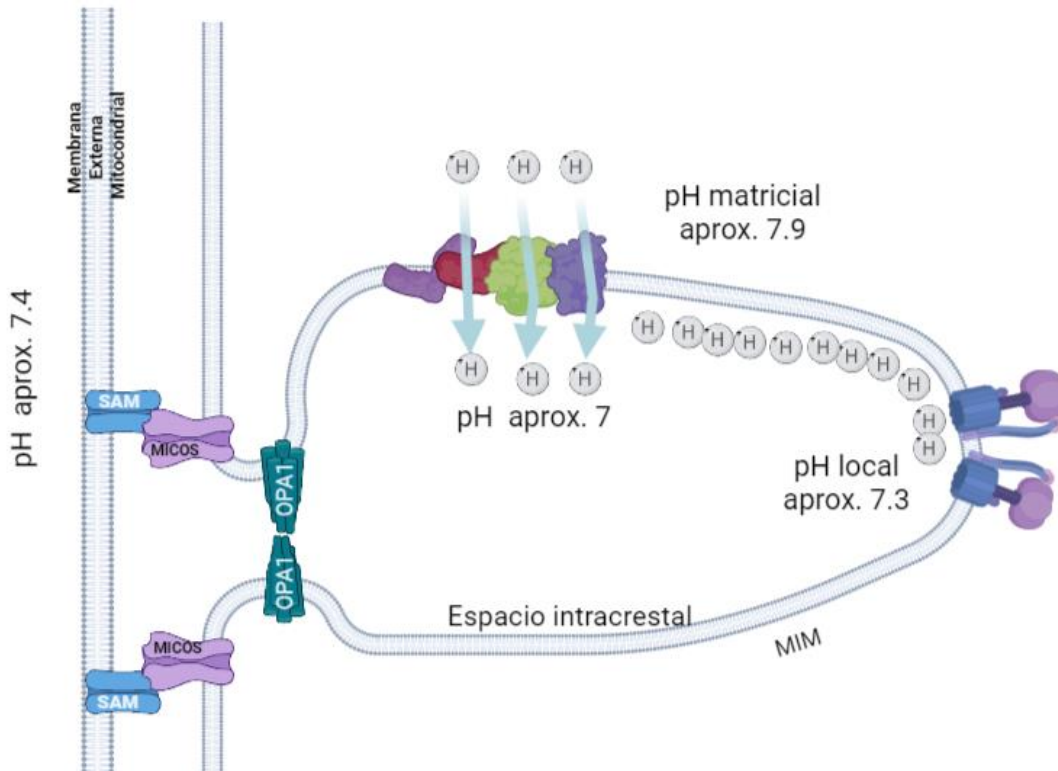


FIGURA 1 ESQUEMA DE CRESTA MITOCONDRIAL. La oligomerización de OPA1 y el ensamblaje completo y las conexiones entre el complejo MICOS de la MIM y el complejo SAM/TOM de la MIM aseguran la conformación de la unión crestal, favoreciendo con esto los microambientes y así la diferencia entre el espacio intracrestal y la matriz mitocondrial; lo cual favorece la acumulación de protones en el interior de la cresta (modificado de Plecítá-Hlavatá&jezek 2005).

Fosforilación Oxidativa (OxPhos)

La mitocondria está encargada de numerosas funciones fisiológicas:

- a) Homeostasis del calcio celular: Junto con el retículo endoplásmico se encarga de almacenarlo y liberar calcio, la regulación fina de la concentración del calcio libre es de suma importancia debido a que modifica la actividad de diversas enzimas; por ejemplo, el calcio dentro de la matriz mitocondrial es capaz de regular varias deshidrogenasas. Esto se ha observado en mitocondrias sometidas a hipoxia donde este catión estimula las deshidrogenasas que resulta en inhibición del 30 al 40 % del consumo de O_2 (Gellerich *et al.*, 2010) y retrasa el inicio de la anoxia; permitiendo que la poca

concentración de O₂ en el microambiente se difunda y evite así que se produzcan EROs en exceso. En las mitocondrias que se encuentran lejos de estos sitios de baja concentración de oxígeno (hipoxia), el calcio (Ca²⁺) activa las deshidrogenasas y aumenta el NADH matricial activando la lanzadera malato/aspartato (Solien, Haynes & Giulivi 2005).

En *Saccharomyces cerevisiae* el Ca²⁺ se usa como segundo mensajero generando pulsos de calcio en respuesta a una variedad de señales como hiperosmolaridad, hipoosmolaridad, estrés celular, concentraciones de glucosa y factor alfa (Fan *et al.*, 2018) . El Ca²⁺ se transporta desde el medio extracelular hacia la levadura (50-200 nM). En orgánulos unidos a la membrana se almacena el catión unido a polifosfato llegando hasta una concentración de 2 mM dentro de estas estructuras (Cyert & Philpott 2013).

- b) Apoptosis: Es la muerte celular programada, tiene varias vías para su inicio y la vía mitocondrial es inducida por proteínas proapoptóticas como BAX y BAK que se oligomerizan e inducen la liberación al citosol de citocromo c, que inicia la apoptosis extrínseca de la célula (Figura 2). Durante las fases iniciales de este proceso BAX es translocado a la MME y se concentran en focos puntiformes submitocondriales con BAK por donde puede salir el citocromo c y unirse a Apaf-1 (proteína proapoptótica citosólica) y activa a las caspasas 9 para poder formar el apoptosoma (Brown & Borutaite 2008).

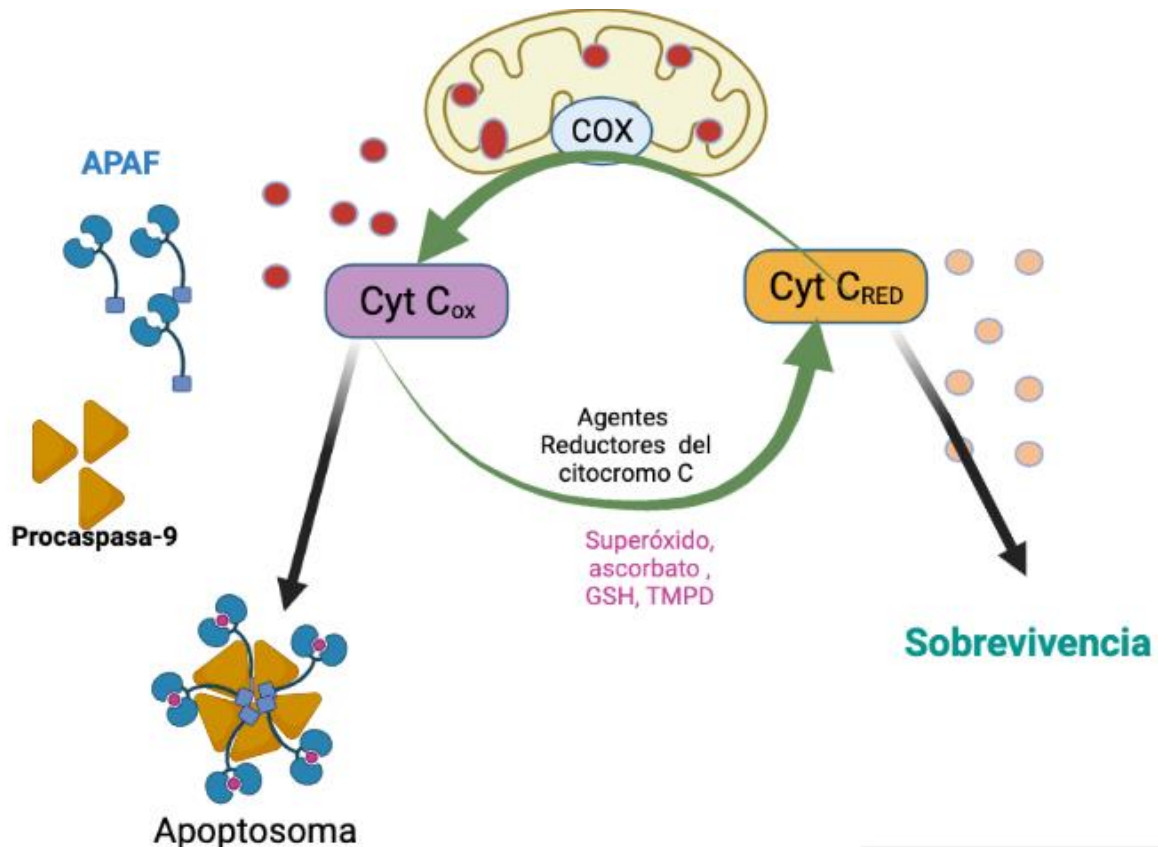


FIGURA 2 APOPTOSIS MITOCONDRIAL. La forma oxidada del citocromo c (Cyt. c_{ox}) en el citosol se une a Apaf-1 formando el apoptosoma que activa la procaspasa-9 que conduce a la apoptosis. El citocromo c citosólico puede reducirse (Cyt. c_{RED}) por varios agentes reductores como: el superóxido, el ascorbato, el glutatión reducido (GSH) y algunos químicos como tetrametilfenilendiamina (TMPD); este citocromo c reducido no puede activar el apoptosoma y, por lo tanto, no promueve la apoptosis (Modificado de Brown & Borutaitė; 2008).

- c) Síntesis de grupo Hemo: Este es necesario para el metabolismo de esteroides, transducción de señales, cadena respiratoria y el procesamiento de micro RNAs. El hemo se genera por la inserción de Fe^{2+} en la protoporfirina IX catalizado por la ferroquelatasa, una enzima de la matriz mitocondrial (Ferreira *et al.*, 1995).
- d) Generación de ATP: es una de las funciones más importantes, ya que gracias a la cadena transportadora de electrones acoplada a la fosforilación oxidativa se obtiene ATP. Esto se revisará en un inciso posterior, donde se incluye la estructura y función de las diferentes enzimas de la fosforilación oxidativa (OxPhos)

Para generar ATP la mitocondria utiliza los NADH o FADH₂ que fueron reducidos por la oxidación de algunas macromoléculas; estas moléculas ceden sus electrones a diversas enzimas redox de la cadena de transporte de electrones (CTE).

La cadena respiratoria clásica está compuesta por cuatro complejos proteicos. Además, en eucariontes primitivos, como las levaduras hay varias deshidrogenasas que ceden sus electrones a la poza de quinonas o a la Aox sin bombear protones. Los sustratos reducidos en el ciclo de Krebs y la glucólisis donan sus electrones a estos complejos que la CTE transfiere al oxígeno. La energía que se libera por esas reacciones redox genera un gradiente de protones a través de la MIM, que es usado por el complejo V (F₁F₀ ATP sintasa) para generar ATP.

El gradiente producido por la fuerza protónmotriz (FPM) tiene dos componentes, el químico y el eléctrico. El componente químico se refiere a la diferencia entre la concentración de protones de la cara del espacio intermembranal de la MIM y la cara matricial de la MIM. El componente eléctrico corresponde a la diferencia de iones cargados positiva o negativamente en los compartimentos separados por la MIM. Combinando estos dos componentes la FPM es calculada como sigue:

ECUACIÓN 4. Fuerza protónmotriz

$$\Delta p = \Delta \psi - \frac{RT}{F} \cdot \ln \left(\frac{[C]_1}{[C]_2} \right)$$

En donde:

Δp : Fuerza protón motriz

$\Delta \Psi$: Potencial de membrana

R: Constante de los gases (1.987 cal/ molK)

T: Temperatura (Kelvin)

F: Constante de Faraday (23.06 kcalmol⁻¹ V⁻¹)

[C₁]: Concentración de protones en la matriz mitocondrial

[C₂]: Concentración de protones en el espacio intermembranal

En condiciones fisiológicas la Δp es de aproximadamente - 220 mV

Cadena transportadora de electrones (CTE)

La transferencia de los electrones por complejos multienzimáticos, que disponen de elementos que son aptos para poder cederlos o aceptarlos fluyen de centros con menor potencial de óxido-reducción hacia centros con mayor potencial de reducción, hasta el oxígeno que es el aceptor final de electrones; el $\Delta G'$ al efectuar la transferencia de electrones depende la diferencia del potencial de reducción entre el aceptor y el donador que constituye el par redox.

Estudios recientes del complejo I han demostrado que la ubiquinona al entrar evoca un cambio conformacional coordinado de las subunidades ND1, NDUFS2 y ND3 que hace posible el bombeo de protones.

Independientemente de que reciba sus electrones en el complejo I o en el complejo II, la quinona se convierte primero en semiquinona y luego adquiere el segundo electrón más dos protones del medio para convertirse en quinol (QH₂). La semiquinona es un radical libre por lo que debe reducirse rápidamente. Si su reducción se retarda, aumenta la posibilidad de que la reducción inespecífica e incompleta del oxígeno genere EROs.

El complejo III oxida al ubiquinol y reduce al citocromo c, bombeando 4 H⁺ al espacio intermembranal; posteriormente, los electrones son llevados a la oxidasa terminal (complejo IV) por el citocromo c. En el CIV se forman 2 moléculas de agua por cada molécula de oxígeno y se bombean 4 H⁺ al EIM. El complejo IV tiene 2 grupos hemo (citocromos a y a₃) y dos centros de cobre (Cu_A y Cu_B). Cuando se reducen el grupo hemo a₃ y el centro Cu_B, un O₂ forma un puente entre los grupos, al romper ese enlace se generan 2 moléculas de agua.

Complejo I

También llamado NADH-ubiquinona oxidoreductasa, está conformado por 15 subunidades centrales y en eucariontes 33 accesorias, es el complejo más grande de la CTE. Las subunidades centrales tienen una configuración en forma de “L”. Las subunidades más hidrofóbicas, se codifican en el genoma mitocondrial.

Este complejo tiene 7 centros FeS (hierro-azufre) que conectan el sitio de unión de NADH con el sitio de reducción de la quinona. El acceso del NADH a esta estructura es controlado por el fragmento NDUFV1/2, para evitar una reducción excesiva del complejo I (Maldonado *et al.*, 2020).

Con respecto al sitio donde se reduce la quinona, el cluster N2 está sumergido en el brazo periférico por encima de la superficie de la membrana y para que llegue la quinona a este sitio (considerando que la quinona es hidrofóbica) se ha descrito la existencia de un túnel creado por las subunidades del brazo periférico. Este túnel se une a los lípidos entrelazándose con la superficie hidrofóbica de sus hélices anfipáticas (Parey *et al.*, 2020).

Se han descrito dos conformaciones del complejo una activa (A) y otra no activa (D). La interconversión D/A puede bloquearse por cationes divalentes (di Luca & Kaila 2021), pH alcalino o por agentes que modifiquen la subunidad ND318 la cual controla esta transición. En el miocardio, el bloqueo del complejo en D previene el daño por isquemia/reperfusión (Cabrera-Orefice *et al.*, 2018.).

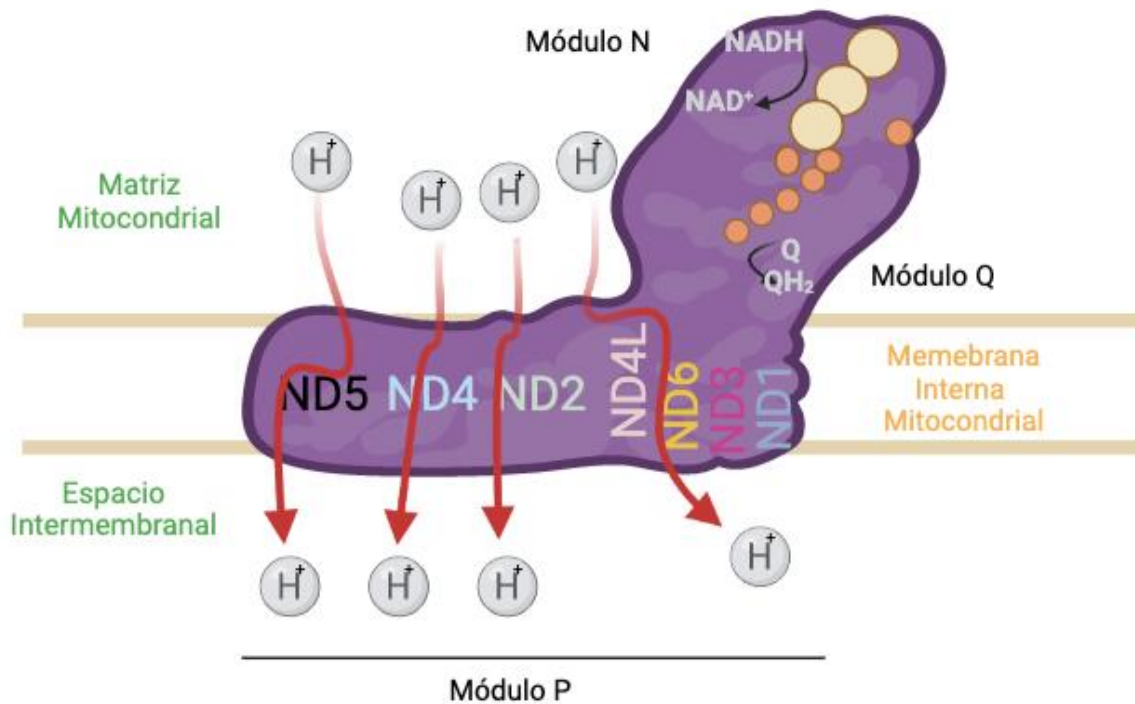


FIGURA 3 . COMPLEJO I. Las subunidades centrales se asignan como módulos funcionales para oxidación del NADH (módulo N), reducción de ubiquinona (módulo Q) y translocación de protones (módulo P). Los módulos N y Q forman la denominada matriz o brazo periférico y el módulo P corresponde al brazo de membrana. Los electrones se transfieren desde el FMN al sitio de reducción Q mediante una cadena de siete grupos de FeS (círculos naranjas). Las tres subunidades similares a antiportadores ND2 (verde), ND4 (rosa) y ND5 (negro) albergan vías de translocación de protones, cada una de las cuales consta de dos medios canales que se conectan al lado N (matriz mitocondrial) y al lado P (espacio intermembrana, EIM), respectivamente; se discute la posición de un cuarto canal de protones (Modificado de Parek, *et al.*,2020).

Complejo II

La succinato:ubiquinona oxidorreductasa contiene 4 subunidades; todas codificadas en el núcleo: SDHA, SDHB, SDHC y SDHD. Se compone de 5 grupos prostéticos y 4 de las cuales la C y D son transmembranales e hidrofóbicas; mientras que A y B contienen 3 centros fierro-azufre, FAD y el sitio de unión al succinato (Figura 4). Este complejo participa tanto en el ciclo de Krebs como en la CTE en donde se oxida el succinato a fumarato transfiriendo los electrones del succinato a la ubiquinona (Bezawork-Geleta *et al.*, 2017). Del succinato, el cofactor FAD acepta, en consecuencia 2 electrones y los trasfiere a través de los grupos fierro-azufre a la quinona en el sitio QP.

En el CII la transferencia de electrones no se acopla con bombeo de protones por lo que no contribuye a la generación de la fuerza protónmotriz, pero; es esencial para la conexión del ciclo de Krebs y la CTE (Kluckova *et al.*, 2013; Cecchini 2003).

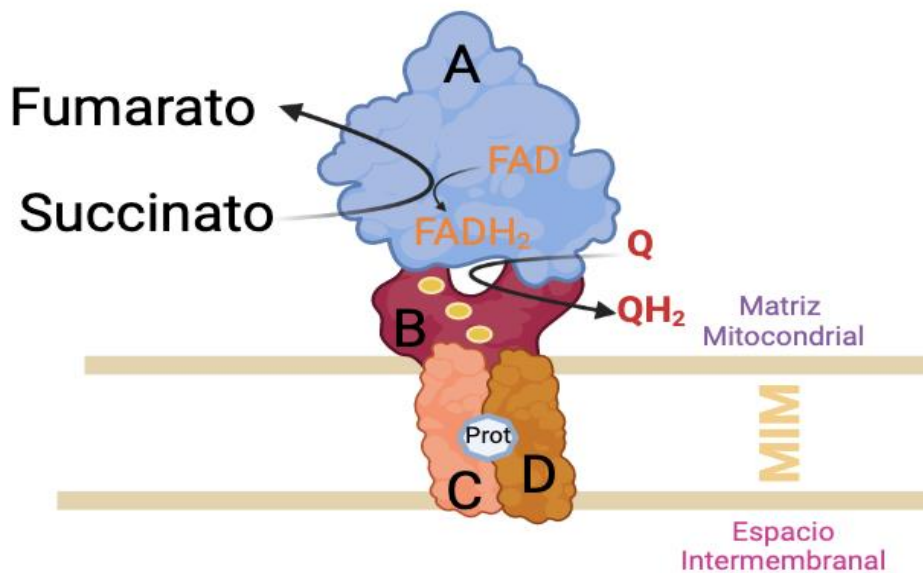


FIGURA 4 COMPLEJO II. Enzima que comparte con el ciclo de Krebs, tiene subunidades hidrofóbicas las cuales están embebidas en la membrana interna mitocondrial. Las cuatro subunidades (Sdh A-D) se indican con letras mayúsculas, las posiciones relativas de los grupos se indican con círculos amarillos (grupos [FeS]), el sitio QP es donde entra una Q y forma QH₂ que es tomado por el complejo III y un anillo de porfirina (hemo b, en hexágono azul) entre las subunidades C y D (Modificado de Dröse, 2012).

Complejo III

La ubiquinol-citocromo c oxido-reductasa (complejo bc₁) funcional consiste en la unión de dos monómeros de 11 subunidades cada uno. Este complejo tiene un hemo tipo b de baja energía de spin (hemo b_L) y otro de alta energía de spin (b_H), así como un hemo tipo C. Aparte de estos hemos también tiene un centro fierro-azufre y dos sitios de unión para la ubiquinona, uno para de oxidar al ubiquinol (Q_o) y el segundo para la reducción de la ubiquinona (Q_i). Esta enzima cataliza la reducción del citocromo c mediante la oxidación del ubiquinol producido por los CI y CII, acoplado la reacción a la translocación de 4 H⁺ (Snyder *et al.*, 2000; Trumpower 1990).

El complejo III bombea cuatro protones por cada par de electrones que recibe de la poza de quinonas. El mecanismo se ha bautizado como Ciclo Q pues se lleva a cabo en dos pasos reciclando un ubiquinol. Primero un ubiquinol es oxidado por el citocromo del lado "P" y queda como quinona que difunde hacia el lado "N". Aquí se bombean los primeros dos protones mientras que los dos electrones tienen destinos diferentes: Un electrón pasa a la proteína FeS de Rieske que a su vez lo dona al citocromo c₁ y de ahí sale hacia el citocromo c. El otro electrón pasa al citocromo b del lado negativo y ahí reduce a la quinona que queda como semiquinona. El segundo paso del ciclo Q inicia de la misma manera: un ubiquinol es oxidado en el sitio P y sus dos protones también se bombean hacia el espacio intermembranal. Esta segunda quinona queda como producto final. El primer electrón reduce secuencialmente a la FeS, al citocromo c₁ y sale hacia el citocromo c. El segundo electrón fluye hacia el lado "N" donde encuentra a la semiquinona producida en el primer paso del ciclo y la reduce recuperando un ubiquinol. En resumen, se oxidaron dos ubiquinoles, pero se recuperó uno. Se bombearon cuatro protones y se redujeron dos citocromos c.

Dos datos importantes de la función del CIII son qué; éste funciona siempre como dímero. Además, existen dos sitios en donde se puede inhibir la transferencia de electrones, uno en el centro N (que está en el lado negativo de la membrana) y otro en el centro P (que está en el lado positivo de la membrana).

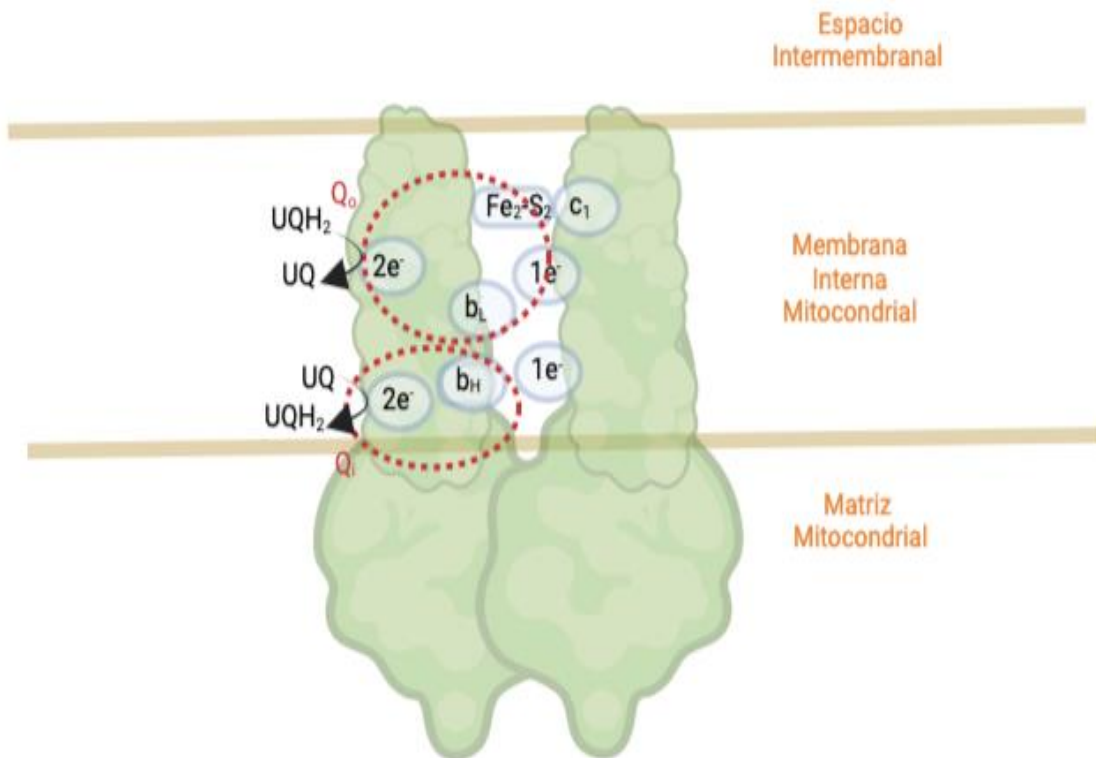


FIGURA 5. COMPLEJO III. La oxidación del UQH₂ por la subunidad Fe₂-S₂ y el citocromo b_L se produce en el sitio Q₀, orientado hacia el espacio intermembranal (EIM); y la reducción de la UQ por el citocromo b_H, en el sitio Q₁, orientado hacia la matriz mitocondrial. La energía liberada en la transferencia de electrones se utiliza para la translocación neta de 2H⁺, desde el lado matricial hacia el lado del espacio intermembranal (Brandt & Trumpower 1994).

Complejo IV

La citocromo c oxidasa cataliza la transferencia de los electrones del citocromo c reducido al O_2 transfiriendo 2 protones de la matriz al EIM. El complejo IV de mamíferos está formado por 14 subunidades de las que 3, COX 1, COX2 y COX3 forman el núcleo catalítico, codificadas en el DNA mitocondrial y son altamente conservadas. La subunidad COX2 tiene un dominio que se extiende hacia el espacio intermembranal, para unirse con el citocromo c soluble.

El centro Cu_A (centro de di-cobre) está ubicado en la interfaz de COX1 y COX2 para que tome los electrones del citocromo c. Estos electrones pasan del Cu_A al hemo a (en la COX1) que los transfiere al centro binuclear del hemo a_3-Cu_B , donde el oxígeno se reduce en agua (figura 6) (Timón-Gómez *et al.*, 2018).

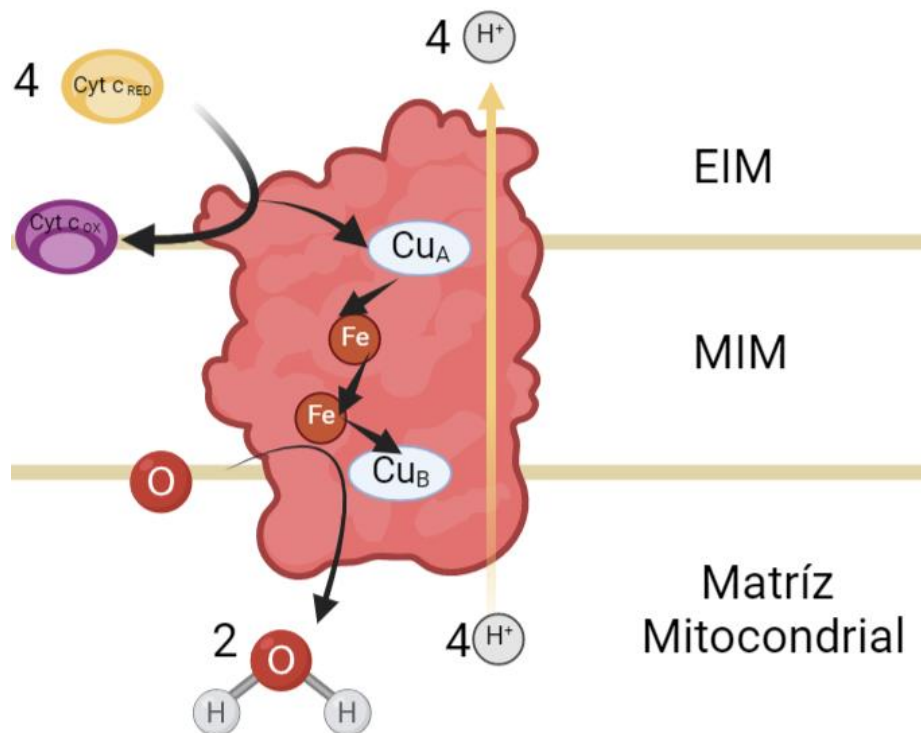


FIGURA 6 COMPLEJO IV. La citocromo c oxidasa capta 4 electrones de 4 citocromo c y los transfiere al oxígeno, para producir dos moléculas de agua. Al mismo tiempo se translocan 4 protones al espacio intermembranal.

Complejo V

La $F_1 F_0$ sintetiza ATP a partir de ADP y fosfato de forma acoplada al gradiente electroquímico generado en la CTE; el mecanismo de acción implica la rotación de algunas subunidades. CV consta de dos segmentos: uno es hidrofóbico (F_0) y está embebido en la membrana interna mitocondrial. Transloca los protones del EMI hacia la matriz mitocondrial. El segmento hidrofílico (F_1) contiene los sitios catalíticos; se proyecta hacia la matriz mitocondrial (Tabla1).

El hemicanal de H^+ , está formado entre la Su6 y Su9, y en cuanto interaccionan los protones inicia el mecanismo rotatorio. El protón forma y deshace alternativamente un puente salino entre estas dos subunidades, provocando el movimiento del anillo y a su vez el movimiento de γ , δ y ϵ . El giro de γ dentro de $\alpha_3\beta_3$ ocasiona cambios conformacionales en donde los reactivos (ADP y fosfato) catalizan la síntesis de ATP (Nakanishi-Matsui & Futai 2008).

TABLA 1. SUBUNIDADES QUE CONFORMAN AL COMPLEJO V, EN LEVADURA (*S. cerevisiae*) Y EN MAMÍFERO (*Bos taurus*).

Sector	<i>S. cerevisiae</i>	<i>B. taurus</i>	Función
F ₁	α	α	Estator
	β	β	Estator
	γ	γ	Rotor
	δ	δ	Rotor
	ε	ε	Rotor
F ₀	OSCP	OSCP	Estator
	Su 6	Su 6	Estator
	Su 9	Su 9	Rotor
	Su 8	A6L	Estator
	Su b	Su b	Estator
	Su d	Su d	Estator
	Su f	Su f	Estator
	Su h	F6	Estator
	Su i/j	-	Estator

Esta enzima se ha descrito como un nanomotor el cual tienen subunidades que funcionan como rotor y otras como estator. ^c funcionan como la parte catalítica en donde la subunidad β se asocia con la subunidad α (forman un heterohexámero) (Modificado de Devenish *et al.*, 2008; Velours *et al.*, 2009).

Mecanismo de acoplamiento mitocondrial

En 1961 Peter Mitchell publicó la teoría quimiosmótica, postulando que la transferencia de los electrones y la síntesis de ATP se acoplan a través de un gradiente de protones y de un potencial de membrana. Contiene a los siguientes postulados:

- 1) Una cadena transportadora de electrones proporciona energía para el transporte vectorial de H^+ de un lado al otro de la membrana.
- 2) La ATP sintasa, que sintetiza/hidroliza ATP de manera acoplada a la translocación de H^+ .
- 3) La impermeabilidad de la MIM a las especies iónicas (incluyendo H^+).

Las especies reactivas de oxígeno (EROs). Producción y detoxificación

Un radical libre es una molécula que contiene un electrón desapareado en su último orbital; es decir, un electrón que no compensa su momento de spin que por lo tanto le confiere un momento magnético. Los radicales libres son muy reactivos pues necesitan donar o aceptar un electrón para lograr el apareamiento. Esta reacción ocurre una y otra vez, generando nuevos radicales y destruyendo a las moléculas orgánicas, en especial donde hay dobles ligaduras de carbono. Un radical libre ubicado en una molécula inmóvil, como por ejemplo el Fe^{++} en el grupo hemo de un citocromo, está fijo y atrapado en una membrana que a su vez tiene poca o nula capacidad de movimiento, lo que limita el área donde puede ejercer su reactividad. Sin embargo, hay radicales libres de estructura sencilla que pueden difundir en la célula, viajando de un compartimento a otro y reaccionando en cada uno.

En los seres vivos existen 3 tipos de radicales libres:

- I. Especies reactivas de nitrógeno (ERNs)
- II. Especie reactiva de cloro (ERCl)

- III. Especies reactivas de oxígeno (EROs)
- I. ERNs: Entre las especies reactivas de nitrógeno está el óxido nítrico (NO) el cual participa en la vasodilatación, inhibición de agregación plaquetaria gracias a que activa la guanilato ciclasa, sin embargo, también puede reaccionar con ácidos grasos que han sido previamente oxidados y por lo tanto provoca el proceso de lipoperoxidación. El NO es lipofílico y se sintetiza gracias al grupo guanidina de la L-arginina en su transformación a L- citrulina. Esta reacción se lleva a cabo por la óxido nítrico sintasa (ONS) la cual requiere de flavín mononucleótido (FMN), flavin adenina dinucleótido (FAD), tetrahidrobiopterina (H4B) y de NADPH (Förstermann & Sessa, 2012).
 - II. ERCl: El ácido hipocloroso (HOCl) es un componente esencial del estallido respiratorio que se forma usando un oxígeno para producir H₂O₂ mediante la NADPH oxidasa. Una vez obtenido el peróxido de hidrógeno la mieloperoxidasa toma al Cl⁻ para formar HOCl. Todo este proceso se lleva a cabo en el fagolisosoma, el cual se acidifica y optimiza la actividad antimicrobiana del HOCl. La generación excesiva o externa a este subcompartimiento puede causar daño tisular y se ha asociado a aterosclerosis y algunos cánceres ya que también puede reaccionar con DNA, proteínas, lípidos, tioles y disulfuros libres (Hawkins *et al.*, 2003).
 - III. EROs: El oxígeno es especialmente propenso a formar radicales libres porque es electronegativo. Las EROs pueden generarse por factores ambientales o intrínsecos:
 - a) Ambientales: contaminación con gases como el monóxido de carbono, luz solar directa u otras fuentes de luz ultravioleta, exposición a isótopos radiactivos.
 - b) Intrínsecas: se crean principalmente en la mitocondria y por las NAD(P)H oxidasas (Xinzhao Wang *et al.*, 2021).

La fuente principal de EROs es la mitocondria. Muchos de los centros redox de las diferentes enzimas del ciclo de Krebs, de la beta-oxidación y principalmente de la cadena respiratoria se convierten en radicales libres durante el ciclo catalítico.

Se han identificado al menos diez sitios diferentes de producción de EROs en la cadena de transporte de electrones (complejo I, II y III) y otras enzimas asociadas. Ver tabla 2 (Quinlan *et al.* 2013).

TABLA 2. SITIOS REDOX QUE PRODUCEN RADICALES LIBRES. Ocurre tanto en la mitocondria como enzimas involucradas en varias vías metabólicas

MITOCONDRIA	NADH:UBIQUINONA OXIDORREDUCTASA
	SUCCINATO:COENZIMA Q OXIDOREDUCTASA
	UBIQUINOL:CITOCROMO-C OXIDOREDUCTASA
ENZIMAS ASOCIADAS	MALATO DESHIDROGENASA
	GLICEROL 3 FOSFATO DESHIDROGENASA
	OXOGLUTARATO DESHIDROGENASA
	PIRUVATO DESHIDROGENASA
	GLICEROL 3 FOSFATO DESHIDROGENASA
	PROLINA DESHIDROGENASA
	DIHIDROOROTATO DESHIDROGENASA

Los radicales libres de la mitocondria pueden reaccionar inespecíficamente con el oxígeno reduciéndolo parcialmente y produciendo el radical superóxido (O_2^-). Este radical se detoxifica por una superóxido-dismutasa (SOD) para formar H_2O_2 y éste a su vez es convertido en agua y O_2 por la catalasa (Blokina, Virolainen, & Fagerstedt 2003). Sin embargo, si el peróxido de hidrógeno no se desactiva rápidamente, puede producir el radical hidroxilo mediante la reacción de Fenton (Deng *et al.*, 2015).

En la cadena respiratoria los mayores productores de EROs son el complejo I y el III. En el complejo I se encuentran el sitio IF, donde se encuentra la flavina donde se oxida el NADH, y el sitio IQ donde se reduce la quinona (Galemou *et al.*, 2021); mientras que en el complejo III el superóxido surge del sitio de oxidación del quinol (sitio IIIQo) (Crofts *et al.*, 2013; Ohnishi *et al.*, 1994). El complejo II produce EROs durante el transporte reverso de electrones al complejo I. Esta reacción es inhibida por la rotenona, que se une al sitio Q del complejo I (Moreno-Sánchez *et al.*, 2013).

La sobreproducción de EROs puede provocar lipoperoxidación, oxidación en cisteínas o daño al DNA (Schieber & Chandel 2014). Por lo tanto, se requiere una producción controlada de éstas para controlar procesos como la proliferación celular (remodelamiento cardíaco), supervivencia celular, migración celular (en queratinocitos involucrados en el proceso de cicatrización) y crecimiento (Ortega & Rosas 2020).

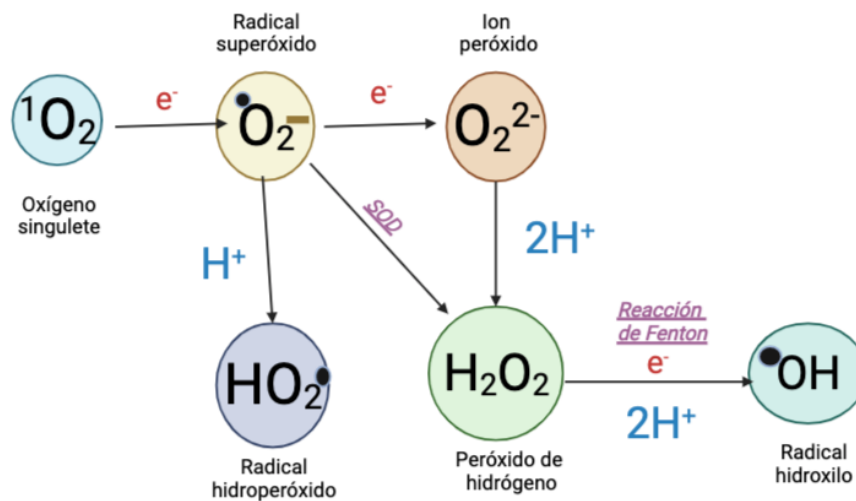
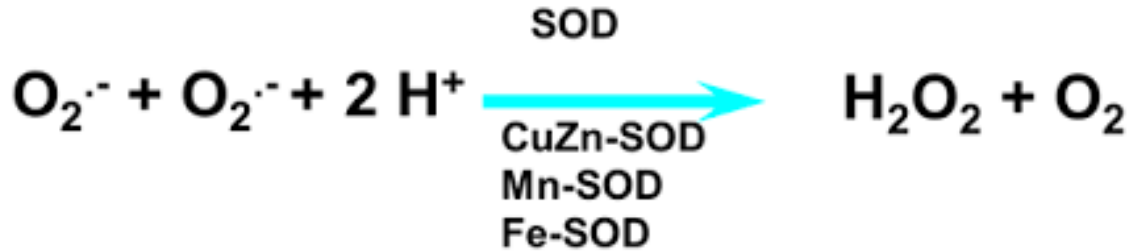


FIGURA 7. GENERACIÓN DE ESPECIES REACTIVAS DE OXÍGENO. El singlete de oxígeno (u oxígeno molecular) es capaz de generar el radical superóxido del cual se pueden formar 3 especies; el ion peróxido gracias a la ganancia de un electrón, el radical hidropéroxido si interviene un protón o gracias a la enzima superóxido dismutasa (SOD) generan peróxido de hidrógeno. Este último también puede formarse si al ion peróxido se agregan 2 protones y aunque no se considera al H_2O_2 como un radical libre este es capaz de formar el radical hidroxilo que se considera el más reactivo de las EROs.

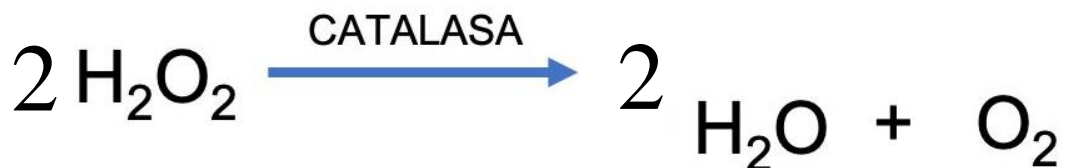
Las EROs son eliminadas por diversos sistemas que son:

- **Sistema enzimático**

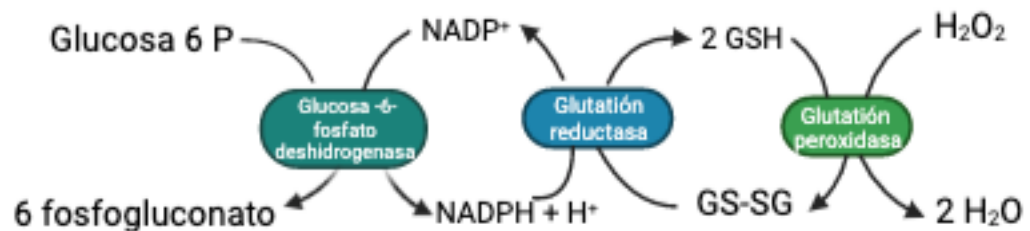
- Superóxido dismutasa (SOD). Es una metaloproteínasa que elimina el $O_2^{\cdot-}$ mediante una dismutación que toma dos moléculas de $O_2^{\cdot-}$ de las cuales una se oxida hasta oxígeno molecular y la otra la reduce a H_2O_2 .



- Catalasa. Es una hemoproteína tetramérica que reduce el H₂O₂ produciendo agua. Usa un átomo de hierro que realiza el intercambio redox.



- Glutatión peróxidasa. Su actividad está modulada por la relación GSH/GSSG; su eficacia reside en impedir la interacción de las EROs entre sí o con los metales de transición. Este complejo cataliza la reducción de H₂O₂ que junto con el grupo prostético de selenio-cisteína de la glutatión reductasa detoxifica esta molécula. Para que este mecanismo funcione a la perfección son necesarias dos enzimas más; la glucosa 6 fosfato deshidrogenasa que toma la glucosa 6 fosfato y el NADP⁺ para crear 6 fosfogluconato y NADPH + H⁺; este último es indispensable para que la glutatión reductasa regenere el GSH.



- **No enzimáticos.**

- Ácido ascórbico: reduce los niveles del daño oxidativo a lípidos y a proteínas, ya que reacciona con OH, H₂O₂ y O₂⁻
- α-tocoferol: es considerado el principal antioxidante de radicales lipofílicos ya que reduce el grupo hidroxilo de su anillo cromano impidiendo la peroxidación lipídica, modulando la fluidez de la membrana, así como cascada de producción de ácido araquidónico.
- Carotenoides: se obtienen de la dieta principalmente de vegetales y frutas reaccionan principalmente con el singulete de oxígeno, son útiles para proteger contra el daño causado por los rayos UV.
- Compuestos fenólicos: pueden inhibir enzimas como las oxidasas, lipooxigenasa, mieloperoxidasa y la NADPH oxidasa lo cual evita la generación de las EROs.

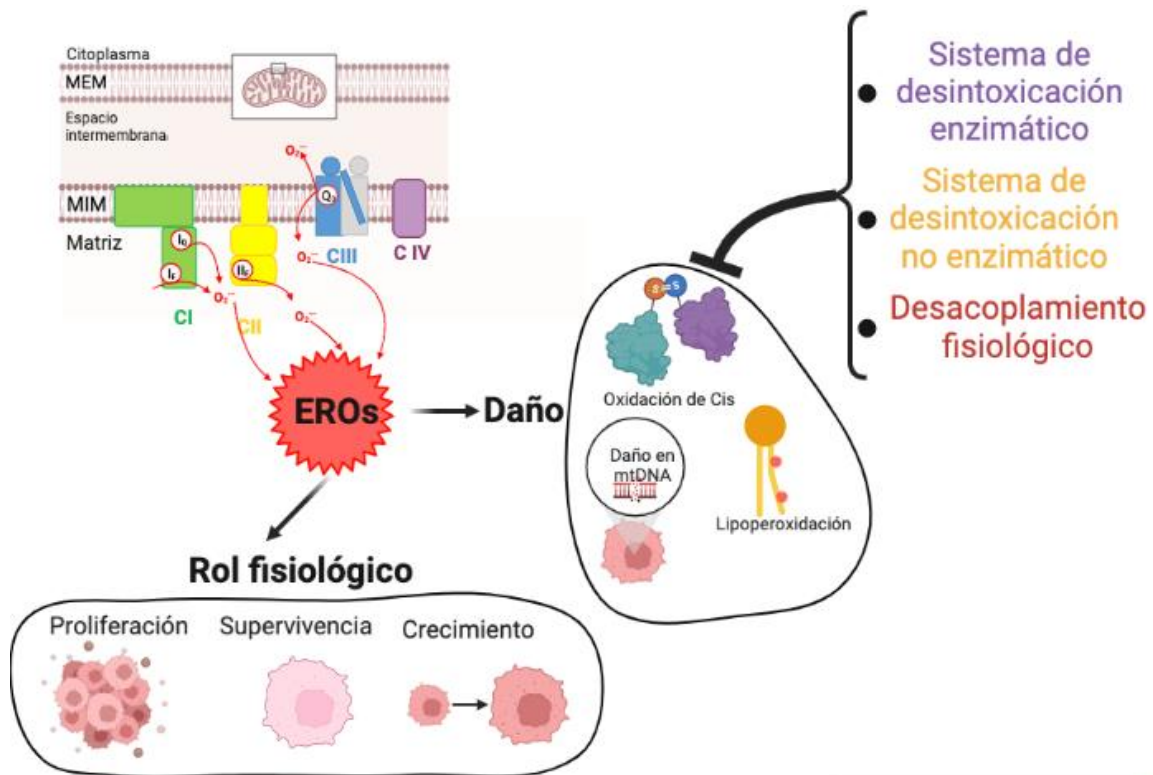


FIGURA 8. PRODUCCIÓN DE LAS EROs Y SUS DESTINOS. Las EROs se producen principalmente en la mitocondria en los complejos I, II y III; dependiendo de las concentraciones pueden ejercer un papel fisiológico en el cual se incluye a la señalización para la proliferación celular, supervivencia y diferenciación celulares. Cuando las concentraciones de EROs se incrementan dañan a las proteínas, lípidos (lipoperoxidación) y hasta el DNA mitocondrial. Para evitar estos efectos dañinos, la célula tiene diferentes mecanismos para evitar estos cambios como los sistemas enzimáticos y no enzimáticos, así como los sistemas de desacoplamiento fisiológico.

Puesto que los radicales libres producidos cuando los electrones fluyen por los grupos prostéticos y coenzimas de la cadena respiratoria como las fierro-azufre proteínas, la semiquinona y los grupos hemo; acelerar el flujo de electrones en la cadena respiratoria disminuye el tiempo que tienen los electrones desapareados para combinarse de manera inespecífica con el oxígeno. El flujo rápido de electrones los lleva hasta la(s) oxidasa(s) donde reducen al oxígeno catalíticamente. Los Sistemas Desacoplantes Fisiológicos de la mitocondria aceleran el paso de electrones en ausencia de síntesis de ATP.

El desacoplamiento fisiológico consiste en la aceleración controlada y reversible del flujo de electrones en la cadena respiratoria independientemente de la síntesis de ATP. Al conjunto de sistemas que evitan la sobreproducción de EROs por la mitocondria se les ha denominado sistemas desacoplantes fisiológicos (Uribe-Carvajal *et al.*, 2011). El mecanismo del desacoplamiento fisiológico consiste en disminuir el gradiente eléctrico de la membrana interna mitocondrial conocido como potencial de membrana ($\Delta\Psi$). Este $\Delta\Psi$ es el principal inhibidor de la cadena respiratoria (Rupprecht *et al.*, 2010; G.C. Brown & Brand 1991). Cuando baja, como en la síntesis de ATP, la CR se acelera. Cuando es alto, la CR se inhibe. Hay dos tipos de sistemas desacoplantes fisiológicos: los intrínsecos y los extrínsecos.

- **Mecanismos intrínsecos de desacoplamiento mitocondrial:** las enzimas redox alternas mitocondriales catalizan el flujo de electrones en la CR pero no son bombas de protones. En consecuencia, no contribuyen a la formación del $\Delta\Psi$ y además no son inhibidas por éste. Las NADH dehidrogenasas tipo 2 (ND2) de la membrana interna mitocondrial, que pueden encontrarse del lado de la matriz mitocondrial (ND2i) o del lado del espacio intermembranal (ND2e). Oxidan al NADH, pero no bombean protones. Las oxidasas alternas (Aox) que en los eucariontes son de un solo tipo, mientras que en

procariontes son muy diversas, también son periféricas de la membrana interna mitocondrial y reciben los electrones del ubiquinol sin bombear protones y reducen al oxígeno (Skulachev 1998; G.C. Brown & Brand 1991). Hay un mecanismo de desacoplamiento fisiológico intrínseco conocido como “slipping”, donde se disocia la actividad redox de la capacidad para bombear protones de un complejo respiratorio. Este fenómeno ha sido descrito en el complejo IV y en el complejo V o F₁F₀ ATP sintasa, donde se dejan pasar los protones por las subunidades “c” sin que haya síntesis de ATP. El slipping de la citocromo c oxidasa provoca una disminución de la estequiometría H⁺/e de 1.0 a 0.5, esto para estimular la termogénesis de manera específica de tejido como en los cardiomiocitos y en el músculo esquelético (Kadenbach 2003).

- **Mecanismos extrínsecos de desacoplamiento mitocondrial.** Específicos para protones como las proteínas desacoplantes o inespecíficos como los poros de transición de la permeabilidad.
 - **Las UCPs.** Son proteínas transmembranales ubicadas en la membrana interna mitocondrial disipan el gradiente de H⁺ y se han descrito en diferentes organismos. La UCP1 se encuentra en el tejido adiposo marrón (BAT, brown adipose tissue); y se especializa en termogénesis. La UCP2 se ha detectado en bazo, riñón, timo, páncreas y la UCP3 está en músculo esquelético (McBride *et al.*, 2019), BAT y en corazón. Se han detectado en levaduras como *C. albicans* o *Y. lipolitica* (Luévano-Martínez 2012), nematodos (*C. elegans*), crustáceos (*L. vannamei*) (Mendez-Romero *et al.*, 2020; 2019) e insectos (*D. melanogaster*), en donde las UCP son tejido específicas y se expresan dependiendo de la etapa de desarrollo de cada organismo (Uribe-Carvajal *et al.*, 2011).
 - **EL PTP:** Es un canal inespecífico ubicado en la mitocondria que al abrirse permite el paso de moléculas hasta 1.5 kDa y desacopla la

OxPhos. Se ha observado que en levaduras como *Saccharomyces cerevisiae* hay un canal similar al PTP que tiene algunas características diferentes y por ello se ha denominado Canal Mitocondrial Inespecífico de *S. cerevisiae* (*sc*MUC); también se ha descrito uno en *Debaryomyces hansenii* (*Dh*MUC), el cual se describe a continuación. Por su importancia para esta tesis se analiza a fondo el PTP en el siguiente inciso.

3. ANTECEDENTES

El poro de transición de la permeabilidad; estructura y función

La transición de la permeabilidad mitocondrial implica el incremento en la permeabilidad de la membrana interna mitocondrial a moléculas de hasta 1.5 kDa a través del PTP el cual es sensible al estrés, a la disminución de adenín-nucleótidos, a bajas concentraciones de fosfato o a la despolarización de la membrana. La apertura del PTP provoca el hinchamiento de la mitocondria, el colapso del potencial transmembranal y el desacoplamiento de la fosforilación oxidativa (Papa, Lorusso, & di Paola 2006; Mitchell 1961; Boyer *et al.*,1977) .

El translocador de adenin-nucleótidos tiene la función de intercambiar ATP/ADP a través de la MIM. Se propuso como componente el PTP ya que su inhibición por el atractilósido o el ácido bongkrelico, regula la transición de la permeabilidad (Allouche *et al.* 2012; Schiffer *et al.* 2022), sin embargo la eliminación genética de las isofomas del translocador (ANT1 y ANT2) aún se lleva a cabo la apertura del PTP con concentraciones altas de Ca^{2+} (como efector de apertura), por lo que el ANT podría contribuir a la regulación pero no se considera un componente esencial de PTP (Karch *et al.*, 2019).

Los VDACs se encuentran en la MEM y funcionan como paso de entrada y salida de los metabolitos mitocondriales, como sustratos respiratorios, iones o nucleótidos de adenina. El VDAC (en especial VDAC1 y VDAC2) es importante ya que, al progresar la transición de la permeabilidad, los componentes citosólicos ingresan a la matriz mitocondrial hasta romper la MEM (Juhaszova *et al.*, 2008; Gutiérrez-Aguilar *et al.*,2007).

La sensibilidad del PTP a mersalil; inhibidor del acarreador de fosfato (PiC), corroboró que esta proteína está involucrada en la conformación del PTP(Gutiérrez-

Aguilar *et al.*, 2010a; 2010d). Otra evidencia de que el PiC es importante en la estructura fue que al eliminar genéticamente este acarreador las mitocondrias requerían una concentración alta de fosfato en comparación con las cepas silvestres para obtener un potencial transmembranal estable y evitar el hinchamiento mitocondrial (Gutiérrez-Aguilar *et al.*, 2010b; Kovačs-Bogdán *et al.*, 2014).

Otra proteína que se describió como posible componente de PTP es SPG7, una proteasa AAA mitocondrial que junto con AFG3L2 es responsable de ensamblar ribosomas y eliminar proteínas no funcionales en las mitocondrias. Se observó su interacción con VDAC lo que demostró una protección contra la sobrecarga de calcio extramitocondrial; así como la interacción con la ciclofilina D, ya que participa en el mecanismo sensible a calcio y a la concentración de EROs (Shanmughapriya *et al.*, 2015).

En estudios de electrofisiología en membranas mitocondriales se ha descrito que el PTP funciona como un canal con transiciones de apertura y cierre de tamaño, cuyos sub-estados muestran variaciones de conductancias. El PTP tiene una conductancia alta si está abierto; pero también se han descrito aperturas moderadas y transitorias (Hurst *et al.*, 2017)

En diferentes órganos como el corazón, el cerebro y el hígado, el PTP participa en procesos de respuesta al estrés, aunque se le ha relacionado con daños celulares en procesos como la isquemia reperusión grave (Griffiths & Halestrap 1993; Solhjoo & O'Rourke 2015).

Otra controversia es la función que el PTP ha tenido a lo largo de la evolución, ya que algunos organismos no presentan la transición de la permeabilidad (algunas levaduras, algas y crustáceos (Gutiérrez-Aguilar 2020; Menze *et al.*, 2005)). También se ha observado que la duración de la apertura de este poro es diferente dependiendo de las condiciones experimentales. Un ejemplo es el daño por isquemia reperusión en miocardiocitos en el cual en un inicio se propuso que la depleción de nutrientes y de oxígeno impide la recuperación de la célula cardíaca

después de un periodo crítico, iniciando la apoptosis en cuanto se establece la reperusión. Esto es muy interesante porque varios grupos de investigación han demostrado que si se realiza un pre acondicionamiento en donde la reperusión sea intermitente; dando tiempo a la célula de recuperar su carga energética y la viabilidad del órgano aumenta (Ramírez-Camacho *et al.*, 2018).

En nuestro grupo tenemos la hipótesis de que el MUC tiene diferentes funciones en cada organismo o tejido, incluyendo diferente protección de la célula al estrés o la tendencia a disparar un programa de muerte.

El $_{sc}$ MUC (canal inespecífico mitocondrial de *S. cerevisiae*) se ha podido estudiar gracias a que esta levadura es de fácil manipulación y es aerobia facultativa; lo cual ha permitido que se pueda usar como modelo para la comprensión de aspectos tanto estructurales como de funcionamiento de esta estructura en levaduras y en otras especies, en especial en mamíferos (PTP).

Entre las diferencias PTP/ $_{sc}$ MUC se encuentran:

1. Tamaño: Aunque en ambos casos son canales iónicos que permiten el transporte no selectivo de moléculas, el $_{sc}$ MUC deja pasar moléculas de hasta 1.1 kDa mientras que el PTP se ha reportado hasta un diámetro de 1.5 kDa.
2. Efectores:
 - a. ATP, ADP y Pi: en donde $_{sc}$ MUC induce su apertura
 - b. Calcio: es capaz de inducir la transición de la permeabilidad en mamíferos, pero en $_{sc}$ MUC (Haworth & Hunter 2000; Halestrap 2004; Pereira *et al.*, 2007; Traba, Satrústegui & Arco 2009) lo cierra (Connern & Halestrap 1994; Giorgio *et al.*, 2018) .
 - c. Ciclosporina A: inhibe a la ciclofilina D en el PTP, mientras que en el $_{sc}$ MUC no se observan efectos (Jung, Bradshaw & Pfeiffer 1997) .

4.PLANTEAMIENTO DEL PROBLEMA

El canal inespecífico mitocondrial de la levadura (MUC) varía en sus propiedades de reversibilidad/irreversibilidad, por lo que es posible que haya casos en los que tenga la función de evitar la precipitación de la muerte celular.

5.HIPÓTESIS

- *Si la apertura del $scMUC$ es reversible a largo plazo, sus efectores antagónicos generarán alternativamente la apertura y cierre del canal aún después de varios minutos.*

6.OBJETIVOS

OBJETIVO GENERAL

Determinar el efecto de la relación ATP/ADP + Pi y de la presencia y ausencia de calcio sobre la apertura y cierre del MUC de *S. cerevisiae* (s_c MUC).

OBJETIVOS PARTICULARES

- Evaluar el potencial transmembranal ($\Delta\Psi$) en presencia de ATP (efector de apertura del s_c MUC) y del ADP (efector de cierre de s_c MUC).
- Analizar el hinchamiento mitocondrial en presencia de ATP (efector de apertura del s_c MUC) y del ADP (efector de cierre de s_c MUC).
- Medir el consumo de oxígeno en la mitocondria aislada al agregar ATP y ADP.
- Caracterizar el efecto del calcio sobre la apertura y cierre del s_c MUC
- Describir el patrón de reversibilidad del s_c MUC bajo diferentes condiciones.

7. MÉTODOS

Cultivo de levadura.

La cepa de *S. cerevisiae* “La Azteca” se estió en medio sólido YPD (extracto de levadura 1%, peptona de gelatina 2%, glucosa 2% y agar 2%) durante 48 hrs a 30°C. Posteriormente se guardaron a 4°C para su uso posterior. Los precultivos se realizaron tomando una colonia de la cepa que se inoculó en 100 mL de YPD (extracto de levadura 1%, peptona de gelatina 2% y glucosa 2%) se incubaron a 30°C por 24 horas con agitación continua. Dicho precultivo se decantó en 900 mL de medio YPGal (extracto de levadura 1%, peptona de gelatina 2% y galactosa 2%) y se cultiva a 30°C en agitación constante por 48 h.

Aislamiento de las mitocondrias.

Se cosecharon los 2 litros de cultivo de 48 h centrifugando a 4380xg por 5 minutos a 4 °C. Se descartó el sobrenadante y se resuspendió el botón de levaduras con 100 mL de agua destilada. Se reunió la suspensión y se centrifugaron a 3500xg por 5 minutos. Se descartó el sobrenadante y se resuspendió el botón en 50 mL de amortiguador de extracción (Manitol 0.6 M, MES 5 mM, pH 6.8 ajustado con trietanolamina) con albúmina al 1%. Se usó un homogenizador (Bead-Beater Biospec Products, USA) con perlas de vidrio de 0.45 mm para romper las células. Se colocó una camisa de hielo para mantener fría la suspensión durante dicha ruptura. Se aplicó tres pulsos de 20 s, dejándola reposar durante 40 minutos entre cada pulso (Uribe *et al.*, 1985). El homogenizado se coloca en tubos de 50 mL (previamente fríos). Se procedió a centrifugar diferencialmente para aislar las mitocondrias a 6°C en rotor Bechman Coulter JA-25.50:

- Se centrifugó el homogenado a 2333xg por 5 minutos.
- El sobrenadante se recuperó y se centrifugó a 7400xg por 10 minutos.
- Se descartó el sobrenadante y se eliminó con una toalla de papel los residuos de grasa adheridos a la pared del tubo.
- El botón se resuspendió con un pincel fino de cerdas naturales y con aproximadamente 100 μ L de amortiguador de extracción.
- Una vez resuspendidos todos los botones se concentraron en uno solo y se llevó a un volumen final de 30 mL (aprox.) con el amortiguador de extracción
- Se centrifugó a 4280xg por 5 minutos.
- Se recuperó el sobrenadante y se centrifugó a 9340xg por 15 min.
- Se descartó el sobrenadante y se resuspendió el botón con pincel en 200 μ L de amortiguador de extracción.
- Se conservó la suspensión de mitocondrias en hielo.

Cuantificación de proteína

Se determinó la concentración de proteína con el método de biuret. A 2 mL del reactivo de biuret se agregó 125 μ L de desoxicolato de sodio al 1%, 350 μ L de agua destilada y 25 μ L de la suspensión de mitocondrias; se dejó incubando la reacción por 15 min a temperatura ambiente. Se determina la absorbancia a 540 nm en un espectrofotómetro Beckman DU-50. (Gornall, Bardawill & David 1949). La interacción del ion Cu^{2+} del reactivo de Biuret con los enlaces peptídicos generan una coloración violeta proporcional a la concentración de proteína de la muestra(Gornall, Bardawill & David 1949)

Microscopía electrónica de transmisión

Se tomaron 500 μ L de mitocondrias aisladas y se fijaron con KMnO_4 al 2% a 4°C durante 12 hr. Durante 15 minutos se lavó con agua estéril desionizada en 6

ocasiones, después de deshidrató con etanol al 50%, 70%, 80% y 90%. Se lavó la muestra con etanol-acetona (1:1) durante 8 minutos, después con acetona anhidra por 5 minutos, se dejó toda la noche con acetona -EPON 821 (1:3) y al día siguiente se resuspendió en acetona -EPON 821 (1:1) por 1 h.

La muestra se incluyó en resina por 24 h, posteriormente se incubó a 37°C por 12 horas seguido; 36 horas a 60°C. Las muestras se cortaron a 70 nm con micrótomo (Ultracut Reicheit-jung) y se observaron en un microscopio electrónico de transmisión (JEOL JEM-1200 EXII).

Hinchamiento mitocondrial

Se determinaron las variaciones del volumen mitocondrial por los cambios en la absorbancia de la muestra usando el espectrofotómetro AMINCO DW2000 en modo Split a 540 nm. La mezcla de reacción fue manitol 0.6 M, MES 5 mM, pH 6.8 (ajustado con TEA); etanol 4 $\mu\text{L}/\text{mL}$, diferentes concentraciones de fosfato (2 mM y 1 mM). Las mitocondrias se agregan a una concentración final de 0.5 mg/mL y fueron incubaron con oligomicina 4 $\mu\text{g}/\text{mg}$ de proteína en un volumen final de 2 mL. A los 30 segundos se agregó 0.1 M de KCl, se registró por 3 minutos el cambio de absorbancia.

Potencial transmembranal ($\Delta\Psi$)

Se usó naranja de safranina, colorante catiónico que es atraído hacia la matriz mitocondrial negativa; cuando se pierde el $\Delta\Psi$ el colorante sale de la mitocondria. Los cambios se determinaron espectrofotométricamente a longitudes de 511 y 533 nm en un espectrofotómetro de doble haz (SLM AMINCO DW2000) en modo dual (Akerman & Wikstrom 1976). La reacción se realizó en un celda de vidrio a un volumen final de 3 mL a temperatura ambiente y en agitación constante en la

siguiente mezcla de reacción: manitol 0.6 M, MES 5 mM , pH 6.8 (ajustado con TEA); etanol 4 μ L/mL, diferentes concentraciones de fosfato (2 mM y 1 mM), 0.1 M de KCl y safranina 10 μ M. Veinte segundos después de iniciado el trazo se detuvo por 5 segundos para agregar las mitocondrias a una concentración final de 0.5 mg/mL, incubadas con oligomicina 4 μ g/mg de proteína y reinició el registro . Al final de todas las adiciones de los nucleótidos se agregó 2 μ M de CCCP para colapsar el potencial transmembranal(Åkerman & Wikström 1976).

Oximetría

Se usó un oxímetro Warner Strathkelvin Instruments, con un electrodo tipo Clark inmerso en una cámara de 1 mL con agitación constante a 30°C. La mezcla de reacción fue: manitol 0.6 M, MES 5 mM, pH6.8 (ajustado con TEA); etanol 4 μ L/mL (como sustrato oxidable), fosfato 2 mM, KCl 0.1 M y 0.5 mM de MgCl₂. Se obtuvo la basal con el medio de respiración y se agregó 0.5 mg/mL de la suspensión de mitocondrias incubadas con 4 μ g de oligomicina por cada mg de proteína y se fue añadiendo ATP (0.5,1 y 2 mM) y ADP (0.5,1 y 2 mM).

Determinación de Especies Reactivas de Oxígeno.

Se usó el método por fluorescencia de resorufina (Zhou 2017) con el Kit de Amplex Red (Invitrogen, Molecular Probes). La reacción se realizó en una placa de 96 pozos y la longitud de excitación fue de 571 nm y emisión de 585 nm en un lector de placas multimodal POLARstar Omega (BMG LABTECH, Ortenberg, Alemania).

Se incubaron 0.3 mg de proteína/mL (mitocondrias frescas) en 0.6 M Manitol, 5 mM MES (pH 6.8, TEA), 0.1 M KCl, 0.5 mM MgCl₂, 4 μ L/mL de etanol y oligomicina. En experimentos independientes se le agrega a la mezcla el fosfato 0.1 mM (con o sin ADP) o 2 mM de fosfato (con o sin ATP) y se deja incubando por 5 minutos.

En la placa se agregaron 20 μ L de la reacción anterior, 10 mM de Amplex red, 0.2 unidades de peróxidos de peroxidasa de rábano/mL, 0.2 unidades superóxido dismutasa/mL y 50 mM fosfato de sodio. La medición se realizó por 1.5 horas tomando el máximo a la hora de exposición. Los resultados se normalizaron con sus controles respectivos sin el efector (Pons *et al.*, 2015).

8.RESULTADOS

Efectos del fosfato sobre el s_c MUC.

El s_c MUC tiene varios efectores y uno de ellos es el fosfato (Pi) (Gutiérrez-Aguilar *et al.* 2010c), bajo las condiciones utilizadas en este estudio se observó que en ausencia de Pi o a muy bajas concentraciones (0.1 mM), no había crestas mitocondriales (Figura 9A) mientras que en presencia de 2 mM fosfato, sí se observaron crestas mitocondriales con una forma similar a la reportada en la literatura (Figura 9B).

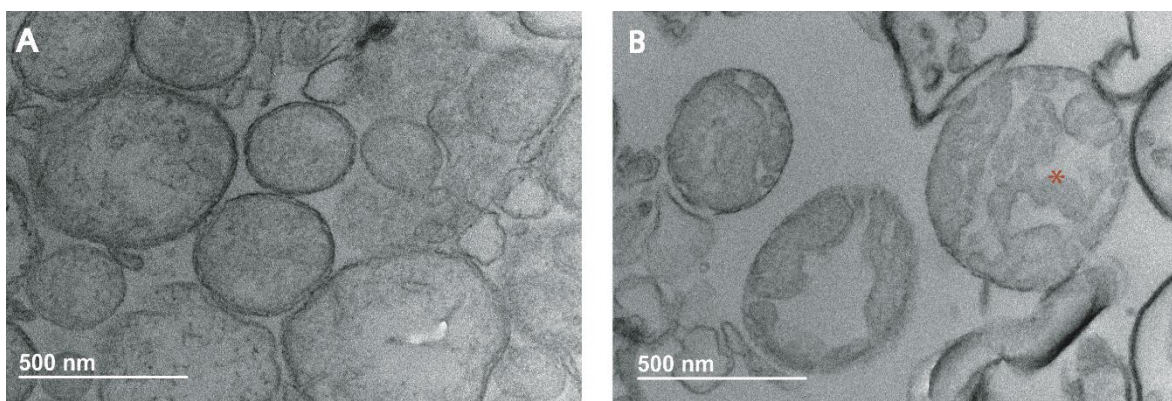


FIGURA 9 ARQUITECTURA DE LAS CRESTAS MITOCONDRIALES EN PRESENCIA DE 0.1 mM Pi (A) Y 2 mM PI(B) donde se observan mitocondrias hinchadas y no se detecta arquitectura de crestas; B Pi 2 mM. Fotografías de microscopio electrónico de transmisión. Se observan crestas (*) mitocondriales dentro de la membrana externa. Las fotografías se analizaron con software Gatan Digital Micrograph.

A altas concentraciones de Pi, cierra el poro evitando el hinchamiento de la mitocondria e incrementando el control respiratorio (Figura 10 y Tabla 3). Se puede observar en los primeros 30 s del trazo de oximetría (Figura 14A y B) la velocidad de consumo de oxígeno aumentó al disminuir el Pi.

Efectos del ATP y del ADP sobre la mitocondria aislada de *S. cerevisiae*.

Se evaluaron los efectos del ATP y del ADP sobre el hinchamiento mitocondrial manteniendo fija la concentración de fosfato y titulando la concentración de ATP y ADP (Figura 10 y 11). Se ha reportado previamente que el ATP es un efector de apertura mientras que el ADP promueve el cierre del s_c MUC. A altas concentraciones de Pi (2 mM) la mitocondria estaba condensada, mientras que al adicionar concentraciones diferentes de ATP se observó cada vez un mayor hinchamiento (Figura 10). En estas condiciones el ATP funciona como antagonista del Pi y ADP.

En 0.1 mM de Pi, la mitocondria estaba hinchada, lo que sugiere que el s_c MUC se encontraba abierto; aquí la adición de concentraciones de ADP promueve la reconstracción sugiriendo que el s_c MUC se cerró (Figura 11).

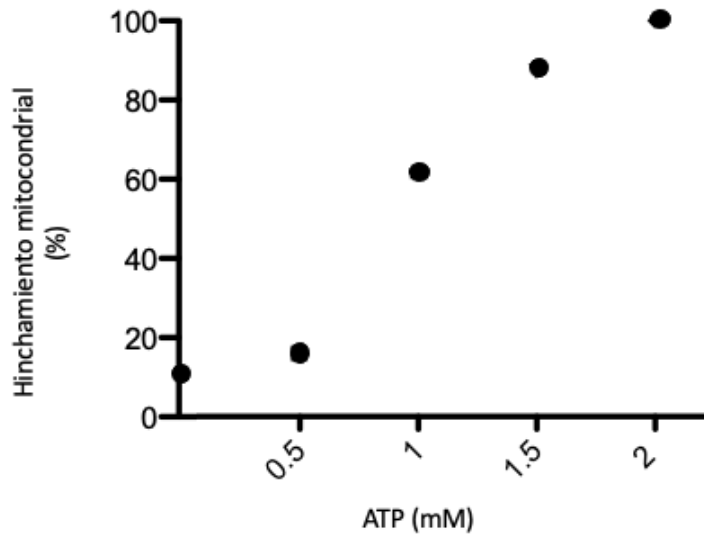


FIGURA 10. HINCHAMIENTO MITOCONDRIAL 2 mM Pi TITULANDO ATP. Porcentaje de hinchamiento mitocondrial partiendo de condiciones en que el scMUC está cerrado (Pi 2 mM) y adicionando diferentes concentraciones de ATP.

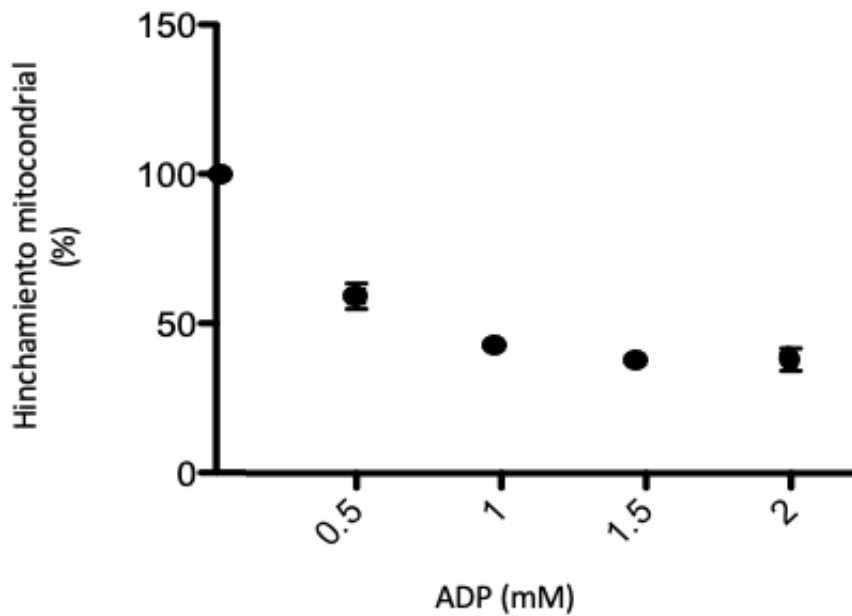


FIGURA 11. HINCHAMIENTO MITOCONDRIAL EN 0.1 mM Pi TITULANDO CON DIFERENTES CONCENTRACIONES DE ADP. El porcentaje de hinchamiento mitocondrial al tener una condición de poro abierto (Pi 0.1 mM) y adicionando concentraciones crecientes de ADP. Se tomó como 100 % al hinchamiento obtenido a la condición sin ADP ya que el PTP está abierto por la baja concentración de fosfato. Se observa como cuando se va incrementando la concentración de un segundo efector (antagónico, ADP) el porcentaje de hinchamiento disminuye.

El hinchamiento mitocondrial se produce por la apertura del s_c MUC y el efecto osmótico que induce el potasio (0.1 M) al ingresar por este canal aumenta la diferencia de la densidad óptica (Δ O.D.).

El ADP inhibió el hinchamiento (Figura 12A, trazo b) consecuencia del cierre del s_c MUC. Una vez cerrado el canal se indujo la reapertura con ATP (Figura 12A, trazo e) observando que al aumentar su concentración aumentó la Δ O.D. por lo que se concluyó que el s_c MUC presentó una apertura reversible.

Iniciando con el s_c MUC cerrado (2 mM Pi en Figura 12B, trazo a) no se observó el hinchamiento de la mitocondria. La adición de ATP (1 mM, Figura 12B, trazos b al e) indujo el hinchamiento. En otros reportes se refiere que es imposible cerrar el s_c MUC; no obstante, al añadir ADP al MUC abierto con ATP, (figura 12B, trazo e) el hinchamiento se frenó, indicando que si fue posible cerrar de nuevo el s_c MUC.

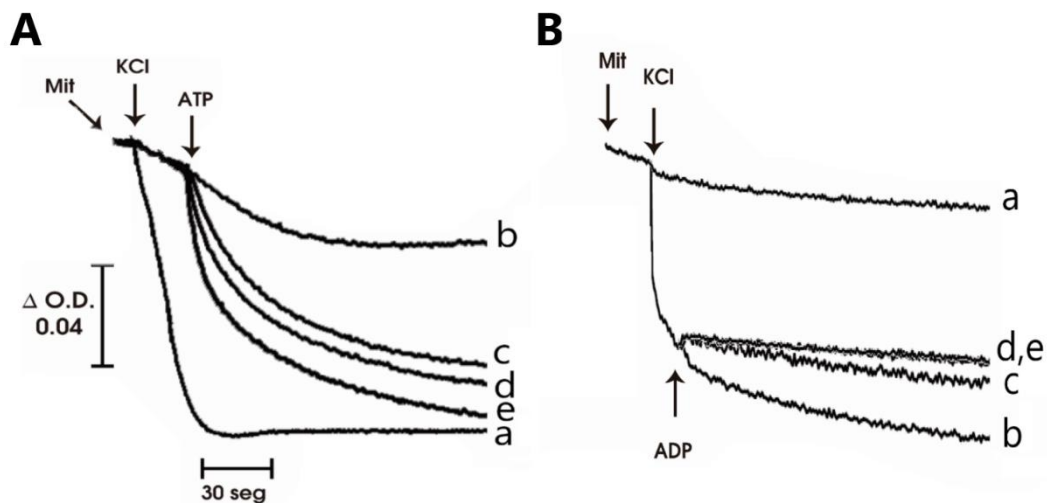


FIGURA 12. EFECTO ANTAGÓNICO DEL ATP Y ADP EN EL HINCHAMIENTO

MITOCONDRIAL. A) El MUC se abre con 0.1 mM Pi (trazo a) la adición de 0.1 M de KCl induce el hinchamiento mitocondrial. La adición de 1 mM ADP cierra el MUC (trazo b). La adición de ATP (1 mM, trazo c; 1.5 mM, trazo d; 2 mM; trazo e) abre el MUC. El MUC se cierra con 2 mM Pi (trazo a). La adición de ATP (1 mM, trazos b-e) lo abre y el potasio induce el hinchamiento mitocondrial. La adición de ADP (1 mM, trazo c; 1.5 mM, trazo d; 2 mM, trazo e) revierte el hinchamiento).

La reversibilidad de la pérdida del potencial transmembranal observada al abrirse el s_c MUC también se analizó para ver si es reversible si este mecanismo no fuese reversible la pérdida de $\Delta\Psi$ sería progresiva hasta que la safranina (colorante catiónico) no tuviera interacción con la carga negativa de la membrana interna mitocondrial. En la figura 13A en el trazo a, se observan que el potencial se mantuvo estable con 2 mM de Pi hasta que se disipó con el desacoplante CCCP. Al agregar ATP el potencial disminuyó (Figura 13A, trazo b) sin embargo al añadir ADP, que cierra el s_c MUC, el $\Delta\Psi$ aumentó corroborando que la apertura puede ser reversible (Figura 13A, trazos c - e). El fenómeno anterior se constata al iniciar con el s_c MUC abierto (0.1 mM Pi) (Figura 11B) en donde una vez que ha perdido el $\Delta\Psi$ se añadió ADP (efector de cierre) incrementándolo y fue posible disminuir este potencial al agregar ATP (Figura 11B, trazos c - e).

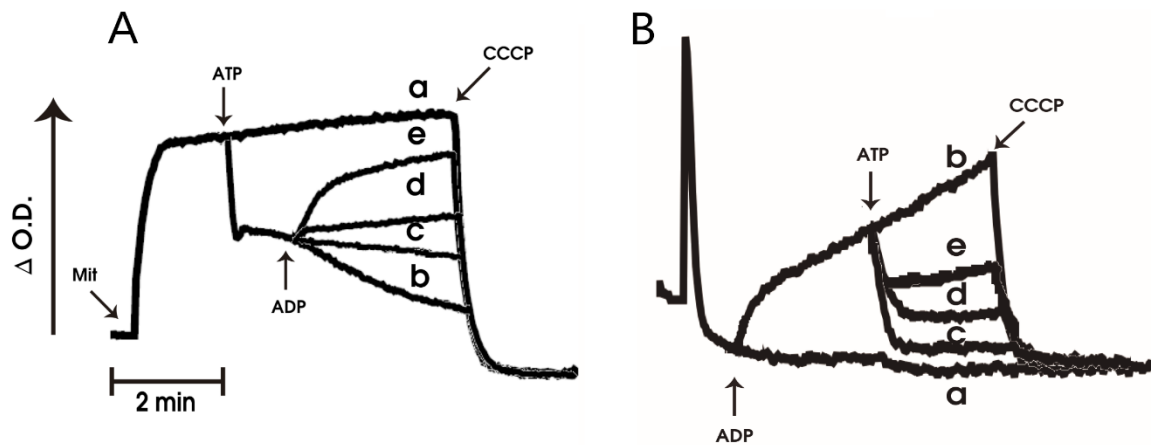


FIGURA 13. EFECTO DEL Pi SOBRE EL POTENCIAL TRANSMEMBRANAL. (A) El MUC se cierra con 2 mM Pi y se genera el $\Delta\Psi$ (trazo a); la adición de ATP (1 mM, trazos b - e) abre el MUC y se abate el $\Delta\Psi$. sin embargo, la adición de ADP (1 mM, trazo c; 1.5 mM, trazo d; 2 mM, trazo e) cierra el MUC y se restablece el $\Delta\Psi$. (B). El MUC está abierto en presencia de 0.1 mM Pi y se colapsa el potencial de membrana. la adición del ADP (1 mM, trazos b-e) cierran el MUC y el potencial se restablece. La adición de ATP (1 mM, trazo c; 1.5 mM, trazo d; 2 mM, trazo e) abre el MUC y abate el potencial transmembranal. La adición de CCCP abate totalmente el $\Delta\Psi$.

En la oximetría se observó con el s_c MUC cerrado un consumo de oxígeno de 59.35 natgO/mgprot*min el cual incrementó conforme se añadió ATP en diferentes concentraciones hasta llegar a 96.5 natgO/mgprot*min con 2 mM de ATP Al cerrar el s_c MUC con ADP el consumo de oxígeno disminuyó parcialmente, sin restablecerse el consumo inicial (solo con el Pi) pero con una velocidad 3 veces menor que al agregar ATP (Tabla 3 y Figura 14).

TABLA 3. CONSUMO DE OXÍGENO (natgO/mgprot*min) CON DIFERENTES CONCENTRACIONES DE ATP Y ADP

Primer efector		Segundo efector		Tercer efector	
Pi		ATP		ADP	
2mM	59.35 ± 4.54	0.5mM	83.44±11.4	0.5mM	44.35±9.26
				1mM	42.65±11.7
				2mM	38±0.41
		1mM	90.27±12.76	0.5mM	59.4±10.3
				1mM	50.72±7.7
				2mM	40±2.26
		2mM	96.5±0.71	2mM	33±2.5

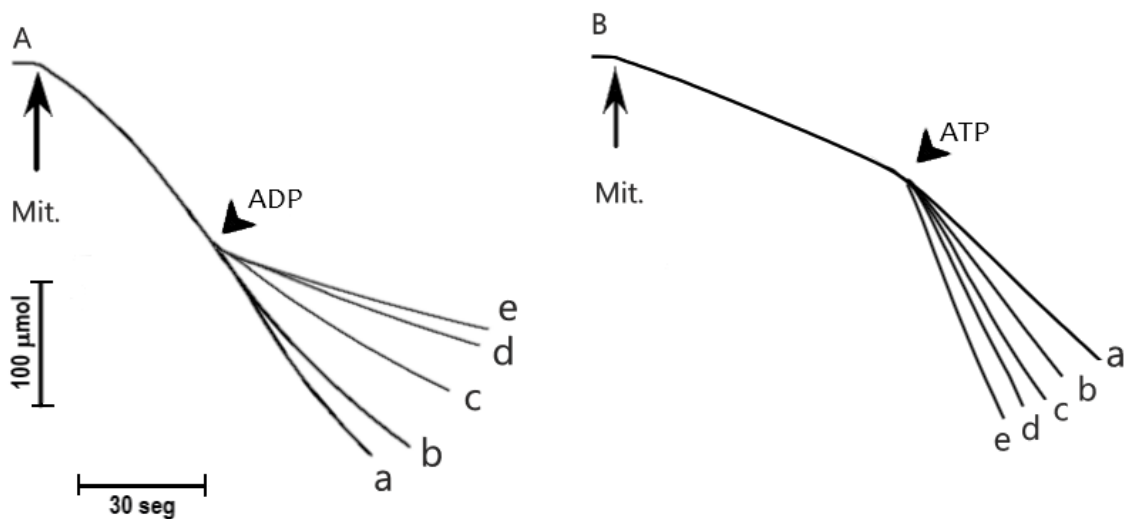


FIGURA 14. CONSUMO DE OXÍGENO. (A) Se inicia con 0.1 mM de Pi (trazo a). Adiciones ADP 0.5 mM (trazo b); ADP 1 mM (trazo c); ADP 1.5 mM (trazo d) y ADP 2 mM (trazo e). **(B)** Se inicia con Pi 2 mM de Pi (trazo a). Se adiciona ATP 0.5 mM (trazo b); ATP 1 mM (trazo c); ATP 1.5 mM (trazo d) y ATP 2 mM (trazo e). En donde se indica Mit. =mitocondrias.

Se ha propuesto que la velocidad del flujo de electrones por la CTE es inversamente proporcional a la producción de EROs (Dröse & Brandt 2008). Como se ha descrito, el s_c MUC al estar abierto incrementa la velocidad de consumo de oxígeno por lo que debería disminuir la producción de EROs. Para poder determinar la cantidad de especies reactivas de oxígeno se midió a producción de EROs y se comparó con la velocidad del flujo de electrones por la CTE.

La producción de H_2O_2 disminuyó conforme el s_c MUC se abrió con ATP (Figura 15A). En el caso de que el s_c MUC se cerró con ADP el porcentaje de producción de H_2O_2 incrementó con respecto al s_c MUC cerrado con 2 mM de Pi (Figura 15B), observando así que es un mecanismo que usa la mitocondria para evitar llegar a concentraciones de EROs que puedan desencadenar daño en la célula.

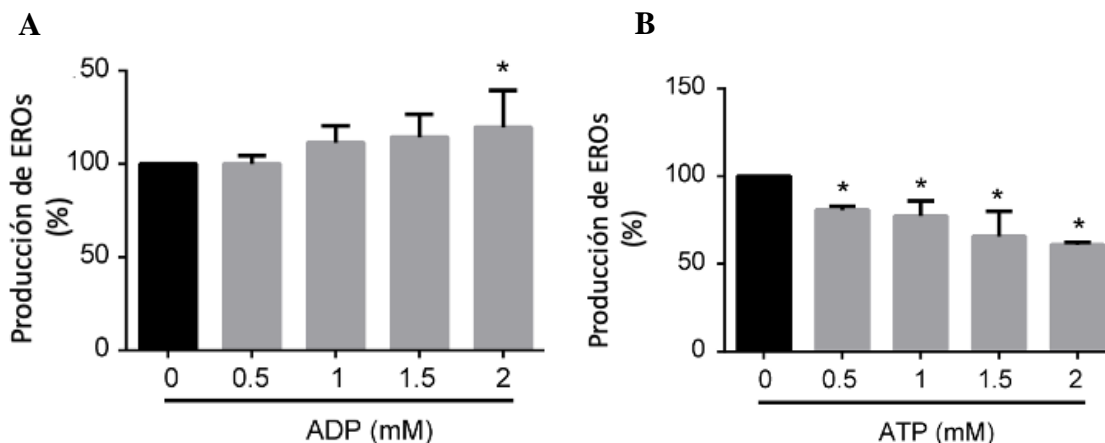


FIGURA 15. PRODUCCIÓN DE ESPECIES REACTIVAS DE OXÍGENO EN MITOCONDRIAS AISLADAS. Producción de EROs en mitocondrias aisladas de *S. cerevisiae*. El porcentaje de 100 % se toma del control en el cual solo se tiene un efector (fosfato) y se observa que en A) con 2 mM de Pi (en donde el PTP está cerrado) y se abre con ATP, el efector antagónico al Pi en donde ocurre la transición de la permeabilidad; el porcentaje de EROs disminuye. En el caso contrario en donde se inicia con baja concentración de Pi (B; 0.1 mM) al agregar ADP (el cual cierra el poro) aumenta la producción de EROs con respecto al control.

Hasta aquí se demostró que el $scMUC$ es una estructura mitocondrial que se puede abrir y cerrar alternando los efectores; sin embargo, no sabemos si esta función (reversibilidad) es permanente o hay un punto en el cual ya no sea capaz de cerrarse. Para esto se determinó el potencial de membrana en mitocondrias aisladas. En condiciones de poro abierto (Figura 16A, trazo b) la adición de ADP (efector de cierre de $scMUC$) a diferentes tiempos (30 seg., 1 min, 2 min y 4 min) permitió volver a cerrar el poro aún después de los 4 minutos de la apertura con ATP. Con respecto al hinchamiento mitocondrial se observó que el ADP frenó el hinchamiento aun después de 4 minutos de apertura del $scMUC$ (Figura 16B, trazo b).

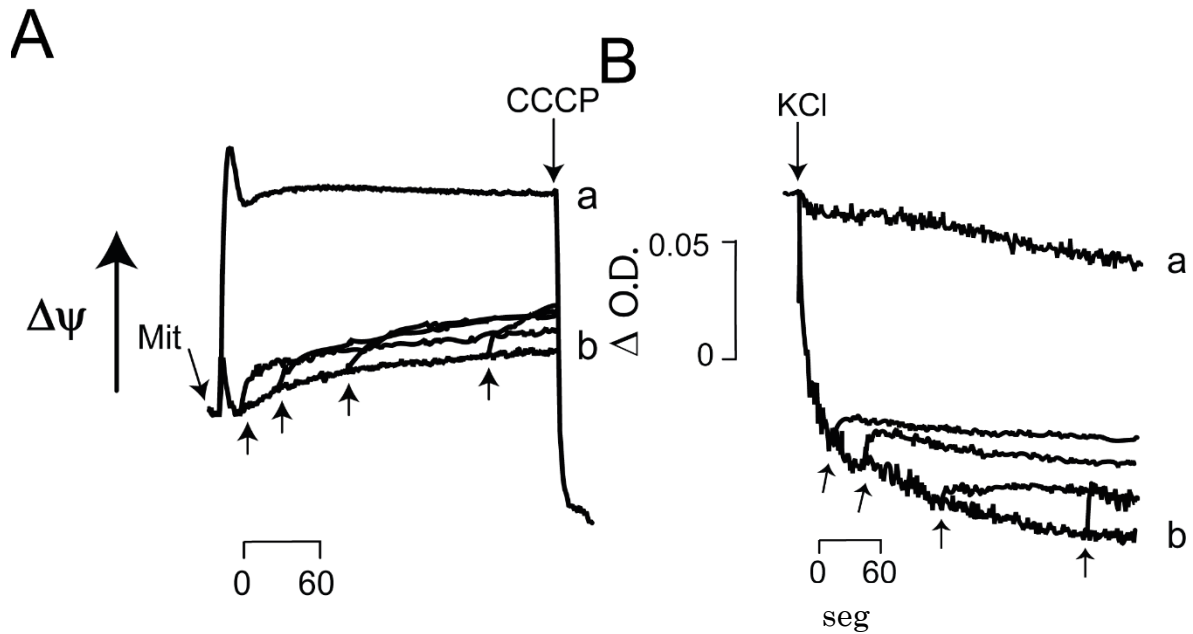


FIGURA 16. REVERSIBILIDAD PARCIAL ADICIONANDO ADP A DIFERENTES TIEMPO EN *S. cerevisiae*. A). $\Delta\Psi$ y B) hinchamiento mitocondrial; (a) 0 mM ATP. (b) 2 mM de ATP; las flechas indican la adición a diferentes tiempos de 1 mM de ADP (30 s, 1, 2 Y 4 min; respectivamente) en las gráficas se observa que es posible cerrar el PTP evitando el hinchamiento mitocondrial al adicionar un efector de cierre (B) y restablecer el potencial transmembranal.

9.DISCUSIÓN

Desde el descubrimiento del PTP se ha propuesto que su función es llevar a la muerte celular (Grimm & Brdiczka 2007); pero podría tener un papel diferente e incluso opuesto al disparo de la apoptosis. Se describió la muerte celular de origen mitocondrial, ya que ocurre a través de este poro, debido a que podría abatirse el potencial eléctrico transmembranal, llevar a la activación de las caspasas y liberarse el citocromo c; que llevaría a una cascada de eventos que llevasen a la apoptosis. Como la activación de las caspasas BAK y BAX que implica la formación de otro poro, el megacanal mitocondrial, ya que el diámetro del PTP que se ha descrito tanto por microscopía como por electrofisiología, no permite que una molécula como el citocromo c pueda atravesar la membrana externa mitocondrial (Priault *et al.*, 2003).

La transición de la permeabilidad que se inicia por la apertura del poro consiste en el movimiento de agua y solutos (menores a 1.1 kDa, en *S. cerevisiae*) a favor de su gradiente de concentración y esta apertura se refleja en el abatimiento del potencial transmembranal, así como en cambios en la estructura de las crestas mitocondriales asociados al hinchamiento mitocondrial (Uribe-Carvajal *et al.* 2011). Este fenómeno se ha descrito en diferentes organismos como parte de los sistemas de desacoplamiento que tienen una función fisiológica (Jarmuszkiewicz *et al.*, 2010; Mendez-Romero *et al.*, 2022).

La apertura/cierres alternados del PTP se propone como una posible estrategia terapéutica para evitar que la zona de isquemia en el tratamiento de reperfusión (que se realiza en oclusiones arteriales de miocardio) sea disminuida. Estas maniobras se describen como pre acondicionamiento (Correa *et al.*, 2008). Como un fundamento que valide al proceso de pre acondicionamiento es importante evaluar si la apertura y cierre del PTP son estados reversibles, que alternen entre sí y que sean modulados por agentes fisiológicos (ATP, ADP y fosfato).

Como se demuestra una vez que el PTP inicia la transición de la permeabilidad con ATP, se puede recuperar el $\Delta\Psi$ con un agente que cierre al PTP como el ADP. Esta reversibilidad puede modularse no sólo con el par ATP/ADP sino también se puede agregar como tercer efector el fosfato, el cual se había probado en otros trabajos en donde señalan que a altas concentraciones se comporta como efector de cierre del PTP.

Sometiendo a las mitocondrias aisladas de *S. cerevisiae* a la adición alternada de estos tres efectores se demostró que la apertura del PTP podría revertirse con un segundo efector que indujera el cierre de éste, recuperando su potencial transmembranal y consecuentemente una velocidad basal en el consumo de oxígeno de la CTE.

En cuanto al papel que el PTP tiene en la fisiología celular, se ha propuesto que es uno de los sistemas de desacoplamiento fisiológico que ayudan a lidiar con los cambios en la demanda y producción de energía.

Una señal que indica que el metabolismo celular (especialmente anabolismo) está muy activo, es cuando los niveles de ADP son mayores a los de ATP, la CTE debe incrementar la velocidad de consumo de oxígeno para poder bombear protones al espacio intermembranal y generar el gradiente electroquímico que pueda ser usado por la ATP sintasa, aumentando la producción de ATP.

Cuando la relación ATP/ADP es mayor a 1 y las pozas de ATP están repletas, la CTE disminuye su actividad provocando que la posibilidad de fugas de los electrones incremente y aumente la concentración de EROs.

Para evitar que los EROs dañen las membranas de la mitocondria e inicien la muerte celular es necesario que actúen sistemas alternativos de abatimiento del gradiente de protones, lo que previene una sobreproducción de EROs.

El PTP al abrirse en respuesta a un incremento en la concentración de ATP acelera el consumo de oxígeno ayudando a que la CTE elimine rápidamente los electrones que fluyen por ella y así se disminuya la formación de EROs.

El PTP tiene un papel de importancia en la regulación de la síntesis de EROs y es de vital importancia que sea capaz de alternar entre sus estados abierto y cerrado.

Lo anterior concuerda con la teoría de CoRR (Co-location for Redox Regulation) postulada por Allen (Allen 2017), en donde el estado redox, que es resultado de cambios en el entorno físico de la célula, repercute directamente en efectos compensatorios de la CTE ya que las proteínas que están codificadas en el ADN mitocondrial (mtDNA) son vitales para ensamblar los complejos de CTE y si existiera un daño en el mtDNA la función de éstos se vería reflejada en el estado redox de la mitocondria (Jeedigunta *et al.*, 2021).

El PTP y lo postulado en la hipótesis de CoRR, proporcionan a las mitocondrias mecanismos de respuesta ante la exposición al estrés e incremento de las EROs y así garantizar la supervivencia de la célula (Allen 2017). Si tomamos como una entidad a la célula se debe de tomar en cuenta que tanto el núcleo , el citosol y la mitocondria deben de trabajar en coordinación; si en algunos de estos niveles se detecta una alteración en la producción de EROs y su detoxificación, entra primero en juego el mecanismo de desacoplamiento fisiológico (PTP), sino es suficiente las enzimas antioxidantes tratan de regular esta sobreproducción, si aún continúa esta alteración (en la regulación redox) se coordinan con la síntesis de proteínas que ayuden a tratar de mantener la viabilidad celular o en caso extremo decidir iniciar la apoptosis celular (Allen & Raven 1996).

10.CONCLUSIONES

- El canal inespecífico mitocondrial (MUC) es reversible.
- El $_{sc}$ MUC es un sistema de desacoplamiento fisiológico capaz de abrirse y cerrarse para optimizar la generación de ATP o en caso de que la célula no requiera ATP prevenir la producción de EROs y el daño a lípidos, proteínas o DNA.
- El $_{sc}$ MUC no es un sistema de muerte celular programada, ya que es reversible y forma parte del sistema de protección mitocondrial.

11.PERSPECTIVAS.

- Hacer una comparación tejido-específica en mitocondrias de mamífero, tanto con los efectores como en la duración de la reversibilidad del PTP
- Dilucidar cual/es son los componentes proteicos esenciales del poro inespecífico mitocondrial
- Iniciar un estudio sobre la importancia de los lípidos de membrana interna mitocondrial sobre la posible función esencial de estos en la formación del poro inespecífico mitocondrial.

12.BIBLIOGRAFÍA

- Åkerman, Karl E.O., and Mårten K.F. Wikström. 1976. "Safranin as a Probe of the Mitochondrial Membrane Potential." *FEBS Letters* 68 (2): 191–97. [https://doi.org/10.1016/0014-5793\(76\)80434-6](https://doi.org/10.1016/0014-5793(76)80434-6).
- Allen, John F. 2017. "The CoRR Hypothesis for Genes in Organelles." *Journal of Theoretical Biology* 434 (December): 50–57. <https://doi.org/10.1016/J.JTBI.2017.04.008>.
- Allen, John F., and John A. Raven. 1996. "Free-Radical-Induced Mutation vs Redox Regulation: Costs and Benefits of Genes in Organelles." *Journal of Molecular Evolution* 42 (5): 482–92. <https://doi.org/10.1007/BF02352278>.
- Allouche, Maya, Claire Pertuiset, Jean Luc Robert, Cécile Martel, Rémi Veneziano, Céline Henry, Ossama Sharaf el Dein, Nathalie Saint, Catherine Brenner, and Joel Chopineau. 2012. "ANT-VDAC1 Interaction Is Direct and Depends on ANT Isoform Conformation in Vitro." *Biochemical and Biophysical Research Communications* 429 (1–2): 12–17. <https://doi.org/10.1016/J.BBRC.2012.10.108>.
- Andrulis, Erik D. 2011. "Theory of the Origin, Evolution, and Nature of Life." *Life (Basel, Switzerland)* 2 (1): 1–105. <https://doi.org/10.3390/life2010001>.
- Bezawork-Geleta, Ayenachew, Jakub Rohlena, Lanfeng Dong, Karel Pacak, and Jiri Neuzil. 2017. "Mitochondrial Complex II: At the Crossroads." <https://doi.org/10.1016/j.tibs.2017.01.003>.
- Blokhina, Olga, Eija Virolainen, and Kurt v. Fagerstedt. 2003. "Antioxidants, Oxidative Damage and Oxygen Deprivation Stress: A Review." *Annals of Botany* 91 (2): 179. <https://doi.org/10.1093/AOB/MCF118>.
- Boyer, Paul D., Britton Chance, Lars Ernster, Peter Mitchell, Efraim Racker, and E. C. Slater. 1977. "Oxidative Phosphorylation and Photophosphorylation." *Annual Review of Biochemistry* 46 (1): 955–66. <https://doi.org/10.1146/ANNUREV.BI.46.070177.004515>.
- Brandt, Ulrich, and Bernard Trumpower. 1994. "The Protonmotive Q Cycle in Mitochondria and Bacteria." *Critical Reviews in Biochemistry and Molecular Biology* 29 (3): 165–97. <https://doi.org/10.3109/10409239409086800>.
- Brown, G.C., and M.D. Brand. 1991. "On the Nature of the Mitochondrial Proton Leak." *Biochim. Biophys. Acta* 1059: 55–62.
- Brown, Guy C., and Vilmante Borutaite. 2008. "Regulation of Apoptosis by the Redox State of Cytochrome c." *Biochimica et Biophysica Acta – Bioenergetics* 1777 (7–8): 877–81. <https://doi.org/10.1016/J.BBABIO.2008.03.024>.
- Cabrera-Orefice, Alfredo, Etienne Galemou Yoga, Christophe Wirth, Karin Siegmund, Klaus Zwicker, Sergio Guerrero-Castillo, Volker Zickermann, Carola Hunte, and Ulrich Brandt. N.d. "Locking Loop Movement in the Ubiquinone Pocket of Complex I Disengages the Proton Pumps." <https://doi.org/10.1038/s41467-018-06955-y>.
- Cecchini, Gary. 2003. "Function and Structure of Complex II of the Respiratory Chain*." <https://doi.org/10.1146/Annurev.Biochem.72.121801.161700> 72 (November): 77–109. <https://doi.org/10.1146/ANNUREV.BIOCHEM.72.121801.161700>.
- Connern, C. P., and A. P. Halestrap. 1994. "Recruitment of Mitochondrial Cyclophilin to the Mitochondrial Inner Membrane under Conditions of Oxidative Stress That Enhance the

- Opening of a Calcium-Sensitive Non-Specific Channel.” *Biochemical Journal* 302 (2): 321–24. <https://doi.org/10.1042/bj3020321>.
- Correa, Francisco, Noemí García, Cinthya Robles, Eduardo Martínez-Abundis, and Cecilia Zazueta. 2008. “Relationship between Oxidative Stress and Mitochondrial Function in the Post-Conditioned Heart.” *Journal of Bioenergetics and Biomembranes* 40 (6): 599–606. <https://doi.org/10.1007/s10863-008-9186-2>.
- Crofts, Antony R., Sangjin Hong, Charles Wilson, Rodney Burton, Doreen Victoria, Chris Harrison, and Klaus Schulten. 2013. “The Mechanism of Ubihydroquinone Oxidation at the Qo-Site of the Cytochrome Bc1 Complex.” *Biochimica et Biophysica Acta* 1827 (11–12): 1362–77. <https://doi.org/10.1016/J.BBABIO.2013.01.009>.
- Cyert, Martha S., and Caroline C. Philpott. 2013. “Regulation of Cation Balance in *Saccharomyces Cerevisiae*.” *Genetics* 193 (3): 677–713. <https://doi.org/10.1534/GENETICS.112.147207>.
- Deng, Hao Hua, Gang Wei Wu, Dong He, Hua Ping Peng, Ai Lin Liu, Xing Hua Xia, and Wei Chen. 2015. “Fenton Reaction-Mediated Fluorescence Quenching of N-Acetyl-L-Cysteine-Protected Gold Nanoclusters: Analytical Applications of Hydrogen Peroxide, Glucose, and Catalase Detection.” *The Analyst* 140 (22): 7650–56. <https://doi.org/10.1039/C5AN01284H>.
- Devenish, Rodney J., Mark Prescott, and Andrew J.W. Rodgers. 2008. “The Structure and Function of Mitochondrial F1F0-ATP Synthases.” *International Review of Cell and Molecular Biology* 267: 1–58. [https://doi.org/10.1016/S1937-6448\(08\)00601-1](https://doi.org/10.1016/S1937-6448(08)00601-1).
- Dodson, E. O. 1979. “Crossing the Prokaryote–Eucaryote Border: Endosymbiosis or Continuous Development?” *Canadian Journal of Microbiology* 25 (6): 651–74. <https://doi.org/10.1139/M79-096>.
- Dröse, Stefan, and Ulrich Brandt. 2008. “The Mechanism of Mitochondrial Superoxide Production by the Cytochrome Bc1 Complex.” *Journal of Biological Chemistry* 283 (31): 21649–54. <https://doi.org/10.1074/jbc.M803236200>.
- Falabella, Micol, Hilary J. Vernon, Michael G. Hanna, Steven M. Claypool, and Robert D.S. Pitceathly. 2021. “Cardiolipin, Mitochondria, and Neurological Disease.” *Trends in Endocrinology and Metabolism* 32 (4): 224. <https://doi.org/10.1016/J.TEM.2021.01.006>.
- Fan, Guihong, Rosalind Huff, Jennifer Muir, Zinayida Nektalova, Jane Kruchowsky, Jennifer L. Kepler, Haiyan Wang, Pamela A. Marshall, and Francisco J. Solis. 2018. “Bifurcations and Limit Cycles in Cytosolic Yeast Calcium.” *Mathematical Biosciences* 298 (April): 58–70. <https://doi.org/10.1016/J.MBS.2017.11.001>.
- Ferreira, Gloria C., Ricardo Franco, Steven G. Lloyd, Isabel Moura, José J.G. Moura, and Boi H. Huynh. 1995. “Structure and Function of Ferrochelatase.” *Journal of Bioenergetics and Biomembranes* 1995 27:2 27 (2): 221–29. <https://doi.org/10.1007/BF02110037>.
- Förstermann, Ulrich, and William C. Sessa. 2012. “Nitric Oxide Synthases: Regulation and Function.” *European Heart Journal* 33 (7). <https://doi.org/10.1093/EURHEARTJ/I304>.
- Galemou Yoga, Etienne, Jonathan Schiller, and Volker Zickermann. 2021. “Ubiquinone Binding and Reduction by Complex I—Open Questions and Mechanistic Implications.” *Frontiers in Chemistry* 9 (April): 266. <https://doi.org/10.3389/FCHEM.2021.672851/BIBTEX>.
- Gellerich, Frank N., Zelfira Gizatullina, Sonata Trumbeckaite, Huu P. Nguyen, Thilo Pallas, Odeta Arandarcikaite, Stephan Vielhaber, Enn Seppet, and Frank Striggow. 2010. “The Regulation of OXPHOS by Extramitochondrial Calcium.” *Biochimica et Biophysica Acta* 1797 (6–7): 1018–27. <https://doi.org/10.1016/J.BBABIO.2010.02.005>.

- Giorgio, Valentina, Lishu Guo, Claudio Bassot, Valeria Petronilli, and Paolo Bernardi. 2018. "Calcium and Regulation of the Mitochondrial Permeability Transition." *Cell Calcium*. <https://doi.org/10.1016/j.ceca.2017.05.004>.
- Gornall, A. G., C. J. Bardawill, and M. M. David. 1949. "Determination of Serum Proteins by Means of the Biuret Reaction." *The Journal of Biological Chemistry* 177 (2): 751–66.
- Gottschalk, Benjamin, Corina T. Madreiter-Sokolowski, and Wolfgang F. Graier. 2022. "Cristae Junction as a Fundamental Switchboard for Mitochondrial Ion Signaling and Bioenergetics." *Cell Calcium* 101 (January): 102517. <https://doi.org/10.1016/J.CECA.2021.102517>.
- Grenfell, J. Lee, Heike Rauer, Franck Selsis, Lisa Kaltenecker, Charles Beichman, William Danchi, Carlos Eiroa, et al. 2010. "Co-Evolution of Atmospheres, Life, and Climate." *Astrobiology* 10 (1): 77–88. <https://doi.org/10.1089/ast.2009.0375>.
- Griffiths, Elinor J., and Andrew P. Halestrap. 1993. "Protection by Cyclosporin A of Ischemia/Reperfusion-Induced Damage in Isolated Rat Hearts." *Journal of Molecular and Cellular Cardiology* 25 (12): 1461–69. <https://doi.org/10.1006/jmcc.1993.1162>.
- Grimm, Stefan, and Dieter Brdiczka. 2007. "The Permeability Transition Pore in Cell Death." *Apoptosis*. <https://doi.org/10.1007/s10495-007-0747-3>.
- Gutiérrez-Aguilar, Manuel. 2020. "Mitochondrial Calcium Transport and Permeability Transition as Rational Targets for Plant Protection." *Biochimica et Biophysica Acta. Bioenergetics* 1861 (12). <https://doi.org/10.1016/J.BBABIO.2020.148288>.
- Gutiérrez-Aguilar, Manuel, Xóchitl Pérez-Martínez, Edmundo Chávez, and Salvador Uribe-Carvajal. 2010a. "In the Phosphate Carrier Is a Component of the Mitochondrial Unselective Channel." *Archives of Biochemistry and Biophysics* 494 (2): 184–91. <https://doi.org/10.1016/j.abb.2009.12.002>.
- . 2010b. "In the Phosphate Carrier Is a Component of the Mitochondrial Unselective Channel." *Archives of Biochemistry and Biophysics* 494 (2): 184–91. <https://doi.org/10.1016/j.abb.2009.12.002>.
- . 2010c. "In the Phosphate Carrier Is a Component of the Mitochondrial Unselective Channel." *Archives of Biochemistry and Biophysics* 494 (2): 184–91. <https://doi.org/10.1016/j.abb.2009.12.002>.
- . 2010d. "In *Saccharomyces Cerevisiae*, the Phosphate Carrier Is a Component of the Mitochondrial Unselective Channel." *Archives of Biochemistry and Biophysics* 494 (2): 184–91. <https://doi.org/10.1016/J.ABB.2009.12.002>.
- Gutiérrez-Aguilar, Manuel, Victoriano Pérez-Vázquez, Odile Bunoust, Stéphen Manon, Michel Rigoulet, and Salvador Uribe. 2007. "In Yeast, Ca²⁺ and Octylguanidine Interact with Porin (VDAC) Preventing the Mitochondrial Permeability Transition." *Biochimica et Biophysica Acta – Bioenergetics* 1767 (10): 1245–51. <https://doi.org/10.1016/j.bbabi.2007.07.002>.
- Halestrap, Andrew P. 2004. "Mitochondrial Permeability: Dual Role for the ADP/ATP Translocator?" *Nature*. <https://doi.org/10.1038/nature02816>.
- Hawkins, C L, D I Pattison, and M J Davies. 2003. "Hypochlorite-Induced Oxidation of Amino Acids, Peptides and Proteins Review Article." *Amino Acids* 25: 259–74. <https://doi.org/10.1007/s00726-003-0016-x>.
- Haworth, Robert A., and Douglas R.M. Hunter. 2000. "Control of the Mitochondrial Permeability Transition Pore by High-Affinity ADP Binding at the ADP/ATP Translocase in Permeabilized Mitochondria." *Journal of Bioenergetics and Biomembranes* 32 (1): 91–96. <https://doi.org/10.1023/A:1005568630151>.

- Hsia, Connie C.W., Anke Schmitz, Markus Lambertz, Steven F. Perry, and John N. Maina. 2013. "Evolution of Air Breathing: Oxygen Homeostasis and the Transitions from Water to Land and Sky." *Comprehensive Physiology* 3 (2): 849–915. <https://doi.org/10.1002/cphy.c120003>.
- Hurst, Stephen, Jan Hoek, and Shey-Shing Sheu. 2017. "MINI-REVIEW Mitochondrial Ca²⁺ and Regulation of the Permeability Transition Pore." *J Bioenerg Biomembr* 49: 27–47. <https://doi.org/10.1007/s10863-016-9672-x>.
- Jarmuszkiewicz, Wiesława, Andrzej Woyda-Ploszczyca, Nina Antos-Krzeminska, and Francis E. Sluse. 2010. "Mitochondrial Uncoupling Proteins in Unicellular Eukaryotes." *Biochimica et Biophysica Acta – Bioenergetics* 1797 (6–7): 792–99. <https://doi.org/10.1016/j.bbabi.2009.12.005>.
- Jeedigunta, Swathi P., Anastasia v. Minenkova, Jonathan M. Palozzi, and Thomas R. Hurd. 2021. "Avoiding Extinction: Recent Advances in Understanding Mechanisms of Mitochondrial DNA Purifying Selection in the Germline." *Annual Review of Genomics and Human Genetics* 22: 55–80. <https://doi.org/10.1146/ANNUREV-GENOM-121420-081805>.
- Juhaszova, Magdalena, Su Wang, Dmitry B. Zorov, H. Bradley Nuss, Marc Gleichmann, Mark P. Mattson, and Steven J. Sollott. 2008. "The Identity and Regulation of the Mitochondrial Permeability Transition Pore: Where the Known Meets the Unknown." In *Annals of the New York Academy of Sciences*, 1123:197–212. Blackwell Publishing Inc. <https://doi.org/10.1196/annals.1420.023>.
- Jung, Dennis W., Patrick C. Bradshaw, and Douglas R. Pfeiffer. 1997. "Properties of a Cyclosporin-Insensitive Permeability Transition Pore in Yeast Mitochondria." *Journal of Biological Chemistry* 272 (34): 21104–12. <https://doi.org/10.1074/jbc.272.34.21104>.
- Kadenbach, Bernhard. 2003. "Intrinsic and Extrinsic Uncoupling of Oxidative Phosphorylation." *Biochimica et Biophysica Acta – Bioenergetics* 1604 (2): 77–94. [https://doi.org/10.1016/S0005-2728\(03\)00027-6](https://doi.org/10.1016/S0005-2728(03)00027-6).
- Karch, Jason, Michael J. Bround, Hadi Khalil, Michelle A. Sargent, Nadina Latchman, Naohiro Terada, Pablo M. Peixoto, and Jeffery D. Molkenin. 2019. "Inhibition of Mitochondrial Permeability Transition by Deletion of the ANT Family and CypD." *Science Advances* 5 (8): 4597. <https://doi.org/10.1126/sciadv.aaw4597>.
- Khosravi, Siavash, and Max E. Harner. 2020. "The MICOS Complex, a Structural Element of Mitochondria with Versatile Functions." *Biological Chemistry* 401 (6–7): 765–78. <https://doi.org/10.1515/HSZ-2020-0103/XML>.
- Kluckova, Katarina, Ayanachew Bezawork-Geleta, Jakub Rohlena, Lanfeng Dong, and Jiri Neuzil. 2013. "Mitochondrial Complex II, a Novel Target for Anti-Cancer Agents." *Biochimica et Biophysica Acta – Bioenergetics* 1827 (5): 552–64. <https://doi.org/10.1016/J.BBABIO.2012.10.015>.
- Kovács-Bogdán, Erika, Yasemin Sancak, Kimberli J. Kamer, Molly Plovanich, Ashwini Jambhekar, Robert J. Huber, Michael A. Myre, Michael D. Blower, and Vamsi K. Mootha. 2014. "Reconstitution of the Mitochondrial Calcium Uniporter in Yeast." *Proceedings of the National Academy of Sciences of the United States of America* 111 (24): 8985–90. <https://doi.org/10.1073/pnas.1400514111>.
- Luca, Andrea di, and Ville R.I. Kaila. 2021. "Molecular Strain in the Active/Deactive-Transition Modulates Domain Coupling in Respiratory Complex I." *Biochimica et Biophysica Acta. Bioenergetics* 1862 (5). <https://doi.org/10.1016/J.BBABIO.2021.148382>.

- Luévano-Martínez, Luis Alberto. 2012. “Uncoupling Proteins (UCP) in Unicellular Eukaryotes: True UCPs or UCP1-like Acting Proteins?” *FEBS Letters* 586 (7): 1073–78. <https://doi.org/10.1016/J.FEBSLET.2012.03.009>.
- Maldonado, Maria, Abhilash Padavannil, Long Zhou, Fei Guo, and James A. Letts. 2020. “Atomic Structure of a Mitochondrial Complex I Intermediate from Vascular Plants.” *Elife* 9 (August): 1–36. <https://doi.org/10.7554/ELIFE.56664>.
- Margulis, L., and D. Bermudes. 1985. “Symbiosis as a Mechanism of Evolution: Status of Cell Symbiosis Theory.” *Symbiosis* 1: 101–24.
- Martin, William F., Sriram Garg, and Verena Zimorski. 2015. “Endosymbiotic Theories for Eukaryote Origin.” *Philosophical Transactions of the Royal Society B: Biological Sciences* 370 (1678). <https://doi.org/10.1098/rstb.2014.0330>.
- McBride, S., L. Wei-LaPierre, F. McMurray, M. MacFarlane, X. Qiu, D. A. Patten, R. T. Dirksen, and M. E. Harper. 2019. “Skeletal Muscle Mitoflashes, PH, and the Role of Uncoupling Protein-3.” *Archives of Biochemistry and Biophysics* 663 (March): 239–48. <https://doi.org/10.1016/J.ABB.2019.01.018>.
- McCord, Joe M. 2000. “The Evolution of Free Radicals and Oxidative Stress.” *The American Journal of Medicine* 108 (8): 652–59. [https://doi.org/10.1016/S0002-9343\(00\)00412-5](https://doi.org/10.1016/S0002-9343(00)00412-5).
- Mendez-Romero, O., C. Ricardez-García, P. Castañeda-Tamez, N. Chiquete-Félix, and S. Uribe-Carvajal. 2022. “Thriving in Oxygen While Preventing ROS Overproduction: No Two Systems Are Created Equal.” *Frontiers in Physiology* 13 (April). <https://doi.org/10.3389/FPHYS.2022.874321>.
- Mendez-Romero, Ofelia, Chrystian Rodriguez-Armenta, Salvador Uribe-Carvajal, and Adriana Muhlia-Almazan. 2020. “Functional Characterization of the Mitochondrial Uncoupling Proteins from the White Shrimp *Litopenaeus Vannamei*.” *Biochimica et Biophysica Acta. Bioenergetics* 1861 (8). <https://doi.org/10.1016/J.BBABIO.2020.148209>.
- Mendez-Romero, Ofelia, Salvador Uribe-Carvajal, Natalia Chiquete-Felix, and Adriana Muhlia-Almazan. 2019. “Mitochondrial Uncoupling Proteins UCP4 and UCP5 from the Pacific White Shrimp *Litopenaeus Vannamei*.” *Journal of Bioenergetics and Biomembranes* 51 (2): 103–19. <https://doi.org/10.1007/s10863-019-09789-5>.
- Menze, Michael A., Kirk Hutchinson, Susan M. Laborde, and Steven C. Hand. 2005. “Mitochondrial Permeability Transition in the Crustacean *Artemia Franciscana*: Absence of a Calcium-Regulated Pore in the Face of Profound Calcium Storage.” *American Journal of Physiology. Regulatory, Integrative and Comparative Physiology* 289 (1). <https://doi.org/10.1152/AJPREGU.00844.2004>.
- Mia, Marcello de, Stéphane D. Lemaire, Yves Choquet, and Francis André Wollmana. 2019. “Nitric Oxide Remodels the Photosynthetic Apparatus upon S-Starvation in *Chlamydomonas Reinhardtii*.” *Plant Physiology* 179 (2): 718. <https://doi.org/10.1104/PP.18.01164>.
- Mitchell, Peter. 1961. “Coupling of Phosphorylation to Electron and Hydrogen Transfer by a Chemi-Osmotic Type of Mechanism.” *Nature* 191 (4784): 144–48. <https://doi.org/10.1038/191144a0>.
- Moreno-Sánchez, Rafael, Luz Hernández-Esquivel, Nadia A. Rivero-Segura, Alvaro Marín-Hernández, Jiri Neuzil, Stephen J. Ralph, and Sara Rodríguez-Enríquez. 2013. “Reactive Oxygen Species Are Generated by the Respiratory Complex II—Evidence for Lack of Contribution of the Reverse Electron Flow in Complex I.” *The FEBS Journal* 280 (3): 927–38. <https://doi.org/10.1111/FEBS.12086>.

- Nakanishi-Matsui, Mayumi, and Masamitsu Futai. 2008. “Stochastic Rotational Catalysis of Proton Pumping F-ATPase.” *Philosophical Transactions of the Royal Society B: Biological Sciences* 363 (1500): 2135–42. <https://doi.org/10.1098/RSTB.2008.2266>.
- Nunn, John F. 1998. “Evolution of the Atmosphere.” *Proceedings of the Geologists’ Association. Geologists’ Association* 109 (1): 1–13. [https://doi.org/10.1016/S0016-7878\(98\)80001-1](https://doi.org/10.1016/S0016-7878(98)80001-1).
- Ohnishi, T., V. D. Sled, N. I. Rudnitsky, S. W. Meinhardt, T. Yagi, Y. Hatefi, T. Link, G. von Jagow, A. S. Saribas, and F. Daldal. 1994. “Topographical Distribution of Redox Centres and the Qo Site in Ubiquinol-Cytochrome-c Oxidoreductase (Complex III) and Ligand Structure of the Rieske Iron-Sulphur Cluster.” *Biochemical Society Transactions* 22 (1): 191–97. <https://doi.org/10.1042/BST0220191>.
- Ortega, Nataly, and Carlos Rosas. 2020. “Cellular Signaling Associated with Reactive Oxygen Species and Their Role in Wound Healing.” *J. Health Med. Sci* 6 (3): 199–205.
- Papa, Sergio, Michele Lorusso, and Marco di Paola. 2006. “Cooperativity and Flexibility of the Protonmotive Activity of Mitochondrial Respiratory Chain.” *Biochimica et Biophysica Acta (BBA) – Bioenergetics* 1757 (5–6): 428–36. <https://doi.org/10.1016/J.BBABIO.2006.03.015>.
- Parey, Kristian, Christophe Wirth, Janet Vonck, and Volker Zickermann. 2020. “Respiratory Complex I — Structure, Mechanism and Evolution.” *Current Opinion in Structural Biology* 63 (August): 1–9. <https://doi.org/10.1016/J.SBI.2020.01.004>.
- Pereira, Clara, Nadine Camougrand, Stéphen Manon, Maria João Sousa, and Manuela Côte-Real. 2007. “ADP/ATP Carrier Is Required for Mitochondrial Outer Membrane Permeabilization and Cytochrome c Release in Yeast Apoptosis.” *Molecular Microbiology* 66 (3): 571–82. <https://doi.org/10.1111/j.1365-2958.2007.05926.x>.
- Plečtitá-Hlavatá, Lydie, and Petr Ježek. 2016. “Integration of Superoxide Formation and Cristae Morphology for Mitochondrial Redox Signaling.” *The International Journal of Biochemistry & Cell Biology* 80 (November): 31–50. <https://doi.org/10.1016/J.BIOCEL.2016.09.010>.
- Pons, Daniel Gabriel, Mercedes Nadal-Serrano, Margalida Torrens-Mas, Adamo Valle, Jordi Oliver, and Pilar Roca. 2015. “UCP2 Inhibition Sensitizes Breast Cancer Cells to Therapeutic Agents by Increasing Oxidative Stress.” *Free Radical Biology and Medicine* 86 (July): 67–77. <https://doi.org/10.1016/j.freeradbiomed.2015.04.032>.
- Priault, Muriel, Nadine Camougrand, Kathleen W. Kinnally, François M. Vallette, and Stéphen Manon. 2003. “Yeast as a Tool to Study Bax/Mitochondrial Interactions in Cell Death.” *FEMS Yeast Research* 4 (1): 15–27. [https://doi.org/10.1016/S1567-1356\(03\)00143-0](https://doi.org/10.1016/S1567-1356(03)00143-0).
- Quinlan, Casey L, Irina v Perevoshchikova, Martin Hey-mogensen, Adam L Orr, and Martin D Brand. 2013. “Redox Biology Sites of Reactive Oxygen Species Generation by Mitochondria Oxidizing Different Substrates \$.” *Redox Biology* 1 (1): 304–12. <https://doi.org/10.1016/j.redox.2013.04.005>.
- Ramírez-Camacho, I., F. Correa, M. el Hafidi, A. Silva-Palacios, M. Ostolga-Chavarría, M. Esparza-Perusquía, S. Olvera-Sánchez, O. Flores-Herrera, and C. Zazueta. 2018. “Cardioprotective Strategies Preserve the Stability of Respiratory Chain Supercomplexes and Reduce Oxidative Stress in Reperfused Ischemic Hearts.” *Free Radical Biology and Medicine* 129 (December): 407–17. <https://doi.org/10.1016/j.freeradbiomed.2018.09.047>.
- Rupprecht, Anne, Elena A. Sokolenko, Valeri Beck, Olaf Ninnemann, Martin Jaburek, Thorsten Trimbuch, Sergey S. Klishin, Petr Jezek, Vladimir P. Skulachev, and Elena E. Pohl. 2010.

- “Role of the Transmembrane Potential in the Membrane Proton Leak.” *Biophysical Journal* 98 (8): 1503–11. <https://doi.org/10.1016/j.bpj.2009.12.4301>.
- Schieber, Michael, and Navdeep S. Chandel. 2014. “ROS Function in Redox Signaling and Oxidative Stress.” *Current Biology : CB* 24 (10). <https://doi.org/10.1016/J.CUB.2014.03.034>.
- Schiffer, Tomas A, Liza Löf, Radosa Gallini, Masood Kamali-Moghaddam, Mattias Carlström, and Fredrik Palm. 2022. “Mitochondrial Respiration-Dependent ANT2-UCP2 Interaction.” *Frontiers in Physiology* 13 (May): 866590. <https://doi.org/10.3389/fphys.2022.866590>.
- Shanmughapriya, Santhanam, Sudarsan Rajan, Nicholas E. Hoffman, Andrew M. Higgins, Dhanendra Tomar, Neeharika Nemani, Kevin J. Hines, et al. 2015. “SPG7 Is an Essential and Conserved Component of the Mitochondrial Permeability Transition Pore.” *Molecular Cell* 60 (1): 47–62. <https://doi.org/10.1016/j.molcel.2015.08.009>.
- Skulachev, V.P. 1998. “Uncoupling: New Approaches to an Old Problem of Bioenergetics.” *Biochim. Biophys. Acta* 1363: 100–124.
- Snyder, Christopher H., Emma Berta Gutierrez-Cirlos, and Bernard L. Trumpower. 2000. “Evidence for a Concerted Mechanism of Ubiquinol Oxidation by the Cytochrome Bc 1 Complex *.” *Journal of Biological Chemistry* 275 (18): 13535–41. <https://doi.org/10.1074/JBC.275.18.13535>.
- Solhjoo, Soroosh, and Brian O’Rourke. 2015. “Mitochondrial Instability during Regional Ischemia-Reperfusion Underlies Arrhythmias in Monolayers of Cardiomyocytes.” *Journal of Molecular and Cellular Cardiology* 78 (January): 90–99. <https://doi.org/10.1016/j.yjmcc.2014.09.024>.
- Solien, Joseph, Virginia Haynes, and Cecilia Giulivi. 2005. “Differential Requirements of Calcium for Oxoglutarate Dehydrogenase and Mitochondrial Nitric-Oxide Synthase under Hypoxia: Impact on the Regulation of Mitochondrial Oxygen Consumption.” *Comparative Biochemistry and Physiology Part A: Molecular & Integrative Physiology* 142 (2): 111–17. <https://doi.org/10.1016/J.CBPB.2005.05.004>.
- Soo, Rochelle M., James Hemp, and Philip Hugenholtz. 2019. “Evolution of Photosynthesis and Aerobic Respiration in the Cyanobacteria.” *Free Radical Biology & Medicine* 140 (August): 200–205. <https://doi.org/10.1016/J.FREERADBIOMED.2019.03.029>.
- Soo, Rochelle M., James Hemp, Donovan H. Parks, Woodward W. Fischer, and Philip Hugenholtz. 2017. “On the Origins of Oxygenic Photosynthesis and Aerobic Respiration in Cyanobacteria.” *Science* 355 (6332): 1436–40. <https://doi.org/10.1126/science.aal3794>.
- Timón-Gómez, Alba, Eva Nývltová, Luciano A. Abriata, Alejandro J. Vila, Jonathan Hosler, and Antoni Barrientos. 2018. “Mitochondrial Cytochrome c Oxidase Biogenesis: Recent Developments.” *Seminars in Cell and Developmental Biology*. <https://doi.org/10.1016/j.semcd.2017.08.055>.
- Traba, Javier, Jorgina Satrustegui, and Araceli del Arco. 2009. “Transport of Adenine Nucleotides in the Mitochondria of *Saccharomyces Cerevisiae*: Interactions between the ADP/ATP Carriers and the ATP-Mg/Pi Carrier.” *Mitochondrion* 9 (2): 79–85. <https://doi.org/10.1016/J.MITO.2009.01.001>.
- Trumpower, B L. 1990. “Cytochrome Bc1 Complexes of Microorganisms.” *Microbiological Reviews* 54 (2): 101–29. <https://doi.org/10.1128/MR.54.2.101-129.1990>.
- Uribe-Alvarez, Cristina, Natalia Chiquete-Félix, Martha Contreras-Zentella, Sergio Guerrero-Castillo, Antonio Peña, and Salvador Uribe-Carvajal. 2016. “Staphylococcus Epidermidis: Metabolic Adaptation and Biofilm Formation in Response to Different Oxygen Concentrations.” *Pathogens and Disease* 74 (1). <https://doi.org/10.1093/FEMSPD/FTV111>.

- Uribe-Carvajal, Salvador, Luís A. Luévano-Martínez, Sergio Guerrero-Castillo, Alfredo Cabrera-Orefice, Norma A. Corona-de-la-Peña, and Manuel Gutiérrez-Aguilar. 2011. "Mitochondrial Unselective Channels throughout the Eukaryotic Domain." *Mitochondrion*. <https://doi.org/10.1016/j.mito.2011.02.004>.
- Velours, Jean, Alain Dautant, Bénédicte Salin, Isabelle Sagot, and Daniel Brèthes. 2009. "Mitochondrial F1F0-ATP Synthase and Organellar Internal Architecture." *The International Journal of Biochemistry & Cell Biology* 41 (10): 1783–89. <https://doi.org/10.1016/J.BIOCEL.2009.01.011>.
- Wu, Youcong, Yang Wu, Tao Zhu, Haiyan Han, Huayong Liu, Tao Xu, Patrice Francois, et al. 2015. "Staphylococcus Epidermidis SrrAB Regulates Bacterial Growth and Biofilm Formation Differently under Oxic and Microaerobic Conditions." *Journal of Bacteriology* 197 (3): 459–76. <https://doi.org/10.1128/JB.02231-14>.
- Xinzhao Wang, Zhaoyun Li, Jujie Sun, Xiang Song, Mengxue Bian, Fukai Wang, Feng Yan, and Zhiyong Yu. 2021. "Inhibition of NADPH Oxidase 4 Attenuates Lymphangiogenesis and Tumor Metastasis in Breast Cancer." *FASEB Journal* 35 (4). <https://doi.org/10.1096/fj.202002533R>.

13.ANEXOS

Publicaciones

Morales-García, L., Ricardez-García, C., Castañeda-Tamez, P., Chiquete-Félix, N., & Uribe-Carvajal, S. (2021). Coupling/Uncoupling Reversibility in Isolated Mitochondria from *Saccharomyces cerevisiae*. *Life (Basel, Switzerland)*, 11(12), 1307.

<https://doi.org/10.3390/life11121307>

Pedroza-Dávila, U., Uribe-Alvarez, C., Morales-García, L., Espinoza-Simón, E., Méndez-Romero, O., Muhlia-Almazán, A., Chiquete-Félix, N., & Uribe-Carvajal, S. (2020). Metabolism, ATP production and biofilm generation by *Staphylococcus epidermidis* in either respiratory or fermentative conditions. *AMB Express*, 10(1), 31.

<https://doi.org/10.1186/s13568-020-00966-z>



Espinoza-Simón, E., Chiquete-Félix, N., Morales-García, L., Pedroza-Dávila, U., Pérez-Martínez, X., Araiza-Olivera, D., Torres-Quiroz, F., & Uribe-Carvajal, S. (2020). In *Saccharomyces cerevisiae*, withdrawal of the carbon source results in detachment of glycolytic enzymes from the cytoskeleton and in actin reorganization. *Fungal biology*, 124(1), 15–23. <https://doi.org/10.1016/j.funbio.2019.10.005>

Uribe-Alvarez, C., Chiquete-Félix, N., Morales-García, L., Bohórquez-Hernández, A., Delgado-Buenrostro, N. L., Vaca, L., Peña, A., & Uribe-Carvajal, S. (2019). *Wolbachia pipientis* grows in *Saccharomyces cerevisiae* evoking early death of the host and deregulation of mitochondrial metabolism. *Microbiology Open*, 8(4), e00675.

<https://doi.org/10.1002/mbo3.675>

Article

Coupling/Uncoupling Reversibility in Isolated Mitochondria from *Saccharomyces cerevisiae*

Lilia Morales-García ^{1,2,†} , Carolina Ricardez-García ^{1,†}, Paulina Castañeda-Tamez ¹, Natalia Chiquete-Félix ¹ and Salvador Uribe-Carvajal ^{1,2,*} 

¹ Department of Genetics and Molecular Biology, Instituto de Fisiología Celular, UNAM, Mexico City 04510, Mexico; lmoga15@gmail.com (L.M.-G.); cricardez@ifc.unam.mx (C.R.-G.); paulinact08@gmail.com (P.C.-T.); nchiquete@ifc.unam.mx (N.C.-F.)

² Department of Biochemistry, Medicine School, UNAM, Mexico City 04510, Mexico

* Correspondence: suribe@ifc.unam.mx; Tel.: +52-5555625632

† Both authors are first authors as they contributed equally to the project.

Abstract: The yeast *Saccharomyces cerevisiae* uses fermentation as the preferred pathway to obtain ATP and requires the respiratory chain to re-oxidize the NADH needed for activity of Glyceraldehyde-3-phosphate. This process is favored by uncoupling of oxidative phosphorylation (OxPhos), which is at least partially controlled by the mitochondrial unspecific pore (s_c MUC). When mitochondrial ATP synthesis is needed as in the diauxic phase or during mating, a large rise in Ca^{2+} concentration ($[Ca^{2+}]$) closes s_c MUC, coupling OxPhos. In addition, s_c MUC opening/closing is mediated by the ATP/ADP ratio, which indicates cellular energy needs. Here, opening and closing of s_c MUC was evaluated in isolated mitochondria from *S. cerevisiae* at different incubation times and in the presence of different ATP/ADP ratios or varying $[Ca^{2+}]$. Measurements of the rate of O_2 consumption, mitochondrial swelling, transmembrane potential and ROS generation were conducted. It was observed that s_c MUC opening was reversible, a high ATP/ADP ratio promoted opening and $[Ca^{2+}]$ closed s_c MUC even after several minutes of incubation in the open state. In the absence of ATP synthesis, closure of s_c MUC resulted in an increase in ROS.

Keywords: physiological uncoupling; yeast mitochondria; mitochondrial permeability transition reversibility; s_c MUC; Ca^{2+}



Citation: Morales-García, L.; Ricardez-García, C.; Castañeda-Tamez, P.; Chiquete-Félix, N.; Uribe-Carvajal, S. Coupling/Uncoupling Reversibility in Isolated Mitochondria from *Saccharomyces cerevisiae*. *Life* **2021**, *11*, 1307. <https://doi.org/10.3390/life11121307>

Academic Editors: Rafael A. Casuso and Giorgio Lenaz

Received: 28 September 2021
Accepted: 22 November 2021
Published: 27 November 2021

Publisher's Note: MDPI stays neutral with regard to jurisdictional claims in published maps and institutional affiliations.



Copyright: © 2021 by the authors. Licensee MDPI, Basel, Switzerland. This article is an open access article distributed under the terms and conditions of the Creative Commons Attribution (CC BY) license (<https://creativecommons.org/licenses/by/4.0/>).

1. Introduction

Fermentative metabolism in *Saccharomyces cerevisiae* requires an active mitochondrial respiratory chain to re-oxidize the NADH produced by glyceraldehyde-3-phosphate dehydrogenase (GAPDH) [1]. NAD^+ is needed in the glycolytic pathway by glyceraldehyde-3-Phosphate dehydrogenase (GAPDH), which may bind to mitochondrial porin and exchange produced NADH for required NAD^+ [2]. A basal high rate of oxygen consumption is possible in *S. cerevisiae* mitochondria due to the substitution of Complex I by three alternative NADH dehydrogenases (NDH2), which do not pump protons and thus decrease the ATP/O [3]. In addition, as Complex-I contains the two most important sites for ROS production in the respiratory chain [4] this substitution probably helps to avoid ROS overproduction in *S. cerevisiae*. In addition, the *S. cerevisiae* mitochondrial unspecific channel (s_c MUC) may open, depleting the transmembrane potential ($\Delta\Psi$), uncoupling oxidative phosphorylation and increasing the rate of oxygen consumption, thus decreasing ROS production further [5–7].

When fermentative substrates are exhausted and O_2 is available, *S. cerevisiae* cells shift their metabolism to become aerobic using accumulated ethanol as respiratory substrate to begin the diauxic phase of growth [8,9]. Physiologically important effectors that alternatively open and close s_c MUC are adenine nucleotides, where ATP opens s_c MUC [7] while hydrolysis products ADP and Pi close it, i.e., a high energy charge opens s_c MUC

while a low energy charge closes it. The second effector of physiological interest is Ca^{2+} , which closes $s_c\text{MUC}$ at high concentrations [10]. In resting yeast, cytoplasmic $[\text{Ca}^{2+}]$ is near $0.1 \mu\text{M}$, while in most extracellular media $[\text{Ca}^{2+}]$ is 1 to 2 mM [11]. Upon stimulation, specialized channels allow large amounts of Ca^{2+} to enter the cell, closing $s_c\text{MUC}$ and enhancing energy production [12]. Thus, Ca^{2+} is an ideal second messenger [12,13]. Activation by Ca^{2+} influx is observed during mating: when an a-type haploid cell is exposed to α -pheromone, this pheromone binds to a specific receptor [14]. When mating, cytoplasmic $[\text{Ca}^{2+}]$ may remain high for up to 20 min signaling the need large morphological changes in the cell due to large modifications in the cellular cytoskeleton [14]. Eventually, an a-cell and an α -cell undergo fusion to generate a diploid [15]. As these processes require a large amount of energy, Ca^{2+} is also needed to close $s_c\text{MUC}$, promote OxPhos coupling and increase ATP availability. When the mating process is over, Ca^{2+} is expelled and a basal metabolism is reinstated [13,16].

Here, we tested in isolated mitochondria the response to either the ratio $\text{ATP}/\text{ADP} + \text{Pi}$ or to $[\text{Ca}^{2+}]$ variations. The role of each effector to control alternative opening and closing was followed using measurements of the rate of O_2 consumption, mitochondrial transmembrane potential ($\Delta\Psi$), mitochondrial swelling and ROS production. The open/close state of $s_c\text{MUC}$ was dependent on the addition of different effectors. Opening and closing were reversible. In addition it was observed that opening was gradual as effector mixtures elicited partial effects. These effects suggest that in fermenting yeast, mitochondria are uncoupled, becoming coupled when a large amount of ATP is required.

2. Materials and Methods

Reagents. All chemicals were analytic grade. Mannitol, MES hydrate, D-Galactose, TEA (triethanolamine), ADP, ATP, safranin-O, oligomycin were from Sigma Chem Co. Bovine serum albumin from Probulmin TM. Bacto-peptone and yeast extract from MCD LAB. H_3PO_4 , KCl and MgCl_2 were from J.T. Baker.

Yeast strain. Experiments were conducted using either a commercial strain of baker's yeast *Saccharomyces cerevisiae* ("La Azteca, S. A." Mexico City) [17] or a laboratory strain W303 (*MAT α* ; *ura3-1*; *trp1 Δ* 2; *leu2-3,112*; *his3-11,15*; *ade2-1*; *can1-100*) [18]. Results were similar for both strains. Yeasts were kept in YPD (1% yeast extract, 2% bacto-peptone, 2% glucose and 2% bacto-agar) plate cultures. Cells were grown as follows: pre-cultures were prepared immersing a loopful of yeast into 100 mL YPD and incubating for 24 h under continuous agitation in an orbital shaker (New Brunswick Scientific, NJ, USA) at 250 rpm in a constant-temperature room (30 °C). Then each 100 mL flask was used to inoculate 900 mL of YPGal (1% yeast extract, 2% bacto-peptone and 2% galactose). Incubation was continued for 48 h.

Isolation of yeast mitochondria. After incubation, yeast was centrifuged ($5000 \times g$ for 5 min and washed twice) and resuspended in 0.6 M mannitol, 5 mM MES, 0.1% bovine serum albumin, pH 6.8 (TEA). The cell suspension was mixed with 0.5 mm diameter glass beads 50% (*v/v*) and disrupted in a Bead Beater, Biospec Products Inc, OK. Mitochondria were isolated from the homogenate by differential centrifugation as previously described [17]. The concentration of mitochondrial protein was determined by Biuret [19]. In all assays we used mitochondria at a final concentration of 0.5 mg prot/mL.

Oxygen consumption. Experiments were conducted using a Clark electrode (Oximeter model 782, Warner/Strathkelvin Instruments, North Lanarkshire, Scotland) in a water-jacketed chamber. Temperature was kept at 30 °C using a water bath (PolyScience 7 L, IL). Total volume 1.0 mL. The reaction mixture was 0.6 M mannitol, 5 mM MES (TEA), pH 6.8 plus 0.1 M KCl, 0.5 mM MgCl_2 and 2 $\mu\text{L}/\text{mL}$ ethanol. In all experiments, samples were preincubated for 5 min with oligomycin 4 $\mu\text{g}/\text{mg}$ prot.

Transmembrane potential. $\Delta\Psi$ was determined as described by Åkerman and Wikström [20], following the changes in absorbance of safranin-O at 511–533 nm using a double beam Aminco-Olis spectrophotometer (GA) in dual mode. The concentrations of ATP, ADP, Ca^{2+} and EGTA are indicated under each figure. At the end of each trace,

the collapse of $\Delta\Psi$ was induced adding 6 μM CCCP. In all experiments, samples were preincubated for 5 min with oligomycin 4 $\mu\text{g}/\text{mg}$ prot.

Mitochondrial swelling. The decrease in absorbance of a mitochondrial suspension at 540 nm was followed as described in the literature [6]. We used a DW2000 Olis/Aminco spectrophotometer in split mode. In all experiments, samples were preincubated for 5 min with oligomycin 4 $\mu\text{g}/\text{mg}$ prot.

Reactive oxygen species were measured in freshly mitochondria using the Amplex Red (Invitrogen, Molecular Probes, Carlsbad, CA, USA) as in [21]. Samples were incubated for 1 min, then 50 μg were placed into a 96-well micro plate with working solution 20 μL (10 μM Amplex red, 0.2 units/mL horseradish peroxidase and 0.2 units superoxide dismutase/mL in 250 mM sodium phosphate pH 7.4), final volume 100 μL . Fluorescence was measured after 30 mins in a POLARstar Omega detector (BGM LABTECH, Offenburg, Germany) set at 571 and 585 nm and results were interpolated against a calibration curve.

3. Results

During fermentation, *Saccharomyces cerevisiae* uncouples OxPhos to oxidize NADH optimizing the rate of glycolysis while in contrast, after glucose depletion a coupled OxPhos is needed and thus $s_c\text{MUC}$ is closed [8]. Among $s_c\text{MUC}$ effectors, the molecules that vary in concentration in different metabolic states such as adenine nucleotides and Pi seem important. Indeed, ATP opens $s_c\text{MUC}$ uncoupling OxPhos, while ADP closes it, coupling OxPhos [22]. Another effector is $[\text{Ca}^{2+}]$, which in eukaryotes increases several orders of magnitude when plasma membrane Ca^{2+} channels open [12–14].

To analyze the possible physiological role of $s_c\text{MUC}$, mitochondria were isolated and used to measure Oxygen consumption, mitochondrial swelling, the transmembrane potential ($\Delta\Psi$) and reactive oxygen species (ROS) production under conditions where $s_c\text{MUC}$ was open or closed (Figure 1).

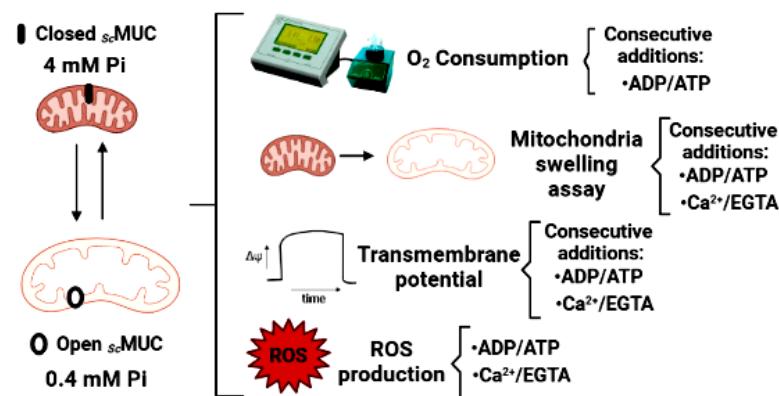


Figure 1. Experimental procedures followed to determine the possible physiological role of $s_c\text{MUC}$ in isolated *S. cerevisiae* mitochondria. Initially, $s_c\text{MUC}$ was open in the presence of 0.4 mM Pi or closed in the presence of 4.0 mM Pi. Then different concentrations of the antagonizing effectors ADP, which closes $s_c\text{MUC}$ or ATP, that opens it, were added. Otherwise, opening or closing was promoted by adding Ca^{2+} to close $s_c\text{MUC}$ or EGTA to chelate the cation and open the channel. Under these conditions, experiments were performed to measure the rate of oxygen consumption, mitochondrial swelling, transmembrane potential or ROS production.

3.1. Effects of ADP/ATP on $s_c\text{MUC}$

Oximetry. The rate of O_2 consumption was measured in the presence of different, fixed Pi concentrations. Then the reversibility of $s_c\text{MUC}$ opening in response to the addition of ATP and/or ADP was evaluated. As described in the literature [5–7], at 2.0 mM Pi we observed a slow rate of oxygen consumption, indicating that OxPhos was coupled (Figure 2A, trace a). Under these conditions, the addition of different concentrations of ATP proportionally increased the rate of oxygen consumption, suggesting that different

concentrations of ATP gradually uncoupled OxPhos (Figure 2A, traces b to e). In contrast, as reported by others [5–7], at 0.1 mM Pi the rate of oxygen consumption was high, indicating that OxPhos was uncoupled due to opening of s_c MUC (Figure 2B trace a). Then, the rate of oxygen consumption gradually decreased upon addition of increasing concentrations of ADP, suggesting different ADP concentrations promoted closure of s_c MUC, promoting coupling (Figure 2B traces b to e). Oxygen consumption results confirmed results by others that increasing concentrations of Pi, and ADP close, while ATP opens s_c MUC [5–7].

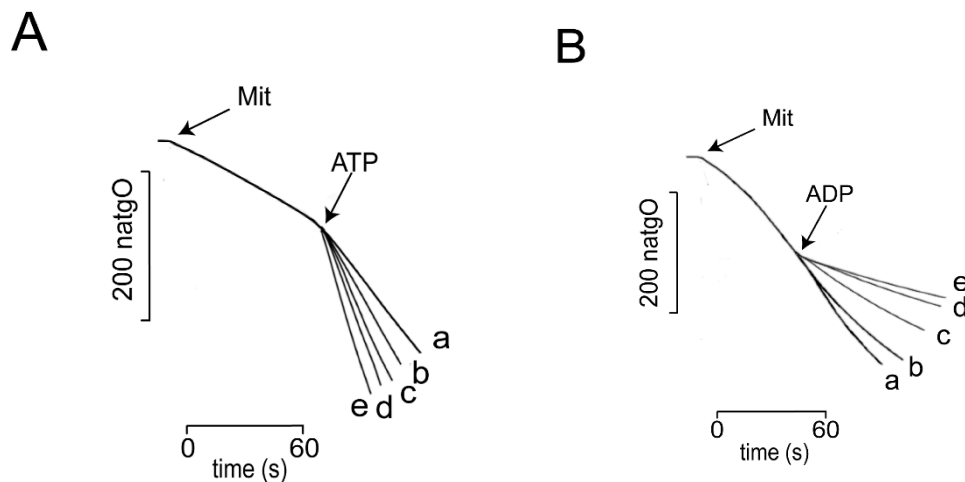


Figure 2. Rate of O_2 consumption by isolated yeast mitochondria in the presence of different concentrations of phosphate (Pi), ATP and ADP. Reaction mixture: 0.6 M mannitol, 5 mM MES, pH 6.8, 0.1 mM KCl, 0.5 mM $MgCl_2$, 2 μ L/mL ethanol. In order to inhibit ATP/ADP interconversion, mitochondria (0.5 mg prot./mL) were incubated for 5 min in the presence of 4 μ g oligomycin/mg prot. (A) Mitochondria were coupled in the presence of 2 mM Pi. Then, ATP was added at a final mM concentration of: (a) 0.5; (b) 1.0; (c) 1.5; (d) 2.0 and (e) 4.0. (B) To promote uncoupling, the experiment was conducted in the presence of 0.1 mM Pi. Then different concentrations of ADP were added to a final mM concentration of (a) 0.5; (b) 1.0; (c) 1.5; (d) 2.0 and (e) 4.0. Experiments were conducted in a Strathkelvin oxymeter equipped with a Clark electrode. $T = 30\text{ }^\circ\text{C}$. Representative experiment, $n = 3$.

Transmembrane potential. The reversibility of s_c MUC opening and closing by ATP and ADP, respectively was evaluated measuring the $\Delta\Psi$ (Figure 3). In these experiments, one adenine nucleotide was added first and the second was added 1.5 min later. At 0.1 mM Pi, $\Delta\Psi$ was almost depleted (Figure 3A trace a) and addition of 2 mM ADP led to $\Delta\Psi$ recovery (Figure 3A trace b). Then, the addition of increasing ATP led to a second fall in $\Delta\Psi$ (Figure 3A, traces c, d and e). The opposite experiment was also performed: when in the presence of 2 mM Pi, $\Delta\Psi$ was high (Figure 3B) and addition of ATP decreased $\Delta\Psi$ (Figure 3B, traces b to e). Then, a later addition of different ADP concentrations resulted in increasing recovery of $\Delta\Psi$, suggesting that s_c MUC closed gradually (Figure 3B traces c, d and e). The reversibility in $\Delta\Psi$ rise/decrease suggests that the alternative addition of ADP and ATP led to alternative, gradual opening/closing of s_c MUC.

Mitochondrial swelling. Another parameter commonly used to follow the open/close state of s_c MUC is mitochondrial swelling [6,23]. At low Pi plus ADP, s_c MUC was closed, so the rate of K^+ -mediated swelling was slow (Figure 4A). Under these conditions, addition of different concentrations of ATP promoted increasing rates in swelling. These data suggested that ATP reverted the ADP-mediated closing of s_c MUC. The opposite experiment, where mitochondria were incubated in the presence of 2 mM Pi plus 2 mM ATP, a rapid rate of K^+ -mediated swelling was observed which indicated s_c MUC was open (Figure 4B, trace b). Then, addition of different concentrations of ADP (Figure 4B, traces c, d, e) inhibited the rate of swelling (Figure 4B traces c, d, and e) suggesting that ADP closed s_c MUC. Therefore, the effect of Pi, ADP or ATP at different times led to changes of swelling rates suggesting that s_c MUC open and close states were reversible [24–26].

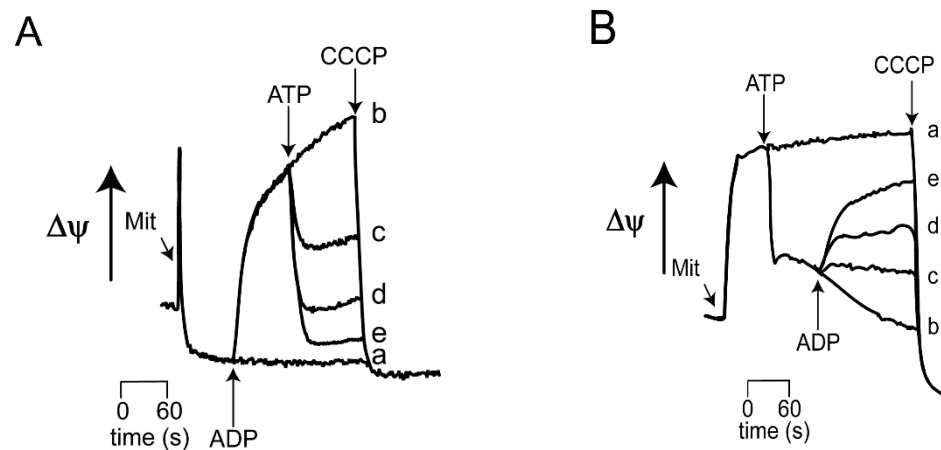


Figure 3. Effect of the sequential addition of ATP and ADP on the mitochondrial transmembrane potential ($\Delta\Psi$). (A) Reaction mixture as in Figure 2A, except 15 μM safranin-O was added. At the arrow, 1 mM ADP, except in trace a, where no ADP was added. Then 1.5 min later ATP was added as follows: traces a and b, 0; trace c, 0.5 mM; trace d, 1 mM; trace e, 1.5 mM. (B) Reaction mixture as in Figure 2B except 15 μM safranin-O. At the arrow, 1 mM ATP except in traces a and b, where no ATP was added. Then 1.5 min of incubation ADP was added as follows: Traces a and b, 0; trace c 0.5 mM; trace d, 1.0 mM; trace e, 1.5 mM. To deplete $\Delta\Psi$, 6 μM FCCP was added at the end of each trace. Absorbance measurements were conducted at 511–533 nm in a Olis/Aminco spectrophotometer in dual mode.

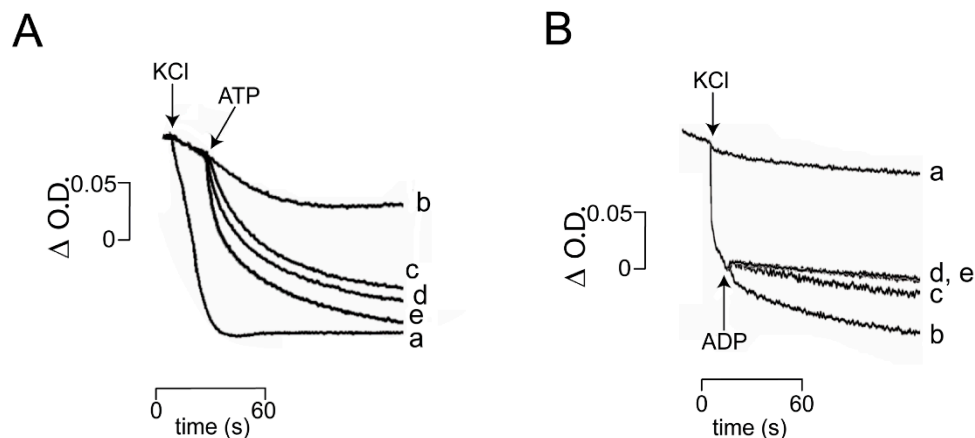


Figure 4. Effect of the sequential addition of ATP and ADP on mitochondrial swelling. (A): Reaction mixture, as in Figure 1, except 0.3 M mannitol. Where indicated 0.1 M KCl. (A) 0.1 mM Pi plus 1 mM ADP (ADP was not added in trace b). Where indicated, ATP was added as follows: (a) and (b) 0; (c) 1 mM; (d) 1.5 mM; (e) 2 mM. (B) 2 mM Pi plus 1 mM ATP ATP was not added in trace (a). Where indicated, ADP was added as follows: traces a and b, 0; trace c, 0.5 mM; trace d, 1 mM; trace (e) 2 mM.

Effects of incubation time on the reversibility ATP-mediated opening of $s_c\text{MUC}$. Preservation of $s_c\text{MUC}$ opening reversibility after different incubation times is critical for survival of the cell. Reversibility of $s_c\text{MUC}$ opening was explored measuring both $\Delta\Psi$ (Figure 5A) and the rate of swelling (Figure 5B). Yeast mitochondria were incubated for different times, from 30 s to 4 min under open $s_c\text{MUC}$ conditions, and then ADP was added (Figure 5). In all cases, ADP promoted partial recovery of $\Delta\Psi$ (Figure 5A) and slight reversal of swelling (Figure 5B). Thus the ATP-mediated opening of $s_c\text{MUC}$ was responsive to ADP for at least 4 min. (Figure 5).

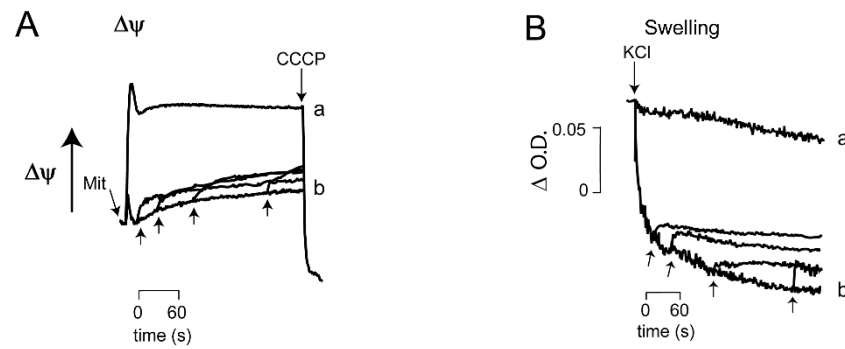


Figure 5. Partial reversion by ADP added at different times of the ATP-mediated opening of s_c MUC. Experimental conditions were as in Figure 3B for $\Delta\Psi$ and Figure 4B for swelling. ATP was 0 (traces a) or 2 mM (all other traces). Upward arrows indicate addition of 1 mM ADP at different incubation times: 30 s, 1, 2 and 4 min. (A) Reaction mixture as in Figure 3B, except 1 mM ATP. (B): Reaction mixture, as in Figure 3B. Where indicated 0.1 M KCl. Representative experiment. $n = 5$.

3.2. Ca^{2+} /EGTA Alternating Effects on s_c MUC

The above results indicate that the opening response of s_c MUC to the sequential additions of ATP and ADP is reversible even after several minutes of incubation. However, neither mitochondrial $\Delta\Psi$ nor swelling returned to the values observed when s_c MUC was closed from the beginning. Thus, it was decided to test whether full reversal of s_c MUC opening could be observed upon depletion of a positive effector after different times of incubation. From previous data, it was reasoned that this could be achieved with Ca^{2+} , an effector closing s_c MUC, and its full chelation with EGTA to open s_c MUC [10,27]. To test whether the EGTA-mediated opening of s_c MUC was reverted adding Ca^{2+} at different incubation times, we conducted measurements of $\Delta\Psi$ (Figure 6A) and mitochondrial swelling (Figure 6B). Mitochondria were incubated in the presence of EGTA for 0.5, 1, 2 and 4 min and then Ca^{2+} was added. Up to 2 min, the addition of Ca^{2+} promoted recovery of a large proportion of $\Delta\Psi$ while a partial effect was obtained at 4 min. (Figure 6A) Mitochondrial swelling was reverted by Ca^{2+} , indicating s_c MUC was closed (Figure 6B). The above data suggest that in isolated mitochondria from *S. cerevisiae*, Ca^{2+} chelation by EGTA evoked the reversible opening of s_c MUC. In contrast to the partial effects of ADP (Figure 5), Ca^{2+} addition resulted in better recovery of $\Delta\Psi$ (Figure 6A) and also at variance with ADP, actual reversal of swelling (Figure 6B).

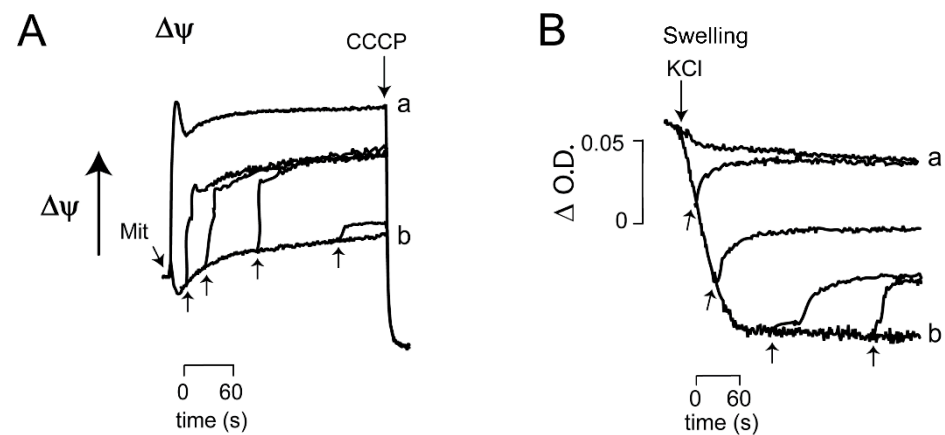


Figure 6. Effect of the addition of Ca^{2+} on mitochondrial transmembrane potential and mitochondrial swelling. (A) Reaction mixture as in Figure 4A. Ca^{2+} 600 μ M (upward arrows) was added at: 30 s, 1, 2 and 4 min. (B) Reaction mixture as in Figure 4B. Where indicated 0.1 M KCl. (upward arrows).

3.3. Reactive Oxygen Species (ROS) Production under Conditions That Open or Close s_c MUC

Physiological uncoupling increases electron flow in the respiratory chain, preventing the over-production of ROS. It has been proposed that permeability transition pores work as unspecific proton sinks thus promoting physiological uncoupling and therefore decrease ROS production [5–7,25]. With this in mind, it was decided to determine whether a correlation exists between the opening/closing of s_c MUC reported above and the control of ROS production (Figure 7).

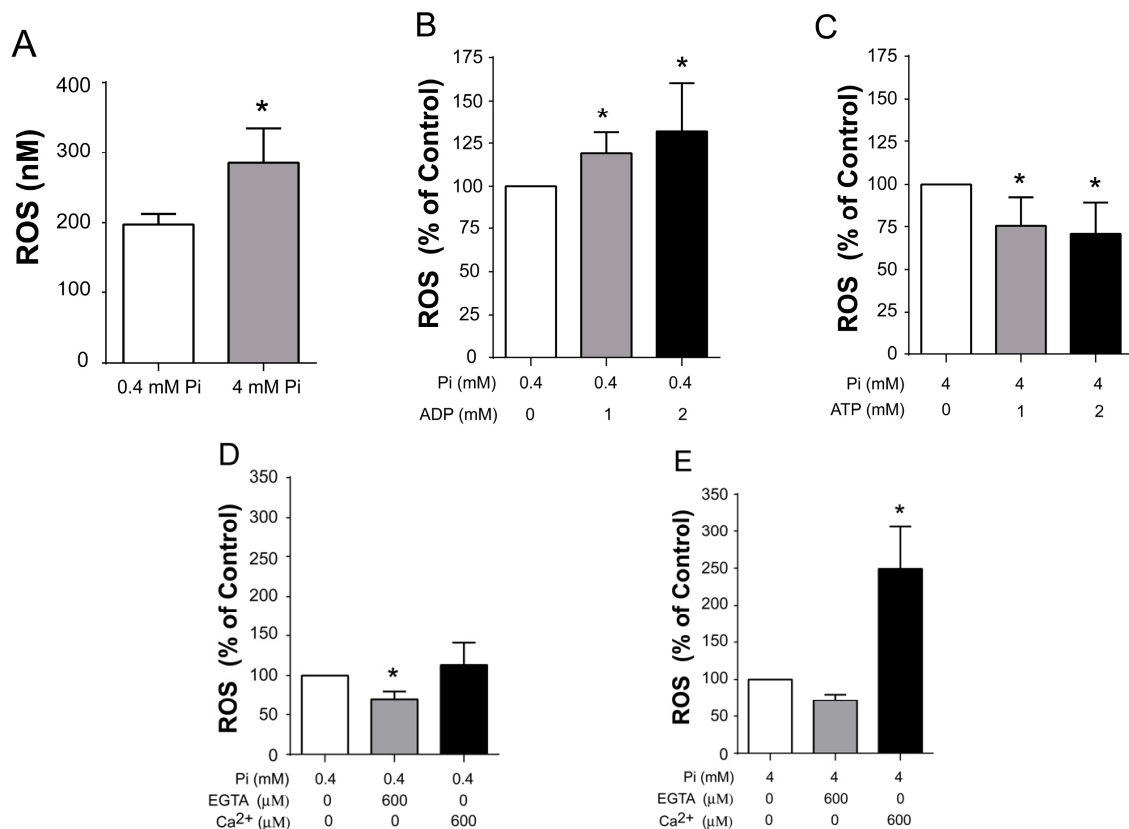


Figure 7. ROS production by *S. cerevisiae* mitochondria under different open/close states of s_c MUC. Production of peroxide was measured following resorufin fluorescence in a PolarStar Omega detector (571–585 nm); the results were interpolated against a calibration curve. (A) Total ROS in nM. Mitochondria incubated with 0.4 mM or 4.0 mM phosphate, data represent the mean \pm standard deviation for three independent experiments (* $p < 0.05$, t test). From B to E, data are percentages of the control in (A,B) Mitochondria incubated with 0.4 mM phosphate with or without 1 or 2 mM ADP, (C) Mitochondria incubated with 4 mM phosphate with or without 1 or 2 mM ATP, (D) Mitochondria incubated with 0.4 mM phosphate with or without 600 μ M EGTA or Ca^{2+} and (E) Mitochondria incubated with 4 mM phosphate with or without 600 μ M EGTA or Ca^{2+} . Data in (B–E) represent the mean \pm standard deviation for three independent experiments (* indicates significant), Dunnett’s multiple comparisons test. (Note that the ROS percentage scale for figures (B and C) are different from (D and E). Raw data for this figure are in Supplementary Table S1.

At 0.4 m Pi, ROS production was lower than at 4.0 mM Pi, suggesting as expected, that a closed s_c MUC enhanced ROS production (Figure 7A, Table S1). Then, to test other effectors used here, at 0.4 mM Pi, ADP was added at 1 or 2 mM, which closed s_c MUC (Figures 2–5), observing that ROS production increased (Figure 7B, Table S1). In contrast, in the presence of 4 mM Pi where s_c MUC was closed, addition of ATP, which opens s_c MUC (Figures 2–5), inhibited ROS production (Figure 7C, Table S1). Under the same low or high Pi concentrations, the effects of Ca^{2+} chelation or addition were tested. As expected from the results shown in Figure 6, at 0.4 mM Pi, EGTA decreased ROS production, while Ca^{2+} addition mildly increased ROS production (Figure 7D, Table S1). Then, at 4.0 mM Pi, EGTA inhibited ROS production, while Ca^{2+} addition resulted in more than twice as

much produced ROS (Figure 7E, Table S1). Thus, when s_c MUC is closed ROS production is higher than when s_c MUC is open. These results are in agreement with the idea that an open s_c MUC is a physiological uncoupler of oxidative phosphorylation that inhibits production of ROS.

Together, our results add to the idea that the permeability transition protects mitochondria and thus the cell against stress. Effectors such as ATP and ADP probably control OxPhos in response with the energy charge, where high ATP signals for uncoupling. In addition, Ca^{2+} promotes a stronger response and prepares the cell in advance for high energy-requiring processes such as duplication of gene exchange with other cells [11–13] (Table 1).

Table 1. Summary of Results.

Low or High Pi without Additions	Effector Additions
s_c MUC is OPEN at 0.4 mM Pi	and CLOSED by ADP 0.5 to 2 mM Ca^{2+} 100 to 600 μ M
s_c MUC is CLOSED at 4.0 mM Pi	and OPENED by ATP 0.5 to 2.0 mM
At both Low and high Pi, alternating ADP/ATP close/open s_c MUC respectively	
At low Pi, Ca^{2+} addition/chelation close/open s_c MUC respectively	
Ca^{2+} is highly efficient to revert opening of s_c MUC, even after 4 min of incubation.	
DATA	
OPEN s_c MUC	CLOSED s_c MUC
High Rate of Oxygen consumption	Low rate of oxygen consumption
Low $\Delta\Psi$	High $\Delta\Psi$
Extensive mitochondrial swelling	Low to nil mitochondrial swelling
Low ROS generation	High ROS production

4. Discussion

During fermentation, *S. cerevisiae* extracts all the energy it needs from glucose, while producing ethanol [28]. Under these conditions, ATP is high, so the F_1F_0 ATP synthase is not required and thus it does not dissipate $\Delta\Psi$. A high $\Delta\Psi$ would inhibit the rate of oxygen consumption by the respiratory chain (RC) [1], however RC does work at a high rate in order to oxidize NADH and produce the NAD^+ needed for glyceraldehyde-3-phosphate dehydrogenase activity [29]. Therefore, during fermentation, mitochondrial OxPhos has to be uncoupled. Uncoupling is due to ATP itself, as it promotes opening of s_c MUC [5–7] (Figures 2–4). An open s_c MUC dissipates the mitochondrial $\Delta\Psi$, accelerating the rate of electron transfer in the respiratory chain [1]. In contrast, when fermentation substrates are depleted, ATP is hydrolyzed to ADP, which is a negative s_c MUC effector and thus promotes the recovery of a high $\Delta\Psi$ [7,8]. Different reports [30–32] and data presented here (Figures 2–4), suggest that opening/closing of s_c MUC is not an all-or-nothing event, but instead partial opening states modulate the degree of uncoupling. Such modulation would be a mechanism to coordinate OxPhos and fermentation as needed [32]. Indeed, our results suggest that the degree of s_c MUC opening is gradual and depends on ATP/(ADP + Pi) concentrations (Figures 2–4). The physiological role of permeability transition may profit from the eventual elucidation of the structure of the pore, which seems to be approaching fast [33].

In addition to adenine nucleotides, Ca^{2+} is an important negative effector of s_c MUC. This contrasts with mammalian cells, where Ca^{2+} works in the opposite sense, i.e., in the mammalian mitochondrial permeability transition pore (mPTP) opening is triggered by Ca^{2+} [34,35]. In the resting state cytoplasmic Ca^{2+} is below 100 nM both in *S. cerevisiae*, and in mammalian cells, while external Ca^{2+} is in the mM range [11]. Several transport systems use this massive gradient to allow Ca^{2+} entry through specialized channels in

the plasma membrane to the cytoplasm where it acts as a secondary messenger [36,37]. Again, at variance with most cells, where these transients last less than a minute, in *S. cerevisiae* cytoplasmic Ca^{2+} may remain high for as long as 20 min [12,13]. Thus, Ca^{2+} closes $s_c\text{MUC}$, enhancing OxPhos, while $s_c\text{MUC}$ may remain open for several minutes and still be reversible. In contrast, in mammals, mPTP opening is dangerous as it uncouples OxPhos and may eventually deplete ATP and trigger cell death through mitochondrial signaling [38].

In yeast, when an event requiring high amounts of energy occurs, Ca^{2+} enters the cell increasing ATP production. One such event may be the mating response, where massive morphologic changes occur that seem to consume a large amount of ATP [39]. Another event where Ca^{2+} enters the cell is phase S1 of the *S. cerevisiae* cell cycle when again it is likely that large amounts of ATP are needed in order to synthesize macromolecules [40]. Both mating and the S1 phase of the cell cycle are events where high mitochondrial ATP production is needed [16]. In these circumstances Ca^{2+} would enable OxPhos coupling by closing $s_c\text{MUC}$ and increasing $\Delta\Psi$.

The mammalian mitochondrial permeability transition pore (mPTP) is widely considered as an equivalent entity to $s_c\text{MUC}$. Indeed, both mPTP and $s_c\text{MUC}$ possess similar cutoff diameters [41] and react in similar fashion to some effectors such as adenine nucleotides [6,22] or to pharmacological agents such as bongkrekic acid or atractyloside [40]. However, the response to Ca^{2+} is the opposite as Ca^{2+} opens mPTP [42] while it closes $s_c\text{MUC}$ [22,27]. In order to obtain coupled mammalian mitochondria, Mg^{2+} or Ca^{2+} chelators have to be added to the isolation medium, while this is not needed in yeast mitochondria [5–7,18]. Additionally, it must be considered that the structure of the channel is still under debate and some components that seem to participate in one channel are not present in the other. One such component may be PiC, which in yeast controls opening and confers sensitivity to Pi [24], but when manipulated in heart mice, it does not modify the properties of mPTP [43]. These results suggest that the still undefined components of mitochondrial permeability transition pores may be different for each species [44]. Furthermore, in mPTP, components of the Ca^{2+} uniporter machinery modify mPTP activity [45,46], while this is not possible in *S. cerevisiae* where there is no Ca^{2+} uniporter [47–49]. Thus, it is probably not safe to assume that mPTP and $s_c\text{MUC}$ are identical entities.

In the mammalian heart, reversal of pore opening has also been reported [24–27], although opening of mPTP seems to react to different events than in *S. cerevisiae*. It is observed during cardiac stress, intermittent episodes of reperfusion allow the cell to empty Ca^{2+} while replenishing ATP pools. Thus, in mammals, mPTP seems important to prevent ROS overproduction through mitochondrial uncoupling, greatly improving survival probabilities [50]. This procedure is termed conditioning. Thus, even though both $s_c\text{MUC}$ and mPTP constitute a mitochondrial uncoupling device, the role of $s_c\text{MUC}$ opening is to oxidize NADH in a species that does not suffer from hypoxia [51].

Other yeast species also present some peculiarities that contribute to the idea that perhaps permeability transition pores are different. It is not clear whether *Yarrowia lipolytica* and perhaps *Endomyces magnusii* undergo mitochondrial permeability transition [52], as this event does not occur except under extreme circumstances, when a calcium ionophore plus massive amounts of calcium are added [53]. Another yeast, *Debaryomyces hansenii*, does undergo PT, however, its channel exhibits a unique sensitivity to Na^+ and K^+ , which are negative effectors and such sensitivity is probably quite important as this yeast resides in marine environments and is used in salted cheese maturation [54].

In many species including *S. cerevisiae*, aging damages mtDNA, possibly through an excess in ROS that in turn increases activity of proteins that promote mtDNA recombination. Then mutations accumulate damaging mitochondria irreversibly in a “vicious cycle” [55,56].

Opening of $s_c\text{MUC}$ increases the rate of O_2 flow in the respiratory chain, preventing overproduction of ROS. This is not the only mechanism accelerating electron flow, as other proton sinks such as uncoupling proteins are differentially expressed upon exposure to stress [31]. A second mechanism promoting physiological uncoupling, where branched

respiratory chains differentially express their alternative redox enzymes such as alternative oxidase (AOX) or NADH dehydrogenases type 2 (NDH2), in order to increase electron flux in the respiratory chain either at the beginning of the stationary phase or when the cell is subjected to stress [56,57].

The Index of Hydrogen Deficiency (IHF) is another exceedingly interesting mechanism mitochondria use to prevent damage by ROS. In aging *Endomyces magnusii* (grown for up to 168 h), unsaturated fatty acids are replaced by their saturated counterparts. So, as palmitic and oleic acid are less susceptible to damage by ROS than unsaturated fatty acids, mitochondrial membranes are protected. In addition, in this species, an alternative AOX is expressed from the beginning of the stationary phase, so physiological uncoupling is also used to protect mitochondria [58].

The “Co-localization for Redox Regulation (CoRR) Hypothesis” must also be considered when explaining how damaged mitochondria are negatively selected to allow cell survival [57]. When protection fails, mitochondria containing damaged mtDNA are negatively selected. This is possible due to the coexistence in the same compartment of mitochondrial DNA with its encoded proteins. These proteins are the most hydrophobic and difficult to move from the nucleus to the mitochondrial matrix. Additionally the CoRR hypothesis proposes that these mtDNA-encoded proteins are vital for the structure of OxPhos complexes I, III, IV and V. Therefore, deleterious mutations in mtDNA proteins would result in OxPhos malfunction and elimination of mitochondria [58].

Together, physiological uncoupling, IHF and mtDNA-encoded proteins (as proposed by the CoRR hypothesis), provide mitochondria with mechanisms to respond to exposure to stress, increased ROS and improve cell survival. Furthermore, regulation of s_c MUC by the energy charge and by Ca^{2+} signaling point to a role of s_c MUC in metabolic control, controlling fermentation, OxPhos and ROS production. In addition, a system to deplete O_2 would confer yeast with an advantage over other organisms as few other cells thrive under hypoxic/anoxic conditions. Probably the equilibrium between ATP and ADP works to graduate s_c MUC responses, while Ca^{2+} signals an event where OxPhos has to be recruited.

Supplementary Materials: The following is available online at <https://www.mdpi.com/article/10.3390/life11121307/s1>. Table S1: Raw data used to generate Figure 7.

Author Contributions: Conceptualization, S.U.-C. and N.C.-F.; methodology; software, formal analysis, investigation, L.M.-G., C.R.-G., P.C.-T., N.C.-F.; writing-original draft preparation, L.M.-G. and C.R.-G.; writing-review and editing; N.C.-F., P.C.-T. and S.U.-C.; supervision, N.C.-F. and S.U.-C. Funding, S.U.-C. All authors have read and agreed to the published version of the manuscript.

Funding: This research was partially funded by DGAPA/PAPIIT/UNAM, Project IN208821.

Institutional Review Board Statement: Not applicable as no humans nor animals were involved in these studies.

Informed Consent Statement: Not applicable as no humans nor animals were involved in these studies.

Acknowledgments: L.M.-G. is a student at the Programa de Doctorado en Ciencias Biomédicas at Universidad Nacional Autónoma de México (UNAM). C.R.-G. is an MsC student at the Programa de Posgrado en Ciencias Bioquímicas at UNAM. P.C.-T. is a student at the Programa de Posgrado en Ciencias Bioquímicas at UNAM, P.C.-T. (CVU 708685), L.M.-G. (CVU 695222) and C.R.-G. (CVU 966402) are CONACyT fellows.

Conflicts of Interest: The authors declare no conflict of interest.

References

1. Nicholls, D.G.; Ferguson, S.J. *Bioenergetics 4*, 4th ed.; Academic Press Inc.: London, UK, 2013; ISBN 9780123884251.
2. Gena, P.; del Buono, N.; D’Abicco, M.; Mastrodonato, M.; Berardi, M.; Svelto, M.; Lopez, L.; Calamita, G. Dynamical Modeling of Liver Aquaporin-9 Expression and Glycerol Permeability in Hepatic Glucose Metabolism. *Eur. J. Cell Biol.* **2017**, *96*, 61–69. [[CrossRef](#)]
3. Hatefi, Y. The Mitochondrial Electron Transport and Oxidative Phosphorylation System. *Annu. Rev. Biochem.* **1985**, *54*, 1015–1069. [[CrossRef](#)]

4. Mazat, J.-P.; Devin, A.; Ransac, S. Modelling mitochondrial ROS production by the respiratory chain. *Cell. Mol. Life Sci.* **2020**, *77*, 455–465. [[CrossRef](#)] [[PubMed](#)]
5. Prieto, S.; Bouillaud, F.; Ricquier, D.; Rial, E. Activation by ATP of a Proton-Conducting Pathway in Yeast Mitochondria. *Eur. J. Biochem.* **1992**, *208*, 487–491. [[CrossRef](#)] [[PubMed](#)]
6. Castrejón, V.; Parra, C.; Moreno, R.; Peña, A.; Uribe, S. Potassium Collapses the ΔP in Yeast Mitochondria While the Rate of ATP Synthesis Is Inhibited Only Partially: Modulation by Phosphate. *Arch. Biochem. Biophys.* **1997**, *346*, 37–44. [[CrossRef](#)] [[PubMed](#)]
7. Guérin, B.; Bunoust, O.; Rouqueys, V.; Rigoulet, M. ATP-Induced Unspecific Channel in Yeast Mitochondria. *J. Biol. Chem.* **1994**, *269*, 25406–25410. [[CrossRef](#)]
8. Di Bartolomeo, F.; Malina, C.; Campbell, K.; Mormino, M.; Fuchs, J.; Vorontsov, E.; Gustafsson, C.M.; Nielsen, J. Absolute Yeast Mitochondrial Proteome Quantification Reveals Trade-off between Biosynthesis and Energy Generation during Diauxic Shift. *Proc. Natl. Acad. Sci. USA.* **2020**, *117*, 7524–7535. [[CrossRef](#)]
9. Lin, Z.; Wang, T.Y.; Tsai, B.S.; Wu, F.T.; Yu, F.J.; Tseng, Y.J.; Sung, H.M.; Li, W.H. Identifying Cis-Regulatory Changes Involved in the Evolution of Aerobic Fermentation in Yeasts. *Genome Biol. Evol.* **2013**, *5*, 1065–1078. [[CrossRef](#)]
10. Cabrera-Orefice, A.; Ibarra-García-Padilla, R.; Maldonado-Guzmán, R.; Guerrero-Castillo, S.; Luévano-Martínez, L.A.; Pérez-Vázquez, V.; Gutiérrez-Aguilar, M.; Uribe-Carvajal, S. The *Saccharomyces cerevisiae* Mitochondrial Unselective Channel Behaves as a Physiological Uncoupling System Regulated by Ca^{2+} , Mg^{2+} , Phosphate and ATP. *J. Bioenerg. Biomembr.* **2015**, *47*, 477–491. [[CrossRef](#)]
11. Carafoli, E. Intracellular Calcium Homeostasis. *Annu. Rev. Biochem.* **1987**, *56*, 395–433. [[CrossRef](#)]
12. Iida, H.; Sakaguchi, S.; Yagawa, Y.; Anraku, Y. Cell Cycle Control by Ca^{2+} in *Saccharomyces cerevisiae*. *J. Biol. Chem.* **1990**, *265*, 21216–21222. [[CrossRef](#)]
13. Iida, H.; Yagawa, Y.; Anraku, Y. Essential Role for Induced Ca^{2+} Influx Followed by $[Ca^{2+}]_i$ Rise in Maintaining Viability of Yeast Cells Late in the Mating Pheromone Response Pathway. A Study of $[Ca^{2+}]_i$ in Single *Saccharomyces cerevisiae* Cells with Imaging of Fura-2. *J. Biol. Chem.* **1990**, *265*, 13391–13399. [[CrossRef](#)]
14. Chalmers, S.; Nicholls, D.G. The Relationship between Free and Total Calcium Concentrations in the Matrix of Liver and Brain Mitochondria. *J. Biol. Chem.* **2003**, *278*, 19062–19070. [[CrossRef](#)]
15. Madden, K.; Snyder, M. Cell Polarity and Morphogenesis in Budding Yeast. *Annu. Rev. Microbiol.* **1998**, *52*, 687–744. [[CrossRef](#)] [[PubMed](#)]
16. Shellhammer, J.P.; Pomeroy, A.E.; Li, Y.; Dujmusic, L.; Elston, T.C.; Hao, N.; Dohlman, H.G. Quantitative Analysis of the Yeast Pheromone Pathway. *Yeast* **2019**, *36*, 495–518. [[CrossRef](#)]
17. Uribe, S.; Ramirez, J.; Peña, A. Effects of Beta-Pinene on Yeast Membrane Functions. *J. Bacteriol.* **1985**, *161*, 1195–1200. [[CrossRef](#)] [[PubMed](#)]
18. Díaz-Ruiz, R.; Avéret, N.; Araiza, D.; Pinson, B.; Uribe-Carvajal, S.; Devin, A.; Rigoulet, M. Mitochondrial Oxidative Phosphorylation Is Regulated by Fructose 1,6-Bisphosphate. *J. Biol. Chem.* **2008**, *283*, 26948–26955. [[CrossRef](#)]
19. Gornall, A.G.; Bardawill, C.J.; David, M.M. Determination of Serum Proteins by Means of the Biuret Reaction. *J. Biol. Chem.* **1949**, *177*, 751–766. [[CrossRef](#)]
20. Åkerman, K.E.O.; Wikström, M.K.F. Safranin as a Probe of the Mitochondrial Membrane Potential. *FEBS Lett.* **1976**, *68*, 191–197. [[CrossRef](#)]
21. Guerrero-Castillo, S.; Cabrera-Orefice, A.; Vázquez-Acevedo, M.; González-Halphen, D.; Uribe-Carvajal, S. During the stationary growth phase, *Yarrowia lipolytica* prevents the overproduction of reactive oxygen species by activating an uncoupled mitochondrial respiratory pathway. *Biochim. Biophys. Acta.* **2012**, *1817*, 353–362. [[CrossRef](#)]
22. Manon, S.; Roucou, X.; Guérin, M.; Rigoulet, M.; Guérin, B. Minireview: Characterization of the Yeast Mitochondria Unselective Channel: A Counterpart to the Mammalian Permeability Transition Pore? *J. Bioenerg. Biomembr.* **1998**, *30*, 419–429. [[CrossRef](#)]
23. Gutiérrez-Aguilar, M.; Pérez-Martínez, X.; Chávez, E.; Uribe-Carvajal, S. In *Saccharomyces cerevisiae*, the Phosphate Carrier Is a Component of the Mitochondrial Unselective Channel. *Arch. Biochem. Biophys.* **2010**, *494*, 184–191. [[CrossRef](#)]
24. Lu, X.; Kwong, J.Q.; Molckentin, J.D.; Bers, D.M. Individual Cardiac Mitochondria Undergo Rare Transient Permeability Transition Pore Openings. *Circ. Res.* **2016**, *118*, 834–841. [[CrossRef](#)]
25. Boyman, L.; Coleman, A.K.; Zhao, G.; Wescott, A.P.; Joca, H.C.; Greiser, B.M.; Karbowski, M.; Ward, C.W.; Lederer, W.J. Dynamics of the Mitochondrial Permeability Transition Pore: Transient and Permanent Opening Events. *Arch. Biochem. Biophys.* **2019**, *666*, 31–39. [[CrossRef](#)] [[PubMed](#)]
26. Belosludtsev, K.N.; Dubinin, M.V.; Belosludtseva, N.V.; Mironova, G.D. Mitochondrial Ca^{2+} Transport: Mechanisms, Molecular Structures, and Role in Cells. *Biochemistry* **2019**, *84*, 593–607. [[CrossRef](#)]
27. Pérez-Vázquez, V.; Saavedra-Molina, A.; Uribe, S. In *Saccharomyces Cerevisiae*, Cations Control the Fate of the Energy Derived from Oxidative Metabolism Through the Opening and Closing of the Yeast Mitochondrial Unselective Channel. *J. Bioenerg. Biomembr.* **2003**, *35*, 231–241. [[CrossRef](#)] [[PubMed](#)]
28. Deed, R.C.; Pilkington, L.I. Lifestyle, Lineage, and Geographical Origin Influence Temperature-Dependent Phenotypic Variation across Yeast Strains during Wine Fermentation. *Microorganisms* **2020**, *8*, 1367. [[CrossRef](#)] [[PubMed](#)]

29. Vemuri, G.N.; Eiteman, M.A.; McEwen, J.E.; Olsson, L.; Nielsen, J. Increasing NADH Oxidation Reduces Overflow Metabolism in *Saccharomyces Cerevisiae*. *Proc. Natl. Acad. Sci. USA* **2007**, *104*, 2402–2407. [[CrossRef](#)]
30. Kruglov, A.G.; Kharechkina, E.S.; Nikiforova, A.B.; Odinkova, I.V.; Kruglova, S.A. Dynamics of the Permeability Transition Pore Size in Isolated Mitochondria and Mitoplasts. *FASEB J.* **2021**, *35*, 1–16. [[CrossRef](#)]
31. Balakirev, M.Y.; Zimmer, G. Gradual Changes in Permeability of Inner Mitochondrial Membrane Precede the Mitochondrial Permeability Transition. *Arch. Biochem. Biophys.* **1998**, *356*, 46–54. [[CrossRef](#)]
32. Guerrero-Castillo, S.; Araiza-Olivera, D.; Cabrera-Orefice, A.; Espinasa-Jaramillo, J.; Gutiérrez-Aguilar, M.; Luévano-Martínez, L.A.; Zepeda-Bastida, A.; Uribe-Carvajal, S. Physiological Uncoupling of Mitochondrial Oxidative Phosphorylation. Studies in Different Yeast Species. *J. Bioenerg. Biomembr.* **2011**, *43*, 323–331. [[CrossRef](#)]
33. Bernardi, P.; Carraro, M.; Lippe, G. The mitochondrial permeability transition: Recent progress and open questions. *FEBS J.* **2021**. [[CrossRef](#)]
34. Bernardi, P. Mechanisms for Ca²⁺-Dependent Permeability Transition in Mitochondria. *Proc. Natl. Acad. Sci. USA* **2020**, *117*, 2743–2744. [[CrossRef](#)]
35. Carraro, M.; Bernardi, P. Measurement of membrane permeability and the mitochondrial permeability transition. *Methods Cell Biol.* **2020**, *155*, 369–379.
36. Burgess, G.M.; Godfrey, P.P.; McKinney, J.S.; Berridge, M.J.; Irvine, R.F.; Putney, J.W. The Second Messenger Linking Receptor Activation to Internal Ca Release in Liver. *Nature* **1984**, *309*, 63–66. [[CrossRef](#)]
37. Kwon, E.; Heo, W. Do Optogenetic Tools for Dissecting Complex Intracellular Signaling Pathways. *Biochem. Biophys. Res. Commun.* **2020**, *527*, 331–336. [[CrossRef](#)] [[PubMed](#)]
38. Naumova, N.; Šachl, R. Regulation of Cell Death by Mitochondrial Transport Systems of Calcium and Bcl-2 Proteins. *Membranes* **2020**, *10*, 299. [[CrossRef](#)] [[PubMed](#)]
39. Prasad, K.R.; Rosoff, P.M. Characterization of the Energy-Dependent, Mating Factor-Activated Ca²⁺ Influx in *Saccharomyces cerevisiae*. *Cell Calcium* **1992**, *13*, 615–626. [[CrossRef](#)]
40. Carbó, N.; Tarkowski, N.; Ipiña, E.P.; Dawson, S.P.; Aguilar, P.S. Sexual Pheromone Modulates the Frequency of Cytosolic Ca²⁺ Bursts in *Saccharomyces cerevisiae*. *Mol. Biol. Cell* **2017**, *28*, 501–510. [[CrossRef](#)] [[PubMed](#)]
41. Carraro, M.; Giorgio, V.; Šileikytė, J.; Sartori, G.; Forte, M.; Lippe, G.; Zoratti, M.; Szabò, I.; Bernardi, P. Channel Formation by Yeast F-ATP Synthase and the Role of Dimerization in the Mitochondrial Permeability Transition. *J. Biol. Chem.* **2014**, *289*, 15980–15985. [[CrossRef](#)]
42. Haworth, R.A.; Hunter, D.R. Control of the Mitochondrial Permeability Transition Pore by High-Affinity ADP Binding at the ADP/ATP Translocase in Permeabilized Mitochondria. *J. Bioenerg. Biomembranes.* **2000**, *32*, 91–96. [[CrossRef](#)]
43. Kim, J.-S.; He, L.; Lemasters, J.J. Mitochondrial Permeability Transition: A Common Pathway to Necrosis and Apoptosis. *Biochem. Biophys. Res. Commun.* **2003**, *304*, 463–470. [[CrossRef](#)]
44. Gutiérrez-Aguilar, M.; Douglas, D.L.; Gibson, A.K.; Domeier, T.L.; Molkentin, J.D.; Baines, C.P. Genetic Manipulation of the Cardiac Mitochondrial Phosphate Carrier Does Not Affect Permeability Transition. *J. Mol. Cell. Cardiol.* **2014**, *72*, 316–325. [[CrossRef](#)]
45. Baines, C.P.; Gutiérrez-Aguilar, M. The Still Uncertain Identity of the Channel-Forming Unit(s) of the Mitochondrial Permeability Transition Pore. *Cell Calcium* **2018**, *73*, 121–130. [[CrossRef](#)] [[PubMed](#)]
46. Shanmughapriya, S.; Rajan, S.; Hoffman, N.E.; Higgins, A.M.; Tomar, D.; Nemani, N.; Hines, K.J.; Smith, D.J.; Eguchi, A.; Vallem, S.; et al. SPG7 Is an Essential and Conserved Component of the Mitochondrial Permeability Transition Pore. *Mol. Cell* **2015**, *60*, 47–62. [[CrossRef](#)] [[PubMed](#)]
47. Hurst, S.; Hoek, J.; Sheu, S.S. Mitochondrial Ca²⁺ and Regulation of the Permeability Transition Pore. *J. Bioenerg. Biomembr.* **2017**, *49*, 27–47. [[CrossRef](#)]
48. Uribe, S.; Rangel, P.; Pardo, J.P. Interactions of Calcium with Yeast Mitochondria. *Cell Calcium* **1992**, *13*, 211–217. [[CrossRef](#)]
49. Carafoli, E.; Lehninger, A.L. A Survey of the Interaction of Calcium Ions with Mitochondria from Different Tissues and Species. *Biochem. J.* **1971**, *122*, 681–690. [[CrossRef](#)]
50. Parks, R.J.; Murphy, E.; Liu, J.C. Mitochondrial Permeability Transition Pore and Calcium Handling. *Methods Mol. Biol.* **2018**, *1782*, 187–196. [[CrossRef](#)]
51. Rigoulet, M.; Bouchez, C.L.; Paumard, P.; Ransac, S.; Cuvellier, S.; Duvezin-Caubet, S.; Mazat, J.P.; Devin, A. Cell Energy Metabolism: An Update. *Biochim. Et Biophys. Acta (BBA)-Bioenerg.* **2020**, *1861*, 148276. [[CrossRef](#)]
52. Trendeleva, T.; Sukhanova, E.; Ural'skaya, L.; Saris, N.-E.; Zvyagil'skaya, R. Mitochondria from *Dipodascus (Endomyces) magnusii* and *Yarrowia lipolytica* Yeasts Did Not Undergo a Ca²⁺-Dependent Permeability Transition Even under Anaerobic Conditions. *J. Bioenerg. Biomembr.* **2011**, *43*, 623–631. [[CrossRef](#)]
53. Deryabina, Y.; Isakova, E.; Antipov, A.; Saris, N.-E.L. The Inhibitors of Antioxidant Cell Enzymes Induce Permeability Transition in Yeast Mitochondria. *J. Bioenerg. Biomembr.* **2013**, *45*, 491–504. [[CrossRef](#)]
54. Cabrera-Orefice, A.; Guerrero-Castillo, S.; Luévano-Martínez, L.A.; Peña, A.; Uribe-Carvajal, S. Mitochondria from the Salt-Tolerant Yeast *Debaryomyces hansenii* (Halophilic Organelles?). *J. Bioenerg. Biomembr.* **2010**, *42*, 11–19. [[CrossRef](#)] [[PubMed](#)]

-
55. Chen, X.J. Mechanism of Homologous Recombination and Implications for Aging-Related Deletions in Mitochondrial DNA. *Microbiol. Mol. Biol. Rev.* **2013**, *77*, 476–496. [[CrossRef](#)]
 56. Ling, F.; Yoshida, M. Rolling-Circle Replication in Mitochondrial Dna Inheritance: Scientific Evidence and Significance from Yeast to Human Cells. *Genes* **2020**, *11*, 514. [[CrossRef](#)] [[PubMed](#)]
 57. Aliyari Rad, S.; Dehghanian, Z.; Asgari Lajayer, B.; Nobaharan, K.; Astatkie, T. Mitochondrial Respiration and Energy Production Under Some Abiotic Stresses. *J. Plant Growth Regul.* **2021**. [[CrossRef](#)]
 58. Jayawardhane, J.; Cochrane, D.W.; Vyas, P.; Bykova, N.V.; Vanlerberghe, G.C.; Igamberdiev, A.U. Roles for Plant Mitochondrial Alternative Oxidase Under Normoxia, Hypoxia, and Reoxygenation Conditions. *Front. Plant Sci.* **2020**, *11*, 566. [[CrossRef](#)] [[PubMed](#)]

ORIGINAL ARTICLE

Open Access



Metabolism, ATP production and biofilm generation by *Staphylococcus epidermidis* in either respiratory or fermentative conditions

Ulrik Pedroza-Dávila¹, Cristina Uribe-Alvarez¹, Lilia Morales-García¹, Emilio Espinoza-Simón¹, Ofelia Méndez-Romero², Adriana Muhlia-Almazán², Natalia Chiquete-Félix¹ and Salvador Uribe-Carvajal^{1*}

Abstract

Staphylococcus epidermidis is a Gram-positive saprophytic bacterium found in the microaerobic/anaerobic layers of the skin that becomes a health hazard when it is carried across the skin through punctures or wounds. Pathogenicity is enhanced by the ability of *S. epidermidis* to associate into biofilms, where it avoids attacks by the host and antibiotics. To test the effect of oxygen on metabolism and biofilm generation, cells were cultured at different oxygen concentrations ($[O_2]$). As $[O_2]$ decreased, *S. epidermidis* metabolism went from respiratory to fermentative. Remarkably, the rate of growth decreased at low $[O_2]$ while a high concentration of ATP ([ATP]) was kept. Under hypoxic conditions bacteria associated into biofilms. Aerobic activity sensitized the cell to hydrogen peroxide-mediated damage. In the presence of metabolic inhibitors, biofilm formation decreased. It is suggested that at low $[O_2]$ *S. epidermidis* limits its growth and develops the ability to form biofilms.

Keywords: *Staphylococcus epidermidis*, Oxygen concentration, Metabolism, Biofilms, Rate of oxygen consumption, Fermentation

Introduction

Saprophytic microorganisms control pathogenic bacteria, digest nutrients and synthesize coenzymes, prosthetic groups and amino acids (Foster et al. 2005; Berg 1996; Sender et al. 2016). In the skin, *Staphylococcus epidermidis* inhibits colonization by *Staphylococcus aureus* or *Streptococcus pyogenes* secreting antimicrobial compounds and proteases (Cogen et al. 2010; Iwase et al. 2010). In the skin, *S. epidermidis* inhabits the epidermis, dermis and the nearly anoxic sebaceous glands (Grice and Segre 2011).

Staphylococcus epidermidis is frequently introduced through wounds and surgical procedures. A recent study reported the presence of antibiotic-resistant

S. epidermidis strains in 46% of hospital secondary infections (Chabi and Momtaz 2019). Many of these strains were resistant to at least three antibiotics (Chabi and Momtaz 2019). Indeed, many antibiotics have to be tested in order to treat *S. epidermidis* nosocomial infections (Roujansky et al. 2020). *S. epidermidis* is also found frequently in implanted devices such as valves and catheters. There is an active search for materials to coat implant surfaces which may prevent biofilm formation (Rabin et al. 2015). Among these, zirconium nitride has shown promise in orthopaedic implants (Pilz et al. 2019), while sphingosine coating is being used with success on implant titanium-surfaces (Beck et al. 2019). Inside the body, this bacterium has to face attack from the immune system, high $[O_2]$ (Fang et al. 2016) and antibiotics (Leid 2009), most likely triggering a stress response. Within the organism, *S. epidermidis* may find areas with low $[O_2]$, similar to its natural habitat; it is likely that the bacterium will make an effort to remain in the hypoxic

*Correspondence: suribe@ifc.unam.mx

¹ Department of Genetics and Molecular Biology, Instituto de Fisiología Celular, Universidad Nacional Autónoma de México (UNAM), Mexico City, Mexico

Full list of author information is available at the end of the article

area, adhering to the surface and organizing into biofilms (Lewis 2007; Uribe-Alvarez et al. 2016). In regard to hypoxic environments within the host, these are often found at or near artificial devices such as catheters or prosthetic valves, where biofilms may force removal of implanted devices (Fey and Olson 2010; Büttner et al. 2015).

Understanding the *S. epidermidis* response to different $[O_2]$ would help optimize treatments (Cotter et al. 2009). We have reported that growing *S. epidermidis* at different $[O_2]$ modifies expression of respiratory chain enzymes and the ability to form biofilms (Uribe-Alvarez et al. 2016). At high $[O_2]$, cytochrome oxidases and NADH dehydrogenases are abundant and biofilms are minimal. In contrast, $[O_2]$ depletion increases nitrate reductase expression and association into biofilms (Uribe-Alvarez et al. 2016).

Here, the effect of $[O_2]$ on both, the aerobic and anaerobic metabolism of *S. epidermidis* was evaluated, together with [ATP]. In addition, the sensitivity of *S. epidermidis* to the toxic effects of hydrogen peroxide was tested. In each case, the biofilm-forming activity of cells was measured (Lewis 2007). When ATP synthesis was inhibited to different degrees by inhibitors of respiration (cyanide) (Uribe-Alvarez et al. 2016) or glycolysis (1,4-bisphosphobutane) (Hartman and Barker 1965; Rosas-Lemus et al. 2016a), biofilm formation also decreased. It is suggested that *S. epidermidis* associates into biofilms as a strategy to avoid high $[O_2]$.

Materials and methods

Bacterial strain and growth media

Staphylococcus epidermidis strain ATCC 12228 was a kind donation from Dr. Juan Carlos Cancino Díaz (Instituto Politécnico Nacional, México). A loopful from the bacterium was suspended in 5 mL of 3% tryptic soy broth (Fluka, Sigma) and incubated at 37 °C for 24 h. Pre-cultures were added to 1 L LB medium (1% tryptone, 0.5% yeast extract, 1% NaCl) plus 2% glucose and incubated 24 h at 30 °C under aerobic (shaking 150 rpm), microaerobic (5% CO_2 , no agitation) or anaerobic (static in oxygen-depleted sealed acrylic chamber) conditions. Then the cells were washed three times at 5000×g for 10 min with distilled water and resuspended in 10 mM HEPES pH 7.4 (Uribe-Alvarez et al. 2016).

Cytoplasmic extracts

All procedures were conducted at 4 °C. Cells (grown under aerobic, microaerobic or anaerobic conditions) were centrifuged at 5000×g for 10 min, washed three times with distilled water and resuspended in 50 mL 10 mM HEPES, pH 7.4, supplemented with one tablet of protease-inhibitor cocktail (Complete) and 1 mM

PMSE. Cells were disrupted by sonication using a Sonics VibraCell sonicator (Sonics & materials, Inc., Newtown, CT) 7 × 20 s with 20 s intervals. To remove unbroken cells the suspension was centrifuged at 10,000×g for 10 min and the supernatant was recovered.

Protein concentration

Protein concentrations from intact *S. epidermidis* cells were determined by the biuret method (Gornall et al. 1949). Absorbance (540 nm) was measured in a Beckman-Coulter DU50 spectrophotometer. For cytoplasmic extracts, protein concentration was measured by Bradford at 595 nm, using 1 or 2 μL aliquots of the sample in a PolarStar Omega (BMG labtech, Ortenberg, Germany) (Bradford 1976).

Rate of oxygen consumption

The rate of oxygen consumption was measured in 10 mM HEPES pH 7.4 plus the indicated respiratory substrate. Bacteria, 0.5 mg prot mL⁻¹ were added to a water-jacketed 1 mL chamber at 37 °C equipped with a Clark type electrode connected to a Strathkelvin model 782 oxymeter. Data were analyzed using the 782 Oxygen System Software (Warner/Strathkelvin Instruments) (Uribe-Alvarez et al. 2016).

Ethanol production

Fermentation by cell cytoplasmic extracts (0.5 mg prot. mL⁻¹) was measured in 0.1 M MES-TEA, pH 7.0, 1.8 mM NAD plus either glucose or glycerol and incubated at 30 °C for 0, 2.5, 5 or 10 min. The reaction was stopped with 30% TCA, 0.1 mL and neutralized with NaOH. Ethanol was measured adding a 10 μL aliquot (0.005 mg) of the supernatant to 0.2 mL 114 mM K_2HPO_4 , pH 7.6. After 1 min, 30 μg ADH mL⁻¹ was added, the sample was incubated for 30 min and O.D. was determined at 340 nm in a POLARstar Omega. Ethanol is reported as μmol ethanol (mg prot)⁻¹ (Araiza-Olivera et al. 2013).

ATP concentration

ATP was measured in cytoplasm extracts resuspended to 0.025 mg protein in 0.15 mL reaction buffer (20 mM KH_2PO_4 , 40 mM Na_2HPO_4 , 80 mM NaCl, 1 mM $MgSO_4$). An ATP calibration curve was prepared freshly each day using lyophilized luciferase (Sigma-Aldrich). Luciferase was prepared following instructions by the provider and 0.02 mL was added to each sample in a 96-well microplate. Bioluminescence was detected in a POLARstar Omega luminometer (BGM LABTECH, Offenburg, Germany). [ATP] was reported as μmol (mg prot)⁻¹ (Palikaras and Tavernarakis 2016; Mendoza-Hoffmann et al. 2018).

Susceptibility to hydrogen peroxide-mediated damage

The effect of $[H_2O_2]$ on the viability of *S. epidermidis* was determined as previously reported (Macvanin and Hughes 2010). Briefly, cells were adjusted to an O.D. = 0.1 (600 nm) and then H_2O_2 (0 to 25 mM as indicated) was added to the reaction mixture. After 30 min, serial dilution of the cultures was performed in 0.9% NaCl and 10 μ L of the 1:1000 diluted sample was plated in LB, 2% glucose agar plates and incubated 24 h at 37 °C. Colony forming units (CFU) mL^{-1} were counted. The sample taken before H_2O_2 addition was assigned as 100%. The average of three experiments is shown with SD. ANOVA test and Tukey's multiple comparison-test were used. Significance was $*P < 0.0001$.

Biofilm formation and detection

Biofilm generation was measured in sterile Costar 96-well polystyrene plates as previously reported (Calà et al. 2015; Uribe-Alvarez et al. 2016). Briefly, in each well, 0.4% crystal violet in 33% glacial acetic acid was mixed with the indicated, inhibitors sodium cyanide (NaCN) (100 μ M), butane-1,4-bisphosphate (B1,4BP) (1 mM) or, carbonyl cyanide *m*-chlorophenyl hydrazone (CCCP) (0.1, 0.5, or 1 μ M, as indicated). Then bacteria were added to O.D. 0.02. Final volume 200 μ L. The plate was incubated 24 h at 37 °C with 5% CO_2 . After incubation, wells were washed twice with 200 μ L phosphate-buffered saline (PBS) to remove non-adherent bacteria. Plates were dried for 1 h at 60 °C, stained with 0.4% crystal violet for 10 min and washed under running tap water to remove excess stain. Absorbance (492 nm) was measured using a microplate reader (Polar Star Omega, BMG Labtech). Each sample was tested in three independent triplicate experiments and compared against the non-treated control using one-way variance analysis (ANOVA) plus Dunnett's post hoc test.

Results

Oxygen is among the most important factors driving evolution (Lane 2002). Its partial reduction products, the reactive oxygen species (ROS) destroy nucleic acids, proteins and membranes (Ezraty et al. 2017). Thus, to profit from its remarkable electron acceptor properties, organisms have to deal carefully with the dangerous oxygen molecule (Lane 2002; Rosas-Lemus et al. 2016b). *S. epidermidis* lives in hypoxic/anoxic environments, although it can adapt to high $[O_2]$. In order to follow the metabolic adaptation of *S. epidermidis* it was cultivated at different $[O_2]$. After 24 h under aerobic conditions biomass yield was 8.58 g/L, three times higher than

under microaerobiosis, 2.11 g/L or anaerobiosis, 1.75 g/L.

In order to further explore the basis for biomass yield variations at different $[O_2]$, the activity of the respiratory chain from *S. epidermidis* grown at different $[O_2]$ was measured (Fig. 1). As expected from previous respiratory chain protein expression results (Uribe-Alvarez et al. 2016), the ability of cells to consume oxygen was proportional to $[O_2]$ in the growth medium. In aerobic conditions and in the presence of lactate the rate of oxygen consumption was 70 natgO (mg prot. min) $^{-1}$, at least five times higher than in microaerobic media, where the rate was 5 natgO (mg prot. min) $^{-1}$ or in those grown under anaerobic conditions, where it was negligible (Fig. 1). Under normoxia the best respiratory fuel was lactate, which was oxidized around three times as fast as glucose or ethanol (Fig. 1).

In *S. epidermidis* respiratory chain activities correlated with growth rates. However, it was reasoned that in hypoxia glycolysis may constitute an important source of energy (Somerville and Proctor 2009). Furthermore, as *S. epidermidis*, normally lives at low $[O_2]$, fermentation may be the preferred energy-yielding pathway in this bacterium. To test this, *S. epidermidis* was grown at different $[O_2]$ and ethanol production from either glucose (Fig. 2a) or glycerol (Fig. 2b) was measured at 2.5, 5 and 10 min of incubation. Both substrates were equally efficient. However, at different $[O_2]$ large variations in the rate of fermentation were observed: bacteria from anaerobic media were the most active, (Fig. 2), suggesting that fermentation increases as $[O_2]$ decreases.

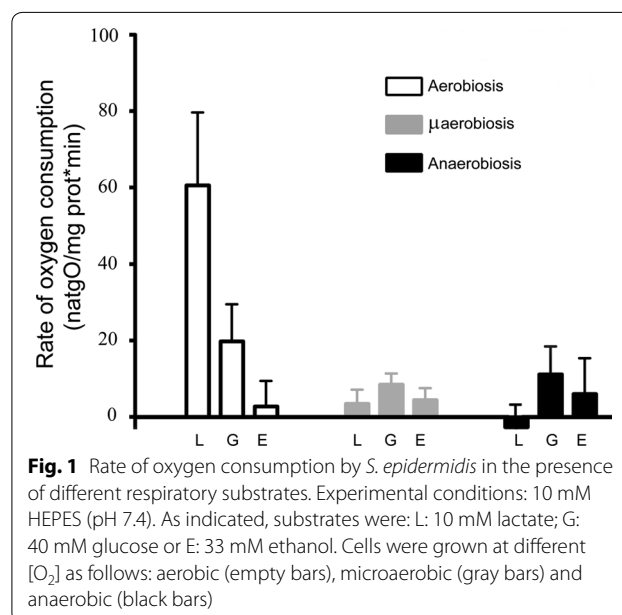
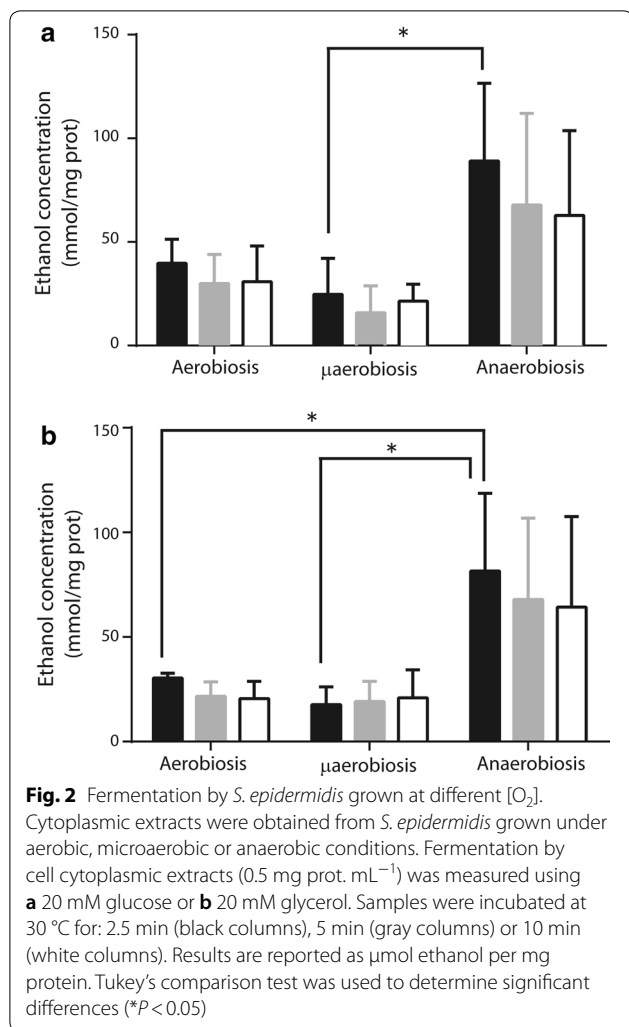
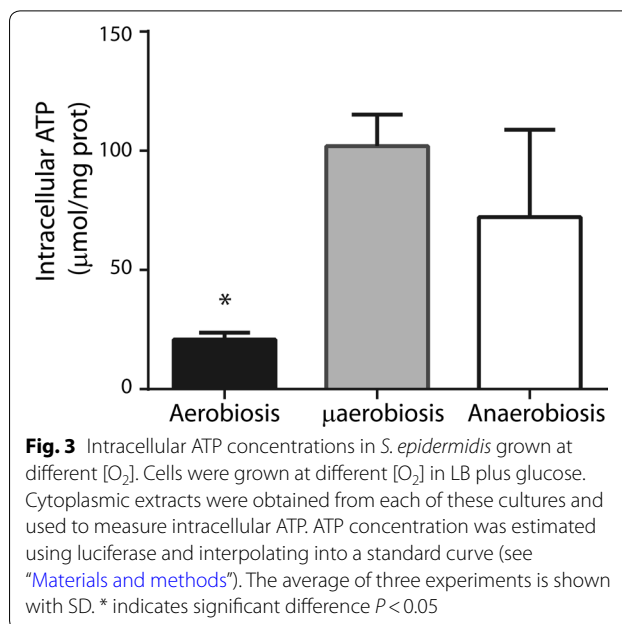


Fig. 1 Rate of oxygen consumption by *S. epidermidis* in the presence of different respiratory substrates. Experimental conditions: 10 mM HEPES (pH 7.4). As indicated, substrates were: L: 10 mM lactate; G: 40 mM glucose or E: 33 mM ethanol. Cells were grown at different $[O_2]$ as follows: aerobic (empty bars), microaerobic (gray bars) and anaerobic (black bars)



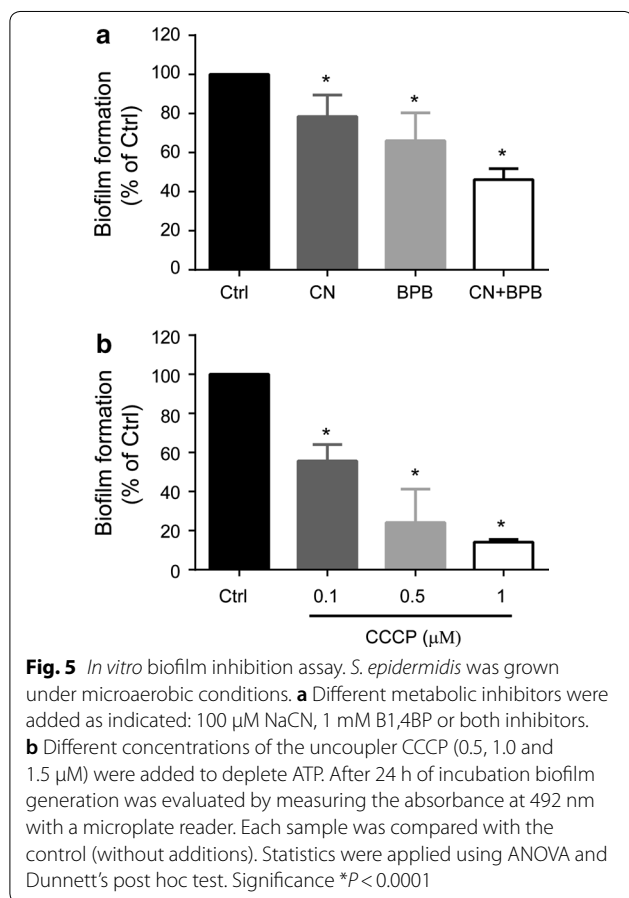
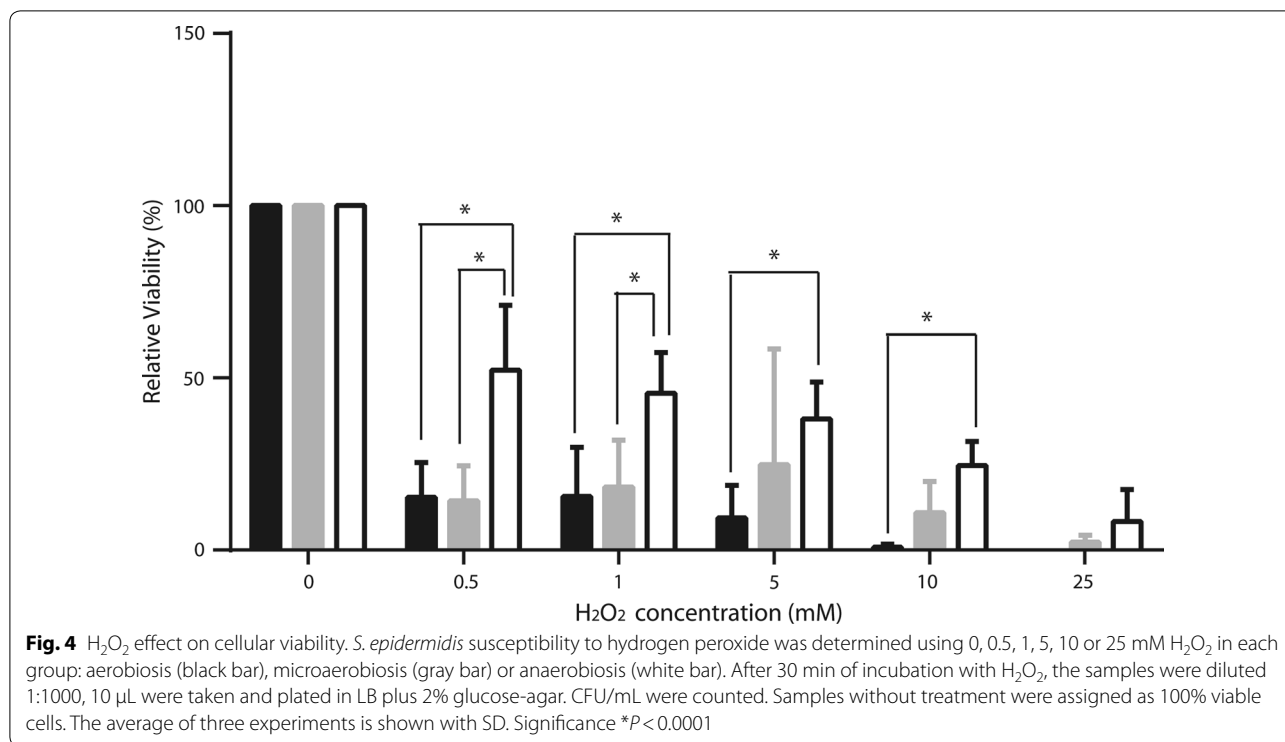
In *S. epidermidis*, increasing $[O_2]$ increased the rate of oxygen consumption while fermentation was inhibited. To determine which of these pathways produced more energy, the concentration of ATP ([ATP]) was measured in *S. epidermidis* grown under normoxia, hypoxia or anoxia (Fig. 3). Contrary to what we expected from the low growth rate and the slow respiratory activity observed, in hypoxia- and anoxia-grown cells, [ATP] was higher than in normoxia as aerobiosis, [ATP] increased roughly five times in hypoxia and three times in anoxia as compared to normoxia (Fig. 3).

In *S. aureus* a deficient respiratory chain confers resistance to H_2O_2 toxicity (Painter et al. 2017), suggesting that anaerobiosis-adapted cells resist oxidative stress better. Thus, we decided to test *S. epidermidis* grown at different $[O_2]$ for its sensitivity to H_2O_2 (Fig. 4) (Lobritz et al. 2015). Even at the lowest concentrations of H_2O_2 we used (0.5 mM), viability decreased in all cells. Aerobic-grown cells exhibited the poorest survival rates, while



cells grown under anaerobiosis survived best, such that even at the highest H_2O_2 concentration tested (25 mM H_2O_2) a small amount of viable cells was detected (Fig. 4). The increase in sensitivity to ROS observed in aerobically grown *S. epidermidis* was probably due to increased expression of the redox enzymes in the respiratory chain (Uribe-Alvarez et al. 2016). These redox enzymes contain different coenzymes and prosthetic groups, which normally become free radicals during their catalytic cycle (Quinlan et al. 2013; Rosas-Lemus et al. 2016b). Thus, as reported for *S. aureus* (Painter et al. 2017) at high $[O_2]$ *S. epidermidis* expressed an active respiratory chain and its sensitivity to H_2O_2 increased.

The highest [ATP] was detected in cells grown at low $[O_2]$, which exhibited a slow growth rate. This seemingly contradictory situation may be explained by proposing that when *S. epidermidis* finds a low $[O_2]$, which resembles that found in its normal niche, it makes an effort to attach itself to a surface, redirecting its energy use from growth to produce polysaccharides and proteins for biofilm generation (Beenken et al. 2004; Lewis 2007). To analyze whether biofilm was dependent on [ATP], *S. epidermidis* was grown under hypoxia and in the presence and absence of different metabolic inhibitors. In hypoxic grown-cells both oxidative phosphorylation and fermentation are active. It was observed that cells incubated in the presence of the respiratory chain inhibitor cyanide or the glycolytic inhibitor 1,4-bisphosphobutane, formed smaller biofilms than the control and that addition of both inhibitors led to even less biofilms (Fig. 5a). This would suggest that biofilm



formation activity is proportional to [ATP]. In addition, the uncoupler CCCP was used at concentrations below those where it killed cells (Result not-shown), observing that biofilm generation decreased further as uncoupler concentration increased (Fig. 5b). These results suggest that, regardless of its source, in *S. epidermidis* high [ATP] is needed to form biofilms.

Discussion

Antibiotic-resistant strains of *S. epidermidis* are increasingly found in nosocomial infections (Chabi and Montaz 2019). Implant removal due to *S. epidermidis* biofilm colonization is also quite frequent (Gristina 1987; Raad et al. 1998). *S. epidermidis* is frequently found in coagulase-negative staphylococci-caused prosthetic valve infective endocarditis cases (Mack et al. 2013), in 30–43% implant infections (Zimmerli et al. 2004) and in 50–70% catheter-related infections (von Eiff et al. 2002). Understanding the physiology of the bacterium is a must in order to design new treatment and prevention methods (Uribe-Alvarez et al. 2016). In biofilms, *S. epidermidis* cells are protected from the host. Thus, it is most important to analyse the association and specialization processes of the cells involved in the genesis of biofilms.

Diverse facultative bacteria adapt to wide $[O_2]$, differentially expressing redox enzymes in its respiratory chain. *S. epidermidis* does express different enzymes

at varying $[O_2]$ (Uribe-Alvarez et al. 2016). Aerobic metabolism enabled cells to grow more (Baez and Shiloach 2014). Still, enhanced growth resulted in higher sensitivity to H_2O_2 , suggesting that high contents of redox enzymes make cells vulnerable to ROS. Indeed, when grown at high $[O_2]$, sensitivity to ROS is enhanced in *S. aureus* and *Enterococcus faecalis*, while their mutant counterparts, lacking an efficient respiratory chain resist ROS better (Painter et al. 2017).

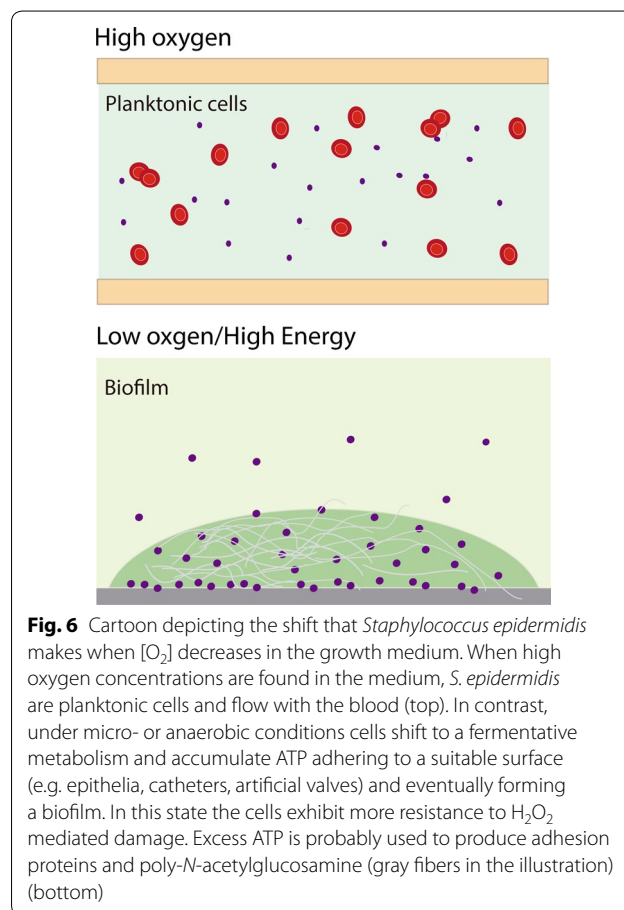
When exposing *S. epidermidis* grown in different $[O_2]$ to oxygen peroxide, we observed a similar phenomenon: cells grown in hypoxic or anoxic environments, which exhibited low respiratory rates were more resistant to oxygen peroxide (Fig. 4). Thus, as in *S. aureus*, the lack of an efficient respiratory chain in *S. epidermidis* enabled cells to survive ROS. This is probably useful when bacteria detached from a biofilm reach other tissues where they may be confronted with the oxidative burst generated by the immune system (Jensen et al. 1992).

The rate of oxygen consumption in aerobic grown cells was highest when lactate was the substrate. This is probably due to the direct donation of electrons to the menaquinone pool by lactate dehydrogenase (Götz and Mayer 2013; Kane et al. 2016). The slower rates observed for alcohol, may be due to an additional step as alcohol dehydrogenase electrons are first donated to Ndi2 (Artzatbanov and Petrov 1990). The rate of respiration was also slow for glucose, probably for the same reason, as intermediaries have to undergo many reactions before releasing electrons to the respiratory chain (Ferreira et al. 2013). In contrast, under anaerobiosis, lactate-dependent oxygen consumption disappeared completely while a small rate of glucose-dependent oxygen consumption was still present. In contrast, in *S. aureus* increased lactate dehydrogenase expression anaerobiosis has been reported (Fuchs et al. 2007).

The normal habitat for *S. epidermidis* is the microaerobic environment found in different epidermic and dermic layers (Peyssonnaud et al. 2008). One strategy *S. epidermidis* uses when confronted with high $[O_2]$ is the differential expression of a diverse number of redox enzymes in the respiratory chain. Reports indicate that when microaerophilic or anaerophilic bacteria find a suitable environment, they react manufacturing proteins and polysaccharides that enable them to form biofilms and attach to surfaces at low $[O_2]$. Avoiding high $[O_2]$ involves both, anchoring in low oxygen environments and building biofilms as barriers against penetration of ROS or toxic substances (Palikaras and Tavernarakis 2016). Metabolic adaptation has also been reported for *Neisseria gonorrhoeae*, when it is stimulated to form biofilms. A proteomic analysis of *N. gonorrhoeae* biofilms evidenced up-regulation of proteins involved in

anaerobic metabolism such as glycolysis and TCA cycle plus increased expression of those proteins involved in biofilm generation like pilus-associated proteins (Phillips et al. 2012). In addition, some oxidative stress genes are required for normal biofilm formation in *N. gonorrhoeae* (Falsetta et al. 2011).

The increase in ATP prior to biofilm formation has been reported in others bacterium. *Bacillus brevis* and *Escherichia coli* react to substrate depletion by adhering to glass surfaces and at the same time increase [ATP] two to fivefold as compared to planktonic cells (Hong and Brown 2009). So, the conditions where bacteria need to make biofilms promote saving ATP even at the expense of the growth rate. ATP is most likely needed to synthesize the extracellular proteins and the polysaccharide fibers that anchor cells to surfaces and to each other. Inhibiting ATP production in micro- or anaerobic conditions by adding cyanide or 1,4-bisphosphobutane resulted in a reduced biofilm formation (Fig. 5). This phenomenon is also observed when treating *S. epidermidis* with the nitrate reductase inhibitor methylamine in anaerobic conditions (Uribe-Alvarez et al. 2016). In contrast, in aerobiosis cyanide promotes biofilm formation (Uribe-Alvarez et al. 2016).



Even when facultative bacteria such as *S. epidermidis* survive at high [O₂], their habitat in the skin is hypoxic to anoxic. While they survive in aerobic environments their susceptibility to ROS-mediated damage and possibly to attack by macrophages increases. They thus present an oxygen avoidance behavior, anchoring and associating in hypoxic environments (Fig. 6). Learning how avoidance works in *S. epidermidis* and other bacteria would impact both the physiologic and therapeutic field.

Aiming to understand such rise in ATP, we found that other bacteria, e.g. *Bacillus brevis* and *Escherichia coli*, react to substrate depletion by adhering to glass surfaces and at the same time increase [ATP] two- to fivefold in comparison to planktonic cells (Hong and Brown 2009). In this regard, it has been reported that hypoxic stimuli induce biofilm formation in *S. epidermidis* (Uribe-Alvarez et al. 2016).

Acknowledgements

Partially funded by UNAM/DGAPA/PAPIIT grant IN203018 to SUC and CONACYT 241670 grant to AMA. UPD (MSc) and EES (PhD) are graduate students in the Biochemistry Program at UNAM. LMG is in the Biomedical PhD program at UNAM. OMR is a graduate student at CIAD. UPD, LMG and OMR are CONACYT fellows. CUA present address: Fox-Chase Cancer Center, Philadelphia, PA. Technical help from Ramón Méndez-Franco is acknowledged.

Authors' contributions

UPD, participated in all experiments and in discussions helping to write and edit the manuscript. CUA contributed to the original idea, she was the first author of the previous paper, participated in oxymetry experiments and in discussions helping to write and edit the manuscript. LMG participated in oxygen-consumption experiments and discussions on the manuscript. EES, participated in fermentation experiments and in discussions. OMR participated in the experiments performed both at CIAD and at UNAM and in discussions. AMA contributed with early ideas and designed some protocols, she provided reagents and facilities at CIAD and edited the manuscript. NCF taught graduate students the techniques involved in each experiment, supervising experimental work and protocols. SUC helped develop the original idea, designed the project, helped in technique application and wrote the manuscript. He provided facilities and found funding. Participated in lab discussions. All authors read and approved the final manuscript.

Ethics approval and consent to participate

This article does not contain any studies with human participants or animals performed by any of the authors.

Competing interests

The authors declare that they have no competing interests.

Author details

¹ Department of Genetics and Molecular Biology, Instituto de Fisiología Celular, Universidad Nacional Autónoma de México (UNAM), Mexico City, Mexico. ² Centro de Investigación y Desarrollo en Alimentos (CIAD), Hermosillo, Sonora, Mexico.

Received: 28 January 2020 Accepted: 31 January 2020

Published online: 11 February 2020

References

- Araza-Olivera D, Chiquete-Felix N, Rosas-Lemus M, Sampetro JG, Peña A, Mujica A, Uribe-Carvajal S (2013) A glycolytic metabolon in *Saccharomyces cerevisiae* is stabilized by F-actin. *FEBS J* 280:3887–3905. <https://doi.org/10.1111/febs.12387>
- Artztbanov VYu, Petrov VV (1990) Branched respiratory chain in aerobically grown *Staphylococcus aureus*—oxidation of ethanol by cells and protoplasts. *Arch Microbiol* 153:580–584
- Baez A, Shiloach J (2014) Effect of elevated oxygen concentration on bacteria, yeasts, and cells propagated for production of biological compounds. *Microb Cell Fact* 13:181. <https://doi.org/10.1186/s12934-014-0181-5>
- Beck S, Sehl C, Voortmann S, Verhasselt HL, Edwards MJ, Buer J, Hasenberg M, Gulbins E, Becker KA (2019) Sphingosine is able to prevent and eliminate *Staphylococcus epidermidis* biofilm formation on different orthopedic implant materials in vitro. *J Mol Med*. <https://doi.org/10.1007/s00109-019-01858-x>
- Beenken KE, Dunman PM, McAleese F, Macapagal D, Murphy E, Projan SJ, Blevins JS, Smeltzer MS (2004) global gene expression in *Staphylococcus aureus* biofilms. *J Bacteriol* 186:4665–4684. <https://doi.org/10.1128/JB.186.14.4665-4684.2004>
- Berg RD (1996) The indigenous gastrointestinal microflora. *Trends Microbiol* 4:430–435. [https://doi.org/10.1016/0966-842X\(96\)10057-3](https://doi.org/10.1016/0966-842X(96)10057-3)
- Bradford MM (1976) A rapid and sensitive method for the quantitation of microgram quantities of protein utilizing the principle of protein-dye binding. *Anal Biochem* 72:248–254
- Büttner H, Mack D, Rohde H (2015) Structural basis of *Staphylococcus epidermidis* biofilm formation: mechanisms and molecular interactions. *Front Cell Infect Microbiol* 5:14. <https://doi.org/10.3389/fcimb.2015.00014>
- Calà C, Amodio E, Di Carlo E, Virruso R, Fasciana T, Giammanco A (2015) Biofilm production in *Staphylococcus epidermidis* strains, isolated from the skin of hospitalized patients: genetic and phenotypic characteristics. *N Microbiol* 38:521–529
- Chabi R, Momtaz H (2019) Virulence factors and antibiotic resistance properties of the *Staphylococcus epidermidis* strains isolated from hospital infections in Ahvaz, Iran. *Trop Med Health* 47:56. <https://doi.org/10.1186/s41182-019-0180-7>
- Cogen AL, Yamasaki K, Sanchez KM, Dorschner RA, Lai Y, MacLeod DT, Torpey JW, Otto M, Nizet V, Kim JE, Gallo RL (2010) Selective antimicrobial action is provided by phenol-soluble modulins derived from *Staphylococcus epidermidis*, a normal resident of the skin. *J Invest Dermatol* 130(1):192–200
- Cotter JJ, O'Gara JP, Mack D, Casey E (2009) Oxygen-mediated regulation of biofilm development is controlled by the alternative sigma factor sigma(B) in *Staphylococcus epidermidis*. *Appl Environ Microbiol* 75:261–264. <https://doi.org/10.1128/AEM.00261-08>
- Ezraty B, Gennaris A, Barras F, Collet J-F (2017) The gain of single electrons by oxygen (O²) generates partially reduced reactive oxygen species (ROS), including superoxide anions (O^{2•-}). *Nat Publ Gr*. <https://doi.org/10.1038/nrmicro.2017.26>
- Falsetta ML, Steichen CT, McEwan AG, Cho C, Ketterer M, Shao J, Hunt J, Jennings MP, Apicella MA (2011) The composition and metabolic phenotype of *Neisseria gonorrhoeae* biofilms. *Front Microbiol* 2:75. <https://doi.org/10.3389/fmicb.2011.00075>
- Fang FC, Frawley ER, Tapscott T, Vázquez-Torres A (2016) Bacterial stress responses during host infection. *Cell Host Microbe* 20:133–143. <https://doi.org/10.1016/j.chom.2016.07.009>
- Ferreira MT, Manso AS, Gaspar P, Pinho MG, Neves AR (2013) Effect of oxygen on glucose metabolism: utilization of lactate in *Staphylococcus aureus* as revealed by in vivo NMR studies. *PLoS ONE* 8:e58277. <https://doi.org/10.1371/journal.pone.0058277>
- Fey PD, Olson ME (2010) Current concepts in biofilm formation of *Staphylococcus epidermidis*. *Future Microbiol* 5:917–933. <https://doi.org/10.2217/fmb.10.56>
- Foster J, Ganatra M, Kamal I, Ware J, Makarova K, Ivanova N, Bhattacharyya A, Kapatal V, Kumar S, Posfai J, Vincze T, Ingram J, Moran L, Lapidus A, Omelchenko M, Kyrpides N, Ghedin E, Wang S, Goltsman E, Joukov V, Ostrovskaya O, Tsukerman K, Mazur M, Comb D, Koonin E, Slatko B (2005) The Wolbachia genome of *Brugia malayi*: endosymbiont evolution within a human pathogenic nematode. *PLoS Biol* 3:e121. <https://doi.org/10.1371/journal.pbio.0030121>
- Fuchs S, Pané-Farré J, Kohler C, Hecker M, Engelmann S (2007) Anaerobic gene expression in *Staphylococcus aureus*. *J Bacteriol* 189:4275–4289. <https://doi.org/10.1128/JB.00081-07>
- Gornall AG, Bardawill CJ, David MM (1949) Determination of serum proteins by means of the biuret reaction. *J Biol Chem* 177:751–766

- Götz F, Mayer S (2013) Both terminal oxidases contribute to fitness and virulence during organ-specific *Staphylococcus aureus* colonization. *MBio* 4:e00976-13. <https://doi.org/10.1128/mBio.00976-13>
- Grice EA, Segre JA (2011) The skin microbiome. *Nat Rev Microbiol* 9:244–253. <https://doi.org/10.1038/nrmicro2537>
- Gristina AG (1987) Biomaterial-centered infection: microbial adhesion versus tissue integration. *Science* 237:1588–1595. <https://doi.org/10.1126/science.3629258>
- Hartman FC, Barker R (1965) An exploration of the active site of aldolase using structural analogs of fructose diphosphate. *Biochemistry* 4:1068–1075. <https://doi.org/10.1021/bi00882a014>
- Hong Y, Brown DG (2009) Variation in bacterial ATP level and proton motive force due to adhesion to a solid surface. *Appl Environ Microbiol* 75:2346–2353. <https://doi.org/10.1128/AEM.02671-08>
- Iwase T, Uehara Y, Shinji H, Tajima A, Seo H, Takada K, Agata T, Mizunoe Y (2010) *Staphylococcus epidermidis* Esp inhibits *Staphylococcus aureus* biofilm formation and nasal colonization. *Nature* 465:346–349. <https://doi.org/10.1038/nature09074>
- Jensen ET, Kharazmi A, Høiby N, Costerton JW (1992) Some bacterial parameters influencing the neutrophil oxidative burst response to *Pseudomonas aeruginosa* biofilms. *APMIS* 100:727–733. <https://doi.org/10.1111/j.1699-0463.1992.tb03991.x>
- Kane AL, Brutinel ED, Joo H, Maysonet R, VanDrise CM, Kotloski NJ, Gralnick JA (2016) Formate metabolism in *Shewanella oneidensis* generates proton motive force and prevents growth without an electron acceptor. *J Bacteriol* 198:1337–1346. <https://doi.org/10.1128/JB.00927-15>
- Lane N (2002) Oxygen: the molecule that made the world. Oxford University Press, Oxford
- Leid JG (2009) Bacterial biofilms resist key host defenses. *Microbe* 4:66–70
- Lewis K (2007) Persister cells, dormancy and infectious disease. *Nat Rev Microbiol* 5:48–56. <https://doi.org/10.1038/nrmicro1557>
- Lobritz MA, Belenky P, Porter CBM, Gutierrez A, Yang JH, Schwarz EG, Dwyer DJ, Khalil AS, Collins JJ (2015) Antibiotic efficacy is linked to bacterial cellular respiration. *Proc Natl Acad Sci USA* 112:8173–8180. <https://doi.org/10.1073/pnas.1509743112>
- Mack D, Davies AP, Harris LG, Jeeves R, Pascoe B, Knobloch JK-M, Rohde H, Wilkinson TS (2013) *Staphylococcus epidermidis* in biomaterial-associated infections. *Biomaterials associated infection*. Springer, New York, pp 25–56
- Macvanin M, Hughes D (2010) Assays of sensitivity of antibiotic-resistant bacteria to hydrogen peroxide and measurement of catalase activity. *Methods in molecular biology*. Humana Press, Clifton, pp 95–103
- Mendoza-Hoffmann F, Pérez-Oseguera Á, Cevallos MÁ, Zarco-Zavala M, Ortega R, Peña-Segura C, Espinoza-Simón E, Uribe-Carvajal S, García-Trejo JJ (2018) The biological role of the ζ subunit as unidirectional inhibitor of the F₁FO-ATPase of *Paracoccus denitrificans*. *Cell Rep* 22:1067–1078. <https://doi.org/10.1016/j.celrep.2017.12.106>
- Painter KL, Hall A, Ha KP, Edwards AM (2017) The electron transport chain sensitizes *Staphylococcus aureus* and *Enterococcus faecalis* to the oxidative burst. *Infect Immun*. <https://doi.org/10.1128/IAI.00659-17>
- Palikaras K, Tavernarakis N (2016) Intracellular assessment of ATP levels in *Caenorhabditis elegans*. *Bio-Protoc*. <https://doi.org/10.21769/BioProtoc.2048>
- Peyssonnaud C, Boutin AT, Zinkernagel AS, Datta V, Nizet V, Johnson RS (2008) Critical role of HIF-1 α in keratinocyte defense against bacterial infection. *J Invest Dermatol* 128:1964–1968. <https://doi.org/10.1038/JID.2008.27>
- Phillips NJ, Steichen CT, Schilling B, Post DMB, Niles RK, Bair TB, Falsetta ML, Apicella MA, Gibson BW (2012) Proteomic analysis of *Neisseria gonorrhoeae* biofilms shows shift to anaerobic respiration and changes in nutrient transport and outer membrane proteins. *PLoS ONE* 7:e38303. <https://doi.org/10.1371/journal.pone.0038303>
- Pilz M, Staats K, Tobudic S, Assadian O, Presterl E, Windhager R, Holinka J (2019) Zirconium nitride coating reduced *Staphylococcus epidermidis* biofilm formation on orthopaedic implant surfaces: an in vitro study. *Clin Orthop Relat Res* 477:461–466. <https://doi.org/10.1097/CORR.000000000000568>
- Quinlan CL, Perevoshchikova IV, Hey-Mogensen M, Orr AL, Brand MD (2013) Sites of reactive oxygen species generation by mitochondria oxidizing different substrates. *Redox Biol* 1:304–312. <https://doi.org/10.1016/j.redox.2013.04.005>
- Raad I, Alrahwani A, Rolston K (1998) *Staphylococcus epidermidis*: emerging resistance and need for alternative agents. *Clin Infect Dis* 26:1182–1187. <https://doi.org/10.1086/520285>
- Rabin N, Zheng Y, Opoku-Temeng C, Du Y, Bonsu E, Sintim HO (2015) Biofilm formation mechanisms and targets for developing antibiofilm agents. *Fut Med Chem* 7:493–512
- Rosas-Lemus M, Chiquete-Félix N, Ruiz-Pérez K, Rigoulet M, Devin A, Hernández-Rodríguez M, Uribe-Carvajal S (2016a) Sensitivity of the mitochondrial unspecific channel of *Saccharomyces cerevisiae* to butane-1,4-bisphosphate, a competitive inhibitor of fructose-1,6-bisphosphate-aldolase. *ChemistrySelect* 1:2930–2934. <https://doi.org/10.1002/slct.201600303>
- Rosas-Lemus M, Uribe-Alvarez C, Contreras-Zentella M, Luévano-Martínez LA, Chiquete-Félix N, Morales-García NL, Simón EE, Muhlia-Almazán A, Escamilla-Marván E, Uribe-Carvajal S (2016b) Oxygen: from toxic waste to optimal (toxic) fuel of life. Free radicals and diseases. Rijeka, InTech
- Roujansky A, Martin M, Gomart C, Hulin A, Mounier R (2020) Multidrug-resistant *Staphylococcus epidermidis* ventriculostomy-related infection successfully treated by intravenous ceftaroline after failure of daptomycin treatment. *World Neurosurg*. <https://doi.org/10.1016/j.wneu.2020.01.013>
- Sender R, Fuchs S, Milo R (2016) Revised estimates for the number of human and bacteria cells in the body. *PLoS Biol*. <https://doi.org/10.1371/journal.pbio.1002533>
- Somerville GA, Proctor RA (2009) At the crossroads of bacterial metabolism and virulence factor synthesis in Staphylococci. *Microbiol Mol Biol Rev* 73:233–248. <https://doi.org/10.1128/MMBR.00005-09>
- Uribe-Alvarez C, Chiquete-Félix N, Contreras-Zentella M, Guerrero-Castillo S, Peña A, Uribe-Carvajal S (2016) *Staphylococcus epidermidis*: metabolic adaptation and biofilm formation in response to different oxygen concentrations. *Pathog Dis* 74:ftv111. <https://doi.org/10.1093/femspd/ftv111>
- von Eiff C, Peters G, Heilmann C (2002) Pathogenesis of infections due to coagulase-negative staphylococci. *Lancet Infect Dis* 2:677–685. [https://doi.org/10.1016/s1473-3099\(02\)00438-3](https://doi.org/10.1016/s1473-3099(02)00438-3)
- Zimmerli W, Trampuz A, Ochsner PE (2004) Prosthetic-joint infections. *N Engl J Med* 351:1645–1654. <https://doi.org/10.1056/NEJMra040181>

Publisher's Note

Springer Nature remains neutral with regard to jurisdictional claims in published maps and institutional affiliations.



In *Saccharomyces cerevisiae*, withdrawal of the carbon source results in detachment of glycolytic enzymes from the cytoskeleton and in actin reorganization

E. Espinoza-Simón^a, N. Chiquete-Félix^a, L. Morales-García^a, U. Pedroza-Dávila^a, X. Pérez-Martínez^a, D. Araiza-Olivera^b, F. Torres-Quiroz^{c,*}, S. Uribe-Carvajal^{a,*}

^a Dept. Molecular Genetics, Inst. de Fisiología Celular, UNAM, Mexico City, Mexico

^b Dept. Biomacromol. Chemistry, Instituto de Química, UNAM, Mexico City, Mexico

^c Dept. Biochem., Inst. de Fisiología Celular, UNAM Mexico City, Mexico

ARTICLE INFO

Article history:

Received 26 June 2019

Received in revised form

20 September 2019

Accepted 9 October 2019

Available online 17 October 2019

Corresponding Editor: Steven Bates

Keywords:

Actin cytoskeleton dynamics

Fermentation

Glycolytic metabolon

Metabolic control

Starving

ABSTRACT

Metabolons are dynamic associations of enzymes catalyzing consecutive reactions within a given pathway. Association results in enzyme stabilization and increased metabolic efficiency. Metabolons may use cytoskeletal elements, membranes and membrane proteins as scaffolds. The effects of glucose withdrawal on a putative glycolytic metabolon/F-actin system were evaluated in three *Saccharomyces cerevisiae* strains: a WT and two different obligate fermentative (OxPhos-deficient) strains, which obtained most ATP from glycolysis. Carbon source withdrawal led to inhibition of fermentation, decrease in ATP concentration and dissociation of glycolytic enzymes from F-actin. Depending on the strain, inactivation/reactivation transitions of fermentation took place in seconds. In addition, when ATP was very low, green fluorescent protein-labeled F-actin reorganized from highly dynamic patches to large, non-motile actin bodies containing proteins and enzymes. Glucose addition restored fermentation and cytoskeleton dynamics, suggesting that in addition to ATP concentration, at least in one of the tested strains, metabolon assembly/disassembly is a factor in the control of the rate of fermentation.

© 2019 The Author(s). Published by Elsevier Ltd on behalf of British Mycological Society. This is an open access article under the CC BY license (<http://creativecommons.org/licenses/by/4.0/>).

1. Introduction

In the highly crowded cytoplasm, macromolecule concentrations reach 200–400 g/l (Fulton, 1982; Zimmerman and Trach, 1991). In this regard, protein and enzyme association inside living cells seems to be a widespread phenomenon (Schmitt and An, 2017) and there are cases where associations improve catalytic efficiency or regulation,

work as depots for functional enzymes or constitute aggregates of dysfunctional enzymes that may even result in pathology as in Alzheimer's, Parkinson's or Huntington's diseases (O'Connell et al., 2012). Associations of enzymes catalyzing consecutive reactions would optimize metabolism: The term “metabolon” was coined to describe a complex of sequential enzymes bound to structural elements (Srere, 1985). Metabolons improve catalytic efficiency through channeling of intermediates and enhancement of enzyme stability; these have been described in the Krebs cycle (Wu and Minter, 2015), in purine synthesis (Pedley and Benkovic, 2017) and in flavonoid synthesis (Jørgensen et al., 2005; Nakayama et al., 2019). Of interest is the ability of plants to rapidly adapt metabolons to produce different molecules as a response to challenges from the environment (Knudsen et al., 2018).

Very early, David Green proposed the existence of a “team of glycolytic enzymes” bound to membranes in both erythrocytes and yeast (Green et al., 1965). Later, glycolytic enzyme associations among themselves and with cytoskeleton elements were described in skeletal muscle (Clarke and Masters, 1975). In erythrocytes,

Abbreviations: ABP, actin binding protein; ALD, fructose 1,6 bis-phosphate aldolase; CCCP, carbonyl cyanide 3-chlorophenyl-hydrazone; FBPase, fructose 1,6 bis-phosphate phosphatase; GAPDH, glyceraldehyde 3 phosphate dehydrogenase; GFP, green fluorescent protein; HRP, horseradish peroxidase; LDH, lactate dehydrogenase; OxPhos, oxidative phosphorylation; PEPCK, phosphoenolpyruvate carboxykinase; PFK, phosphofructokinase; PGK, phosphoglycerate kinase; PKM, pyruvate kinase M; TBS, tris-buffered saline.

* Corresponding author. Circuito Exterior s/n Ciudad Universitaria, Coyoacán, 04510 D.F. Mexico. Fax: +52 55 56225630.

** Corresponding author. Circuito Exterior s/n Ciudad Universitaria, Coyoacán, 04510 D.F. Mexico. Fax: +52 55 56225630.

E-mail addresses: ftq@ifc.unam.mx (F. Torres-Quiroz), suribe@ifc.unam.mx (S. Uribe-Carvajal).

<https://doi.org/10.1016/j.funbio.2019.10.005>

1878-6146/© 2019 The Author(s). Published by Elsevier Ltd on behalf of British Mycological Society. This is an open access article under the CC BY license (<http://creativecommons.org/licenses/by/4.0/>).

proteins such as band 3, alpha-spectrin, beta-spectrin and ankyrin have been detected in association with glycolytic enzymes (Puchulu-Campanella et al., 2013). Association of the glycolytic enzymes to cytoskeletal elements include aldolase (ALD) and phosphofructokinase (PFK), which are stabilized by microtubules, optimizing their combined activity (Ra, 2000). In breast cancer cells, PFK co-localizes with pyruvate kinase (PK) or fructose 1,6 bis-phosphate phosphatase (FBPase) and phosphoenolpyruvate carboxykinase (PEPCK) (Kohnhorst et al., 2017). In hamster ovary cancer cells, glyceraldehyde-3-phosphate dehydrogenase (GAPDH) and lactate dehydrogenase (LDH) participate in a putative “glycolytic metabolon” bound to actin (Hudder et al., 2003). In this regard, it was predicted by an *in silico* assay that ALD binds actin (Menard et al., 2014).

Enzyme organization and dynamics depend on energy. In yeast, glucose starvation inhibits dynamics of chromatin and messenger ribonucleoproteins (mRNP) (Joyner et al., 2016), autophagy (Lu et al., 2004) and protein uptake (Ashe et al., 2000), while it enhances vacuolar hydrolysis (Lang et al., 2014). Also, enzymes involved in lipid biosynthesis are sequestered in foci (Suresh et al., 2015). When yeast cultures reach saturation or when incubated without glucose, enzymes, such as cytidine triphosphate synthase form filaments that disassemble upon returning to a rich medium (Noree et al., 2010).

The actin cytoskeleton plays a role in cell structure, migration, polarization, division and traffic. In yeast, actin is in equilibrium between monomeric and filamentous states (Moseley and Goode, 2006). Actin dynamics require accessory proteins such as Actin related protein (Arp2/3) and the Wiskott-Aldrich syndrome protein (Wasp) (Smith et al., 2001). Actin filaments may form actomyosin rings, cables and patches. Actin and accessory proteins as Abp1 (actin binding protein 1), Arp, Las 17 and Sla2 among others form highly motile patches that participate in endocytosis and exocytosis (Moseley and Goode, 2006). Upon cell division, patches are distributed equally into mother and daughter cells (Apodaca, 2001; Moseley and Goode, 2006). In the stationary phase, F-actin and actin-binding proteins form immobile “actin bodies”. Few hours after glucose deprivation, actin cables become stabilized and myosin cables release their cargo (Xu and Bretscher, 2014). Probably actin bodies are a reservoir from which actin cables and patches assemble as soon as nutrients become available (Sagot et al., 2006).

The glycolytic *Scerevisiae* enzymes GAPDH and phosphoglycerate kinase (PGK) are inhibited by viscosity unless ALD is added. Indeed, upon association with ALD, GAPDH increases twenty times its enzymatic activity and resists viscosity-mediated inhibition (Araiza-Olivera et al., 2010). Pharmacological stabilization of F-actin increases glycolytic enzyme binding and increases the rate of fermentation. Cytochalasin-mediated monomerization of actin filaments decreases both, metabolon assembly and rate of fermentation (Araiza-Olivera et al., 2013).

It was decided to study the effect of carbon source withdrawal on the stabilization/destabilization of a glycolytic metabolon. The response to carbon source starving was tested in WT yeast or in two different oxidative-phosphorylation-deficient, fermentation obligate *S. cerevisiae* strains, namely ρ^0 (Friis and Schultz, 2016) and *pet122Δ*, which fails to produce COX-III (Costanzo and Fox, 1990). The *pet122Δ* strain lacks the ability to translate COX-III, as it lacks PET122, a translation promoter that bridges the small ribosomal subunit with the COX-III mRNA. Still, this strain is ρ^+ and thus contains all the metabolic regulators that respond to glucose variations (Costanzo and Fox, 1990) In contrast, the ρ^0 strain has lost all its mitochondrial DNA and thus lacks many mechanisms to adapt to starvation (Friis and Schultz, 2016) Both mutants were highly sensitive to glucose starvation. ATP concentration ([ATP]) decreased and actin filaments were reorganized from patches to immotile bodies. The WT strain underwent these changes only in the

presence of an uncoupler. In all strains, glucose addition led to recovery of [ATP], actin dynamics and binding of enzymes to actin.

2. Materials and methods

2.1. Strains and culture media

The *S. cerevisiae* strains we acquired and/or generated are listed in Table 1. As indicated, culture media were: YP (1 % Yeast extract, 2 % Peptone), YPD (YP plus 2 % Dextrose), SD (Difco: YNB 1.7 g/100 mL, $(\text{NH}_4)_2\text{SO}_4$ 5 % and an amino acid mix) or SD-Gluc (SD plus 2 % glucose) at 30 °C. Cells were grown overnight at 30 °C in a rotating carousel at 50 rpm (Cel-Gro Tissue Culture Rotator, Thermo Scientific). Where indicated, cultures were transferred to Erlenmeyer flasks and incubated under agitation at 250 rpm.

2.2. Glycolytic enzymes binding to F-actin or among themselves

Actin association of ALD, GAPDH and PGK was evaluated by co-immunoprecipitation (Araiza-Olivera et al., 2013). In addition, the association of ALD with GAPDH and PGK was evaluated using the same method. Mouse monoclonal anti-actin (ab 14128; Abcam), protein G agarose (sc-2002; Santa Cruz Biotech), mouse monoclonal anti-ALD (ab 169544; Abcam), rabbit polyclonal anti-GAPDH (FC335, Santa Cruz Biotech) and rabbit polyclonal anti-PGK (sc-28784, Santa Cruz Biotech) were used. In each case, antibodies (3 $\mu\text{g}/\text{mL}$) against actin or ALD were incubated with 20 μL protein A/G agarose during 30 min at 4 °C, mixed with cytoplasmic extract protein (1 mg/mL) and incubated at 4 °C overnight under agitation. Samples were collected and washed by centrifugation at $2000\times g$ for 10 min twice using IP buffer (50 mM Tris-HCl, pH 7.4, 1 mM PMSF, 0.1 % Tween 20), and protease inhibitor cocktail (sc 29130; Santa Cruz). All samples were diluted in sample buffer (62.5 mM Tris, pH 6.8, 10 % glycerol, 2 % SDS, 5 % β -mercaptoethanol and 0.01 % bromophenol blue) and boiled for 5 min. SDS/PAGE were performed in 10 % polyacrylamide. Proteins were electrotransferred to polyvinylidene difluoride (PVDF) membranes and blocked with 0.5 % albumin in TBS-T (10 mM Trizma base, 150 mM NaCl, 0.1 % Tween 20, pH 7.5) for 1 h and incubated overnight at 4 °C with primary antibody, washed with TBS-T and incubated 1 h with secondary antibody. Once membranes were washed exhaustively, bands were developed with Immobilon Western Chemiluminescent HRP substrate (Millipore).

2.3. ATP concentration

The concentration of ATP was determined by bioluminescence, using the ATP dependency of the luciferase catalyzed light-emitting oxidation of luciferin, which is capable of measuring extremely low concentrations of ATP (Deluca and McElroy, 1978). Intracellular ATP was measured using the ATP Bioluminescence Assay Kit CLS II (Roche); this Kit is especially optimized for the use in luminometers, exhibits a constant light signal sustaining for several minutes. To calculate the intracellular ATP concentration, an ATP calibration curve was prepared freshly each day, as indicated by the manufacturer of the ATP Bioluminescent Kit and using lyophilized luciferase reagent. The procedure was the following, cultures were grown as mentioned above for 4 h and 1×10^7 cells/mL were taken and resuspended in 100 mM Tris-HCl, 4 mM EDTA, pH 7.8. Cells were immersed in boiling water for 2 min and cell debris were removed by centrifugation at $15\,000\times g$. To quantify ATP concentration the supernatants were placed in the wells of a microplate and then the luciferase reagent was added. Measurements of experimental samples and standards were conducted in a POLARstar Omega luminometer (BMG Labtech, Germany) as reported by Mendoza-Hoffmann et al. (2018).

Table 1
S. cerevisiae strains used in this study.

Strain name	Strain genotype	Source
W3031-A	<i>MATa</i> { <i>leu2-3,112 trp1-1 can1-100 ura3-1 ade2-1 his3-11,15</i> }	Dr. A. Tzagaloff
W303 1-A Abp1-GFP	<i>MATa</i> { <i>leu2-3,112 trp1-1 can1-100 ura3-1 ade2-1 ABP1-GFP:HIS3</i> }	This work
W303 ρ^0	<i>MATa</i> { <i>leu2-3,112 trp1-1 can1-100 ura3-1 ade2-1 his3-11,15, rho0</i> }	Dr. Xochitl Perez-Martinez
W303 ρ^0 Abp1-GFP	<i>MATx</i> { <i>leu2-3,112 trp1-1 can1-100 ura3-1 ade2-1 ABP1-GFP:HIS3, rho0</i> }	This work
W303 JPM66a	<i>MATx</i> { <i>leu2-3,112 trp1-1 can1-100 ura3-1 ade2-1 his3-11,15 pet122delta::KANMX</i> }	Dr. Xochitl Perez-Martinez
W303 J11 Abp1-GFP	<i>MATx</i> { <i>leu2-3,112 trp1-1 can1-100 ura3-1 ade2-1 ABP1-GFP:HIS3 pet122delta::KANMX</i> }	This work

2.4. Rate of fermentation

Yeast cells from SD-Gluc or YPD 24 h cultures were washed three times using sterile water (2900×g 5 min in an Avant J-26 XPI centrifuge, Beckman Coulter, USA) and inoculated in YP or YPD-Gluc, incubating at 30 °C for 4 h under agitation at 250 rpm in a Excella E24 incubator Shaker (New Brunswick Scientific, USA). Then, cells were washed and the pellet was resuspended again in YP or YPD. To measure the rate of fermentation, cells (1×10^7) were incubated in 20 mM glucose, for up to 6 min and 0.1 mL of 30 % trichloroacetic acid (TCA) was added. Samples were centrifuged at 2900×g for 5 min at 4 °C. The supernatant was neutralized with NaOH and ethanol was quantified using an enzymatic method coupled to NAD⁺ (1.8 mM) reduction by alcohol dehydrogenase ($100 \mu\text{g} \mu\text{L}^{-1}$) (Bonnichsen, 1965). Briefly 1 mg prot./mL of each supernatant was suspended in 1 mL of 300 mM Na₄P₂O₇·10H₂O, 75 mM Semicarbazide hydrochloride, 22 mM Glycine, 66 mM NaOH pH 8.8, and 1.8 mM NAD (Bonnichsen, 1965). After 10 s, 100 μg/mL ADH was added and incubated 1 h at 24 °C. Absorbance was determined at 340 nm in an Aminco-Olis DW2000 spectrophotometer (Olis Inc., Bogart, GA, USA). Ethanol standard curve was used, and the results are reported as nmol ethanol per mg cells.

2.5. Fluorescent labeling of the actin-binding protein and of actin

In order to analyze actin distribution and dynamics, green-fluorescent protein-tagged strains were created to observe actin patches (Huckaba et al., 2004; Vasicova et al., 2015). For the actin-binding protein (Abp1p), its C-terminus of Abp1p was tagged with GFPy by PCR-based insertion of the gene into a chromosomal copy of ABP1 using plasmid pFA6a-link-yoEGFP-SpHis5 (gift from Wendell Lim & Kurt Thorn) (Addgene plasmid # 44836) (Lee et al., 2013) and primers Abp1fluoF, Abp1fluoR (Table S2) as described previously (Huckaba et al., 2004). Yeast were transformed using a lithium acetate protocol (Gietz et al., 1995) and the correct integration of GFP cassette at the ABP1 locus was characterized using PCR. GFP tagging had no effect on growth, glucose fermentation or actin organization (Results not shown).

To confirm the colocalization of GFP-Abp1 and actin, each GFP-Abp1-labeled strain was fixed in 3.7 % paraformaldehyde. Actin was labeled as follows: cells were washed and stained with 1.65 μM rhodamine-phalloidin (Sigma Aldrich) and incubated for 30 min at room temperature. Next, cells were washed and mounted for imaging (Higuchi-Sanabria et al., 2016). Samples were observed under a Nikon Eclipse E600 fluorescence microscope equipped with a DXM 1200 high resolution digital camera with a 460 nm–490 nm filter for GFP excitation and 530 nm–550 nm filter for rhodamine excitation. Merging was performed using ImageJ software (Hartig, 2013).

2.6. Time-lapse microscopy

To evaluate actin patch dynamics, live cells were layered onto SD agarose pads (Pemberton, 2014). Then, we evaluated actin patch dynamics in a Leica TCS-SP5 confocal microscope in a 63× objective

with an Argon laser exciting at 488 nm and generating 60 images/min. Image processing was performed with the LAS X (Leica) and ImageJ software.

2.7. Actin patch dynamics in pharmacological uncoupled yeast

To evaluate actin dynamics, the WT strain was cultured in SD-Gluc overnight and yeasts were washed and inoculated in SD. Where indicated, 20 μM carbonyl cyanide 3-chlorophenylhydrazone (CCCP) was added. Then, cells were mounted on agarose pads and analyzed with a Nikon Eclipse E600 fluorescence microscope with a DXM 1200 high resolution color digital camera.

2.8. Statistics

Where indicated, one-way ANOVA (Tukey's multiple comparisons test) was used to compare the differences between strains, using GraphPad Prism version 6 (GraphPad Software, Inc. La Jolla, CA, USA).

3. Results

3.1. Glycolytic enzyme/F-actin affinity decreased upon carbon source withdrawal

To test the modifications in actin-enzyme affinity brought by starvation, co-immunoprecipitation of three glycolytic pathway enzymes, namely ALD (Fig. 1, upper panel), PGK (Fig. 1, second panel) and GAPDH (Fig. 1, third panel) with actin was evaluated in glucose-fed (G) and in starved (S) cells. Tested strains were W303 WT, W303 ρ^0 and W303 *pet122Δ*. In glucose-fed strains, a strong interaction between actin and glycolytic enzymes was observed (Fig. 1, odd lanes). This was already expected from a previous report (Araiza-Olivera et al., 2013). In contrast, glycolytic enzymes from starved yeast exhibited a decrease in co-immunoprecipitation in all cases (Fig. 1, even lanes). It is interesting to observe that in starved samples GAPDH detachment seemed to be complete. Thus, the glycolytic enzyme/F-actin organization expected for a putative metabolon was disrupted by carbon source withdrawal and this should inhibit the glycolytic pathway in starved cells. To test this, it was decided to determine the association of the aforementioned enzymes in glucose-fed (G) and in starved (S) cells and whether starvation effects were magnified in the fermentative obligate strains.

3.2. Glycolytic enzyme–enzyme affinity decreased mildly upon carbon source withdrawal

The effect of glucose withdrawal on affinity among glycolytic enzymes was analyzed in extracts from G or S cells. ALD was immunoprecipitated (Fig. 2, lower panel) and co-immunoprecipitation of PGK (Fig. 2 upper panel) and GAPDH (middle panel) was evaluated. Samples from each of the strains

W303 WT (lanes 1 and 2), W303 ρ^0 (lanes 3 and 4) and W303 *pet122* Δ (lanes 5 and 6) were used. In all cases PGK co-immunoprecipitation decreased markedly upon starving (Fig. 2, upper panel), while GAPDH co-immunoprecipitation decreased only mildly. The effects of starving on GAPDH-ALD association were milder than those reported upon F-actin destabilization with latrunculin or cytochalasin (Araiza-Olivera et al., 2013). Thus, the glycolytic enzyme/F-actin organization expected for a putative metabolon was only mildly disrupted by carbon source withdrawal and it is not clear whether this would inhibit the glycolytic pathway in starved cells. To test this, it was decided to determine the concentration of ATP ([ATP]) in fed and starved cells from each strain and whether starvation effects were magnified in the obligate fermentative strains.

3.3. Starving decreases [ATP] in yeast. More so in obligate fermentative strains

The effect of carbon source withdrawal on [ATP] was determined, both in the WT strain (Fig. 3, black bars) and in each of the

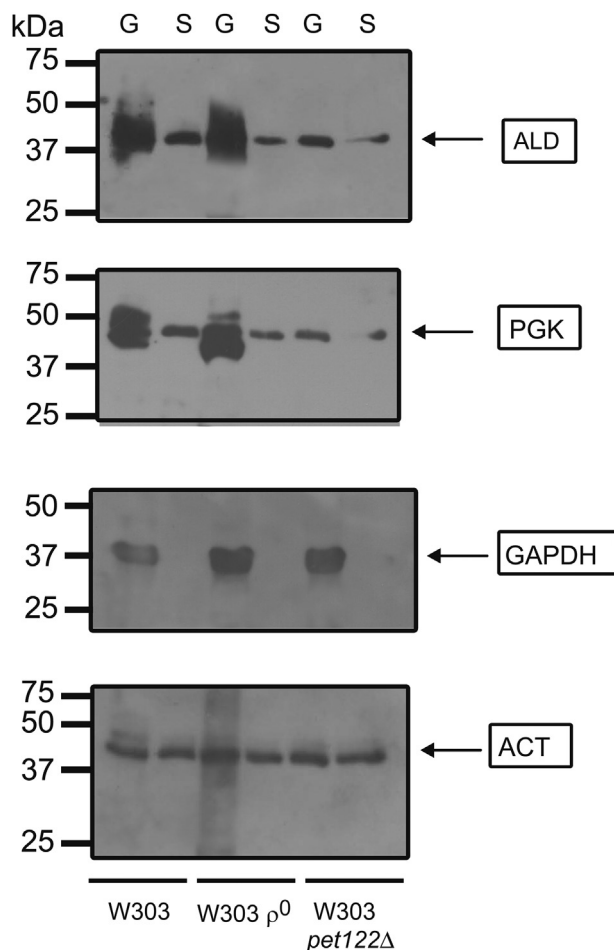


Fig. 1. Under starvation, glycolytic enzymes detach from actin. Cells were cultured overnight in SD-Gluc. Then, cells were washed and incubated in SD (S) or SD-Gluc (G) 4 h at 30 °C. Yeast extracts were obtained and actin was immunoprecipitated. Precipitates were immunoblotted against ALD (top panel), PGK (second panel) or GAPDH (third panel), with actin (ACT) as loading control (bottom panel). Lane 1: W303 WT Abp1-GFP in SD-Gluc, Lane 2: W303WT Abp1-GFP in SD, Lane 3: W303 ρ^0 Abp1-GFP in SD-Gluc, lane 4: W303 ρ^0 Abp1-GFP in SD, lane 5: W303 *pet122* Δ Abp1-GFP in SD-Gluc, lane 6: W303 *pet122* Δ Abp1-GFP in SD. Representative image of three independent experiments. Lanes with glucose-fed yeast are labeled “G” while those from starved yeast are labeled “S”.

OxPhos-deficient mutants: W303 ρ^0 (Fig. 3, white bars) and W303 *pet122* Δ (gray bars). After incubating for 4 h in the presence of glucose, [ATP] was: in WT, [ATP] = 2.3 nmol (mg prot)⁻¹ and slightly higher [ATP] = 2.6–2.8 nmol (mg prot)⁻¹ in the fermentative mutants (Fig. 3A). Then, after a starving period of 30 min, a slight decrease was observed in WT where [ATP] = 1.8 nmol (mg prot)⁻¹, while in the fermentative strains [ATP] decreased to near 1.0 nmol (mg prot)⁻¹ in each case (Fig. 3B). After 4 h in the absence of glucose, [ATP] differences became more evident. The WT still contained high [ATP] = 2.0 nmol (mg prot)⁻¹ while in each of the fermentative mutants a much lower [ATP] = 0.6 nmol (mg prot)⁻¹ was observed (Fig. 3C). These results indicated that [ATP] was more sensitive to carbon depletion in each obligate fermentative strain than in WT. i.e., after starving for 4 h, [ATP] decreased 60–75 % in each mutant while in the WT the decrease was only 16 % (Fig. 3). The decrease in [ATP] could be due to a simple lack of substrate or might be evidencing the disorganization a glycolytic metabolon.

3.4. At low [ATP] glucose addition increased fermentation activity

Glucose withdrawal resulted in glycolytic enzyme detachment from F-actin (Fig. 1), in mild loss of enzyme–enzyme affinity (Fig. 2) and in decreased [ATP] (Fig. 3), suggesting that glycolysis was inactivated. To test this, the rate of fermentation was measured in starved (S, dots) and glucose-fed (G, circles) samples from each of the three strains (Fig. 4). In S samples the rate of fermentation was as least five times faster than in G samples (Fig. 4), suggesting that a low [ATP] activated glycolysis. In addition, while the WT (Fig. 4-A circles) and the W303 ρ^0 strain (Fig. 4-B circles) exhibited a nearly constant activity from the beginning, the fermentation rate for the W303 *pet122* Δ strain was slow for the first two minutes and increased at later incubation times (Fig. 4-C, circles). The WT strain, where [ATP] was higher after fasting, was the least active (Fig. 4-A, circles). The W303 *pet122* Δ strain exhibited an initial fermentation rate of 3 nmols EtOH (min·mg. prot⁻¹), which increased to 12 nmols EtOH (min·mg. prot⁻¹) after two minutes (Fig. 4-C, circles).

In contrast, in the G samples a very slow rate of fermentation was observed (Fig. 4, dots) in all cases. Furthermore, when these plots were magnified (Fig. 4, inserts), a slightly faster fermentation rate was detected for the first minute in each case, which decreased at later time points. In addition, for glucose-fed strains rates of fermentation were smaller than in the fasted samples. In the glucose-fed WT, the initial rate of fermentation was 3 μ mol EtOH

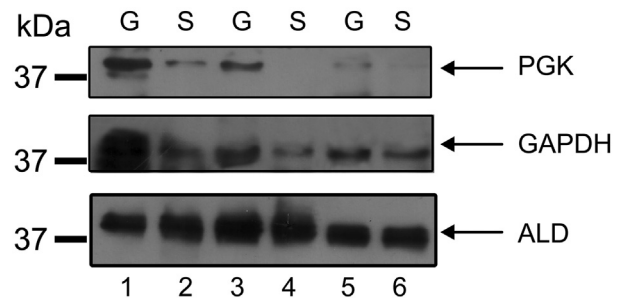


Fig. 2. Glucose withdrawal results in decreased affinity of glyceraldehyde-phosphate dehydrogenase and 2-phosphoglycerate for aldolase. Experimental conditions as in Fig. 1, except aldolase (ALD) was immunoprecipitated from yeast extracts. Precipitates were immunoblotted against PGK (upper panel) or GAPDH (middle panel), using ALD as loading control (bottom panel). Lane 1: W303 WT Abp1-GFP in SD-Gluc, Lane 2: W303WT Abp1-GFP in SD, Lane 3: W303 ρ^0 Abp1-GFP in SD-Gluc, lane 4: W303 ρ^0 Abp1-GFP in SD, lane 5: W303 *pet122* Δ Abp1-GFP in SD-Gluc, lane 6: W303 *pet122* Δ Abp1-GFP in SD. Representative image of three independent experiments. Lanes with glucose-fed yeast are labeled “G” while those from starved yeast are labeled “S”.

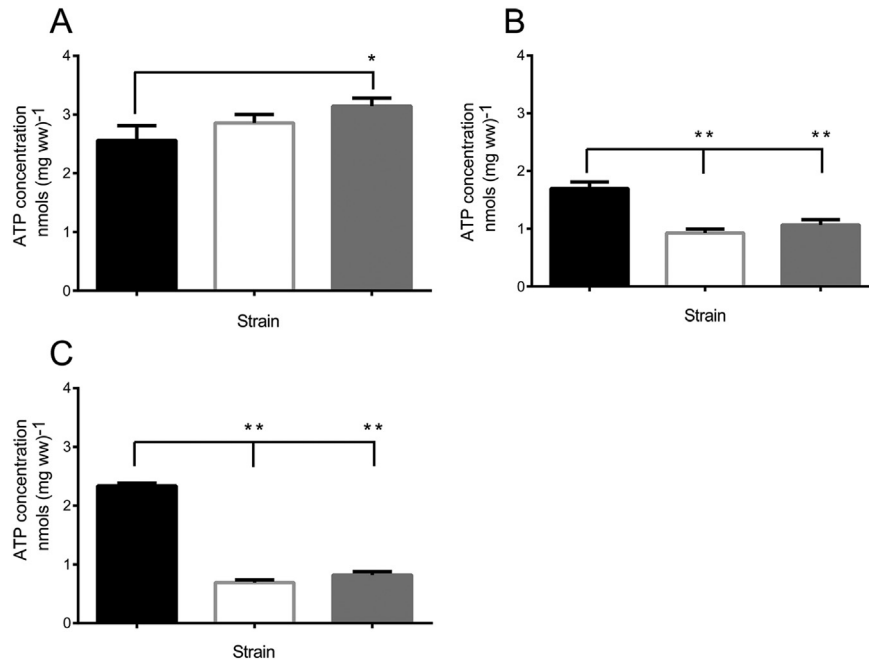


Fig. 3. ATP concentration in different yeast strains subjected to starving. Intracellular ATP in W303 Abp1-GFP (black bars), W303 ρ^0 Abp1-GFP (white bars) and W303 *pet122* Δ Abp1-GFP (gray bars) were measured. Experimental conditions as in Fig. 1. Yeasts were incubated as follows: (A) in SD-Gluc for 4 h or (B) in SD for 30 min or (C) in SD for 4 h. Then yeasts were harvested, washed and ATP was quantified using a bioluminescence assay. Values are means \pm SD of three independent experiments, each performed in triplicate. Statistical differences were determined using One way ANOVA plus Tukey's multiple comparisons test: *P < 0.05, **P < 0.01.

($\mu\text{mol}\cdot\text{mg}\cdot\text{prot}^{-1}$) and decreased after two minutes to 1.2 μmol EtOH ($\text{min}\cdot\text{mg}\cdot\text{prot}^{-1}$) (Fig. 4-A insert). The W303 ρ^0 strain exhibited an initial fermentation rate of 3.6 μmol EtOH ($\text{min}\cdot\text{mg}\cdot\text{prot}^{-1}$), which after two minutes decreased to 1.5 μmol EtOH ($\text{min}\cdot\text{mg}\cdot\text{prot}^{-1}$) (Fig. 4-B, insert). The W303 *pet122* Δ exhibited an initial fermentation rate of 5 μmol EtOH ($\text{min}\cdot\text{mg}\cdot\text{prot}^{-1}$), which decreased after two minutes to 2.0 μmol EtOH ($\text{min}\cdot\text{mg}\cdot\text{prot}^{-1}$) (Fig. 4-C, insert). Thus, in the fasted samples fermentation was active, probably aiming to replenish the low ATP pool. In contrast, the glucose-fed samples were active from the start of the experiment, although these did not reach high rates probably as a result of the presence of high [ATP]. The only indication of a lag in fermentation activity after fermentation was from W303 *pet122* Δ where a one to two minute lag was observed before full activity was observed (Fig. 4-C, circles).

3.5. Actin-binding protein 1 (Abp1) reports structural cytoskeleton modifications promoted by glucose withdrawal

The glycolytic metabolon is most likely organized around the actin cytoskeleton (Araiza-Olivera et al., 2013). As actin is not amenable to labeling, it was decided to label the actin-binding protein (Abp1) instead. Then in order to confirm that the fluorescence from Abp1 was an efficient reporter of actin localization, strains were fixed and GFP-Abp1 fluorescence was followed (Fig. 5 left panels). In the same samples, F-actin was labeled using rhodamine-phalloidin (Fig. 5 middle panels) and co-localization was evaluated (Fig. 5 right panels). Green fluorescence from GFP-Abp1 co-localization with the red fluorescence from rhodamine-phalloidin was analyzed (Fig. 5). In all glucose-fed strains, and in the starved W303 WT, small fluorescent patches were detected, both in the green and in the red fluorescence channels (Fig. 5A and B, C and E), while in the starved fermentative-obligate strains large fluorescent bodies were observed both in the W303 ρ^0 (Fig. 5-D) and in the W303 *pet122* Δ (Fig. 5-F). The CCCP-uncoupled W303 WT

(to deplete ATP) also exhibited large fluorescent bodies (Result not shown). Thus, incubation without glucose led to reorganization of F-actin that correlated with the decrease in [ATP]. Upon glucose addition, [ATP] increased and modifications observed in the actin cytoskeleton were reversed (Result not shown). Images from reorganized F-actin in the S mutants (Fig. 5) suggested the presence of actin bodies, which according to the literature should be immotile (Sagot et al., 2006). To confirm the presence of immotile actin bodies, it was decided to evaluate cytoskeleton dynamics from each strain and condition.

3.6. In starving oxidative-phosphorylation-deficient strains, small, highly dynamic F-actin patches are replaced by large non-motile bodies

When yeast reach the stationary phase, actin cables and patches reorganize, forming immotile actin bodies (Sagot et al., 2006). Thus, it was decided to determine whether glucose withdrawal led to modifications of actin cytoskeleton dynamics in each strain under study, using a time-lapse microscopy assay and following the fluorescence of GFP-Abp1. In all glucose-fed strains and in the starved W303 WT strain, small, motile actin patches were observed (see supplementary videos 1, 2, 4 and 6). The W303-WT strain exhibited highly motile actin patches regardless of whether it was glucose fed (Suppl-video 1) or starved (Suppl-video 2). In contrast, the W303 ρ^0 mutant exhibited motile patches when glucose fed (Suppl-video 3), while it exhibited immotile actin bodies when starved (Suppl-video 4). The W303 *pet122* Δ strain also exhibited motile actin patches when glucose-fed (Suppl-video 5) and non-motile actin bodies when starved (Suppl-video 6).

Supplementary video related to this article can be found at <https://doi.org/10.1016/j.funbio.2019.10.005>.

The interactions of enzymes in a putative glycolytic metabolon and F-actin were explored in cells subjected to carbon source depletion. Upon starving, the cytoskeleton reorganized and lost its

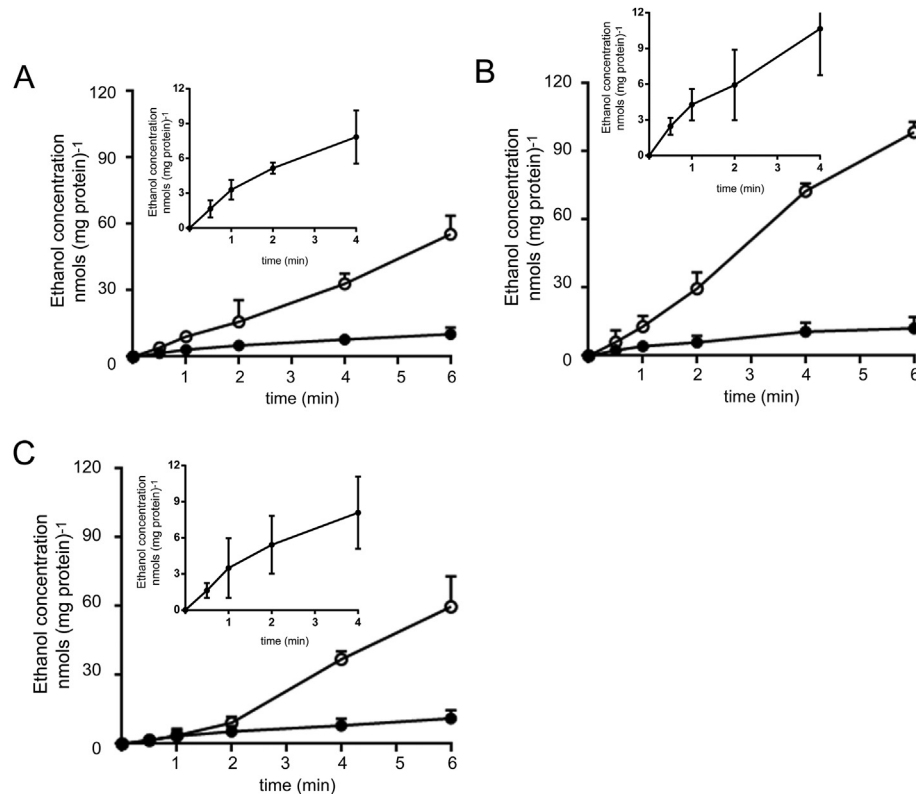


Fig. 4. In *S. cerevisiae*, the rate of fermentation reacts rapidly to glucose withdrawal and re-addition. Ethanol production kinetics were measured in (A) W303 Abp1-GFP, (B) W303 ρ^0 Abp1-GFP or (C) W303 *pet122* Δ Abp1-GFP. Experimental conditions, as in Fig. 1. Cells were washed and incubated 4 h in YP (empty circles) or YPD (full dots) at 30 °C. The rate of fermentation was determined at 30 s, 1, 2, 4 and 6 min. Produced ethanol was quantified using an enzyme-coupled assay (see methods). Results are reported as nmol EtOH/mg protein. Three independent experiments were performed, values are means \pm SD. * $P < 0.05$. Inserts are a 10 time magnification of the YPD plot for each strain, aiming to show that during the first one to two minutes fermentation was slightly faster than at later points.

affinity for glycolytic enzymes. ATP concentration seemed to be an important factor regulating both cytoskeleton organization and fermentation activity. In W303 ρ^0 and W303 *pet122* Δ , cells that depend strongly on glycolysis for ATP production, starving also resulted in re-distribution of the cytoskeleton and in actin storage into immotile bodies. All effects disappeared upon glucose re-addition.

4. Discussion

Membrane-less enzyme complexes in the cytoplasm vary in stoichiometry and protein dwelling time (Case et al., 2019). Up to 180 intermediary metabolism enzymes may exhibit non-diffusible behavior (O'Connell et al., 2012). An interactome involving both the enzymes in a given metabolon and the membrane transporters would result in channeling of substrates from uptake by the cell all the way to the last product of the pathway (Morales and Reithmeier, 2012). Such seems to be the case in erythrocytes, where a docking site in the vicinity of the membrane-spanning segment of band 3 binds both glycolytic enzymes and a glucose transporter (GLUT1) (Puchulu-Campanella et al., 2013). The tendency of proteins exhibiting quaternary structures to form fibers seems to be high and may optimize function as in purinosomes or become a source of disease as in sickle cell anemia or as in amyloid diseases (O'Connell et al., 2012).

Signaling pathways are another example where protein association has been reported recently (Strzyz, 2019). Actin polymerization is optimized by signaling clusters on the plasma membrane where Nephren–Nck–N-WASP associate (Case et al., 2019). Also on the plasma membrane, the mitogen-activated protein kinase

(MAPK) pathway recruits proteins such as SOS, needed to optimize signaling (Huang et al., 2019). Protein clusters may sequester small molecules, as in adenosine A_{2A} or A_{2B} signalosomes, where each specific isoform of adenosine receptor, adenylate cyclase and A-Kinase-Anchoring Protein (AKAP) generate a sequestered cAMP pool and evoke receptor-specific responses (Guinzeberg et al., 2017).

Glycolytic metabolons optimize catalysis and protect enzymes against external conditions (Araiza-Olivera et al., 2013; Menard et al., 2014). Most likely, metabolons are dynamic structures (Sweetlove and Fernie, 2018). In *C. elegans* neurons under energy stress, glycolytic enzymes move near synapses, probably with the aim of increasing local [ATP] (Jin et al., 2017). Hypoxia drives *S. cerevisiae* glycolytic enzymes into G bodies where glycolysis becomes more efficient (Jin et al., 2017).

The rate of fermentation in glucose-fed versus starved cells were explored. The energy dependence of assembly was analyzed in three different yeast strains. A WT OxPhos facultative strain (W303 WT) and two obligate fermentative strains, namely a ρ^0 (W303 ρ^0) and a strain where a promoter (PET122) needed for translation of subunit three of complex IV was deleted (W303 *pet122* Δ) (Costanzo and Fox, 1988). The obligate fermentative strains magnified the effects of glucose withdrawal on ATP production (Friis and Schultz, 2016). Cells were incubated four hours in the presence or in the absence of a carbon source. Under starvation, the glycolytic enzymes, ALD, GAPDH and PGK lost their affinity for F-actin (Fig. 1), and decreased enzyme–enzyme affinity (Fig. 2). Starving led to a decrease in the concentration of ATP that was more accentuated in the fermentative obligate strains (Fig. 3). When the rate of glycolysis was tested it was observed that low [ATP] led to high fermentation activity. In regard to the possible inactivation of

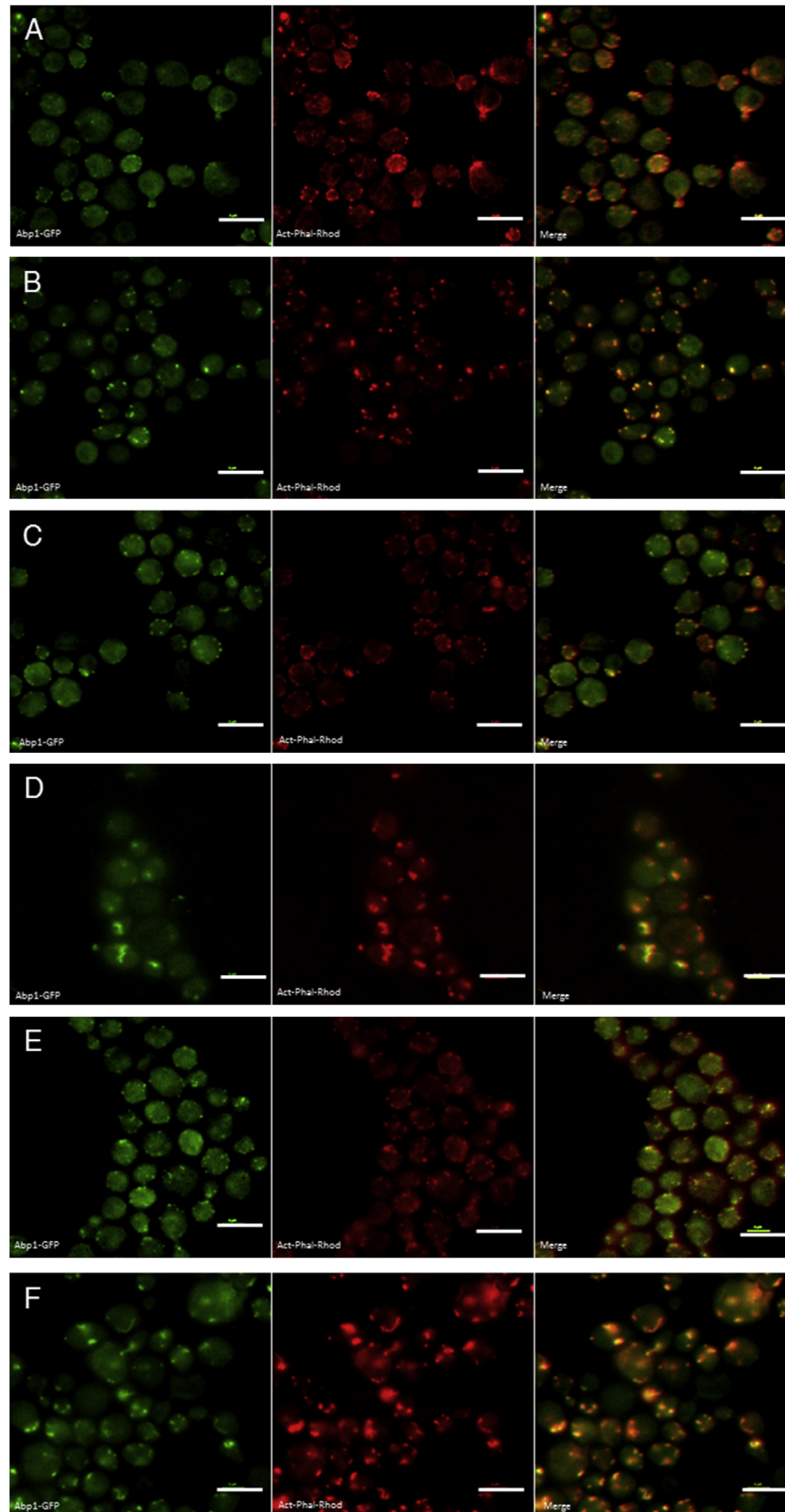


Fig. 5. Abp1-GFP and F-actin co-localize in the *S. cerevisiae* Abp1-GFP-derived W303 strains. Experimental conditions as in Fig. 4. Yeasts were incubated overnight in SD-Gluc, then cells were washed and incubated in SD-Gluc (A, C and E) or SD (B, D and F) at 30 °C and under agitation for 4 h. After incubation, cells were fixed and stained with rhodamine phalloidin for 30 min. Cell Images were obtained in an epifluorescence microscope. Strains are W303 Abp1-GFP, glucose fed (A) or starved (B) W303 ρ^0 Abp1-GFP, Glucose fed (C) or starved (D) and W303 *pet122* Δ A Glucose-fed (E) or starved (F). Bar = 10 μ m. Images are representative from three independent experiments.

glycolysis resulting from enzyme dissociation, only the W303 *pet122Δ* strain exhibited a degree of inactivation by starving, which rapidly reverted after two minutes (Fig. 4-C). In contrast, the rate of fermentation after glucose addition to well-fed yeast was never as high as in the starved cells and it decreased after two minutes. We suggest that [ATP] controls the rate of fermentation. The two-minute delay in activation of fermentation in the starved W303 *pet122Δ* probably reflects the need to reassemble a glycolytic metabolon. This was not observed in the W303 ρ^0 strain, perhaps due to its reported inability to respond to changes in the environment (Friis and Schultz, 2016).

The response to carbon source withdrawal was more pronounced in obligate fermentative cells, which depend heavily on glycolysis for energy production. Both OxPhos-deficient strains decreased their total ATP concentration by 80 % while in the WT the decrease was only 10 %. In addition, large reorganization of the cytoskeleton took place as F-actin was redistributed from small, dynamic patches to large immotile bodies. It has been suggested that actin bodies may be a storage form of actin designed to save energy (Sagot et al., 2006). Thus it is possible that these bodies stop functions such as cargo and endocytosis, where a motile cytoskeleton would be required (Goode et al., 2015). The cytoskeleton role as a scaffold for enzyme association in the glycolytic metabolon (Menard et al., 2014) would also be lost in large actin bodies. The critical role of the metabolon to produce energy has been documented in other systems, such as in *gpdh-3* null flies which do not exhibit glycolytic complex organization in muscle, which results in the inability to fly (Wojtas et al., 1997).

Redistribution of the actin cytoskeleton into immotile bodies correlated with ATP availability. In the mutants, [ATP] decreased and the cytoskeleton was modified. However, in the WT it was necessary to uncouple oxidative phosphorylation in order to obtain immotile bodies. Actin cytoskeleton redistribution experiments were conducted using the GFP-Abp1, which as expected from the literature (Sagot et al., 2006), remained bound to actin following its distribution, regardless of the metabolic conditions in the cell.

In *S. cerevisiae*, a carbon source starve-feed cycle controlled the rate of fermentation. It is likely that the mechanism of control involved the assembly/disassembly of a putative glycolytic metabolon that used the F-actin cytoskeleton as a scaffold. In addition, the concentration of ATP was a major factor controlling the maximal rate of fermentation. Obligate fermentative strains were more sensitive to the effects of starving on their metabolism and on cytoskeleton dynamics.

Declaration of Competing Interest

The authors have no conflicts of interest to declare.

Acknowledgements

Partially funded by DGAPA-PAPIIT, UNAM, Mexico, Grant numbers: SUC: IN204015; FTQ: IA202217 and IN209219 and by Conacyt Mexico SUC: Grant: 239487. EES was a COMECYT Mexico PhD fellow, LMG and UPD are CONACYT fellows, EES and UPD are enrolled in the Biochemistry Graduate Program at UNAM. LMG is in the Biomedical Research Graduate program at UNAM. We received technical help from the Microscopy (R. Rincón Heredia), Molecular Biology and Computation units at the IFC.

Appendix A. Supplementary data

Supplementary data to this article can be found online at <https://doi.org/10.1016/j.funbio.2019.10.005>.

References

- Apodaca, G., 2001. Endocytic traffic in polarized epithelial cells: role of the actin and microtubule cytoskeleton. *Traffic* 2, 149–159. <https://doi.org/10.1034/j.1600-0854.2001.020301.x>.
- Araiza-Olivera, D., Chiquete-Felix, N., Rosas-Lemus, M., Sampedro, J.G., Peña, A., Mujica, A., Uribe-Carvajal, S., 2013. A glycolytic metabolon in *Saccharomyces cerevisiae* is stabilized by F-actin. *FEBS J.* 280, 3887–3905. <https://doi.org/10.1111/febs.12387>.
- Araiza-Olivera, D., Sampedro, J.G., Mújica, A., Peña, A., Uribe-Carvajal, S., 2010. The association of glycolytic enzymes from yeast confers resistance against inhibition by trehalose. *FEMS Yeast Res.* 10, 282–289. <https://doi.org/10.1111/j.1567-1364.2010.00605.x>.
- Ashe, M.P., Long, S.K., De Sachs, A.B., 2000. Glucose depletion rapidly inhibits translation initiation in yeast. *Mol. Biol. Cell* 11, 833–848.
- Bonnichsen, R., 1965. Ethanol: determination with alcohol dehydrogenase and DPN. In: *Methods of Enzymatic Analysis*, pp. 285–289. <https://doi.org/10.1016/B978-0-12-395630-9.50061-X>.
- Case, L.B., Zhang, X., Ditlev, J.A., Rosen, M.K., 2019. Stoichiometry controls activity of phase-separated clusters of actin signaling proteins. *Science* 363, 1093–1097. <https://doi.org/10.1126/science.aau6313> (80).
- Clarke, F.M., Masters, C.J., 1975. On the association of glycolytic enzymes with structural proteins of skeletal muscle. *Biochim. Biophys. Acta* 381, 37–46. [https://doi.org/10.1016/0304-4165\(75\)90187-7](https://doi.org/10.1016/0304-4165(75)90187-7).
- Costanzo, M.C., Fox, T.D., 1990. Control of mitochondrial gene expression in *Saccharomyces cerevisiae*. *Annu. Rev. Genet.* 24, 91–113. <https://doi.org/10.1007/BF00219314>.
- Costanzo, M.C., Fox, T.D., 1988. Specific translational activation by nuclear gene products occurs in the 5' untranslated leader of a yeast mitochondrial mRNA. *Proc. Natl. Acad. Sci. U.S.A.* 85, 2677–2681. <https://doi.org/10.1073/pnas.85.8.2677>.
- Deluca, M., McElroy, W.D., 1978. Purification and properties of firefly luciferase. In: *Methods in Enzymology. Bioluminescence and Chemiluminescence*, 57. Acad. Press, San Diego, New York, pp. 3–15.
- Friis, R.M.N., Schultz, M.C., 2016. Attenuation of transcriptional and signaling responses limits viability of ρ^0 *Saccharomyces cerevisiae* during periods of glucose deprivation. *Biochim. Biophys. Acta - Gen. Subj* 1860, 2563–2575. <https://doi.org/10.1016/j.bbagen.2016.07.029>.
- Fulton, A.B., 1982. How crowded is the Cytoplasm? *Minireviews. Water* 30, 345–347. [https://doi.org/10.1016/0092-8674\(82\)90231-8](https://doi.org/10.1016/0092-8674(82)90231-8).
- Gietz, R.D., Schiestl, R.H., Willems, A.R., Woods, R.A., 1995. Studies on the transformation of intact yeast cells by the LiAc/SS??DNA/PEG procedure. *Yeast* 11, 355–360. <https://doi.org/10.1002/yea.320110408>.
- Goode, B.L., Eskin, J.A., Wendland, B., 2015. Actin and endocytosis in budding yeast. *Genetics* 199, 315–358. <https://doi.org/10.1534/genetics.112.145540>.
- Green, D.E., Murer, E., Richardson, S.H., Salmon, B., Brierley, G.P., Baum, H., 1965. Association of integrated metabolic pathways with membranes. *Arch. Biochem. Biophys.* 112, 635–647.
- Guinberg, R., Díaz-Cruz, A., Acosta-Trujillo, C., Vilchis-Landeros, M.M., Vázquez-Meza, H., Lozano-Flores, C., Chiquete-Felix, N., Varela-Echavarría, A., Uribe-Carvajal, S., Riveros-Rosas, H., Pina, E., 2017. Newly synthesized cAMP is integrated at a membrane protein complex signalosome to ensure receptor response specificity. *FEBS J.* 284, 258–276. <https://doi.org/10.1111/febs.13969>.
- Hartig, S.M., 2013. Basic image analysis and manipulation in imagej. *Curr. Protoc. Mol. Biol.* 1–12. <https://doi.org/10.1002/0471142727.mb1415s102>.
- Higuchi-Sanabria, R., Swayne, T.C., Boldogh, I.R., Pon, L.A., 2016. Imaging of the actin cytoskeleton and mitochondria in fixed budding yeast cells. In: Gavin, R.H. (Ed.), *Cytoskeleton Methods and Protocols: Methods and Protocols*. Springer New York, New York, NY, pp. 63–81. https://doi.org/10.1007/978-1-4939-3124-8_3.
- Huang, W.Y.C., Alvarez, S., Kondo, Y., Kwang Lee, Y., Chung, J.K., Monatrice Lam, H.Y., Biswas, K.H., Kuriyan, J., Groves, J.T., 2019. A molecular assembly phase transition and kinetic proofreading modulate Ras activation by SOS. *Science* 363, 1098–1103. <https://doi.org/10.1126/science.aau5721> (80).
- Huckaba, T.M., Gay, A.C., Pantalena, L.F., Yang, H.C., Pon, L.A., 2004. Live cell imaging of the assembly, disassembly, and actin cable-dependent movement of endosomes and actin patches in the budding yeast, *Saccharomyces cerevisiae*. *J. Cell Biol.* 167, 519–530. <https://doi.org/10.1083/jcb.200404173>.
- Hudder, A., Nathanson, L., Deutscher, M.P., 2003. Organization of mammalian cytoplasm. *Mol. Cell. Biol.* 23, 9318–9326. <https://doi.org/10.1128/MCB.23.24.9318-9326.2003>.
- Jin, M., Han, T., Yao, Y., Alessi, A.F., Freeberg, M.A., Inoki, K., Klionsky, D.J., Kim, J.K., Jin, M., Klionsky, D.J., Han, T., Freeberg, M.A., Karnovsky, A., Moresco, J.J., Yates, J.R., Baba, M., Gitler, A.D., Inoki, K., Fuller, G.G., Alessi, A.F., Freeberg, M.A., Roach, N.P., Kim, J.K., Han, T., 2017. Glycolytic enzymes coalesce in G bodies under hypoxic stress. *Cell Rep.* 20, 895–908. <https://doi.org/10.1016/j.celrep.2017.06.082>.
- Jørgensen, K., Rasmussen, A.V., Morant, M., Nielsen, A.H., Bjarnholt, N., Zagrobelny, M., Bak, S., Møller, B.L., 2005. Metabolon formation and metabolic channeling in the biosynthesis of plant natural products. *Curr. Opin. Plant Biol.* 8, 280–291. <https://doi.org/10.1016/j.pbi.2005.03.014>.
- Joyner, R.P., Tang, J.H., Helenius, J., Dultz, E., Brune, C., Holt, L.J., Huet, S., Müller, D.J., Weis, K., 2016. A glucose-starvation response regulates the diffusion of macromolecules. *Elife* 5, 1–26. <https://doi.org/10.7554/eLife.09376>.

- Knudsen, C., Gallage, N.J., Hansen, C.C., Møller, B.L., Laursen, T., 2018. Dynamic metabolic solutions to the sessile life style of plants. *Nat. Prod. Rep.* 11, 1140–1155. <https://doi.org/10.1039/c8np00037a>.
- Kohnhorst, C.L., Kyoung, M., Jeon, M., Schmitt, D.L., Kennedy, E.L., Ramirez, J., Bracey, S.M., Luu, B.T., Russell, S.J., An, S., 2017. Identification of a multienzyme complex for glucose metabolism in living cells. *J. Biol. Chem.* 292, 9191–9203. <https://doi.org/10.1074/jbc.M117.783050>.
- Lang, M.J., Martínez-Marquez, J.Y., Prosser, D.C., Ganser, L.R., Buelto, D., Wendland, B., Duncan, M.C., 2014. Glucose starvation inhibits autophagy via vacuolar hydrolysis and induces plasma membrane internalization by down-regulating recycling. *J. Biol. Chem.* 289, 16736–16747. <https://doi.org/10.1074/jbc.M113.525782>.
- Lee, S., Lim, W.A., Thorn, K.S., 2013. Improved blue, green, and red fluorescent protein tagging Vectors for *S. cerevisiae*. *PLoS One* 8, 4–11. <https://doi.org/10.1371/journal.pone.0067902>.
- Lu, M., Sautin, Y.Y., Holliday, L.S., Gluck, S.L., 2004. The glycolytic enzyme aldolase mediates assembly, expression, and activity of vacuolar H⁺-ATPase. *J. Biol. Chem.* 279, 8732–8739. <https://doi.org/10.1074/jbc.M303871200>.
- Menard, L., Maughan, D., Vigoreaux, J., 2014. The structural and functional coordination of glycolytic enzymes in muscle: evidence of a metabolon? *Biology (Basel)* 3, 623–644. <https://doi.org/10.3390/biology3030623>.
- Mendoza-Hoffmann, F., Pérez-Oseguera, A., Cevallos, M.A., Zarco-Zavala, M., Ortega, R., Peña-Segura, C., Espinoza-Simón, E., Uribe-Carvajal, S., García-Trejo, J.J., 2018. The biological role of the ζ subunit as unidirectional inhibitor of the F1FO-ATPase of paracoccus denitrificans. *Cell Rep.* 22, 1067–1078. <https://doi.org/10.1016/j.celrep.2017.12.106>.
- Moraes, T.F., Reithmeier, R.A.F., 2012. Membrane transport metabolons. *Biochim. Biophys. Acta* 1818, 2687–2706. <https://doi.org/10.1016/j.bbame.2012.06.007>.
- Moseley, J.B., Goode, B.L., 2006. The yeast actin cytoskeleton: from cellular function to biochemical mechanism. *Microbiol. Mol. Biol. Rev.* 70, 605–645. <https://doi.org/10.1128/MMBR.00013-06>.
- Nakayama, T., Takahashi, S., Waki, T., 2019. Formation of flavonoid metabolons: functional significance of protein-protein interactions and impact on flavonoid chemodiversity. *Front. Plant Sci.* 10 <https://doi.org/10.3389/fpls.2019.00821>.
- Noree, C., Sato, B.K., Broyer, R.M., Wilhelm, J.E., 2010. Identification of novel filament-forming proteins in *Saccharomyces cerevisiae* and *Drosophila melanogaster*. *J. Cell Biol.* 190, 541–551. <https://doi.org/10.1083/jcb.201003001>.
- O'Connell, J.D., Zhao, A., Ellington, A.D., Marcotte, E.M., 2012. Dynamic reorganization of metabolic enzymes into intracellular bodies. *Annu. Rev. Cell Dev. Biol.* 28, 89–111. <https://doi.org/10.1146/annurev-cellbio-101011-155841>.
- Pedley, A.M., Benkovic, S.J., 2017. A new View into the regulation of purine metabolism: the purinosome. *Trends Biochem. Sci.* 42, 141–154. <https://doi.org/10.1016/j.tibs.2016.09.009>.
- Pemberton, L.F., 2014. Preparation of yeast cells for live-cell imaging and indirect immunofluorescence. In: Smith, J.S., Burke, D.J. (Eds.), *Yeast Genetics: Methods and Protocols*. Springer New York, New York, NY, pp. 79–90. https://doi.org/10.1007/978-1-4939-1363-3_6.
- Puchulu-Campanella, E., Chu, H., Anstee, D.J., Galan, J.A., Tao, W.A., Low, P.S., 2013. Identification of the components of a glycolytic enzyme metabolon on the human red blood cell membrane. *J. Biol. Chem.* 288, 848–858. <https://doi.org/10.1074/jbc.M112.428573>.
- Ra, B., 2000. Quantitative characterization of homo- and heteroassociations of muscle phosphofructokinase with aldolase. *Biochim. Biophys. Acta Gen. Subj.* 1479, 303–314.
- Sagot, I., Pinson, B., Salin, B., Daignan-Fornier, B., 2006. Actin bodies in yeast quiescent cells: an immediately available actin reserve? *Mol. Biol. Cell* 17, 4645–4655. <https://doi.org/10.1091/mbc.E06>.
- Schmitt, D.L., An, S., 2017. Spatial organization of metabolic enzyme complexes in cells. *Biochemistry* 56, 3184–3196. <https://doi.org/10.1021/acs.biochem.7b00249>.
- Smith, M.G., Swamy, S.R., Pon, L. a., 2001. The life cycle of actin patches in mating yeast. *J. Cell Sci.* 114, 1505–1513.
- Srere, P.A., 1985. The metabolon. *Trends Biochem. Sci.* 10, 109–110. [https://doi.org/10.1016/0968-0004\(85\)90266-X](https://doi.org/10.1016/0968-0004(85)90266-X).
- Strzyz, P., 2019. Phase separation tunes signal transduction. *Nat. Rev. Mol. Cell Biol.* 20, 263. <https://doi.org/10.1038/s41580-019-0121-7>.
- Suresh, H.G., da Silveira dos Santos, A.X., Kukulski, W., Tyedmers, J., Riezman, H., Bukau, B., Mogk, A., 2015. Prolonged starvation drives reversible sequestration of lipid biosynthetic enzymes and organelle reorganization in *Saccharomyces cerevisiae*. *Mol. Biol. Cell* 26, 1601–1615. <https://doi.org/10.1091/mbc.E14-11-1559>.
- Sweetlove, L.J., Fernie, A.R., 2018. The role of dynamic enzyme assemblies and substrate channelling in metabolic regulation. *Nat. Commun.* 9, 2136. <https://doi.org/10.1038/s41467-018-04543-8>.
- Vasicova, P., Lejskova, R., Malcova, I., Hasek, J., 2015. The stationary-phase cells of *Saccharomyces cerevisiae* display dynamic actin filaments required for processes extending chronological life span. *Mol. Cell Biol.* 35, 3892–3908. <https://doi.org/10.1128/MCB.00811-15>.
- Wojtas, K., Laurence, S., Sullivan, D., 1997. Flight muscle function in *Drosophila* requires colocalization of glycolytic enzymes. *Mol. Biol. Cell* 8, 1665–1675.
- Wu, F., Minter, S., 2015. Krebs cycle metabolon: structural evidence of substrate channelling revealed by cross-linking and mass spectrometry. *Angew. Chemie - Int. Ed.* 54, 1851–1854. <https://doi.org/10.1002/anie.201409336>.
- Xu, L., Bretscher, A., 2014. Rapid glucose depletion immobilizes active myosin v on stabilized actin cables. *Curr. Biol.* 24, 2471–2479. <https://doi.org/10.1016/j.cub.2014.09.017>.
- Zimmerman, S.B., Trach, S.O., 1991. Estimation of macromolecule concentrations and excluded volume effects for the cytoplasm of *Escherichia coli*. *J. Mol. Biol.* 222, 599–620. [https://doi.org/10.1016/0022-2836\(91\)90499-V](https://doi.org/10.1016/0022-2836(91)90499-V).

Wolbachia pipientis grows in *Saccharomyces cerevisiae* evoking early death of the host and deregulation of mitochondrial metabolism

Cristina Uribe-Alvarez^{1*} | Natalia Chiquete-Félix^{1*} | Lilia Morales-García¹ |
 Arlette Bohórquez-Hernández² | Norma Laura Delgado-Buenrostro³ |
 Luis Vaca² | Antonio Peña¹ | Salvador Uribe-Carvajal¹

¹Depto. de Genética Molecular, Instituto de Fisiología Celular, Universidad Nacional Autónoma de México, Ciudad de México, México

²Depto. de Biología Celular y del Desarrollo, Instituto de Fisiología Celular, Universidad Nacional Autónoma de México, Ciudad de México, México

³Unidad de Biomedicina UBIMED, Facultad de Estudios Superiores Iztacala, Universidad Nacional Autónoma de México, Tlanepantla, Edo. de México, México

Correspondence

Antonio Peña and Salvador Uribe-Carvajal
 Depto. de Genética Molecular, Instituto de Fisiología Celular, Universidad Nacional Autónoma de México, Ciudad de México, México.
 Emails: apd@ifc.unam.mx; suribe@ifc.unam.mx

Funding information

Dirección General de Asuntos del Personal Académico, Universidad Nacional Autónoma de México, Grant/Award Number: IN204015 and IN2114; Consejo Nacional de Ciencia y Tecnología, Grant/Award Number: 239487 and 344726

Abstract

Wolbachia sp. has colonized over 70% of insect species, successfully manipulating host fertility, protein expression, lifespan, and metabolism. Understanding and engineering the biochemistry and physiology of *Wolbachia* holds great promise for insect vector-borne disease eradication. *Wolbachia* is cultured in cell lines, which have long duplication times and are difficult to manipulate and study. The yeast strain *Saccharomyces cerevisiae* W303 was used successfully as an artificial host for *Wolbachia* wAlbB. As compared to controls, infected yeast lost viability early, probably as a result of an abnormally high mitochondrial oxidative phosphorylation activity observed at late stages of growth. No respiratory chain proteins from *Wolbachia* were detected, while several *Wolbachia* F₁F₀-ATPase subunits were revealed. After 5 days outside the cell, *Wolbachia* remained fully infective against insect cells.

KEYWORDS

bioenergetics, endosymbiosis, oxidative phosphorylation, *Saccharomyces cerevisiae*, *Wolbachia pipientis*

1 | INTRODUCTION

Construction of artificial ecosystems mimicking symbiotic relationships have been proposed to study ecology and evolution of symbioses (Hosoda et al., 2011; Momeni, Chen, Hillesland, Waite, & Shou, 2011), to engineer microbial consortia (Brenner, You, & Arnold, 2008; French, 2017; Frey-Klett et al., 2011; Mee & Wang, 2012), and

to host uncultivable bacteria (Stewart, 2012). Synthetic mutualism of species that do not interact naturally has been established in co-culture between bacteria, yeast, amoeba, alga, cell lines, and tissues (Buchsbbaum & Buchsbbaum, 1934; Hosoda & Yomo, 2011; Hosoda et al., 2011; Kubo et al., 2013; Lórcincz et al., 2010; Shou, Ram, & Vilar, 2007). Several bacterial endosymbionts have been found in yeast (Kang, Jeon, Hwang, & Park, 2009; Saniee & Siavoshi, 2015) as

*Cofirst authors.

well as in fungal hyphae and spores (Bertaux et al., 2003; Bianciotto et al., 2004; de Boer et al., 2004; Hoffman & Arnold, 2010; Lumini, Ghignone, Bianciotto, & Bonfante, 2006; Partida-Martinez & Hertweck, 2005; Sato et al., 2010). In this work, we cultured the obligate endosymbiont bacterium *Wolbachia* in an artificial host: the nonpathogenic yeast *Saccharomyces cerevisiae*.

Wolbachia pipientis is an exceedingly successful obligate endoparasite/endosymbiont in nematodes and arthropods (Taylor & Hoerauf, 1999; Werren, 1997; Werren, Baldo, & Clark, 2008). The size of the *Wolbachia* genome varies widely depending on the strain. Arthropod endoparasites have much larger genomes than nematode endosymbionts (Bandi, Slatko, & O'Neill, 1999; Darby et al., 2012; Foster et al., 2005; Klasson et al., 2008; Salzberg, Puiu, Sommer, Nene, & Lee, 2009; Wu et al., 2004). In regard to a possible aerobic metabolism, the *Wolbachia* from the plant hopper *Leodelphax stratellus* (*wStr*) is ten times more sensitive to paraquat than the insect host cell, suggesting that *wStr* does not possess the enzymes needed for reactive oxygen species (ROS) detoxification and thus it may be anaerobic or microaerophilic (Fallon, Kurtz, & Carroll, 2013). In contrast, eliminating *Wolbachia* with tetracycline in filaria, increases respiratory-chain gene expression in the host and causes an early death. This result, lead to the hypothesis that at least in filariae *Wolbachia* contributes as an energy generator for the host (Strübing, Lucius, Hoerauf, & Pfarr, 2010; Darby et al., 2012, 2014).

Culturing obligate intracellular bacteria is a challenge. Insect cells support *Wolbachia* growth, but culture times are long and cells are difficult to manipulate. Alternative systems such as mammalian blood have proven helpful to grow intracellular organisms such as *Sodalis* (Dale & Maudlin, 1999). However, *Wolbachia* did not seem to grow in blood and this was not pursued further (Result not-shown; see Methods). In contrast, *Saccharomyces cerevisiae* did support the growth of *Wolbachia* strain *wAlbB*.

As it can be extensively manipulated, *S. cerevisiae* is widely used as a model organism in biochemistry and molecular biology. In *S. cerevisiae*, it is possible to study processes such as the Crabtree effect observed in tumor cells (Diaz-Ruiz, Rigoulet, & Devin, 2011) and to model cell death in response to anoxia or ischemia/reperfusion (Stella, Burgos, Chapela, & Gamondi, 2011). In addition, it is used as a host to study DNA and RNA viral replication (Alves-Rodrigues, Galão, Meyerhans, & Díez, 2006), to identify and characterize bacterial effectors and toxins (Siggers & Lesser, 2008) and to analyze the function of heterologously expressed proteins such as the *Yarrowia lipolytica* and the mammalian brown-fat mitochondrial uncoupling proteins (UCPs) (Guerrero-Castillo et al., 2011). Thus, when it was observed that *Wolbachia* grew in *S. cerevisiae*, the system was characterized and the effects of *Wolbachia* infection on its host were analyzed.

Growing *Wolbachia* in insect cell cultures or in live hosts presents difficulties that have precluded detailed biochemistry and physiology studies (Baldrige et al., 2014; Khoo, Venard, Fu, Mercer, & Dobson, 2013). Here, we used the *S. cerevisiae* strain W303 as an alternative host for *Wolbachia* *wAlbB* and analyzed the host/endosymbiont system. Infected yeasts died earlier than controls. This probably

resulted from an abnormally high mitochondrial oxidative phosphorylation activity observed at late stages of growth. Understanding *Wolbachia* and host-*Wolbachia* interactions holds great promise for medical, parasitological, and biotechnological applications.

2 | EXPERIMENTAL PROCEDURES

2.1 | Aa23 cell line maintenance

Aa23 cell line (*Aedes albopictus* infected with *wAlbB*) (O'Neill et al., 1997) was kindly donated by Professor Anne Fallon (U. Minnesota) and maintained in Eagle's minimal essential medium (MEM, Sigma Chemical Co. M0643). MEM was supplemented as indicated elsewhere (Shih, Gerenday, & Fallon, 1998). The medium was filter-sterilized (Millipore, 0.22 μ m) and stored in 200 ml aliquots at 4°C. Prior to use, heat-inactivated fetal bovine serum (FBS; 30 min at 56°C) was added to a final concentration of 10% (Shih et al., 1998). The insect cell line was grown on True Line TR 4003 140 mm sterile petri dishes at 27°C in a 5% CO₂ atmosphere (ESCO CelCulture CO₂ incubator or in Corning culture flasks, Shanghai, China). Subcultures were performed in a 1:10 split at 90% confluence. A sample from this cell line was treated with tetracycline to eliminate *Wolbachia* infection (Aa23Tet) (Dobson, Marsland, Veneti, Bourtzis, & O'Neill, 2002).

2.2 | Cell viability assays

Viability of Aa23 cell line, *Wolbachia* or yeast was assessed using the BacLight live-dead staining kit (Molecular Probes, Carlsbad, CA). Ten microliters of cell suspension were stained according to the manufacturer suggested protocol and viewed in an epifluorescence NIKON microscope.

2.3 | Failed attempts to grow *Wolbachia* ex-vivo and a serendipitous finding

The original idea was to find a system where *Wolbachia* would grow ex-vivo. To do this, diverse protocols used for other endosymbionts such as *Sodalis* and *Coxiella* were followed (Dale & Maudlin, 1999; Omsland et al., 2009, 2013). It was found that some components did improve survival in isolated *Wolbachia*, even if we never observed substantial growth. Some of these agents were: (1) Trehalose and other compatible solutes such as mannitol, glycerol and sucrose, known to stabilize pollen (Crowe, Reid, & Crowe, 1996; Leslie, Israeli, Lighthart, Crowe, & Crowe, 1995) and isolated proteins (Sampedro & Uribe, 2004) (2) Actin, which supports binding and movements of some endosymbionts in vivo. (3) Catalase which deactivates hydrogen peroxide (Dale & Maudlin, 1999) and (4) Blood from large mammals, which has been used to grow *Sodalis* (Dale & Maudlin, 1999) and increases *Wolbachia* titers (Amuzu, Simmons, & McGraw, 2015; McMeniman, Hughes, & O'Neill, 2011). Human blood was also effective.

First, we tried growing *Wolbachia* using sheep blood. However, it was easily contaminated at the sites of extraction, so cultures

had to be discarded often. On one occasion we obtained positive *wsp* gene amplification from a yeast colony grown in one of the agar plates. Out of curiosity, we studied the host, which turned out to be *S. cerevisiae*. From this accidental finding we decided to test a known strain of *S. cerevisiae* as an alternative host. We learned that, in order to support growth of *Wolbachia*, yeast culture media needed to be supplemented with blood, which eventually was substituted with ammonium ferric citrate with excellent results and none of the contamination problems. Neither compatible solutes, nor catalase nor actin enhanced growth. The second addition needed was bovine fetal serum, which was present in all original growth media but not in yeast culture media. FBS was titrated and we ended up using 1%.

Among laboratory strains, infection was successful in W303 and NB40, while infection % in BY was milder (Figure 1). The *S. cerevisiae* strain W303-1A (MAT α ; *ura3-1*; *trp1* Δ 2; *leu2-3,112*; *his3-11,15*; *ade2-1*; *can1-100*) (Gutierrez-Aguilar et al., 2014), where *Wolbachia* was abundant at 10 days of infection was chosen for further experiments (See Results).

2.4 | *Wolbachia wAlbB* infection of the *Saccharomyces cerevisiae* W303 yeast strain (*wScW303*)

A first yeast infection was performed following a modified cell line infection protocol (Dobson et al., 2002). All procedures were performed under sterile conditions. The Aa23 cell line (containing *Wolbachia*) was grown in Corning cell culture flasks (225 cm²) as described in (Shih et al., 1998). After 20 days of culture, cells were scrapped and concentrated by centrifugation at 3,000g for 5 min. For homogenization, $\sim 1 \times 10^7$ cells were resuspended in 10 ml Eagles medium and vortexed for 10 min with (50% v/v) 3 mm sterile borosilicate glass beads (Rasgon, Gamston, & Ren, 2006). The homogenate was centrifuged at 3,000g for 10 min to remove unbroken cells. The supernatant was passed through a 2.7 μ m syringe filter and the filtrate containing bacteria was centrifuged at 16,500g for 10 min. The pellet was resuspended in 2 ml of Mitsubishi-Maramorosch medium (MM) supplemented with 1 mmol L⁻¹ ammonium ferric citrate and 20% fetal bovine serum (FBS) (MM Fe FBS). In parallel, yeasts were

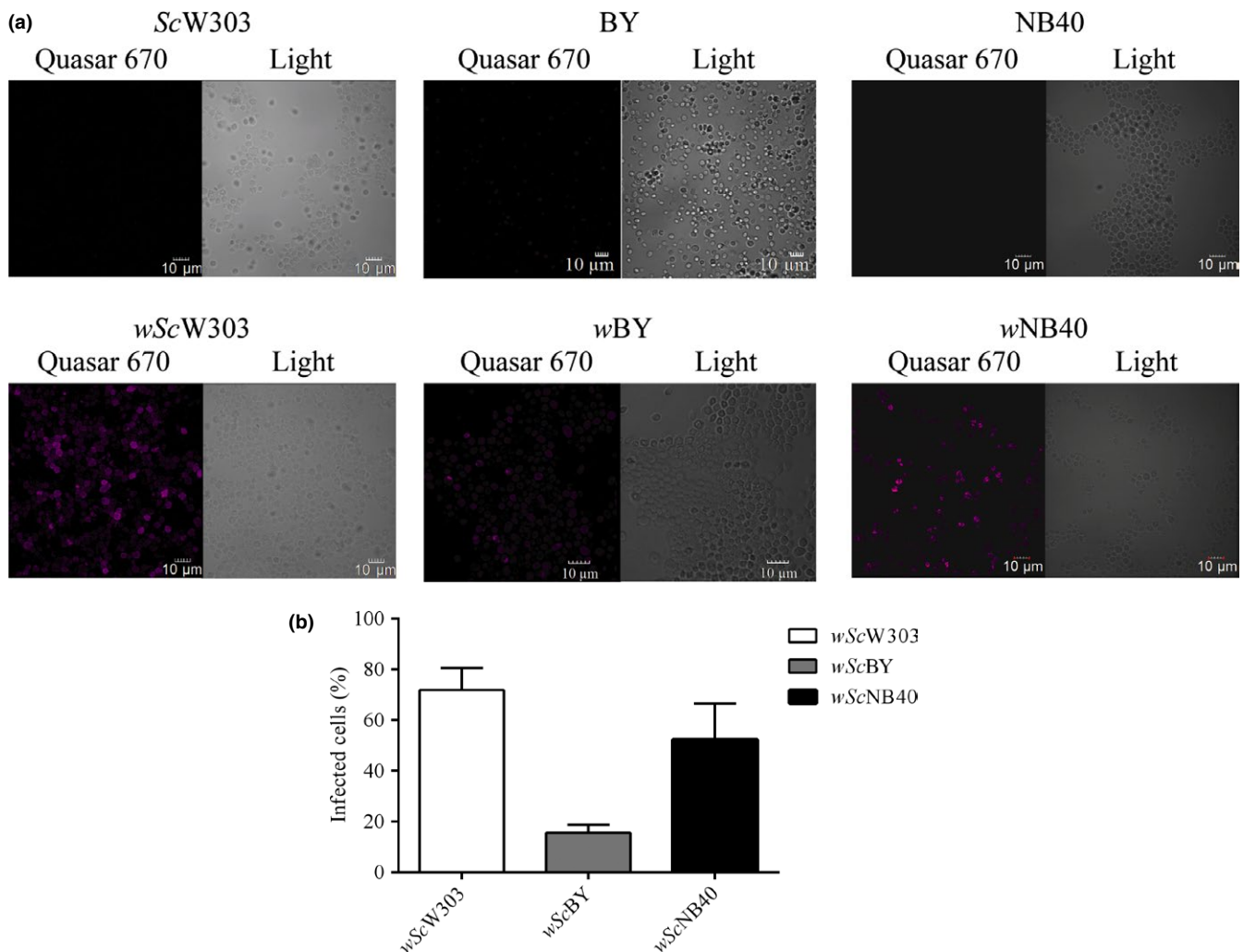


FIGURE 1 Infection of *Saccharomyces cerevisiae* with *Wolbachia*. (a) FISH using a *Wolbachia* 16S rDNA specific probe labeled with Quasar 670 (pink) was performed on 14 day old cultures of infected and control *S. cerevisiae* strains W303 (*ScW303*), BY (*ScBY*), and NB40 (*ScNB40*) (b) After 14 days postinfection, the percentage of infected cells were counted as those with positive hybridization.

grown in a liquid YPD culture for 3 hr, harvested and centrifuged at 3,000g for 3 min. Culturing yeast in low oxygen environments prevents thickening of the cell wall (Aguilar-Uscanga & Francois, 2003; Smith et al., 2000; Avrahami-Moyal, Braun, & Engelberg, 2012). To induce contact between bacteria and yeast both bacteria (the whole 2 ml sample) and yeast (60 mg ww) were mixed and centrifuged at 2,500g for 1 hr at 20°C (Dobson et al., 2002). Bacteria-infected yeast were plated (all 2 ml) on a Petri dish containing MM supplemented with 1 mmol L⁻¹ ammonium ferric citrate plus 25% v/v outdated human packaged erythrocytes and 2% agar (MM Fe-blood) and incubated at 27°C in a 5% CO₂ chamber (ESCO, Cell Culture CO₂ incubator, Singapore) for 14 days (Dale & Maudlin, 1999). Infection was confirmed by FISH and PCR. Infected yeast was transferred to a fresh agar plate every month for up to 6 months, then yeast was discarded and a new sample was used. Some aliquots were added with 40% glycerol, frozen and stored at -80°C, these samples have remained infective for nearly 10 months.

To transfer *Wolbachia* from yeast to yeast, slight modifications to the protocol were made: An aliquot of 100 µl of yeast taken from a glycerol-frozen sample or a loophole of infected yeast cells was diluted in 2 ml YPD Fe 20% FBS and plated in YPD Fe-blood agar plates, which were grown in 5% CO₂. After 14 days, all cells grown in a Petri dish were collected and washed by centrifugation at 3,000g for 3 min at 20°C with sterile water and the pellet was suspended in 10 ml MM. The suspension was vortexed for 10 min in the presence of 0.425–0.600 mm sterile borosilicate glass beads (60% v/v) to disrupt yeast cells (note that beads were smaller than those used for insect cell lines). Disrupted yeasts were centrifuged at 3,000g for 10 min and the supernatant was centrifuged again 3,000g for 10 min. The washed supernatant was filtered through different 0.8–0.65–0.45 µm syringe filters. Again, we used filters with smaller pores than those used for cell lines due to the small size of yeast cells. The last filtrate was centrifuged at 16,500g for 10 min. The pellet (~60 mg ww) was suspended in 2 ml MM Fe FBS and used to infect yeast from 3-h cultures as described above. The yeast-bacterium mixture was plated in a YPD Fe agar plate and incubated at 27°C with 5% CO₂ for at least 7 days. Infection was evaluated using FISH and PCR.

2.5 | Culture and maintenance of wAlbB-infected *Saccharomyces cerevisiae* W303

Infected *S. cerevisiae* strains were kept in YPD plus 1 mmol L⁻¹ ammonium ferric citrate agar plates. When transferring to liquid medium, a loophole from the desired strain was suspended in 100 ml of sterile YPDS and incubated at 28°C, 130 rpm for 48 hr. Precultures were decanted in one liter YPDS and incubated at the same conditions for up to 14 days. When transferring from solid to solid media, a loophole of yeast was suspended in 1 ml YPD supplemented with 1 mmol L⁻¹ ammonium ferric citrate plus 20% FBS and plated on YPD agar. A cell passage every 2–3 weeks was performed in order to maintain the infection. When it was desired to eliminate *Wolbachia*

from yeast, tetracycline 30 µg/ml was added five consecutive times to the medium as passages were performed (Dobson et al., 2002).

2.6 | *Wolbachia* wAlbB infection of the C6C36 *Aedes albopictus* cell line

To determine whether *Wolbachia* cells retained its infective ability after all treatments, *Wolbachia* were isolated from *S. cerevisiae* grown in liquid YPD Fe 1% FBS and they were tested for infection against a C6C36 insect cell line.

2.7 | *Wolbachia* surface protein (*wsp*) gene PCR identification

The *Wolbachia* *wsp* gene was amplified using the following primers: *wsp* 81F (5' TGGTCCAATAAGTGATGAAGAAAC 3') and *wsp* 691R (5' AAAAATTAACGCTACTCCA 3') (Braig, Zhou, Dobson, & O'Neill, 1998) in a 25 µl reaction volume using recombinant Taq DNA polymerase (Thermo Fisher Scientific). PCR amplification was performed as reported elsewhere (Braig et al., 1998; Xi, Khoo, & Dobson, 2006). The PCR product was electrophoresed on a 1% agarose gel and stained with ethidium bromide. PCR product was purified using a GeneJET PCR purification Kit (Thermo Fisher Scientific) and sequenced in the Molecular Biology Unit at the Institute of Cellular Physiology, UNAM.

2.8 | Fluorescence in-situ hybridization (FISH)

Wolbachia 16S rDNA oligonucleotide probe labeled with Quasar 670 dye (λ_{em} 647, λ_{ex} 670) W1, 5'-AATCCGGCCGARCCGACCC-3' was used for FISH assays (Heddi, Grenier, Khatchadourian, Charles, & Nardon, 1999). One milliliter of the desired culture was centrifuged at 3,000g for Aa23, C6C36 and yeast, and 18,500g for purified *Wolbachia* for 5 min. Protocol was followed as reported elsewhere (Genty, Bouchon, Raimond, & Bertaux, 2014). Samples were viewed in a FluoView FV-1,000 Olympus confocal microscope, NA 1.4 with a 100X objective. Images were analyzed with the FV-Viewer Olympus software.

2.9 | Z-cut images for cell reconstruction

Fourteen day old infected and noninfected yeast samples were visualized with a Olympus-FV1000 or FV-3000 microscopes. Z-cut images were reconstructed using Imaris 7.2.1 and Image J software. Calcofluor-white (0.05 mmol L⁻¹ in 20% DMSO-20 mmol L⁻¹ Bicine Buffer) was used to stain fungus cell wall.

2.10 | Antibodies

Primary antibodies: Mouse monoclonal Anti-*Wolbachia* Surface Protein NR-31029 was from BEI Resources, NIAID, NIH. Mouse monoclonal Anti-VDAC was from Abcam. Secondary antibody: HRP

coupled Anti-mouse antibody from Jackson ImmunoResearch (West Grove, PA).

2.11 | Western blot

A loop-hole from yeast grown in solid media was suspended in 200 μl of water; otherwise, 200 μl from liquid culture samples were centrifuged at 3,000g for 5 min and washed twice in water. The pellet was solubilized in 200 μl RIPA buffer (25 mmol L^{-1} Tris•HCl pH 7.6, 150 mmol L^{-1} NaCl, 1% NP-40, 1% sodium deoxycholate, 0.1% SDS) supplemented with protease inhibitors 1 mmol L^{-1} PMSF (Sigma-Aldrich) and Complete protease inhibitor cocktail (Roche-CO-RO) as recommended by the abcam protocol. Samples were lysed in a Sonics VibraCell sonicator (Sonics & materials, Inc., Newtown, CT) at 80% amplitude for 10 s and left under agitation in a Multi-Vortex V-32 (Biosan, Riga, Latvia) for 30 min at 4°C. Samples were centrifuged at 15,160g for 5 min. The supernatant was recovered and protein concentration was measured by Bradford in a PolarStar Omega (BMG labtech, Ortenberg, Germany) [(Bradford, 1976) #64]. Samples were diluted in a 4X buffer (500 mmol L^{-1} Tris, pH 6.8, 10% glycerol, 10% SDS, 0.05% beta-mercapto-ethanol, and 0.01% bromophenol blue) and boiled for 5 min. SDS/PAGE was performed in 10% polyacrylamide gels and electrotransferred to poly(vinylidenedifluoride) membranes as reported elsewhere (Chiquete-Felix et al., 2009). Membranes were blocked with 5% Blotto nonfat dry milk in TBS-T (50 mmol L^{-1} Tris, 104 mmol L^{-1} NaCl, pH 7.6, 0.1% Tween 20) for 1 hr, and incubated overnight at 4°C with the primary antibody. Membranes were washed with TBS-T and incubated at 37°C for 1 hr with secondary antibody. Membranes were washed again and the bands were developed by chemiluminescence using an ECL kit (Amersham Biosciences, GE, Healthcare) (Chiquete-Felix et al., 2009). PVDF membranes were stripped as indicated by abcam protocol using a mild-stripping buffer, blocked with 5% Blotto nonfat dry milk in TBS-T and reprobed with a different antibody as indicated.

2.12 | Transmission electron microscopy of wScW303

Infection was assessed by transmission electron microscopy (TEM) following a protocol from (Sun et al., 2015). Briefly, 500 μl of cells were harvested from 100 ml cultures of infected and uninfected *Saccharomyces cerevisiae* cultures from the first unintentional infection (wSc) at 10 days and wScW303 of fourteen days. Yeast and *Wolbachia* samples were washed twice in distilled water at 740 g for 5 min for yeast and 23400 g for 10 min for bacteria in an Eppendorff Centrifuge 5415C. Samples were fixed in 2% KMnO_4 at 4°C overnight. Next day, samples were washed for 15 min with deionized water six times and dehydrated with sequential 10-minute washes with 50%, 70%, 80%, 90% ethanol and three washes with 100% ethanol. Samples were washed with ethanol-propanone (1: 1) for 8 min, then with anhydrous propanone for 5 min, then with propanone-EPON 821 (3: 1) for 1 hr and left in propanone-EPON 821 (1 : 3) overnight. Next day, samples were

concentrated and resuspended in propanone-EPON 821 (1: 1) for 1 hr. Then, samples were concentrated again and left in resin for 24 hr. Then they were incubated for 12 hr at 37°C and then further incubated for 36 hr at 60°C. Resins were cut into 70 nm slices on an ultra-microtome (Ultracut Reicheit-jung) and observed in a JEOL JEM-1200 EXII electron microscope. Data were processed using Gatan Digital Micrograph Software.

2.13 | Mitochondrial (or Mitochondria/Wolbachia mixture) isolation

Yeast were centrifuged at 3,000g for 5 min, washed twice in water and resuspended in MES-mannitol buffer (5 mmol L^{-1} MES, 0.6 mol L^{-1} mannitol, 0.1% BSA pH 6.8 adjusted with triethanolamine). Yeast were disrupted using a Bead Beater cell homogenizer (Biospec Products, OK, USA, final volume 50 ml) with 0.425–0.6 mm glass beads during three 20 s pulses separated by 40 s resting periods in ice (Uribe, Rangel, Espínola, & Aguirre, 1990). The homogenate was differentially centrifuged to isolate mitochondria similar to described in (Peña, Piña, Escamilla, & Piña, 1977). Briefly, cells were centrifuged at 1,100g for 5 min. The supernatant was centrifuged at 9,798g for 10 min and the pellet was resuspended in MES-mannitol buffer and centrifuged at 3,000g for 5 min. Finally, the supernatant was centrifuged at 17,500g for 10 min. The resulting pellet was resuspended in minimal volume and protein concentration was measured by Biuret (Gornal, 1957) using a Beckman Coulter spectrophotometer at 540 nm.

2.14 | Oxymetry

Mitochondrial high resolution respirometry was assessed in an Oroboros oxygraph (Oroboros Intrs Corp, Innsbruck, Austria) using 5 mmol L^{-1} MES, 0.6 mol L^{-1} mannitol pH 6.8, 10 mmol L^{-1} KCl and 4 mmol L^{-1} Pi at 30°C. Final volume in the closed chamber was 1.5 ml with a protein concentration of 0.5 mg prot/ml. Bacterial protein concentration of 0.5 mg prot/ml was used. The trace was started by the addition of 5 mmol L^{-1} of the indicated substrate: glycerol-3-phosphate, ethanol, NADH, pyruvate-malate, succinate, glutamine or glutamate. For Complex IV evaluation, 5 mmol L^{-1} ascorbate (pH 7.6)-0.05 mmol L^{-1} TMPD was used (Uribe, Ramirez, & Peña, 1985). Respiratory control was measured using 0.5 $\mu\text{l}/\text{ml}$ ethanol to induce state II respiration and 1 mmol L^{-1} ADP to induce the phosphorylated state (Uribe et al., 1985). Respiratory chain inhibitors were used in the following concentrations: 0.1 $\mu\text{mol L}^{-1}$ rotenone, 0.15 mmol L^{-1} flavone, 0.1 $\mu\text{mol L}^{-1}$ antimycin A, and 2 mmol L^{-1} cyanide (Uribe et al., 1985). 0.5 $\mu\text{mol L}^{-1}$ CCCP was added as an uncoupler. Data were analyzed using the Oroboros Lab software.

2.15 | Electrophoretic techniques and in-gel activities

Blue native gel electrophoresis (BN-PAGE) and high-resolution clear native electrophoresis (hrCN-PAGE) were performed as in (Wittig,

Braun, & Schagger, 2006; Wittig, Karas, & Schagger, 2007). Whole cells were solubilized with 2 mg dodecylmaltoside/mg protein plus 1 mmol L⁻¹ PMSF and Complete protease inhibitor cocktail (Roche-CO-RO) and shaken for 30 min at 4°C. Membranes were centrifuged at 23,680g at 4°C for 1 hr. Protein concentration in the supernatants was determined by Bradford (1976). Between 0.1 and 0.15 mg of protein were loaded in 5%–15% polyacrylamide gradient gels. When hr-CN PAGE electrophoresis was performed 0.01% Lauryl maltoside and 0.05% sodium deoxycholate were added to the cathode buffer [(Wittig et al., 2007) #69]. Gels were run for about an hour at 15 mA/gel in a Bio-rad electrophoresis chamber. In-gel NADH-NBT oxidoreductase (100 µg protein), succinate-NBT oxidoreductase (150 µg protein), cytochrome *c* oxidase (100 µg protein), and in-gel ATPase (100 µg protein) activities were done as reported previously (Uribe-Alvarez et al., 2016). 20 µg protein of solubilized Bovine Heart Mitochondria (BHM) were loaded in each gel as controls.

2.16 | LC-MALDI-MS/MS

Indicated bands from hr-CN PAGE or BN-PAGE were enzymatically digested, separated on a HPLC EksperNanoLC 425 (Eksigent, Redwood City CA) and analyzed in a MALDI-TOF/TOF 4800 Plus mass spectrometer (ABSciex, Framingham MA) (Shevchenko, Tomas, Havli, Olsen, & Mann, 2006) in the Unidad de Genómica, Proteómica y Metabolómica, CINVESTAV-IPN. Generated MS/MS spectra were compared using Protein Pilot software v. 4.0 (ABSciex, Framingham MA) against the *Saccharomyces cerevisiae* ATCC 204508 database (downloaded of Uniprot, 6721 protein sequences) and *Wolbachia* genus database (downloaded of Uniprot, 47781 protein sequences) using Paragon algorithm.

3 | RESULTS

3.1 | At the expense of its own viability, the artificial host *Saccharomyces cerevisiae* W303 supports growth of *Wolbachia* wAlbB

To study *Wolbachia* (wAlbB) large biomass yields plus a host that is easy to manipulate are needed. After testing different alternatives (see Methods), it was discovered that different *S. cerevisiae* strains were susceptible to infection and supported active *Wolbachia* proliferation. At 14 days of infection, *Wolbachia* grew efficiently in *S. cerevisiae* strains W303 (ScW303) and NB40 (ScNB40), while strain BY (ScBY) supported only a weak infection (Figure 1a). After 14 days the percentage of infected cells counted by FISH using probes against the *Wolbachia* 16S rDNA was 71.8% ± 8.7% for ScW303 and 52.3% ± 14.3% for ScNB40, while in ScBY less than 20% cells were positive for FISH (Figure 1b). Strain ScW303 was chosen for further studies. ScW303 maintains high rate of oxidative phosphorylation regardless of the carbon source, it is highly resistant to oxidative stress (Ocampo, Liu, Schroeder, Shadel, & Barrientos, 2012) and it has a weak cell wall (Avrahami-Moyal et al., 2012). Strains used in this study are detailed in Table S1.

3.2 | Proliferation of *Wolbachia* in ScW303 was further confirmed using different independent methods as follows (Figure 2)

3.2.1 | PCR of the *Wolbachia* outer surface protein gene (*wsp*)

Both the Aa23 cell line (Figure 2a) and infected *S. cerevisiae* (wScW303) (Figure 2b) amplified 650 bp fragments exhibiting sequences 100% identical to the surface protein of the *Wolbachia* endosymbiont of *Aedes albopictus* (NCBI database: KC242223.1) (Table S2). PCR amplification bands were not observed in the tetracycline-treated Aa23 cell line (Figure 2a, Aa23 Tet) and in the noninfected yeast (Figure 2b, ScW303). Tetracycline used continuously in cell cultures is reported to kill *Wolbachia* (Dobson et al., 2002).

3.2.2 | Western Blot analysis detected *Wolbachia* *wsp* in *S. cerevisiae*

In the Aa23 cell line, a ~37 kDa protein corresponding to the *Wolbachia* Surface protein (*wsp*) was revealed with anti *wsp* antibodies (Bei resources, NIH, MD) (Figure 2c, Aa23). This band disappeared after growth in the presence of tetracycline (Aa23 Tet). VDAC (Voltage dependent anionic channel) protein was used as a loading control. In non-infected yeast *wsp* was not detected, (Figure 2c, ScW303), while in infected yeast the *wsp* western blot signal was first detected at day 3 and increased gradually up to day 10, remaining stable until day 14 (Figure 2c, wScW303). (For images of original Western Blots, see Figure S1a). When tetracycline was added to the medium, the *wsp* signal decreased, disappearing by day 10 (Figure S1b, wScW303Tet).

3.2.3 | Normal growth and early death were observed in infected *S. cerevisiae*

During the first 12 days of culture, growth curves of infected wScW303 were similar to the controls (Figure 3a). Then, beginning at day 14, wScW303 absorbance decreased. Cell wall degradation (Figure S2) and viability staining (Figure 3b) confirmed that wScW303 viability was rapidly lost during the late stages of the stationary phase, from 14 to 18 days of culture.

In addition, during growth the transcriptional activity of both *S. cerevisiae* 18S rRNA and the *Wolbachia* *wsp* were tested. Transcription was high in *S. cerevisiae* from the first day, decreased at day fourteen and became negligible at days 16 and 18 (Figure 3c). In contrast, transcription of the *wsp* from *Wolbachia* became detectable only after 3 days, increased exponentially until day 10 and remained constant until day 14. Then, at days 16 and 18, transcription decreased abruptly (Figure 3c). Transcription data in the *Wolbachia*/*S. cerevisiae* system indicated that *Wolbachia* activity grew later than *S. cerevisiae*, reaching a maximum at 10 days. Later, beginning at 14 days both transcription activities decreased abruptly in parallel with the death of the host.

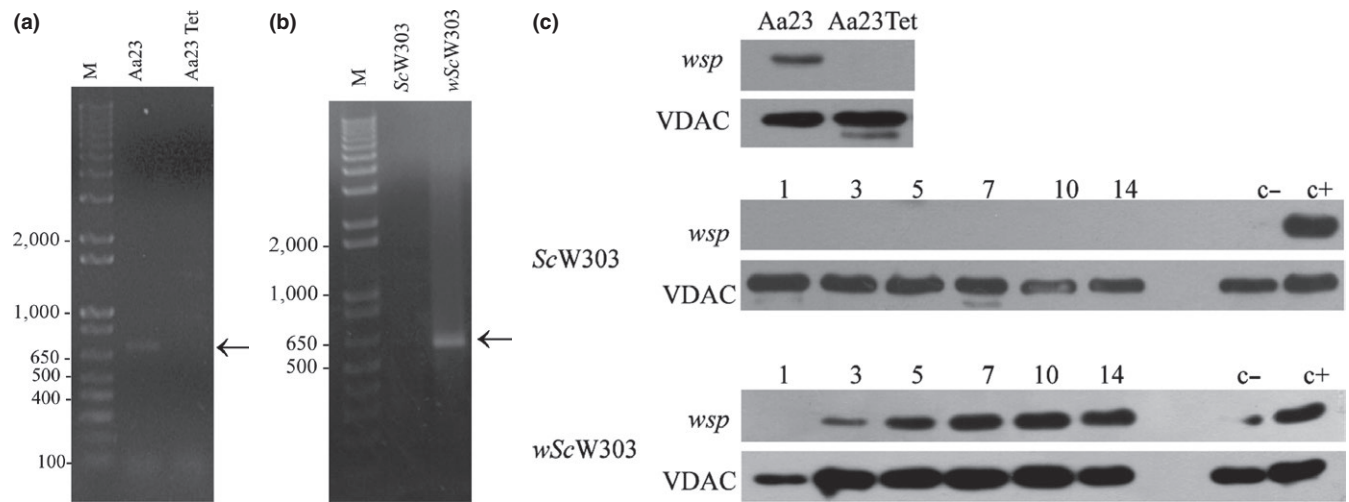


FIGURE 2 Detection of *Wolbachia* in *Saccharomyces cerevisiae* W303. (a) Agarose gel electrophoresis of the *wsp* PCR products predicted as a ~600 bp band in the Aa23 cell line. Lanes: M, Invitrogen 1 kb plus DNA ladder; Aa23, infected cell line; Aa23 Tet, noninfected cell line. (b) Agarose gel electrophoresis of the *wsp* PCR products for *S. cerevisiae*. Lanes: M, Invitrogen 1 kb plus DNA ladder; ScW303, uninfected original yeast; wScW303, infected yeast. (c) Western blot against the *wsp* and VDAC proteins. First row, first lane Aa23 infected cell line and second lane Aa23 Δ w tetracycline-cured cell line. Yeast samples were taken at 1, 3, 5, 7, 10, and 14 days postinfection. A positive control was taken from a 20 day YPD-2% agar culture infected-wScW303. Negative control was a noninfected sample ScW303

3.2.4 | Yeast cell/endosymbiont images were observed by staining *S. cerevisiae* with Calcofluor white and wAlbB with Quasar 670

Both the western blot and the RT-PCR experiments suggested that *Wolbachia* grew in the presence of *S. cerevisiae* becoming abundant at days 10–14. In order to determine whether *Wolbachia* was inside yeast, samples from infected and noninfected yeast cells from 14-day old cultures were hybridized using a *Wolbachia* specific 16S rDNA probe labeled with Quasar-670 (FISH). Then, the yeast cell wall was stained with Calcofluor white (Figure 4, Movie S1, Movie S2), Staining of the *S. cerevisiae* cell wall allowed observation of labeled bacteria inside yeast. Figure 4 shows that the Quasar-670 label was detectable only in wScW303 and not in ScW303. Merge of the Calcofluor, Quasar-670 and Clear field (Light) images show bacteria are inside the cell (Figure 4). Tridimensional reconstructions of z-cuts performed in a wScW303 sample show the intracellular location of different bacteria (movies S1 and S2). In the periphery of movies S1 and S2, few independent bacterial labels were detected, which we speculate, may come from bacteria inside heavily deteriorated host cells whose cell wall was not stained by Calcofluor (movies S1 and S2).

3.2.5 | TEM images detected *Wolbachia* inside *S. cerevisiae*

Transmission electron microscopy images further suggested the intracellular location of *Wolbachia*. Cultures of 10 and 14 days of control and infected *S. cerevisiae* were analyzed. In infected yeast cells (Figure 5b–f, g), bacteria-like bodies (Figure 5, labeled *) that are not present in the uninfected yeast (Figure 5a and d) can be

observed. At 10 days both infected and noninfected yeast present mitochondria, which can be identified by the presence of inner membrane cristae (Figure 5, labeled m). In contrast 14 day-old cultures of ScW303 lost most mitochondrial structures, which suggest that these organelles are dysfunctional probably because cells are in late stationary phase. In contrast, 14 days-old infected wScW303 show *Wolbachia* plus mitochondria where the typical cristae pattern may be observed, suggesting abnormal preservation of mitochondria in infected yeast (Figure 5e–g). In wScW303 cultures, we can observe different cell images: most cells had an intact plasma membrane and contained mitochondria and bacteria-like bodies inside (Figure 5e). Other cells exhibited damaged membranes but the bacteria like structures were still present (Figure 5f). Among the whole population, we found some budding yeast, where bacteria-like bodies can be seen concentrated in the bud (Figure 5g). None of the latter populations was found in control ScW303 cultures.

3.2.6 | *Wolbachia*-infected yeast retained high mitochondrial oxidative phosphorylation activity for abnormally long periods

A possible mechanism for the early death of infected yeast was explored in our infected ScW303/wAlbB system. This system exhibited an abnormal preservation of mitochondria (Figure 5), so it was logical to explore aerobic metabolic activity. The relationship between *Wolbachia* and aerobic metabolism in the host is a matter of controversy. Some authors have proposed that these endo-cellular organisms possess an aerobic metabolism that contributes to overall activity (Strübing et al., 2010) while others suggest that *Wolbachia* optimizes aerobic metabolism by supplying heme groups for respiratory complexes (Darby et al., 2012; Fallon, Baldrige, Carroll, &

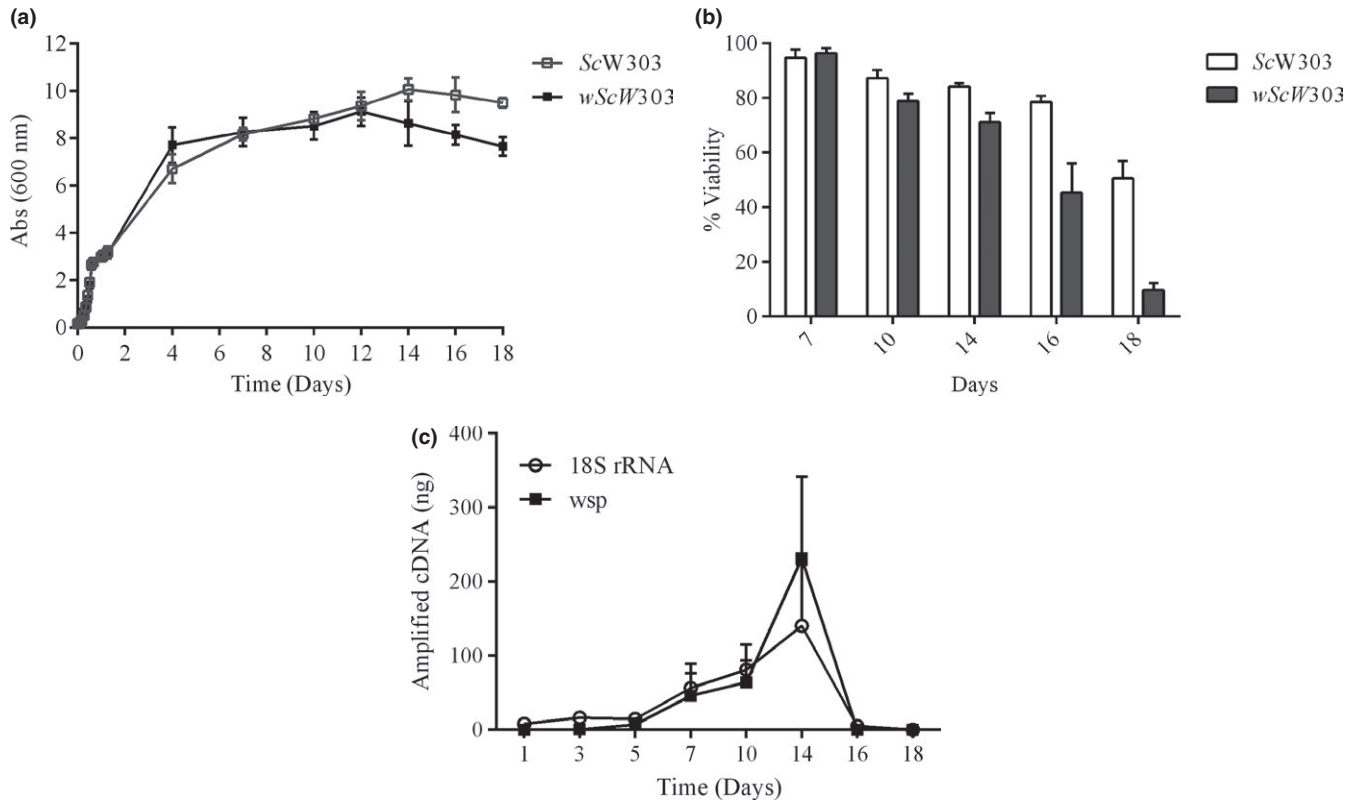


FIGURE 3 *S. cerevisiae* growth, viability, and transcriptional activity in the absence and presence of *Wolbachia*. (a) Growth curves of ScW303 and wScW303 grown in YPDS at 30°C, 130 rpm for 18 days. (b) Yeast cell viability in different days of culture quantified by microscopy with the BacLight viability kit. (c) Amplification of the *wsp* gene of *Wolbachia* and the 18S rRNA gene of *S. cerevisiae* of samples taken at different days of culture

Kurtz, 2014; Foster et al., 2005; Heddi et al., 1999; Strübing et al., 2010). Thus, we decided to evaluate oxidative phosphorylation activities in our system, which preserved mitochondrial structure beyond the stationary phase (Figure 5).

When isolation of *Wolbachia* was attempted, it was found that the bacterium and mitochondria migrated together (Baldrige et al.,

2014; Uribe et al., 1985). Thus, it was decided to characterize oxidative phosphorylation activity in the mitochondria/*Wolbachia* mixture and then determine the contribution of each entity using different bioenergetics techniques. The rate of oxygen consumption was measured using ethanol as a substrate (Table 1). We isolated the mitochondria/*Wolbachia* fraction from either one-day cultures

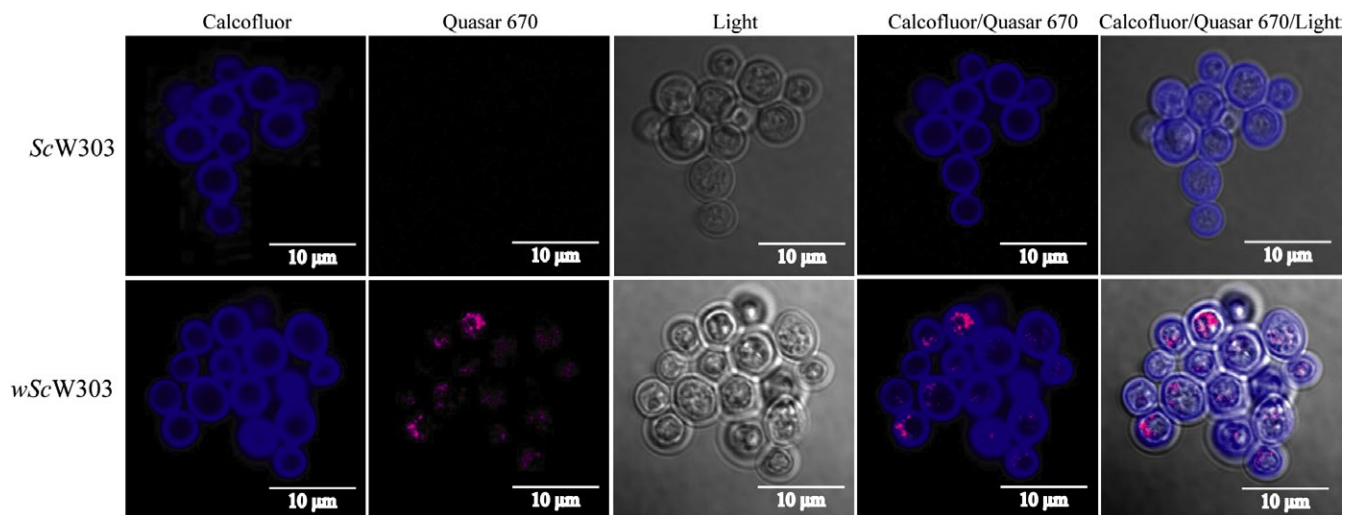


FIGURE 4 *Wolbachia* in calcofluor-labeled *S. cerevisiae*. Infected (wScW303) and noninfected (ScW303) *S. cerevisiae* cells were hybridized with the 16S rDNA *Wolbachia* probe (Quasar 670, pink). Then, the yeast cell wall was stained with calcofluor-white (Calcofluor, blue) to confirm the endosymbiosis. Merge images are shown to evaluate the presence of *Wolbachia* inside yeast

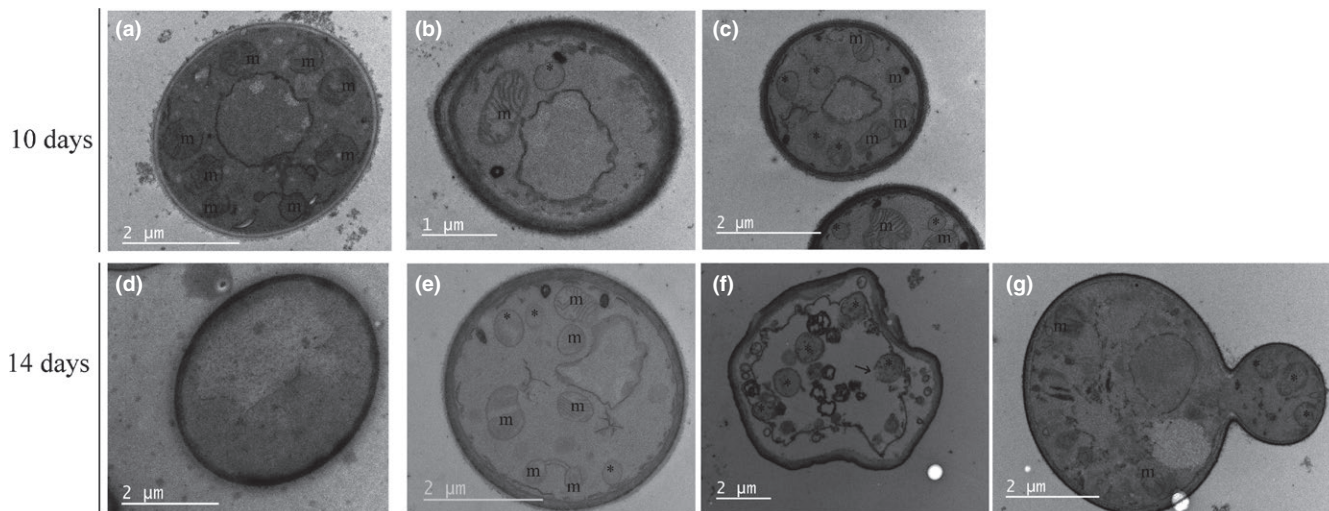


FIGURE 5 Electron microscopy images of infected and noninfected *Saccharomyces cerevisiae* at different times of incubation.

Transmission electron microscopy images confirm the intracellular location of *Wolbachia*. 10-day images were taken with uninfected (a) Sc and infected (b–c) wSc; 14 day-old images were taken with (d) ScW303 and (e–g) wScW303. Images show the presence of bacteria-like bodies (*) that are not present in uninfected yeast and mitochondria (m) whose cristae can be easily identified

TABLE 1 Oxygen consumption rates of mitochondrial fractions from 1 and 14 day-old cultures of *Wolbachia*-infected (wScW303) and noninfected (ScW303) *Saccharomyces cerevisiae* cells

	State IV (natgO/min*mg prot)	State III (natgO/min*mg prot)	RCIII/IV
1 Day ScW303	25.2 ± 3.1	52.5 ± 6.8	2.1 ± 0.15
1 Day wScW303	27.4 ± 4.6	65.4 ± 9.0	2.4 ± 0.2
14 Days ScW303	22.6 ± 5.1	29.0 ± 6.3	1.3 ± 0.2
14 Days wScW303	34.2 ± 5.1	73.3 ± 11.1	2.1 ± 0.1

Reaction mixture: 0.6 mol L⁻¹ mannitol, 5 mmol L⁻¹ MES, pH 6.8, 4 mmol L⁻¹ Pi, 10 mmol L⁻¹ KCl. As substrate, 5 mmol L⁻¹ ethanol. For state III, 1 mmol L⁻¹ ADP.

where there are very few *Wolbachia* cells or from 14-day cultures, where *Wolbachia* numbers were high (Table 1). In one-day cultures from ScW303 and wScW303 respiratory activities were very similar. However, at 14 days the rates of oxygen consumption and respiratory controls (RC) were widely different as follows: In noninfected yeast, both the rate of oxygen consumption and respiratory control decreased at the expense of state 3 inhibition, while in contrast, wScW303 retained high rates of oxygen consumption plus high respiratory controls, i.e. in 14-day old *Wolbachia*-infected yeast exhibited high oxidative phosphorylation activity, consistent with the presence of mitochondria observed by TEM in the infected cells (Table 1).

3.2.7 | In the presence of *Wolbachia* the activity of different mitochondrial respiratory complexes was preserved

In the isolated mitochondria/*Wolbachia* mixture, we tested specific substrates for each respiratory chain complex/enzyme (Table S3). In one-day cultures the rates of oxygen consumption were similar in infected and noninfected *S. cerevisiae* (Figure 6). In

aged mitochondria from noninfected yeast, external NADH dehydrogenase (NDH2e, Pyruvate-Malate), succinate dehydrogenase (Succinate) and Complex IV (Ascorbate-TMPD) activities were strongly diminished. In contrast, in the 14 day-old mitochondrial fractions from *Wolbachia*-infected cells, respiratory activities in the presence of glycerol-3-phosphate, pyruvate-malate, and succinate were increased in comparison to 1-day cultures. Since *S. cerevisiae* does not have complex I and pyruvate-malate dependent respiration was insensitive to rotenone, redox activity was most likely from the mitochondrial NDH2 and not a bacterial complex I. Succinate oxidation was completely inhibited by antimycin A, indicating the absence of an alternative oxidase. Complex IV and NADH-dependent oxygen consumption rates were still decreased as compared to mitochondria from one-day cultures (Figure 6). Other respiratory substrates, namely glutamate and glutamine, which are used by *Rickettsia* (Winkler & Turco, 1988) where assayed and they did not support oxygen consumption. The respiratory activities measured indicate that the mitochondria/*Wolbachia* fractions from the infected and noninfected yeast consume the same substrates and are inhibited by the same respiratory chain inhibitors.

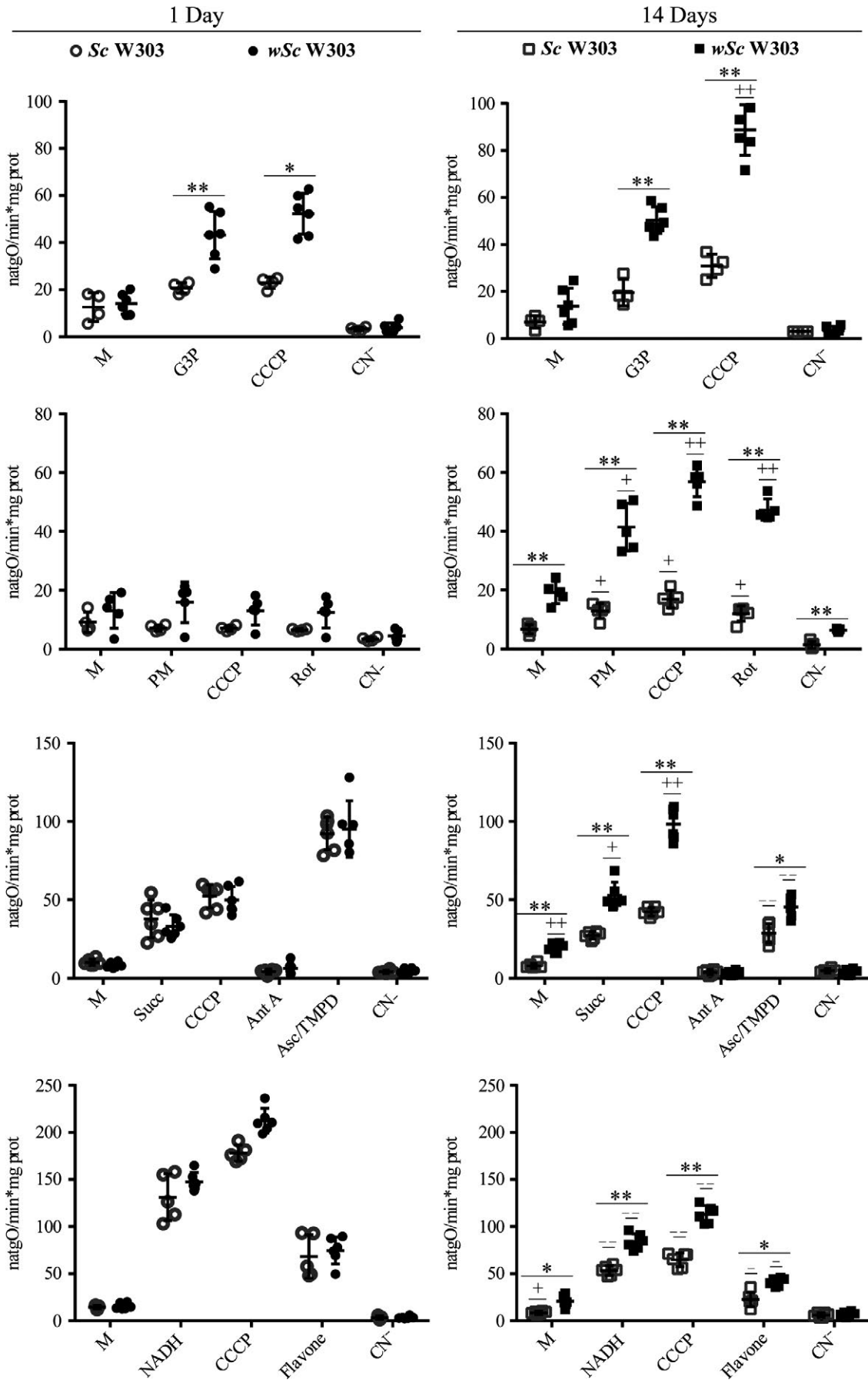


FIGURE 6 *Wolbachia*-mediated effects on the oxygen consumption activity of isolated yeast mitochondria. High-resolution respirometry. 1 day-old cultures of noninfected (1 Day ScW303) and infected (1 Day wScW303) yeast and 14 day-old cultures of noninfected (14 Days ScW303) and infected (14 Days wScW303) yeast. 5 mmol L⁻¹ from each substrate was added as indicated: glycerol-3-phosphate (G3P), NADH, pyruvate-malate (Pyr-Mal), succinate (Succ), and ascorbate-TMPD (Asc/TMPD). Where indicated, 0.5 μmol L⁻¹ CCCP, 0.1 μmol L⁻¹ rotenone (Rot), 0.1 μmol L⁻¹ antimycin A (Ant A), 1 mmol L⁻¹ cyanide (CN⁻), and 0.15 mmol L⁻¹ flavone. 0.5 mg prot/ml of mitochondria (M) were added. Data represent mean ± SEM. T test **p* < .005, ***p* < .001 for ScW303 versus wScW303 yeast on the same day. T test ^{-/+}*p* < .05 ^{-/+}*p* < .001 (–, decrease; +, increase) for ScW303 in day one versus day 14 cultures or wScW303 in day one versus day 14 cultures

3.2.8 | Under the experimental conditions tested, infected wScW303 oxygen consumption activity was mitochondrial

The experiments above suggested that either *Wolbachia* has the exact same electron transport chain as mitochondria or *Wolbachia* respiratory proteins may be damaged when the mitochondria/*Wolbachia* fraction is isolated and exposed to oxygen.

To explore this possibility further, we measured in-gel activities in the mitochondria/bacterium fraction. As eukaryote and prokaryote respiratory complexes I, II, III, and IV have different molecular masses the contribution from each organism to a given activity would be easily detected by native gel electrophoresis. The in-gel activities for each complex from infected and noninfected yeast from 1 and 14 day-old cultures were analyzed and, in all cases, activities were detected only at MWs corresponding to the mitochondrial enzymes (Table S3, Figure 7) suggesting that in the artificial ScW303/wAlbB system and under the specific conditions of growth reported here, *Wolbachia* did not express any functional respiratory chain proteins. The above results suggest that mitochondria were responsible for all the observed oxygen consumption activity. Still,

one NADH dehydrogenase (Table S4) was weakly expressed making it impossible to conclude on whether different *Wolbachia* strains may be aerobic or not.

3.2.9 | F₁F₀-ATPase subunits from *Wolbachia* were detected in wScW303

In the in gel ATPase activity from the mitochondria/*Wolbachia* isolate no differential bands were observed. This was expected as the proposed MWs are similar for of both ATPases: 543 kDa for the eukaryote *S. cerevisiae* and 530 kDa for prokaryotes *Escherichia coli* and *Paracoccus denitrificans* (Bakhtiari, Lai-Zhang, Yao, & Mueller, 1999; Jonckheere, Smeitink, & Rodenburg, 2012; Morales-Rios, Montgomery, Leslie, & Walker, 2015; Robinson et al., 2013; Schagger, 2002). However, the ATPase activity band (Figure 7A1, Table S4) sequence exhibited a mixture of yeast and *Wolbachia* ATPase proteins. BN and hrCN-PAGE results indicate that if *Wolbachia* expresses any electron transport chain proteins (still a possibility), under our experimental conditions their concentration was negligible when compared to the mitochondrial proteins and to its own F₁F₀-ATPase.

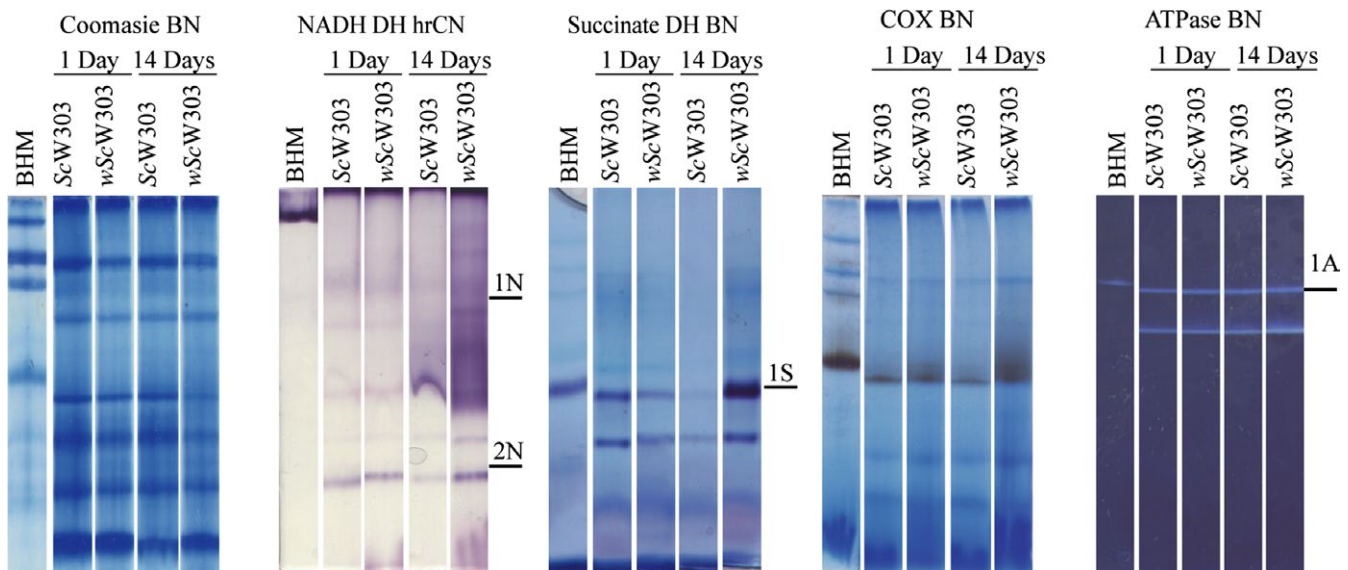


FIGURE 7 *Wolbachia*-mediated effects on the activity of each mitochondrial respiratory complex. BN-PAGE Coomassie-stained gel of ScW303 and wScW303 cells harvested at one and 14 days. In gel NADH-NBT oxido-reductase, succinate dehydrogenase, cytochrome c oxidase and ATPase enzyme activities in hrCN-PAGE or BN-PAGE, from 14 day old culture of wScW303. Bands 1N, 2N, 1S, and 1A were sequenced (Table S4). Bovine heart mitochondria (BHM) were used as a control

3.2.10 | *Wolbachia* remains infective against insect cell lines

After being cultured in a yeast cell, the question arose on whether *Wolbachia* remained viable and infective when isolated. To test this, we extracted *Wolbachia* from wScW303, incubated it in isolation for 5 days and then infected a C6C36 insect cell line which was previously reported to support bacterial infection (Baldrige et al., 2014). Aged *Wolbachia* infection was successful as assessed by specific staining using FISH (Figure 8 Movie S3).

4 | DISCUSSION

Growing obligate endosymbionts in cell lines yields low biomass at high costs (Baldrige et al., 2014; Khoo et al., 2013). To circumvent this problem, we built a synthetic host-endosymbiont system by artificially infecting the commonly used yeast *Saccharomyces cerevisiae* strain W303 with *Wolbachia* wAlbB from *A. albopictus* (Figures 1–5, Movies S1–S2). Culturing *Wolbachia* in yeast allowed us to study the complex relationship between the host and the bacterium. Using *S. cerevisiae* as an artificial host confers benefits such as a high resistance to changing environments (Gasch, 2002; Gasch & Werner-Washburne, 2002), use of inexpensive liquid cultures and most importantly, the ease of manipulating and genetically engineering the host cell. Following our approach, it may be possible to construct other synthetic parasite-mutualistic systems for obligate endosymbionts. Our system requirements for a successful infection were: supplementing YPD with iron and bovine fetal serum, plus low speed agitation of the nonbaffled Erlenmeyer flask and keeping the temperature between 28 and 30°C. These adjustments resulted in successful yeast infection and considerable *Wolbachia* yields in 14 days as compared with available methods that need up to 100 days. Even if the *Saccharomyces/Wolbachia* system is only a model of the interactions that occur in a naturally infected eukaryote

cell, its manageability is outstanding and it may yield results that are not possible in cell lines.

Since *Wolbachia* is an alpha-proteobacterium closely related to mitochondria, it seemed likely that the aerobic metabolic machinery of *Wolbachia* might mimic, enhance, or supplement the respiratory activity from the host. (Strübing et al., 2010). However, under our conditions, *Wolbachia* respiratory chain proteins were not detectable, instead, we found an increase in host mitochondrial activity. Another obligate endosymbiont, the *Sytophilus oryzae* Principal Endosymbiont (SOPE), has also been reported to increase the mitochondrial activity in the host, probably by providing nutrients such as riboflavin (Heddi, Lefebvre, & Nardon, 1993; Heddi et al., 1999). Several authors suggest that *Wolbachia* provides riboflavin or heme groups to their arthropod and nematode hosts (Brownlie et al., 2009; Darby et al., 2012; Foster et al., 2005; Wu et al., 2009). This may vary with strains as *Wolbachia* from *Brugia malayi* (wBm) contains complete sets of riboflavin, heme and nucleotide biosynthesis genes the filarial host lacks (Darby et al., 2012; Foster et al., 2005; Klasson et al., 2008; Wu et al., 2004). In return, the host provides amino acid, proteins and a safe, stable environment (Brownlie et al., 2009; Darby et al., 2012; Foster et al., 2005; Wu et al., 2009). The possibility that *Wolbachia*, behaves as SOPE, donating riboflavin or heme groups to the host may be explored in auxotrophic yeast mutants. *S. cerevisiae* libraries have a mutant for almost every enzyme on the riboflavin and heme synthesis pathways e.g. *S. cerevisiae* genome database (<https://www.yeast-genome.org/>).

Under the conditions tested here, expression of *Wolbachia* electron transport proteins was not detected. The reported *Wolbachia pipientis* wAlbB genome (Mavingui et al., 2012) shows that some respiratory complex subunits are missing, e.g. *nuoC* and *nuoD* for a functional complex I (Sazanov, 2015); yet other *Wolbachia* sequenced genomes contain all the genes necessary for a functional electron transport chain (Klasson et al., 2008), so maybe under different growth conditions, hosts and *Wolbachia* strains, bacterial respiratory proteins may be detected. It is suggested that other *Wolbachia* strains should be tested in order to determine whether some consume oxygen.

In our hands, *Wolbachia* infection resulted in activation of mitochondria beyond the stationary growth phase. It may be speculated that such activation constitutes an advantage for *Wolbachia* either due to quenching of oxygen in the cytoplasm (Rosas-Lemus et al., 2016) or because *Wolbachia* needs high ATP that an active mitochondria provides (Potter, Badder, Hoade, Johnston, & Morten, 2016). It has already been suggested by experiments using paraquat that *Wolbachia* sensitivity to free radicals is higher than that of the host (Fallon et al., 2013) and it cannot survive outside a host cell unless it is kept in a 5% CO₂ atmosphere (Rasgon et al., 2006). Also, high agitation speeds, which would increase oxygen concentrations, lead to loss of the *Wolbachia* infection (Result not shown). Thus, it is possible that *Wolbachia* enters the cytoplasm to hide from high atmospheric oxygen and then it optimizes cell metabolism to both, use host metabolites and find low cytoplasmic oxygen concentrations.

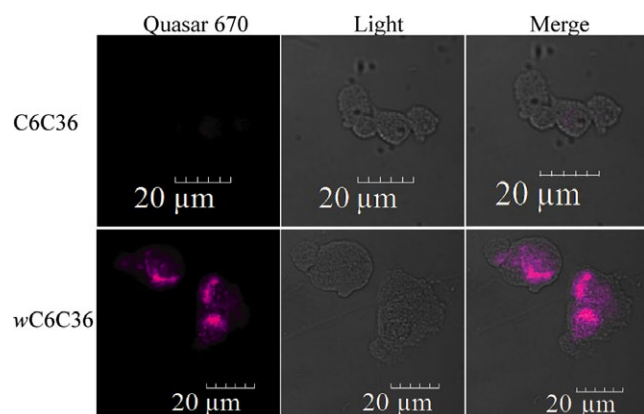


FIGURE 8 *Wolbachia* remains infective after being cultured in *S. cerevisiae*. FISH (Quasar 670-pink) of the wC6C36 cell line. Light/Quasar images show hybridization only inside the infected cell line. The noninfected cell line C6C36 does not have any of the pink hybridization mark identified as *Wolbachia*

Avoidance, i.e. hiding from oxygen, is a common behavior in oxygen conformers (Rosas-Lemus et al., 2016). In air, oxygen saturation concentration is ~21% (200 $\mu\text{mol L}^{-1}$) while intracellular oxygen concentration ranges between 13.2% and 14% (126–133 $\mu\text{mol L}^{-1}$) for rhabdomyosarcoma (RD) cells (Potter et al., 2016) or HEK293T cells (Abcam, 2016). When cells are exposed to lower ambient oxygen, intracellular oxygen concentration is also decreased: HEK293T cells exposed to 6% oxygen (50 $\mu\text{mol L}^{-1}$) have an intracellular oxygen concentration below 2% (19 $\mu\text{mol L}^{-1}$) (Abcam, 2016); RD cells exposed to 10% or 5% ambient oxygen reduce their intracellular oxygen concentration to 5.4% and 2.1% respectively (Potter et al., 2016). In addition, there is an intracellular oxygen gradient in the area surrounding the mitochondria in rat heart and hepatocytes, where oxygen concentration ranges between 3 (Gnaiger, 2003) and 6 $\mu\text{mol L}^{-1}$ (Jones & Kennedy, 1982; Tamura, Oshino, Chance, & Silver, 1978). Thus, a mitochondrion-containing host such as cell lines and yeast would probably provide the endosymbiont with a microaerobic environment. The mechanism for the increase in host mitochondrial activity needs to be defined.

In conclusion, we describe the infection of *S. cerevisiae* strain W303 by *Wolbachia* wAlbB. Infection led to premature death of the host and to an abnormal pattern of oxygen consumption. Further experiments using other yeast and other *Wolbachia* strains are needed to further explore oxidative phosphorylation patterns in the host/endosymbiont relationship. This system holds a large potential for different evaluations of biochemical and genetical processes in *Wolbachia*. Large biofermentors may be used to yield large amounts of biomass as required for different genomics and proteomics studies.

ACKNOWLEDGMENTS

Aa23 cell line was kindly donated by Dr. Ann Fallon from the University of Minnesota. The wsp antibody was a kind gift from Bei resources. CUA is a CONACYT PhD fellow enrolled in the Biochemistry PhD Program at UNAM. LMG is a CONACYT PhD fellow enrolled in the Biomedical Sciences PhD Program at UNAM. We received technical help from the Molecular Biology, the Microscopy and the Computation Units at IFC, UNAM. MALDI-TOF sequencing was performed by E. Ríos Castro from the Unidad de Genómica, Proteómica y Metabolómica, CINVESTAV-IPN, R Méndez-Franco, M. Contreras-Zentella, N.S. Sánchez and M. Calahorra are recognized for their technical assistance. M. Rigoulet, A. Devin (U-Bordeaux), D. González-Halphen, and G. Dreyfus-Cortés (IFC, UNAM) critically read the manuscript.

CONFLICT OF INTEREST

None declared.

REFERENCES

Abcam. (2016). ab197245 intracellular oxygen concentration assay. Retrieved from <http://www.abcam.com/ps/products/197/>

- ab197245/documents/ab197245%20Intracellular%20Oxygen%20Concentration%20Assay%20protocol%20v4%20(website).pdf.
- Aguilar-Uscnaga, B., & Francois, J. M. (2003). A study of the cell wall composition and structure in response to growth conditions and mode of cultivation. *Letters in Applied Microbiology*, 37(3), 268–274. <https://doi.org/10.1046/j.1472-765X.2003.01394.x>
- Alves-Rodrigues, I., Galão, R. P., Meyerhans, A., & Díez, J. (2006). *Saccharomyces cerevisiae*: A useful model host to study fundamental biology of viral replication. *Virus Research*, 120(1–2), 49–56. <https://doi.org/10.1016/j.virusres.2005.11.018>
- Amuzu, H. E., Simmons, C. P., & McGraw, E. A. (2015). Effect of repeat human blood feeding on *Wolbachia* density and dengue virus infection in *Aedes aegypti*. *Parasit Vectors*, 8, 246. <https://doi.org/10.1186/s13071-015-0853-y>
- Avrahami-Moyal, L., Braun, S., & Engelberg, D. (2012). Overexpression of PDE2 or SSD1-V in *Saccharomyces cerevisiae* W303-1A strain renders it ethanol-tolerant. *FEMS Yeast Research*, 12(4), 447–455. <https://doi.org/10.1111/j.1567-1364.2012.00795.x>
- Bakhtiari, N., Lai-Zhang, J., Yao, B., & Mueller, D. M. (1999). Structure/function of the beta-barrel domain of F1-ATPase in the yeast *Saccharomyces cerevisiae*. *Journal of Biological Chemistry*, 274(23), 16363–16369. <https://doi.org/10.1074/jbc.274.23.16363>
- Baldrige, G. D., Baldrige, A. S., Witthuhn, B. A., Higgins, L., Markowski, T. W., & Fallon, A. M. (2014). Proteomic profiling of a robust *Wolbachia* infection in an *Aedes albopictus* mosquito cell line. *Molecular Microbiology*, 94(3), 537–556. <https://doi.org/10.1111/mmi.12768>
- Bandi, C., Slatko, B., & O'Neill, S. L. (1999). *Wolbachia* genomes and the many faces of symbiosis. *Parasitol Today*, 15(11), 428–429. [https://doi.org/10.1016/S0169-4758\(99\)01543-4](https://doi.org/10.1016/S0169-4758(99)01543-4)
- Bertaux, J., Schmid, M., Prevost-Boure, N. C., Churin, J. L., Hartmann, A., Garbaye, J., & Frey-Klett, P. (2003). In situ identification of intracellular bacteria related to *Paenibacillus* spp. in the mycelium of the ectomycorrhizal fungus *Laccaria bicolor* S238N. *Applied and Environment Microbiology*, 69(7), 4243–4248. <https://doi.org/10.1128/AEM.69.7.4243-4248.2003>
- Bianciotto, V., Genre, A., Jargeat, P., Lumini, E., Becard, G., & Bonfante, P. (2004). Vertical transmission of endobacteria in the arbuscular mycorrhizal fungus *Gigaspora margarita* through generation of vegetative spores. *Applied and Environment Microbiology*, 70(6), 3600–3608. <https://doi.org/10.1128/AEM.70.6.3600-3608.2004>
- de Boer, W., Leveau, J. H., Kowalchuk, G. A., Gunnewiek, P. J. K., Abeln, E. C., Figue, M. J., ... van Veen, J. A. (2004). *Collimonas fungivorans* gen. nov., sp. nov., a chitinolytic soil bacterium with the ability to grow on living fungal hyphae. *International Journal of Systematic and Evolutionary Microbiology*, 54(Pt 3), 857–864. <https://doi.org/10.1099/ijs.0.02920-0>
- Bradford, M. M. (1976). A rapid and sensitive method for the quantification of microgram quantities of protein utilizing the principle of protein-dye binding. *Veterinary Parasitology*, 98(1–3), 215–238.
- Braig, H. R., Zhou, W., Dobson, S. L., & O'Neill, S. L. (1998). Cloning and characterization of a gene encoding the major surface protein of the bacterial endosymbiont *Wolbachia pipientis*. *Journal of Bacteriology*, 180(9), 2373–2378.
- Brenner, K., You, L., & Arnold, F. H. (2008). Engineering microbial consortia: A new frontier in synthetic biology. *Trends in Biotechnology*, 26(9), 483–489. <https://doi.org/10.1016/j.tibtech.2008.05.004>
- Brownlie, J. C., Cass, B. N., Riegler, M., Witsenburg, J. J., Iturbe-Ormaetxe, I., McGraw, E. A., & O'Neill, S. L. (2009). Evidence for metabolic provisioning by a common invertebrate endosymbiont, *Wolbachia pipientis*, during periods of nutritional stress. *PLoS Pathogens*, 5(4), e1000368.
- Buchsbaum, R., & Buchsbaum, M. (1934). An artificial symbiosis. *Science*, 80(2079), 408–409.
- Chiquete-Felix, N., Hernández, J. M., Méndez, J. A., Zepeda-Bastida, A., Chagolla-López, A., & Mujica, A. (2009). In guinea pig sperm, aldolase

- A forms a complex with actin, WAS, and Arp2/3 that plays a role in actin polymerization. *Reproduction*, 137(4), 669–678. <https://doi.org/10.1530/REP-08-0353>
- Crowe, L. M., Reid, D. S., & Crowe, J. H. (1996). Is trehalose special for preserving dry biomaterials? *Biophysical Journal*, 71(4), 2087–2093. [https://doi.org/10.1016/S0006-3495\(96\)79407-9](https://doi.org/10.1016/S0006-3495(96)79407-9)
- Dale, C., & Maudlin, I. (1999). *Sodalis* gen. nov. and *Sodalis glosinidius* sp. nov., a microaerophilic secondary endosymbiont of the tsetse fly *Glossina morsitans morsitans*. *International Journal of Systematic Bacteriology*, 49 (Pt 1), 267–275. <https://doi.org/10.1099/00207713-49-1-267>
- Darby, A. C., Armstrong, S. D., Bah, G. S., Kaur, G., Hughes, M. A., Kay, S. M., ... Tanya, V. N. (2012). Analysis of gene expression from the *Wolbachia* genome of a filarial nematode supports both metabolic and defensive roles within the symbiosis. *Genome Research*, 22(12), 2467–2477. <https://doi.org/10.1101/gr.138420.112>
- Darby, A. C., Gill, A. C., Armstrong, S. D., Hartley, C. S., Xia, D., Wastling, J. M., & Makepeace, B. L. (2014). Integrated transcriptomic and proteomic analysis of the global response of *Wolbachia* to doxycycline-induced stress. *ISME Journal*, 8(4), 925–937. <https://doi.org/10.1038/ismej.2013.192>
- Diaz-Ruiz, R., Rigoulet, M., & Devin, A. (2011). The Warburg and Crabtree effects: On the origin of cancer cell energy metabolism and of yeast glucose repression. *Biochimica et Biophysica Acta*, 1807(6), 568–576. <https://doi.org/10.1016/j.bbabbio.2010.08.010>
- Dobson, S. L., Marsland, E. J., Veneti, Z., Bourtzis, K., & O'Neill, S. L. (2002). Characterization of *Wolbachia* host cell range via the in vitro establishment of infections. *Applied and Environment Microbiology*, 68(2), 656–660. <https://doi.org/10.1128/AEM.68.2.656-660.2002>
- Fallon, A. M., Baldrige, G. D., Carroll, E. M., & Kurtz, C. M. (2014). Depletion of host cell riboflavin reduces *Wolbachia* levels in cultured mosquito cells. *In Vitro Cellular & Developmental Biology - Animal*, 50(8), 707–713. <https://doi.org/10.1007/s11626-014-9758-x>
- Fallon, A. M., Kurtz, C. M., & Carroll, E. M. (2013). The oxidizing agent, paraquat, is more toxic to *Wolbachia* than to mosquito host cells. *In Vitro Cellular & Developmental Biology - Animal*, 49(7), 501–507. <https://doi.org/10.1007/s11626-013-9634-0>
- Foster, J., Ganatra, M., Kamal, I., Ware, J., Makarova, K., Ivanova, N., ... Vincze, T. (2005). The *Wolbachia* genome of *Brugia malayi*: Endosymbiont evolution within a human pathogenic nematode. *PLoS Biology*, 3(4), e121. <https://doi.org/10.1371/journal.pbio.0030121>
- French, K. E. (2017). Engineering mycorrhizal symbioses to alter plant metabolism and improve crop health. *Frontiers in Microbiology*, 8, 1403. <https://doi.org/10.3389/fmicb.2017.01403>
- Frey-Klett, P., Burlinson, P., Deveau, A., Barret, M., Tarkka, M., & Sarniguet, A. (2011). Bacterial-fungal interactions: Hyphens between agricultural, clinical, environmental, and food microbiologists. *Microbiology and Molecular Biology Reviews*, 75(4), 583–609. <https://doi.org/10.1128/MMBR.00020-11>
- Gasch, A. P. (2002). Yeast genomic expression studies using DNA microarrays. *Methods in Enzymology*, 350, 393–414. [https://doi.org/10.1016/S0076-6879\(02\)50976-9](https://doi.org/10.1016/S0076-6879(02)50976-9)
- Gasch, A. P., & Werner-Washburne, M. (2002). The genomics of yeast responses to environmental stress and starvation. *Functional & Integrative Genomics*, 2(4–5), 181–192. <https://doi.org/10.1007/s10142-002-0058-2>
- Genty, L. M., Bouchon, D., Raimond, M., & Bertaux, J. (2014). *Wolbachia* infect ovaries in the course of their maturation: Last minute passengers and priority travellers? *PLoS ONE*, 9(4), e94577. <https://doi.org/10.1371/journal.pone.0094577>
- Gnaiger, E. (2003). Oxygen conformance of cellular respiration. In R. C. Roach, P. D. Wagner, & P. H. Hackett (Eds.), *Hypoxia: Through the lifecycle* (pp. 39–55). Boston, MA: Springer. <https://doi.org/10.1007/978-1-4419-8997-0>
- Gornal, A. G. (1957). Spectrophotometric and turbidimetric methods for measuring proteins III: Biuret method. *Methods in Enzymology*, 3, 447–454.
- Guerrero-Castillo, S., Araiza-Olivera, D., Cabrera-Orefice, A., Espinasa-Jaramillo, J., Gutiérrez-Aguilar, M., Luévano-Martínez, L. A., ... Uribe-Carvajal, S. (2011). Physiological uncoupling of mitochondrial oxidative phosphorylation. Studies in different yeast species. *Journal of Bioenergetics and Biomembranes*, 43(3), 323–331. <https://doi.org/10.1007/s10863-011-9356-5>
- Gutiérrez-Aguilar, M., López-Carbajal, H. M., Uribe-Alvarez, C., Espinoza-Simón, E., Rosas-Lemus, M., Chiquete-Félix, N., & Uribe-Carvajal, S. (2014). Effects of ubiquinone derivatives on the mitochondrial unselective channel of *Saccharomyces cerevisiae*. *Journal of Bioenergetics and Biomembranes*, 46(6), 519–527. <https://doi.org/10.1007/s10863-014-9595-3>
- Heddi, A., Grenier, A. M., Khatchadourian, C., Charles, H., & Nardon, P. (1999). Four intracellular genomes direct weevil biology: Nuclear, mitochondrial, principal endosymbiont, and *Wolbachia*. *Proceedings of the National Academy of Sciences of the United States of America*, 96(12), 6814–6819. <https://doi.org/10.1073/pnas.96.12.6814>
- Heddi, A., Lefebvre, F., & Nardon, P. (1993). Effect of endocytobiotic bacteria on mitochondrial enzymatic activities in the weevil *Sitophilus oryzae* (Coleoptera: Curculionidae). *Insect Biochemistry and Molecular Biology*, 23(3), 8.
- Hoffman, M. T., & Arnold, A. E. (2010). Diverse bacteria inhabit living hyphae of phylogenetically diverse fungal endophytes. *Applied and Environment Microbiology*, 76(12), 4063–4075. <https://doi.org/10.1128/AEM.02928-09>
- Hosoda, K., Suzuki, S., Yamauchi, Y., Shiroguchi, Y., Kashiwagi, A., Ono, N., ... Yomo, T. (2011). Cooperative adaptation to establishment of a synthetic bacterial mutualism. *PLoS ONE*, 6(2), e17105. <https://doi.org/10.1371/journal.pone.0017105>
- Hosoda, K., & Yomo, T. (2011). Designing symbiosis. *Bioengineered Bugs*, 2(6), 338–341. <https://doi.org/10.4161/bbug.2.6.16801>
- Jonckheere, A. I., Smeitink, J. A., & Rodenburg, R. J. (2012). Mitochondrial ATP synthase: Architecture, function and pathology. *Journal of Inherited Metabolic Disease*, 35(2), 211–225. <https://doi.org/10.1007/s10545-011-9382-9>
- Jones, D. P., & Kennedy, F. G. (1982). Intracellular oxygen supply during hypoxia. *American Journal of Physiology*, 243(5), C247–C253. <https://doi.org/10.1152/ajpcell.1982.243.5.C247>
- Kang, S. W., Jeon, B. Y., Hwang, T. S., & Park, D. H. (2009). Symbiotic relationship between *Microbacterium* sp. SK0812 and *Candida tropicalis* SK090404. *The Journal of Microbiology*, 47(6), 721–727. <https://doi.org/10.1007/s12275-009-0146-2>
- Khoo, C. C. H., Venard, C. M. P., Fu, Y., Mercer, D. R., & Dobson, S. L. (2013). Infection, growth and maintenance of *Wolbachia pipientis* in clonal and non-clonal *Aedes albopictus* cell cultures. *Bulletin of Entomological Research*, 103(3), 251–260. <https://doi.org/10.1017/S0007485312000648>
- Klasson, L., Walker, T., Sebahia, M., Sanders, M. J., Quail, M. A., Lord, A., ... Sinkins, S. P. (2008). Genome evolution of *Wolbachia* strain wPip from the *Culex pipiens* group. *Molecular Biology and Evolution*, 25(9), 1877–1887. <https://doi.org/10.1093/molbev/msn133>
- Kubo, I., Hosoda, K., Suzuki, S., Yamamoto, K., Kihara, K., Mori, K., & Yomo, T. (2013). Construction of bacteria-eukaryote synthetic mutualism. *Biosystems*, 113(2), 66–71. <https://doi.org/10.1016/j.biosystems.2013.05.006>
- Leslie, S. B., Israeli, E., Lighthart, B., Crowe, J. H., & Crowe, L. M. (1995). Trehalose and sucrose protect both membranes and proteins in intact bacteria during drying. *Applied and Environment Microbiology*, 61(10), 3592–3597.
- Lőrincz, Z., Preininger, É., Kósa, A., Pónyi, T., Nyitrai, P., Sarkadi, L., ... Gyurján, I. (2010). Artificial tripartite symbiosis involving a green alga (*Chlamydomonas*), a bacterium (*Azotobacter*) and a fungus

- (*Alternaria*): Morphological and physiological characterization. *Folia Microbiologica (Praha)*, 55(4), 393–400. <https://doi.org/10.1007/s12223-010-0067-9>
- Lumini, E., Ghignone, S., Bianciotto, V., & Bonfante, P. (2006). Endobacteria or bacterial endosymbionts? To be or not to be. *New Phytologist*, 170(2), 205–208. <https://doi.org/10.1111/j.1469-8137.2006.01673.x>
- Mavingui, P., Moro, C. V., Tran-Van, V., Wisniewski-Dyé, F., Raquin, V., Minard, G., ... Lozano, L. (2012). Whole-genome sequence of *Wolbachia* strain wAlbB, an endosymbiont of tiger mosquito vector *Aedes albopictus*. *Journal of Bacteriology*, 194(7), 1840. <https://doi.org/10.1128/JB.00036-12>
- McMeniman, C. J., Hughes, G. L., & O'Neill, S. L. (2011). A *Wolbachia* symbiont in *Aedes aegypti* disrupts mosquito egg development to a greater extent when mosquitoes feed on nonhuman versus human blood. *Journal of Medical Entomology*, 48(1), 76–84. <https://doi.org/10.1603/ME09188>
- Mee, M. T., & Wang, H. H. (2012). Engineering ecosystems and synthetic ecologies. *Molecular BioSystems*, 8(10), 2470–2483. <https://doi.org/10.1039/c2mb25133g>
- Momeni, B., Chen, C. C., Hillesland, K. L., Waite, A., & Shou, W. (2011). Using artificial systems to explore the ecology and evolution of symbioses. *Cellular and Molecular Life Sciences*, 68(8), 1353–1368. <https://doi.org/10.1007/s00018-011-0649-y>
- Morales-Rios, E., Montgomery, M. G., Leslie, A. G., & Walker, J. E. (2015). Structure of ATP synthase from *Paracoccus denitrificans* determined by X-ray crystallography at 4.0 Å resolution. *Proceedings of the National Academy of Sciences of the United States of America*, 112(43), 13231–13236. <https://doi.org/10.1073/pnas.1517542112>
- Ocampo, A., Liu, J., Schroeder, E. A., Shadel, G. S., & Barrientos, A. (2012). Mitochondrial respiratory thresholds regulate yeast chronological life span and its extension by caloric restriction. *Cell Metabolism*, 16(1), 55–67. <https://doi.org/10.1016/j.cmet.2012.05.013>
- Omsland, A., Cockrell, D. C., Howe, D., Fischer, E. R., Virtaneva, K., Sturdevant, D. E., ... Heinzen, R. A. (2009). Host cell-free growth of the Q fever bacterium *Coxiella burnetii*. *Proceedings of the National Academy of Sciences of the United States of America*, 106(11), 4430–4434. <https://doi.org/10.1073/pnas.0812074106>
- Omsland, A., Cockrell, D. C., Howe, D., Fischer, E. R., Virtaneva, K., Sturdevant, D. E., ... Heinzen, R. A. (2013). Bringing culture to the uncultured: *Coxiella burnetii* and lessons for obligate intracellular bacterial pathogens. *PLoS Pathogens*, 9(9), e1003540. <https://doi.org/10.1371/journal.ppat.1003540>
- O'Neill, S. L., Pettigrew, M., Sinkins, S. P., Braig, H. R., Andreadis, T. G., & Tesh, R. B. (1997). In vitro cultivation of *Wolbachia pipientis* in an *Aedes albopictus* cell line. *Insect Molecular Biology*, 6(1), 33–39. <https://doi.org/10.1046/j.1365-2583.1997.00157.x>
- Partida-Martinez, L. P., & Hertweck, C. (2005). Pathogenic fungus harbours endosymbiotic bacteria for toxin production. *Nature*, 437(7060), 884–888. <https://doi.org/10.1038/nature03997>
- Peña, A., Piña, M. Z., Escamilla, E., & Piña, E. (1977). A novel method for the rapid preparation of coupled yeast mitochondria. *FEBS Letters*, 80(1), 209–213.
- Potter, M., Badder, L., Hoade, Y., Johnston, I. G., & Morten, K. J. (2016). Monitoring intracellular oxygen concentration: Implications for hypoxia studies and real-time oxygen monitoring. *Advances in Experimental Medicine and Biology*, 876, 257–263. <https://doi.org/10.1007/978-1-4939-3023-4>
- Rasgon, J. L., Gamston, C. E., & Ren, X. (2006). Survival of *Wolbachia pipientis* in cell-free medium. *Applied and Environment Microbiology*, 72(11), 6934–6937. <https://doi.org/10.1128/AEM.01673-06>
- Robinson, G. C., Bason, J. V., Montgomery, M. G., Fearnley, I. M., Mueller, D. M., Leslie, A. G., & Walker, J. E. (2013). The structure of F(1)-ATPase from *Saccharomyces cerevisiae* inhibited by its regulatory protein IF(1). *Open Biology*, 3(2), 120164. <https://doi.org/10.1098/rsob.120164>
- Rosas-Lemus, M., Uribe-Alvarez, C., Contreras-Zentella, M., Luévano-Martínez, L. A., Chiquete-Félix, N., Espinosa-Simón, E., ... Uribe-Carvajal, S. (2016). Oxygen: from toxic waste to optimal (Toxic) fuel of life. In *Free Radicals and Diseases*. InTech.
- Salzberg, S. L., Puiu, D., Sommer, D. D., Nene, V., & Lee, N. H. (2009). Genome sequence of the *Wolbachia* endosymbiont of *Culex quinquefasciatus* JHB. *Journal of Bacteriology*, 191(5), 1725. <https://doi.org/10.1128/JB.01731-08>
- Sampedro, J. G., & Uribe, S. (2004). Trehalose-enzyme interactions result in structure stabilization and activity inhibition. The role of viscosity. *Molecular and Cellular Biochemistry*, 256–257(1–2), 319–327. <https://doi.org/10.1023/B:MCBI.0000009878.21929.eb>
- Sanjeev, P., & Siavoshi, F. (2015). Endocytotic uptake of FITC-labeled anti-*H. pylori* egg yolk immunoglobulin Y in *Candida* yeast for detection of intracellular *H. pylori*. *Frontiers in Microbiology*, 6, 113.
- Sato, Y., Narisawa, K., Tsuruta, K., Umezu, M., Nishizawa, T., Tanaka, K., ... Ohta, H. (2010). Detection of betaproteobacteria inside the mycelium of the fungus *Mortierella elongata*. *Microbes and Environments*, 25(4), 321–324. <https://doi.org/10.1264/jsme2.ME10134>
- Sazanov, L. A. (2015). A giant molecular proton pump: Structure and mechanism of respiratory complex I. *Nature Reviews Molecular Cell Biology*, 16(6), 375–388. <https://doi.org/10.1038/nrm3997>
- Schagger, H. (2002). Respiratory chain supercomplexes of mitochondria and bacteria. *Biochimica et Biophysica Acta*, 1555(1–3), 154–159. [https://doi.org/10.1016/S0005-2728\(02\)00271-2](https://doi.org/10.1016/S0005-2728(02)00271-2)
- Shevchenko, A., Tomas, H., Havli, J., Olsen, J. V., & Mann, M. (2006). In-gel digestion for mass spectrometric characterization of proteins and proteomes. *Nature Protocols*, 1(6), 2856–2860.
- Shih, K. M., Gerenday, A., & Fallon, A. M. (1998). Culture of mosquito cells in Eagle's medium. *In Vitro Cellular & Developmental Biology - Animal*, 34(8), 629–630. <https://doi.org/10.1007/s11626-996-0010-1>
- Shou, W., Ram, S., & Vilar, J. M. (2007). Synthetic cooperation in engineered yeast populations. *Proceedings of the National Academy of Sciences of the United States of America*, 104(6), 1877–1882. <https://doi.org/10.1073/pnas.0610575104>
- Siggers, K. A., & Lesser, C. F. (2008). The yeast *Saccharomyces cerevisiae*: A versatile model system for the identification and characterization of bacterial virulence proteins. *Cell Host & Microbe*, 4(1), 8–15. <https://doi.org/10.1016/j.chom.2008.06.004>
- Smith, A. E., Zhang, Z., Thomas, C. R., Moxham, K. E., & Middelberg, A. P. (2000). The mechanical properties of *Saccharomyces cerevisiae*. *Proceedings of the National Academy of Sciences of the United States of America*, 97(18), 9871–9874.
- Stella, C., Burgos, I., Chapela, S., & Gamondi, O. (2011). Ischemia-reperfusion: A look from yeast mitochondria. *Current Medicinal Chemistry*, 18(23), 3476–3484. <https://doi.org/10.2174/092986711796642553>
- Stewart, E. J. (2012). Growing unculturable bacteria. *Journal of Bacteriology*, 194(16), 4151–4160. <https://doi.org/10.1128/JB.00345-12>
- Strübing, U., Lucius, R., Hoerauf, A., & Pfarr, K. M. (2010). Mitochondrial genes for heme-dependent respiratory chain complexes are up-regulated after depletion of *Wolbachia* from filarial nematodes. *International Journal for Parasitology*, 40(10), 1193–1202. <https://doi.org/10.1016/j.ijpara.2010.03.004>
- Sun, X. Y., Zhao, Y., Liu, L. L., Jia, B., Zhao, F., Huang, W. D., & Zhan, J. C. (2015). Copper tolerance and biosorption of *Saccharomyces cerevisiae* during alcoholic fermentation. *PLoS ONE*, 10(6), e0128611. <https://doi.org/10.1371/journal.pone.0128611>
- Tamura, M., Oshino, N., Chance, B., & Silver, I. A. (1978). Optical measurements of intracellular oxygen concentration of rat heart in vitro. *Archives of Biochemistry and Biophysics*, 191(1), 8–22. [https://doi.org/10.1016/0003-9861\(78\)90062-0](https://doi.org/10.1016/0003-9861(78)90062-0)
- Taylor, M. J., & Hoerauf, A. (1999). *Wolbachia* bacteria of filarial nematodes. *Parasitology Today*, 15(11), 437–442. [https://doi.org/10.1016/S0169-4758\(99\)01533-1](https://doi.org/10.1016/S0169-4758(99)01533-1)

- Uribe, S. A., Ramirez, J. O., & Peña, A. N. (1985). Effects of beta-pinene on yeast membrane functions. *Journal of Bacteriology*, 161(3), 1195–1200.
- Uribe, S., Rangel, P. A., Espínola, G. L., & Aguirre, G. A. (1990). Effects of cyclohexane, an industrial solvent, on the yeast *Saccharomyces cerevisiae* and on isolated yeast mitochondria. *Applied and Environment Microbiology*, 56(7), 2114–2119.
- Uribe-Alvarez, C., Chiquete-Félix, N., Contreras-Zentella, M., Guerrero-Castillo, S., Peña, A., & Uribe-Carvajal, S. (2016). *Staphylococcus epidermidis*: Metabolic adaptation and biofilm formation in response to different oxygen concentrations. *Pathogens and Disease*, 74(1), ftv111. <https://doi.org/10.1093/femspd/ftv111>
- Werren, J. H. (1997). Biology of *Wolbachia*. *Annual Review of Entomology*, 42, 587–609. <https://doi.org/10.1146/annurev.ento.42.1.587>
- Werren, J. H., Baldo, L., & Clark, M. E. (2008). *Wolbachia*: Master manipulators of invertebrate biology. *Nature Reviews Microbiology*, 6(10), 741–751. <https://doi.org/10.1038/nrmicro1969>
- Winkler, H. H., & Turco, J. (1988). *Rickettsia prowazekii* and the host cell: entry, growth and control of the parasite. *Current Topics in Microbiology and Immunology*, 138, 81–107.
- Wittig, I., Braun, H. P., & Schägger, H. (2006). Blue native PAGE. *Nature Protocols*, 1(1), 418–428. <https://doi.org/10.1038/nprot.2006.62>
- Wittig, I., Karas, M., & Schägger, H. (2007). High resolution clear native electrophoresis for in-gel functional assays and fluorescence studies of membrane protein complexes. *Molecular & Cellular Proteomics: MCP*, 6(7), 1215–1225. <https://doi.org/10.1074/mcp.M700076-MCP200>
- Wu, B., Novelli, J., Foster, J., Vaisvila, R., Conway, L., Ingram, J., ... Slatko, B. (2009). The heme biosynthetic pathway of the obligate *Wolbachia* endosymbiont of *Brugia malayi* as a potential anti-filarial drug target. *PLoS Neglected Tropical Diseases*, 3(7), e475. <https://doi.org/10.1371/journal.pntd.0000475>
- Wu, M., Sun, L. V., Vamathevan, J., Riegler, M., Deboy, R., Brownlie, J. C., ... Wiegand, C. (2004). Phylogenomics of the reproductive parasite *Wolbachia pipientis* wMel: A streamlined genome overrun by mobile genetic elements. *PLoS Biology*, 2(3), E69. <https://doi.org/10.1371/journal.pbio.0020069>
- Xi, Z., Khoo, C. C., & Dobson, S. L. (2006). Interspecific transfer of *Wolbachia* into the mosquito disease vector *Aedes albopictus*. *Proceedings. Biological sciences Royal Society*, 273(1592), 1317–1322. <https://doi.org/10.1098/rspb.2005.3405>

SUPPORTING INFORMATION

Additional supporting information may be found online in the Supporting Information section at the end of the article.

How to cite this article: Uribe-Alvarez C, Chiquete-Félix N, Morales-García L, et al. *Wolbachia pipientis* grows in *Saccharomyces cerevisiae* evoking early death of the host and deregulation of mitochondrial metabolism. *MicrobiologyOpen*. 2019;8:e675. <https://doi.org/10.1002/mbo3.675>